AD-A167 269 AN INVESTIGATION OF DIELECTRIC LOADED RIDGED WAVEGUIDE (U) NAVAL RESEARCH LAB WASHINGTON DC C W YOUNG 31 MAR 86 NRL-8917 1/2

UNCLASSIFIED F/G 9/1 NL

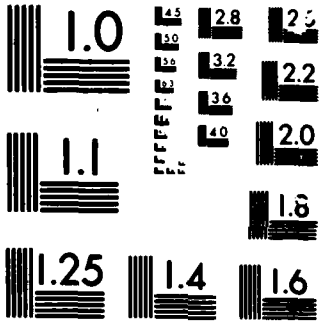

MICROCOPY CHART

AD-A167 269

NRL Report 8917

An Investigation of Dielectric Loaded Ridged Waveguide

C. W. YOUNG, JR.

Microwave Technology Branch
Electronics Technology Division

March 31, 1986

DTIC FILE COPY

DTIC
ELECTE
MAY 1 5 1986
S D
E

NAVAL RESEARCH LABORATORY
Washington, D.C.

86 5 15 032

Approved for public release; distribution unlimited.

SECURITY CLASSIFICATION OF THIS PAGE

REPORT DOCUMENTATION PAGE

1a. REPORT SECURITY CLASSIFICATION UNCLASSIFIED	1b. RESTRICTIVE MARKINGS
2a. SECURITY CLASSIFICATION AUTHORITY 2b. DECLASSIFICATION / DOWNGRADING SCHEDULE	3. DISTRIBUTION / AVAILABILITY OF REPORT Approved for public release; distribution unlimited.
4. PERFORMING ORGANIZATION REPORT NUMBER(S) NRL Report 8917	5. MONITORING ORGANIZATION REPORT NUMBER(S)
6a. NAME OF PERFORMING ORGANIZATION Naval Research Laboratory 6b. OFFICE SYMBOL (If applicable)	7a. NAME OF MONITORING ORGANIZATION
6c. ADDRESS (City, State, and ZIP Code) Washington, DC 20375-5000	7b. ADDRESS (City, State, and ZIP Code)
8a. NAME OF FUNDING / SPONSORING ORGANIZATION Naval Electronic Systems Command 8b. OFFICE SYMBOL (If applicable)	9. PROCUREMENT INSTRUMENT IDENTIFICATION NUMBER
8c. ADDRESS (City, State, and ZIP Code) Arlington, VA 22202	10. SOURCE OF FUNDING NUMBERS PROGRAM ELEMENT NO. 62762N; PROJECT NO. XF62584; TASK NO.; WORK UNIT ACCESSION NO. DN480-805

11. TITLE (Include Security Classification)

An Investigation of Dielectric Loaded Ridged Waveguide

12. PERSONAL AUTHOR(S)
Young, Charles W., Jr.

13a. TYPE OF REPORT	13b. TIME COVERED	14. DATE OF REPORT (Year, Month, Day)	15. PAGE COUNT
Final	FROM 6/81 TO 12/84	1986 March 31	146

16. SUPPLEMENTARY NOTATION

17. COSATI CODES			18. SUBJECT TERMS (Continue on reverse if necessary and identify by block number)
FIELD	GROUP	SUB-GROUP	Ridged waveguide; Modal analysis; Dielectric loaded; Power breakdown

19. ABSTRACT (Continue on reverse if necessary and identify by block number)

The single mode bandwidth of any waveguide is the cutoff frequency ratio of the first higher order mode and the principal, or dominant, waveguide mode. Ridged waveguide may be designed to achieve a much larger single mode bandwidth than conventional rectangular waveguide, but suffers from a drastic decrease in peak power breakdown. Dielectric slab loaded rectangular waveguide also is capable of large single mode bandwidths. However, the aspect ratio of the latter waveguide must be reduced if the single mode bandwidth criterion is used, with a corresponding reduction of peak power breakdown. In this report, a complete modal analysis is made for ridged waveguide partially loaded with dielectric. Cutoff frequency calculations are derived for the different waveguide modes to provide the actual single mode bandwidth. Mathematical solutions for propagation characteristics, both phase and loss, and for peak power breakdown levels are derived for the dominant mode. It is shown that

(Continues)

20. DISTRIBUTION / AVAILABILITY OF ABSTRACT ☐ UNCLASSIFIED/UNLIMITED ☒ SAME AS RPT ☐ DTIC USERS	21. ABSTRACT SECURITY CLASSIFICATION UNCLASSIFIED
22a. NAME OF RESPONSIBLE INDIVIDUAL Charles W. Young, Jr.	22b. TELEPHONE (Include Area Code) (202)767-3008; 22c. OFFICE SYMBOL 6853

DD FORM 1473, 84 MAR — 83 APR edition may be used until exhausted. All other editions are obsolete.

SECURITY CLASSIFICATION OF THIS PAGE

19. ABSTRACT (Continued)

true TE or TM modes do not exist in the dielectric loaded ridged waveguide, contrary to the assumption made in the only published analysis of such waveguide. Numerical examples are cited to demonstrate the large single mode bandwidths that may be achieved with dielectric loaded ridge waveguide and the considerable increase in theoretical peak power breakdown levels over that of either empty ridged waveguide or dielectric slab loaded rectangular waveguide having the same single mode bandwidth.

CONTENTS

SYMBOLS AND DEFINITIONS iv

1.0 INTRODUCTION 1

2.0 WAVEGUIDE THEORETICAL ANALYSIS 4

3.0 COMPARISON OF EXPERIMENTAL DATA WITH THEORY 62

4.0 WAVEGUIDE PERFORMANCE CHARACTERISTICS 75

5.0 REFERENCES 91

APPENDIX A—Transverse Resonance Method Analysis 96

APPENDIX B—Dielectric Center Loaded Rectangular Waveguide 100

APPENDIX C—Scattering Matrix Properties of Lossless Waveguide Junctions 108

APPENDIX D—Effects of Standing Wave Patterns on Sample Measurements 112

APPENDIX E—Computer Programs 122

QUALITY INSPECTED 3

A-1

SYMBOLS AND DEFINITIONS

VPS	— vertical plane of symmetry
HPS	— horizontal plane of symmetry
TE	— transverse electric
TM	— transverse magnetic
LSE	— longitudinal section electric
LSM	— longitudinal section magnetic
QLSE	— quasi-LSE
QLSM	— quasi-LSM
FHOM	— first higher order mode
DRWG	— double ridged waveguide (empty)
DSLRWG	— dielectric slab loaded rectangular waveguide
DLDRWG	— dielectric loaded double ridged waveguide
P_{BD}	— peak power breakdown
P_{MVE}	— maximum voltage equivalent power
(M,E)	— magnetic wall at VPS, electric wall at HPS
(E,E)	— electric wall at VPS, electric wall at HPS
(M,M)	— magnetic wall at VPS, magnetic wall at HPS
(E,M)	— electric wall at VPS, magnetic wall at HPS
BW	— bandwidth
j	— $\sqrt{-1}$
ω	— radian frequency
f	— cyclic frequency
ϵ	— permittivity
ϵ_r	— relative permittivity
μ_0	— permeability of free space
p	— x-directed component of wave vector
k	— y-directed component of wave vector
β	— z-directed component of wave vector
α	— loss term of complex propagation constant
γ	— complex propagation constant, $= \alpha + j\beta$
δ_{mn}	— Kronecker delta function

AN INVESTIGATION OF DIELECTRIC LOADED RIDGED WAVEGUIDE

1.0 INTRODUCTION

1.1 Background

Many types of transmission media are used in the microwave portion of the frequency spectrum for guidance of electromagnetic energy. Waveguide, coaxial cable, twin lead, stripline, and microstrip constitute some of the more common types, and a variety of different configurations exists for each. In this report such waveguide types as dielectric waveguide and coplanar waveguide are not considered, and the term waveguide is restricted to mean conducting cylindrical tubes with a uniform, but not necessarily homogeneous, cross-sectional geometry.

Two important characteristics of waveguide are: (1) low insertion loss and (2) high-power capability. In both of these categories, waveguide is distinctly superior to other transmission media, and for many high-power applications, waveguide is the only choice. Waveguide is not without its disadvantages, however. Factors such as size, weight, and cost are outside the scope of this investigation, but the dispersive nature of waveguide [1,2] and the problems that can arise from multimoding, or the simultaneous propagation of different waveguide modes [2,3], are important considerations and are discussed in detail in Section 1.2.

Most early waveguide development [4-7] concentrated on rectangular and circular cross sections with homogeneous loading. The solutions to the boundary value problems posed by these regular cross sections are straightforward [1,8], and the real effort was in work on special features (bends, tuning posts, junctions, coupling slits, etc.). One of the first nonregular waveguide cross sections to receive much attention was ridged waveguide (Fig. 1). Early analyses of such waveguide geometry have been done with a number of different approaches [2,7,9-13]. One of the first investigations using numerical solutions was conducted by Montgomery [14] in 1971 using the Ritz-Galerkin method.

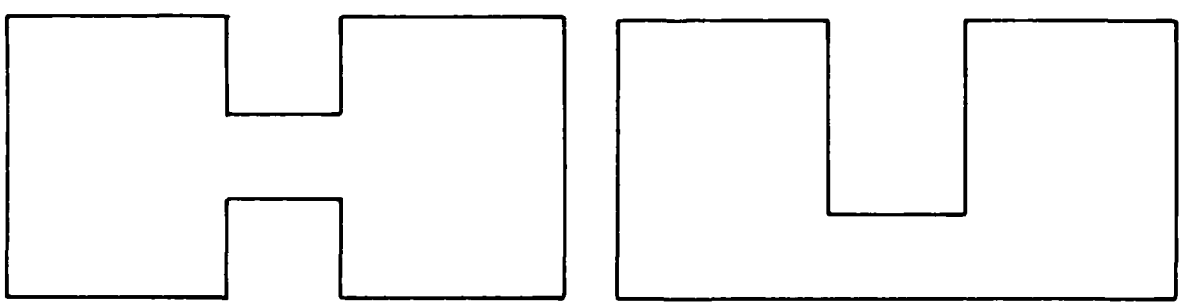

(a) double ridged (b) single ridged

Fig. 1 — Cross section of ridged waveguide

Every mode of propagation in any waveguide may be characterized by its field distribution. For homogeneous waveguides, modes are usually classified as TE (transverse electric) or TM (transverse magnetic) [1,2,8]. The principal, or dominant, waveguide mode is the mode with the lowest cutoff frequency. A fractional bandwidth may be defined as the ratio of the cutoff frequency of some higher

Manuscript approved May 29, 1985.

order mode and the cutoff frequency of the dominant mode. For a true single mode bandwidth, the maximum operating frequency is limited to the cutoff frequency f_c of the first higher order mode that can propagate; thus, the single mode bandwidth is

$$BW_{sm} = \frac{f_c\,(\text{first higher order mode})}{f_c\,(\text{dominant mode})}.$$

Ridged waveguide achieves a large single-mode bandwidth as a result of the excess capacitance in the center of the waveguide (a consequence of the reduced height in the gap region) which has the effect of lowering the cutoff frequency of the dominant $TE_{1,0}$ mode. The next propagating mode is the $TE_{2,0}$ mode which has an electric field null in the center; thus, the added capacitance has only a second order effect on the $TE_{2,0}$ cutoff frequency. A characteristic of ridged waveguide is the high wall current density in the ridge region, which results in a greater transmission loss than conventional waveguide. For many applications, a more serious disadvantage is the greatly reduced peak power breakdown level due to the increased electric field intensity in the ridge gap.

An alternative method for increasing the $TE_{1,0}$-$TE_{2,0}$ bandwidth of rectangular waveguide is placement of a dielectric slab vertically in the center (Fig. 2). This dielectric slab loaded rectangular waveguide has received considerable attention [15-24]. The two most notable features [18] are: (1) $TE_{1,0}$-$TE_{2,0}$ bandwidths comparable to those of ridged waveguide could be achieved, and (2) the power-handling capacity was increased over that of air-filled rectangular waveguide as a consequence of the higher breakdown strength of the dielectric material. The increase in power-handling capacity was emphasized in 1976 by Findakly and Haskel [23]. Dielectric slab loaded rectangular waveguide also achieves a large $TE_{1,0}$-$TE_{2,0}$ bandwidth as a result of the added capacitance in the center of the waveguide, but with the added capacitance due to the higher dielectric constant of the slab rather than to a reduced height. However, the first higher order mode to propagate in this waveguide structure usually is not the $TE_{2,0}$ mode. Because of the dielectric loading, LSE (longitudinal section electric) and LSM (longitudinal section magnetic) modes [1-3,18] may propagate prior to the $TE_{2,0}$ mode. Except for waveguides with small aspect ratios (height-to-width ratios), the first higher order mode to propagate will be the $LSE_{1,1}$ mode as shown by Gardiol [19]. The extensive bandwidth-power capacity design information of [23] uses a $TE_{1,0}$-$TE_{2,0}$ definition for bandwidth, assuming that intervening LSE and LSM modes could be suppressed or eliminated. The importance of limiting the waveguide propagation to a single mode is shown in [3] and [24].

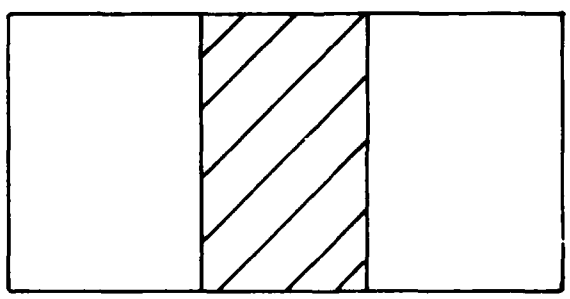

Fig. 2 — Cross section of dielectric slab loaded rectangular waveguide

One shortcoming of dielectric slab loaded rectangular waveguide is the limited increase in bandwidth provided by dielectric materials with low to moderate values of relative dielectric constant ϵ_r. The $TE_{1,0}$-$TE_{2,0}$ bandwidth is dependent on the thickness of the dielectric slab as well as ϵ_r; however, the minimum required value of ϵ_r increases very rapidly with bandwidth. From [23], a fractional bandwidth of 5.25 requires a value of ϵ_r of at least 50. High dielectric materials are available but generally have much greater loss than low ϵ_r materials [25,26]. Also, large ϵ_r materials are usually more

difficult to machine, can be very sensitive to temperature and atmospheric humidity, and in many cases are anisotropic.

1.2 Objectives

The purpose of this investigation is a theoretical analysis of a waveguide structure which is a composite of the two types discussed in Section 1.1, air-filled ridged waveguide and dielectric slab loaded rectangular waveguide. The generalized cross section of this partially dielectric loaded double ridged waveguide is shown in Fig. 3. The principal objective will be a complete modal analysis of this waveguide structure. The only previous theoretical investigation of this waveguide found in the technical literature was conducted by Magerl [27], with analysis restricted to a geometry where the dielectric width was exactly that of the ridge and with only a limited discussion of modes other than presumed $TE_{m,0}$ modes. Although Magerl's analysis is valid for cutoff frequencies of the $TE_{m,0}$ modes, true TE modes do not exist above cutoff [28]. With the complete modal analysis of this investigation, the cutoff frequency of any waveguide mode may be calculated, thus allowing the true single mode bandwidth to be determined. Also, this analysis will take into account the deviation of the dominant mode from a true TE mode for frequencies above cutoff, and will allow numerical evaluation of propagation terms (phase and loss) and peak power breakdown levels as a function of frequency for the waveguide of Fig. 3. A secondary objective of this investigation will be to show that the dielectric loaded ridged waveguide may be designed to have a much greater theoretical peak power breakdown level than either air-filled ridged waveguide or dielectric slab loaded rectangular waveguide having an equal single mode bandwidth.

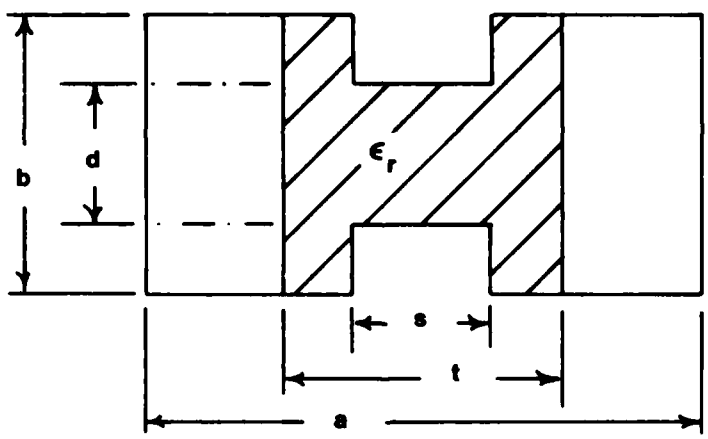

Fig. 3 — Cross section of dielectric loaded double ridged waveguide

The single mode bandwidth condition, where the maximum operating frequency is limited to the cutoff frequency of the first higher order mode that can propagate, is an important consideration. Although waveguides may be used in an overmoded condition where more than one mode may propagate, it is standard practice to limit if possible the operating frequency to the frequency range where only the dominant mode propagates. This is done to prevent coupling between modes. If more than one mode may propagate, some degree of coupling is inevitable in any real device because of slight geometrical imperfections. Energy coupled from the dominant mode into any propagating higher order mode may then be trapped between discontinuities, such as bends, and give rise to cavity effects. For high Q cavities, even a small coupling may thus produce sharp absorption peaks at the resonant frequencies of the cavities [2,8,19]. Mode suppression techniques such as properly oriented resistive film act to increase the attenuation for the higher order modes [3,24], thereby lowering the Q factor of the corresponding cavities and greatly reducing the absorption peaks. For high-power operation, where

such techniques for higher order mode suppression may be impractical due to arcing or melting of the resistive film, single mode bandwidth operation is therefore highly desirable.

A simplified explanation of how the composite waveguide structure of Fig. 3 could achieve a larger single mode bandwidth-power breakdown product than either of its constituent waveguide types may be made from an intuitive viewpoint. The added capacitance in the center of this waveguide is a combined effect of the reduced height in the gap and the dielectric loading. The added capacitance lowers the cutoff frequency of the dominant ($TE_{1,0}$-like) mode which has a maximum electric field in the center of the waveguide, but has little effect on the cutoff frequency of the $TE_{2,0}$-like mode which has an electric field null at the center. The modes are referred to as $TE_{m,o}$-like because true TE modes do not exist in this structure (nor do true TM, true LSE, or true LSM modes), as will be shown. The effect on the power breakdown level of the increased electric field intensity for the dominant mode in the region of the gap is offset by the increased breakdown strength of the dielectric. Since the vertical walls of the ridge are conducting surfaces, tangential electric fields may not exist there. The higher order LSE-like and LSM-like modes, which have electric fields tangential to the ridge wall, will therefore have an effective height less than the waveguide height, with a corresponding increase in cutoff frequency.

The dielectric slab must extend past either wall of the ridge, with the *H* shape shown in Fig. 3, if the addition of the dielectric is to maximize the power breakdown level. This is necessary because the strong fringing fields from the gap could cause arcing in air.

In Section 2, the mathematical development of the theoretical analysis is made to confirm this intuitive explanation. Numerical results obtained from this theoretical analysis are compared with the results of other theory. In Section 3, this analysis is further substantiated by comparison of theoretical results with experimental data from measurements on waveguide samples with varing geometries. Section 4 presents some of the characteristics of dielectric loaded ridged waveguide and compares the waveguide performance parameters with those of air-filled ridged waveguide and dielectric slab loaded rectangular waveguide.

2.0 WAVEGUIDE THEORETICAL ANALYSIS

2.1 Discussion of Analysis Approach

As noted by Lewin [29], the number of waveguide problems capable of exact solution is limited to a few very simple shapes, even when the common approximations of ideal geometry and infinite wall conductivity are made. Approximate solutions for more complicated waveguide shapes may be found via a number of methods and techniques. Some classes of waveguides are more suited to certain analysis methods than to other methods. Of the variety of methods available for finding numerical solutions to the hollow waveguide problem [30,31], many are not applicable for analysis of inhomogeneous waveguides. A review of different analysis methods which are suitable for obtaining a solution to the general inhomogeneous dielectric loaded waveguide problem may be found in Ref. 32. These methods include the transverse equivalent transmission line concept [1,7,9,11,33-39], perturbation methods [1,40-45], variational methods [1,38,41,46-50], Rayleigh-Ritz methods [1,38,41, 46,47,51-53], reaction concepts [41,47,54], and finite difference or finite element methods [55-60].

The transverse resonance method is probably the least complex of the possible approaches that may be used to find solutions for waveguide configurations of the type shown in Fig. 3. In this method, an equivalent transmission line circuit is formed to represent propagation characteristics in one of the transverse dimensions of the waveguide rather than along the waveguide axis [1,2]. Discontinuities along the transverse axis are reflected as lumped elements in the equivalent circuit. In general, each propagating mode will require a different equivalent circuit for analysis.

The computational requirements of the transverse resonance method are much less than those of other numerical methods, but there are two drawbacks to the use of this method to analyze the

waveguide of Fig. 3. First, the transverse resonance method gives only the propagation characteristics with no insight into the behavior of the fields; the electric field distribution is required to determine the power breakdown of the waveguide. Second is the question of a suitable equivalent circuit to represent the discontinuity formed by the ridge walls. This discontinuity is reflected as a change of the waveguide height in the transverse direction. By use of quasistatic methods and conformal mapping, such a discontinuity may be shown to have an equivalent transmission line circuit consisting of a shunt capacitance at the junction of two transmission lines of unequal characteristic impedance [7,33,38,39]. However, this derivation of the shunt capacitance assumes a propagating TE mode with only a vertical component of electric field incident upon the discontinuity formed by the height change, and further assumes the discontinuity to be isolated, i.e., far removed from other discontinuities in the waveguide. In the case of air-filled (or any homogeneous dielectric loaded) ridged waveguide, the $TE_{1,0}$ and $TE_{2,0}$ propagating modes each satisfy the first assumption: the propagating component of the transverse wave is TE to the ridge wall with no axial component of electric field [7,9,11]. Corrections to the value of the shunt capacitance in the equivalent transmission line circuit may be made to correct for proximity effects due to narrow ridges and/or close in sidewalls [10].

When attempting to find an equivalent circuit to represent the ridge wall in the partially dielectric loaded ridged waveguide of Fig. 3, several problems arise as a consequence of the inhomogeneous dielectric loading. In the absence of the ridge, modes other than $TE_{m,0}$ are characterized as LSE or LSM. Introduction of the ridge will cause distortion of the fields from true LSE or LSM nature, but as in the undistorted case the propagating components of the transverse wave will have axial components of electric field. Equivalent circuits to represent the change in waveguide height for incident modes other than the dominant mode (no axial electric field component) were not found in the technical literature. Without a suitable equivalent circuit to represent the effects of the ridge walls, the transverse resonance method is not applicable for analysis of the distorted $LSE_{m,n}$ ($n \neq 0$) and LSM modes. Even for the distorted $TE_{m,0}$ ($LSE_{m,0}$) modes, the accuracy of an equivalent circuit such as that from [7] may be questionable. An axial component of electric field must exist to satisfy the required boundary conditions at frequencies above cutoff [28]. Although this axial electric field may be evanescent, leaving the propagating portion of the transverse wave incident on the effective waveguide height change the dominant mode, the equivalent circuit derivation does not consider any axial electric field since none exists for the homogeneous case. An additional limitation on the accuracy of the derived shunt capacitance is due to the possible proximity of the discontinuity at the air-dielectric interface to the discontinuity at the ridge walls. Corrections to the shunt capacitive term for proximity effects such as in Ref. 10 do not consider a change of the dielectric media.

Despite the drawbacks of the transverse resonance method for analysis of the waveguide of Fig. 3, approximate solutions for the propagation characteristics of the dominant mode that may be obtained using this method are useful for several reasons. As the ridge depth becomes small ($d \rightarrow b$ in Fig. 3), the solution must approach that of the dielectric slab loaded rectangular waveguide for which the dominant mode is the $TE_{1,0}$ mode. At the dominant mode cutoff frequency of the actual ridged waveguide, the axial component of electric fields vanishes, thus the equivalent circuit derivation from Ref. 7 to represent the effect of the ridge walls need only consider proximity effects. At frequencies above cutoff, the dominant mode may be considered as a $TE_{1,0}$ mode distorted by the presence of the ridge. To a first order approximation, the evanescent axial component of electric field may be ignored and the dominant mode treated as true $TE_{1,0}$. The departure of the dominant mode from a true $TE_{1,0}$ mode will increase as the ridge gap becomes smaller. The solution obtained by the transverse resonance method thus will not be exact, but may provide sufficient accuracy for many purposes. Since the computational requirements are minor, the method is useful to provide approximate propagation characteristics of the dominant mode as a starting point in the search for a numerical solution of the more rigorous (and considerably more complex) analysis developed in Section 2.2.

Appendix A outlines a detailed development of the transverse resonance method to solve for the propagation characteristics of the waveguide of Fig. 3. The development includes the $TE_{2,0}$ mode as

well as the $TE_{1,0}$ mode since all of the arguments made concerning the approximations of the method for the distorted $TE_{1,0}$ mode apply to the distorted $TE_{2,0}$ mode as well.

As pointed out in Section 1.1, the first higher order mode to propagate in dielectric slab loaded rectangular waveguide may not be the $TE_{2,0}$ mode. Both the $LSE_{1,1}$ and $LSM_{0,1}$ mode are likely to have lower cutoff frequencies than the $TE_{2,0}$ mode. For the partially dielectric loaded double ridged waveguide, the distorted versions of these longitudinal section modes must have their cutoff frequencies determined if the single mode bandwidth criteria is to be used. For lack of a suitable equivalent circuit to represent the effects of the discontinuity at the ridge walls, the transverse resonance method is unsuitable for analysis of these higher order modes, thus another analysis approach must be found. A second reason for finding another means of waveguide analysis is the questionable approximations that were made for the distorted $TE_{m,0}$ modes. A more rigorous solution is desirable, preferably one that uses the same analysis method for all waveguide modes.

A perturbation method was rejected as a viable analysis approach for the partially dielectric loaded ridged waveguide because of the possible large deviation from the unperturbed problem, the dielectric slab loaded rectangular waveguide, for which the solution is readily available (Appendix B). Some consideration was given to the possibility of deriving an equivalent circuit to represent the effects of the ridge walls for higher order LSE- and LSM-type modes, as well as to account for the axial electric fields for the distorted $TE_{m,0}$ modes, thus allowing a more accurate analysis with the transverse resonance method. It was determined that an accurate equivalent circuit could not be derived for which the element values would be a function of the ridge wall discontinuity alone; all of the geometry parameters (Fig. 3) would be required to numerically define the element values. Such a process essentially would constitute the rationale "solve the problem to find the quantity needed to solve the problem," an obviously circuitous approach.

Many of the analysis approaches described in Ref. 32 are appropriate for obtaining numerical solutions for waveguides with arbitrary or very complex cross sections. While such methods could be used to obtain numerical solutions for the partially dielectric loaded double ridged waveguide, the computational requirements would be considerably in excess of a method which utilized the rectangular features of this waveguide with analysis restricted to the generalized cross section shown in Fig. 3. The approach of the latter method was selected for the waveguide analysis. Section 2.2 presents the mathematical development of the analysis. This analysis uses the Galerkin form [46,47] of the Rayleigh-Ritz method. This procedure is commonly referred to as the Ritz-Galerkin method [14] and constitutes a mode-matching technique [48,58].

2.2 Analysis of Lossless Waveguide

The appropriate physical parameters of the partially dielectric loaded double ridged waveguide under investigation are defined in Fig. 3. Only those configurations possessing physical symmetry in both the vertical and horizontal planes are considered. For the initial analysis, the following assumptions will be made:

- The waveguide is lossless, with the metal walls being perfect conductors and the loss tangent of the dielectric material equal to zero. Loss calculations will be made at a later stage by using perturbational techniques.
- The dielectric material is homogeneous and isotropic with a relative permittivity ϵ_r and a permeability equal to that of free space, μ_0.
- The interior volume of the waveguide is charge-free.
- Axial propagation is unidirectional in the $+z$ direction.
- Time dependence of all fields has the form $\exp(+j\omega t)$, where $j = \sqrt{-1}$ and ω is the radian frequency.

Advantage may be taken of the horizontal symmetry to reduce the model for analysis to a half cross section as shown in Fig. 4, with either a magnetic wall or an electric wall placed at the vertical plane of symmetry (VPS) at $x = x_3$. The model could be further reduced to one quadrant of the cross section by virtue of the vertical symmetry, but such a further reduction would offer no real advantages for this analysis. Because of the vertical symmetry, however, either an electric wall or a magnetic wall may alternatively exist at the horizontal plane of symmetry (HPS) at $y = 0$. The type of wall, electric (E) or magnetic (M), at the VPS is independent of the wall type at the HPS. The resulting solutions will be different for the four possible combinations of symmetry conditions. Until further clarification can be made, the wall conditions at the planes of symmetry will be indicated by a two-letter combination with the first letter denoting the wall type at the VPS and the second denoting the wall type at the HPS. The four solutions will then be defined as (M, E), (M, M), (E, M), and (E, E).

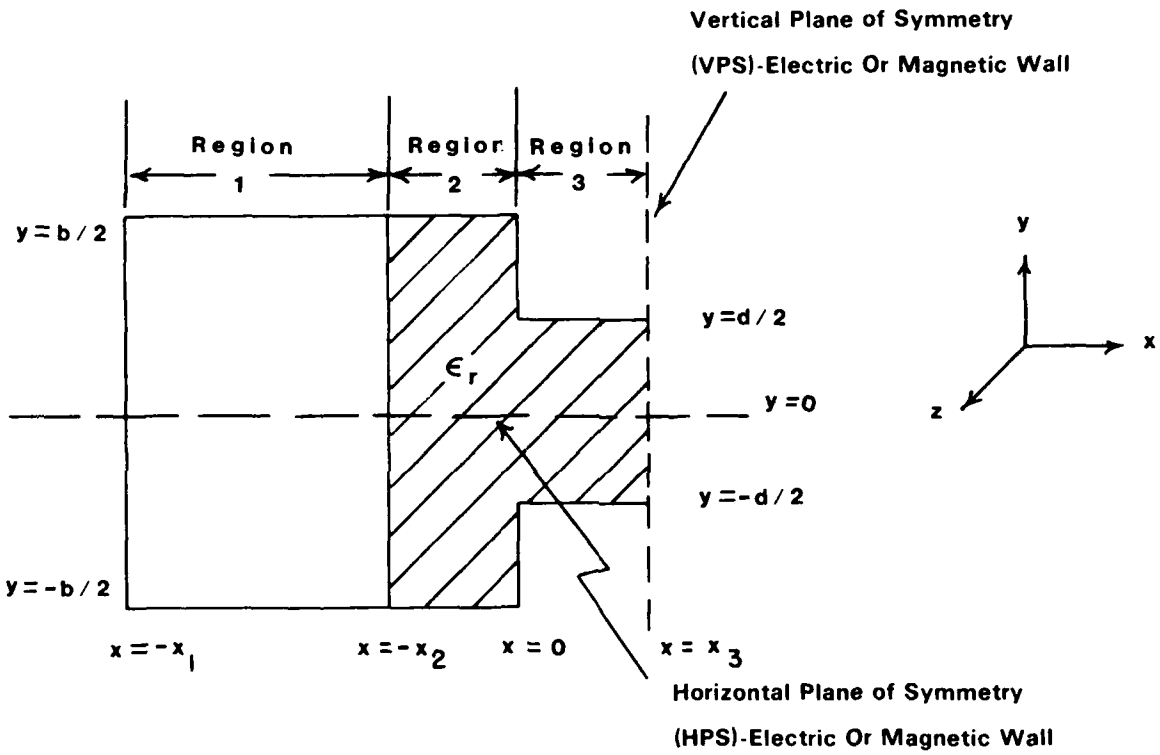

Fig. 4 — Model for analysis

The relationship between the x-direction parameters of the model for analysis (Fig. 4) and those of the waveguide (Fig. 3) are given by:

$$x_1 = (a - s)/2 \tag{2.1a}$$

$$x_2 = (t - s)/2 \tag{2.1b}$$

$$x_3 = s/2. \tag{2.1c}$$

The model will be separated into three homogeneous rectangular regions:

Region 1 $\quad -x_1 \leqslant x < -x_2,\ -b/2 \leqslant y \leqslant b/2$

Region 2 $\quad -x_2 \leqslant x < 0,\ -b/2 \leqslant y \leqslant b/2$

Region 3 $\quad 0 \leqslant x \leqslant x_3,\ -d/2 \leqslant y \leqslant d/2$

The rectangular coordinate system is the natural choice for an analysis of this configuration. The axes are defined in Fig. 4. The respective unit vectors are $\mathbf{a}_x$, $\mathbf{a}_y$, and $\mathbf{a}_z$.

For the assumptions noted, Maxwell's equations reduce to:

$$\nabla \times \mathbf{E} = -j\omega\mu_0\mathbf{H} \tag{2.2a}$$

$$\nabla \times \mathbf{H} = j\omega\epsilon\mathbf{E} \tag{2.2b}$$

$$\nabla \cdot \mathbf{E} = 0 \tag{2.2c}$$

$$\nabla \cdot \mathbf{H} = 0. \tag{2.2d}$$

Amplitudes are peak rather than RMS. Appropriate boundary conditions are:

$$\left.\begin{array}{l}\mathbf{n} \times \mathbf{E} = 0 \\ \mathbf{n} \cdot \mathbf{H} = 0\end{array}\right\} \text{at all electric walls} \tag{2.3a}$$

$$\left.\begin{array}{l}\mathbf{n} \cdot \mathbf{E} = 0 \\ \mathbf{n} \times \mathbf{H} = 0\end{array}\right\} \text{at all magnetic walls} \tag{2.3b}$$

$$\left.\begin{array}{l}\mathbf{n} \times \mathbf{H} \\ \mathbf{n} \times \mathbf{E}\end{array}\right\} \begin{array}{l}\text{continuous across the} \\ \text{air-dielectric interface}\end{array} \tag{2.3c}$$

where $\mathbf{n}$ is the unit vector normal to the applicable surface. Taking the curl of both sides of Eq. (2.2a) and substituting Eq. (2.2b) gives

$$\nabla \times \nabla \times \mathbf{E} = \omega^2\mu_0\,\epsilon\mathbf{E}.$$

Using the vector identity

$$\nabla \times \nabla \times \mathbf{E} = -\nabla_v^2\mathbf{E} + \nabla\,(\nabla \cdot \mathbf{E})$$

and (2.2c) gives the Helmholtz equation [40]

$$\nabla_v^2\,\mathbf{E} + \omega^2\,\mu_0\epsilon\,\mathbf{E} = 0 \tag{2.4a}$$

where ∇_v^2 is the vector Laplacian operator [44]. A similar derivation for $\mathbf{H}$ gives

$$\nabla_v^2\,\mathbf{H} + \omega^2\,\mu_0\,\epsilon\,\mathbf{H} = 0. \tag{2.4b}$$

In rectangular coordinates,

$$\nabla_v^2 = \mathbf{a}_x\nabla^2 + \mathbf{a}_y\,\nabla^2 + \mathbf{a}_z\,\nabla^2$$

where

$$\nabla^2 = \frac{\partial^2}{\partial x^2} + \frac{\partial^2}{\partial y^2} + \frac{\partial^2}{\partial z^2}.$$

Thus

$$\left(\frac{\partial^2}{\partial x^2} + \frac{\partial^2}{\partial y^2} + \frac{\partial^2}{\partial z^2}\right)\Psi = -\omega^2\,\mu_0\,\epsilon\,\Psi \tag{2.5}$$

for $\Psi = E_x, E_y, E_z, H_x, H_y$ or H_z.

Because of the homogeneous nature and rectangular shape of each region in Fig. 4, a separable solution may be presumed to exist [61] for all the fields in the region. The full solution will be a superposition, or linear combination, of particular solutions each of which satisfies Maxwell's equations at all points within the region. The required boundary conditions for the region will be satisfied by the

full solution, but in general may not be satisfied completely by any particular solution. For Ψ representing any of the six field quantities,

$$\Psi\ (x,y,z) = \sum_n a_n\ \Psi_n\ (x,y,z)$$

where the constants a_n must be determined and each particular solution has the form

$$\Psi_n\ (x,y,z) = X_n(x)\ Y_n(y)\ Z_n(z).$$

The vector representation of the particular solution may be expressed as

$$\mathbf{E}_n = \mathbf{a}_x\ E_{x,n} + \mathbf{a}_y\ E_{y,n} + \mathbf{a}_z\ E_{z,n}$$

$$\mathbf{H}_n = \mathbf{a}_x\ H_{x,n} + \mathbf{a}_y\ H_{y,n} + \mathbf{a}_z\ H_{z,n}.$$

Since each particular solution must satisfy Maxwell's equations,

$$\nabla \times \mathbf{E}_n = -j\omega\ \mu_0\ \mathbf{H}_n \tag{2.6a}$$

$$\nabla \times \mathbf{H}_n = j\omega\ \epsilon\ \mathbf{E}_n \tag{2.6b}$$

$$\nabla \cdot \mathbf{E}_n = 0 \tag{2.6c}$$

$$\nabla \cdot \mathbf{H}_n = 0. \tag{2.6d}$$

Also, Eq. (2.5) must hold for all field components of each particular solution, thus $X_n'' Y_n Z_n + X_n Y_n'' Z_n + X_n Y_n Z_n'' = -\omega^2\mu_0\ \epsilon\ X_n Y_n Z_n$ where the double prime superscript denotes the second derivative with respect to the corresponding variable. The time dependence has been stipulated to be harmonic with the form $\exp(j\omega t)$ and is implicit for all fields. Since the product $X_n Y_n Z_n$ cannot be zero if a solution is to exist, $X_n''/X_n + Y_n''/Y_n + Z_n''/Z_n = -\omega^2\mu_0\epsilon$. Since x, y, and z are independent variables, each function must separately equal a constant. With

$$X_n''/X_n = p_n^2 \tag{2.7a}$$

$$Y_n''/Y_n = -k_n^2 \tag{2.7b}$$

$$Z_n''/Z_n = -\beta_n^2 \tag{2.7c}$$

the separation equation is given by

$$\beta_n^2 + k_n^2 - p_n^2 = \omega^2\mu_0\ \epsilon. \tag{2.7d}$$

The general solution for Eq. (2.7c) is

$$Z_n(z) = c_1 \exp\ (j\beta_n z) + c_2 \exp\ (-j\beta_n z).$$

Any propagating mode must have a unique axial dependence. Since propagation has been assumed to be unidirectional in the $+z$ direction, β_n^2 is single valued, $\beta_n^2 = \beta^2$, and because the time dependence is taken as $\exp\ (j\omega t)$, the axial dependence for all fields is $Z(z) = \exp\ (-j\beta z)$. Like the time dependence, the axial dependence will be implicit henceforth for all field quantities. The amplitude will be absorbed into the individual field amplitude term.

The general solution for the differential equation of Eq. (2.7b) is

$$Y_n(y) = c_1 \sin\ (k_n y) + c_2 \cos(k_n y).$$

In a region with height h, the fields E_x, E_z, and H_y must be zero at $y = h/2$ and at $y = -h/2$ by virtue of Eq. (2.3a). Then for $\Psi = E_x$, E_z, or H_y,

$$\Psi|_{y=\pm h/2} = \sum_n X_n(x)\ Y_n(y)|_{y=\pm h/2} = 0$$

which can be true for all x in the region only if Y_n $(y = \pm h/2) = 0$ for all n. Thus,

$$c_1 \sin (k_n h/2) + c_2 \cos (k_n h/2) = 0$$

and

$$-c_1 \sin (k_n h/2) + c_2 \cos (k_n h/2) = 0.$$

Addition and subtraction of these last two equations will show that Y_n (neglecting the amplitude term which will be absorbed into the overall amplitude for Ψ_n) must have one of two forms:

$$Y_n(y) = \cos (k_n y), \text{ with } k_n = (2n + 1)\pi/h \tag{2.8a}$$

or

$$Y_n(y) = \sin (k_n y), \text{ with } k_n = 2n\pi/h \tag{2.8b}$$

for n=0, 1, 2, 3, ... If Maxwell's equations are to hold at all points within the region, then $E_{x,n}$, $E_{z,n}$, and $H_{y,n}$ must have the same y-dependence. Furthermore, $E_{y,n}$, $H_{x,n}$, and $H_{z,n}$ must have the complementary y dependence. If the y-dependence of the nth term of E_x, E_z, and H_y is $\cos [(2n + 1) \pi y/h]$, then the y dependence of the nth term of E_y, H_x , and H_z must be $\sin [(2n + 1) \pi y/h]$; if the y-dependence of the nth term of E_x, E_z, and H_y is $\sin (2n \pi y/h)$, the y-dependence of the nth term of E_y, H_x , and H_z is $\cos (2n \pi y/h)$.

The boundary condition (electric or magnetic wall) at the HPS will determine the type of y-dependence for the fields. For (M,E) and (E,E) solutions, E_x, E_z, and H_y must vanish at $y = 0$. The y-dependence for $E_{x,n}$, $E_{z,n}$, and $H_{y,n}$ is therefore $\sin (2n \pi y/h)$ and that for $E_{y,n}$, $H_{x,n}$, and $H_{z,n}$ is $\cos (2n \pi y/h)$. The (M,M) and (E,M) solutions require E_y, H_x, and H_z to vanish at $y = 0$, thus $E_{x,n}$, $E_{z,n}$, and $H_{y,n}$ must have the y-dependence $\cos [(2n + 1) \pi y/h]$ while $E_{y,n}$, $H_{x,n}$, and $H_{z,n}$ have $\sin [(2n + 1) \pi y/h]$ as their y-dependence.

The general solution to the differential equation of Eq. (2.7a) may be expressed in several forms. For positive values of p_n^2, the solution is normally expressed as

$$X_n(x) = a_{1,n} \cosh p_n x + a_{2,n} \sinh p_n x$$

where $p_n = \sqrt{p_n^2}$. For negative values of p_n^2, the solution is normally expressed as

$$X_n(x) = a_{1,n} \cos (\sqrt{-p_n^2}\, x) + a_{2,n} \sin (\sqrt{-p_n^2}\, x).$$

The solution when p_n^2 equals zero is

$$X_n(x) = a_{1,n} + a_{2,n}\, x.$$

The hyperbolic form may be used for p_n^2 negative or zero if for the former case p_n is taken as imaginary,

$$p_n = \sqrt{p_n^2} = j\sqrt{-p_n^2} \text{ for } p_n^2 < 0.$$

This would result in a complex representation for $X_n(x)$ when p_n^2 is negative since

$$\cosh j|\theta| = \cos |\theta| \qquad \text{(real)}$$

$$\sinh j|\theta| = j \sin |\theta| \qquad \text{(imaginary)}.$$

Such a complex representation may be avoided by expressing the general solution to (2.7a) as

$$X_n(x) = a_{1,n} \cosh (p_n x) + a_{2,n} \sinh (p_n x)/p_n. \tag{2.9}$$

This expression is equivalent to the conventional hyperbolic solution, differing only in the form of the constant of the sinh term. To conform with the known solution when p_n^2 is zero, the limiting definition will be used:

$$\left.\frac{\sinh p_n x}{p_n}\right|_{p_n = 0} = \lim_{p_n \to 0} \frac{\sinh p_n x}{p_n}$$

$$= x \qquad \text{for } p_n^2 = 0.$$

By using Eq. (2.9) to represent the x-dependence of the fields regardless of the value of p_n^2, unnecessary complications in the mathematical notation will be avoided as will the need for imaginary amplitude coefficients. Examination of Eq. (2.9) will show that $X_n(x)$ and all of its derivatives remain real when the amplitude terms are real, regardless of the value of p_n^2 (positive, negative, or zero).

The development of the field expression thus far may be summarized as follows: in each region, the x- and y-dependence of each of the field quantities may be expressed as a series,

$$\Psi\ (x, y) = \sum_n X_n(x)\ Y_n(y).$$

The x-dependence will have the general form

$$X_n(x) = a_n \cosh\ (p_n x) + b_n \sinh\ (p_n x)\ / p_n$$

where the amplitude terms a_n and b_n will differ for the different fields. The value of p_n in each region is determined by the separation equation, with

$$p_n^2 = \beta^2 + k_n^2 - \omega^2 \mu_0 \epsilon$$

and

$$p_n = \sqrt{p_n^2} \text{ for } p_n^2 \geqslant 0$$

$$p_n = j\sqrt{|p_n^2|} \text{ for } p_n^2 < 0.$$

The y-dependence will use a double notation for compactness. The fields E_x, E_z, and H_y will have

$$Y_n(y) = \begin{Bmatrix} \sin \\ \cos \end{Bmatrix} k_n y$$

while the fields E_y, H_x, and H_z will have

$$Y_n(y) = \begin{Bmatrix} \cos \\ \sin \end{Bmatrix} k_n y,$$

where the upper trigonometric function is to be used for (M,E) and (E,E) solutions (an electric wall at $y = 0$) with $k_n = 2n\pi/h$ and h is the waveguide height in the particular region. For (M,M) and (E,M) solutions (a magnetic wall at $y = 0$), the lower trigonometric function is to be used, with $k_n = (2n + 1)\ \pi/h$. The question of limits on the summation in the series representation for the fields will be deferred until a later stage in the analysis development.

The boundary conditions at the horizontal conducting surfaces of the waveguide have been used to formulate the field expressions to this point. The remaining boundary conditions to be satisfied are at the vertical side wall, at the air-dielectric interface, at the plane of the ridge wall, and at the vertical plane of symmetry. Before proceeding to these boundary conditions, it is necessary to consider in more detail the analysis approach and how it will be expected to yield a numerical solution. In Appendix B,

the general solution for the dielectric slab loaded rectangular waveguide is shown to reduce to an eigenvalue problem of the form

$$[M]\begin{bmatrix} \mathbf{E}_x \\ \cdots \\ \mathbf{H}_x \end{bmatrix} = 0$$

where the eigenvectors are the modal coefficients of the x-directed electric and magnetic fields. The field distribution for any mode of the partially dielectric loaded double ridged waveguide may be viewed as a distorted field distribution of the corresponding mode in dielectric slab loaded rectangular waveguide, with the distortion resulting from the presence of the conducting surfaces of the ridges. Therefore for this analysis the approach follows that for the dielectric slab loaded rectangular waveguide.

If the eigenvectors of the eigenvalue problem are to represent the x-directed electric and magnetic fields, it will be necessary to find the relationship between these fields and the orthogonal fields. Maxwell's curl Eqs. (2.2a, 2.2b) may be expanded as

$$-j\omega\,\mu_0\,H_x = \frac{\partial}{\partial y}\,E_z - \frac{\partial}{\partial z}\,E_y \tag{2.10a}$$

$$-j\omega\,\mu_0\,H_y = \frac{\partial}{\partial z}\,E_x - \frac{\partial}{\partial x}\,E_z \tag{2.10b}$$

$$-j\omega\,\mu_0\,H_z = \frac{\partial}{\partial x}\,E_y - \frac{\partial}{\partial y}\,E_x \tag{2.10c}$$

$$j\omega\,\epsilon\,E_x = \frac{\partial}{\partial y}\,H_z - \frac{\partial}{\partial z}\,H_y \tag{2.10d}$$

$$j\omega\,\epsilon\,E_y = \frac{\partial}{\partial z}\,H_x - \frac{\partial}{\partial x}\,H_z \tag{2.10e}$$

$$j\omega\,\epsilon\,E_z = \frac{\partial}{\partial x}\,H_y - \frac{\partial}{\partial y}\,H_x. \tag{2.10f}$$

Since the z-dependence for all fields is implicit as $\exp(-j\beta z)$, the differential operator $\partial/\partial z$ may be replaced by $-j\beta$. Substitution of Eq. (2.10c) into Eq. (2.10e) will yield the relation

$$(\omega^2\mu_0\,\epsilon + \frac{\partial^2}{\partial x^2})\,E_y = \frac{\partial}{\partial x}\,\frac{\partial}{\partial y}\,E_x - \omega\,\mu_0\,\beta\,H_x. \tag{2.11a}$$

In a similar fashion, substitution of Eq. (2.10b) into Eq. (2.10f) will give

$$(\omega^2\mu_0\epsilon + \frac{\partial^2}{\partial x^2})\,E_z = -j\beta\,\frac{\partial}{\partial x}E_x + j\,\omega\,\mu_0\,\frac{\partial}{\partial y}\,H_x, \tag{2.11b}$$

while substitution of Eq. (2.10f) into Eq. (2.10b) gives

$$(\omega^2\mu_0\epsilon + \frac{\partial^2}{\partial x^2})\,H_y = \omega\,\epsilon\,\beta E_x + \frac{\partial}{\partial x}\,\frac{\partial}{\partial y}\,H_x, \tag{2.11c}$$

and substitution of Eq. (2.10e) into Eq. (2.10c) gives

$$(\omega^2\mu_0\epsilon + \frac{\partial^2}{\partial x^2})\,H_z = -j\omega\,\epsilon\,\frac{\partial}{\partial y}\,E_x - j\beta\,\frac{\partial}{\partial x}\,H_x. \tag{2.11d}$$

Since Eq. (2.11) were derived directly from Maxwell's equations, they may used to determine the relationship between fields on a term-by-term basis in the series expansion for the fields.

In Region 1, the conducting sidewall at $x = -x_1$ (Fig. 4) requires E_y, E_z, and H_x to vanish at this plane. This boundary condition may be used to eliminate one of the unknown amplitude coefficients in

the generalized form of the x-dependence for each term in the field expansion. With $\Psi(x, y) = \Sigma_m X_n(x) Y_n(x)$ representing any field, E_y, E_z, or H_x, it is easily shown that each term X_n must be zero at $x = -x_1$ if Ψ is to vanish at all points on the sidewall. Using the generalized form for $X_n(x)$ from (2.9),

$$a_{1,n} \cosh(-p_n x_1) + a_{2,n} \sinh(-p_n x_1)/p_n = 0,$$

thus

$$a_{1,n} = a_{2,n} \frac{\sinh(p_n x_1)}{p_n \cosh(p_n x_1)}.$$

The x-dependence for these fields now becomes

$$X_n(x) = \frac{a_{2,n}}{p_n \cosh(p_n x_1)} \Big[\sinh(p_n x_1) \cosh(p_n x) + \cosh(p_n x_1) \sinh(p_n x)\Big].$$

A new constant may be defined as

$$b_n = a_{2,n}/\cosh(p_n x_1)$$

and the mathematical identity

$$\cosh\theta \sinh\phi + \sinh\theta \cosh\phi = \sinh(\theta + \phi)$$

used to further reduce the x dependence to

$$X_n(x) = b_n \sinh[p_n(x + x_1)]/p_n$$

for the fields E_y, E_z, and H_x. Since Maxwell's equations must be satisfied on a term-by-term basis, and at every point within the region, the x-dependence for the nth modal component of the field E_x, H_y, and H_z must have the form

$$X_n(x) = c_n \cosh[p_n(x + x_1)].$$

The $1/p_n$ term is absorbed into the constant to maintain consistency with the form of Eq. (2.9).

The fields of Region 1 are now expressed as

$$E_x^{(1)} = \sum_n A_{1,n} \cosh[p_{1,n}(x + x_1)] \cdot \begin{Bmatrix}\sin\\ \cos\end{Bmatrix} k_{1,n} y \tag{2.12a}$$

$$E_y^{(1)} = \sum_n B_{1,n} \frac{\sinh[p_{1,n}(x + x_1)]}{p_{1,n}} \cdot \begin{Bmatrix}\cos\\ \sin\end{Bmatrix} k_{1,n} y \tag{2.12b}$$

$$E_z^{(1)} = \sum_n jC_{1,n} \frac{\sinh[p_{1,n}(x + x_1)]}{p_{1,n}} \cdot \begin{Bmatrix}\sin\\ \cos\end{Bmatrix} k_{1,n} y \tag{2.12c}$$

$$H_x^{(1)} = \sum_n D_{1,n} \frac{\sinh[p_{1,n}(x + x_1)]}{p_{1,n}} \cdot \begin{Bmatrix}\cos\\ \sin\end{Bmatrix} k_{1,n} y \tag{2.12d}$$

$$H_y^{(1)} = \sum_n F_{1,n} \cosh[p_{1,n}(x + x_1)] \cdot \begin{Bmatrix}\sin\\ \cos\end{Bmatrix} k_{1,n} y \tag{2.12e}$$

$$H_z^{(1)} = \sum_n jG_{1,n} \cosh[p_{1,n}(x + x_1)] \cdot \begin{Bmatrix}\cos\\ \sin\end{Bmatrix} k_{1,n} y \tag{2.12f}$$

where the extra subscript 1 on the amplitude constants and the constants p_n and k_n, and the extra superscript (1) on the fields are to distinguish these quantities from the corresponding quantities in the other regions. The constant j is included in the expressions for the axial (z-directed) fields to allow the amplitude coefficients to be real, thus avoiding the need for complex arithmetic in the numerical computations. The dual y-dependence notation will avoid much of the notational repetition that otherwise would be necessary for separate derivations to correspond to the two different types of wall conditions (electric or magnetic) at $y = 0$ imposed by symmetry consideration. For (M,E) and (E,E) solutions, the upper trigonometric function is applicable, with

$$k_{1,n} = 2n\pi/b. \tag{2.13a}$$

For (E,M) and (M,M) solutions, the lower trigonometric function is applicable, with

$$k_{1,n} = (2n + 1)\ \pi/b. \tag{2.13b}$$

The separation equation for Region 1 becomes

$$p_{1,n}^2 = \beta^2 + k_{1,n}^2 - \omega^2\mu_0\epsilon_0 \tag{2.13c}$$

and $p_{1,n}$ will be real or imaginary, depending on the sign of $p_{1,n}^2$.

Equations (2.11) may be used on a modal component, or term-by-term, basis with the fields given in Eqs. (2.12) to obtain a relationship between the various amplitude coefficients. Applying Eq. (2.11a) to (2.12) yields

$$\begin{aligned}(\omega^2\mu_0\epsilon_0 + p_{1,n}^2)\ B_{1,n} \sinh\,[p_{1,n}\ (x + x_1)]\,/p_{1,n} \cdot \begin{Bmatrix}\cos\\ \sin\end{Bmatrix} k_{1,n} \\ = (\pm\ k_{1,n})\ p_{1,n}\ A_{1,n} \sinh\,[p_{1,n}\ (x + x_1)] \cdot \begin{Bmatrix}\cos\\ \sin\end{Bmatrix} k_{1,n}\ y \\ - \omega\mu_0\,\beta\ D_{1,n} \sinh\,[p_{1,n}\ (x + x_1)]\,/p_{1,n} \cdot \begin{Bmatrix}\cos\\ \sin\end{Bmatrix} k_{1,n}\ y.\end{aligned} \tag{2.14}$$

The $\pm$ notation on $k_{1,n}$ is the result of the dual notation for the y-dependence; whenever the $\pm$ (or $\mp$) notation is encountered, the upper symbol is to be used for (M,E) or (E,E) solutions while the lower symbol is to be used for (M,M) or (E,M) solutions. The expression $p_{1,n} \sinh\,[p_{1,n}\ (x + x_1)]$ may be replaced by the expression $p_{1,n}^2 \sinh\,[p_{1,n}\ (x + x_1)]\,/p_{1,n}$ for all $p_{1,n}^2$ ($p_{1,n}$ real or imaginary) if the limiting definition is used,

$$\begin{aligned}\left.\frac{\sinh\,[p_{1,n}(x + x_1)]}{p_{1,n}}\right|_{p_{1,n}=0} &= \lim_{p_{1,n}\to 0} \frac{\sinh\,[p_{1,n}\ (x + x_1)]}{p_{1,n}} \\ &= x + x_1.\end{aligned}$$

With this replacement in Eq. (2.14), the relationship between the amplitude coefficients must be

$$(\omega^2\mu_0\epsilon_0 + p_{1,n}^2)\ B_{1,n} = \pm\ k_{1,n}\ p_{1,n}^2\ A_{1,n} - \omega\ \mu_0\,\beta\ D_{1,n}$$

for Eq. (2.14) to hold at all points in the region. From Eq. (2.13c)

$$\omega^2\mu_0\,\epsilon_0 + p_{1,n}^2 = \beta^2 + k_{1,n}^2;$$

thus

$$(\beta^2 + k_{1,n}^2)\ B_{1,n} = \pm\ k_{1,n}\ p_{1,n}^2\ A_{1,n} - \omega\mu_0\,\beta\ D_{1,n}.$$

In a similar fashion, Eqs. (2.11b), (2.11c) and (2.11d) may be used with Eqs. (2.12) to obtain the relationship of the amplitude coefficients of $E_z^{(1)}$, $H_y^{(1)}$, and $H_z^{(1)}$, respectively, with the amplitude coefficients of $E_x^{(1)}$ and $H_x^{(1)}$. The complete results are given by

$$(\beta^2 + k_{1,n}^2)B_{1,n} = \pm\, k_{1,n}\, p_{1,n}^2\, A_{1,n} - \omega\, \mu_0\, \beta\, D_{1,n} \tag{2.15a}$$

$$(\beta^2 + k_{1,n}^2)\, C_{1,n} = -\, \beta\, p_{1,n}^2\, A_{1,n} \mp k_{1,n}\, \omega\, \mu_0\, D_{1,n} \tag{2.15b}$$

$$(\beta^2 + k_{1,n}^2)\, F_{1,n} = \omega\, \epsilon_0\, \beta\, A_{1,n} \mp k_{1,n}\, D_{1,n} \tag{2.15c}$$

$$(\beta^2 + k_{1,n}^2)\, G_{1,n} = \mp\, k_{1,n}\omega\, \epsilon_0\, A_{1,n} - \beta\, D_{1,n}. \tag{2.15d}$$

The relationships expressed in Eq. (2.15) may be reduced to matrix form as

$$\left[\begin{array}{c|c} \psi_1 & 0 \\ \hline 0 & \psi_1 \end{array}\right]\left(\begin{array}{c} \mathbf{C}_1 \\ \hline \mathbf{B}_1 \end{array}\right) = \left[\begin{array}{c|c} -\Phi & \pm K_1 \\ \hline \pm K_1 & \Phi \end{array}\right]\left[\begin{array}{c|c} P_1^2 & 0 \\ \hline 0 & -\omega\, \mu_0\, U \end{array}\right]\left(\begin{array}{c} \mathbf{A}_1 \\ \hline \mathbf{D}_1 \end{array}\right) \tag{2.16}$$

$$\left[\begin{array}{c|c} \psi_1 & 0 \\ \hline 0 & \psi_1 \end{array}\right]\left(\begin{array}{c} \mathbf{F}_1 \\ \hline \mathbf{G}_1 \end{array}\right) = -\left[\begin{array}{c|c} -\Phi & \pm K_1 \\ \hline \pm K_1 & \Phi \end{array}\right]\left[\begin{array}{c|c} \omega\, \epsilon_0\, U & 0 \\ \hline 0 & U \end{array}\right]\left(\begin{array}{c} \mathbf{A}_1 \\ \hline \mathbf{D}_1 \end{array}\right) \tag{2.17}$$

where the vectors $\mathbf{C}_1$, $\mathbf{B}_1$, $\mathbf{F}_1$, $\mathbf{G}_1$, $\mathbf{A}_1$, and $\mathbf{D}_1$ are column vectors having the ordered components $C_{1,n}$, $B_{1,n}$, $F_{1,n}$, $G_{1,n}$, $A_{1,n}$, and $D_{1,n}$, respectively.

The matrices ψ_1, Φ, K_1, and P_1^2 are diagonal matrices with elements

$$\{\psi_1\}_{m,n} = (\beta^2 + k_{1,n}^2)\, \delta_{mn} \tag{2.18a}$$

$$\{\Phi\}_{m,n} = \beta\, \delta_{mn} \tag{2.18b}$$

$$\{K_1\}_{m,n} = k_{1,n}\, \delta_{mn} \tag{2.18c}$$

$$\{P_1^2\}_{m,n} = p_{1,n}^2\, \delta_{mn} \tag{2.18d}$$

where δ_{mn} is the Kronecker delta function

$$\delta_{mn} = 1 \quad \text{for } m = n$$
$$\phantom{\delta_{mn}} = 0 \quad \text{for } m \neq n$$

and U is the unit matrix. Since the question of limits on the summation in the series expansion for the fields has yet to be addressed, no attempt will be made in the analysis to make the index notation of the various vectors and matrices conform with the conventional notation in which the integer indices start at one. Such a departure from convention should not cause confusion in the mathematical treatment of the analysis. When programming a computer to solve for a numerical solution, however, caution must be exercised since most computer routines require the conventional indexing method.

From Eqs. (2.12), it is apparent that for terms where $k_{1,n}$ is zero (encountered only in (M,E) and (E,E) solutions with n equal to zero) the corresponding modal components of $E_y^{(1)}$, $E_z^{(1)}$, and $H_y^{(1)}$ vanish everywhere, and the amplitude coefficients $A_{1,0}$, $C_{1,0}$, and $F_{1,0}$ are therefore meaningless. To maintain a consistent notation, these elements will be carried in the development

when k_n is zero, but strictly as dummy elements not to be included in the final solution. There is further discussion of this issue later in the development of the analysis.

The situation at the waveguide cutoff frequency (where by definition $\beta = 0$) for any mode containing terms with $k_{i,n} = 0$, where $i = 1, 2,$ or 3, in the series expansion for the fields will be referred to as a singular condition. For a singular condition (2.15) losses meaning for $k_{1,n} = 0$ since both sides of each equation are zero. However, Eq. (2.10c) may be applied directly to Eq. (2.12) to give

$$B_{1,0} = \omega\, \mu_0\, G_{1,0} \quad \text{for } \beta = 0,\ k_{1,n} = 0. \tag{2.19}$$

The result of Eq. (2.19) alternatively could be obtained by a limiting definition with Eqs. (2.15a) and (2.15d). With $k_{1,0} = 0$

$$\beta^2\, B_{1,0} = -\,\omega\, \mu_0\, \beta\, D_{1,0}$$

$$\beta^2\, G_{1,0} = -\,\beta\, D_{1,0}.$$

Obviously, $\lim_{\beta \to 0} D_{1,0} = 0$; however,

$$\lim_{\beta \to 0} \frac{B_{1,0}}{G_{1,0}} = \omega\, \mu_0.$$

For the matrix equations of (2.16) and (2.17) to remain valid for the singular condition, the matrices ψ_1 and Φ must be modified as

$$\{\psi\}_{m,n} = (\beta^2 + k_{1,n}^2 + \delta^0)\, \delta_{mn} \tag{2.20}$$

$$\{\Phi\}_{m,n} = (\beta + \delta^0)\, \delta_{mn} \tag{2.21}$$

where

$$\delta^0 = \begin{cases} 1 & \text{for } \beta = 0,\ k_{i,n} = 0 \\ 0 & \text{otherwise.} \end{cases} \tag{2.22}$$

Also, for the singular condition the leading element of the vector $\mathbf{D}_1$ must be $-\,G_{1,0}$ rather than $D_{1,0}$. The modifications to the matrices ψ and Φ will cause (2.16) and (2.17) to give

$$C_{1,0} = -\,p_{1,0}^2\, A_{1,0}$$

$$F_{1,0} = \omega\, \epsilon_0\, A_{1,0}$$

for the singular condition, but the relationship of these three coefficients is meaningless since they are dummy elements.

In Region 3, the development of the x-dependence for the fields is similar to that for Region 1. For (M,E) and (M,M) solutions, the vertical plane of symmetry represents a magnetic wall, thus E_x, H_y, and H_z must vanish at $x = x_3$, and the x-dependence for the modal components of these fields is found to be of the form

$$X_n(x) = c_{3,n} \sinh\, [p_{3,n}(x - x_3)]\, / p_{3,n}. \tag{2.23}$$

For Maxwell's equations to hold for all points in the region, the x-dependence for the modal components of the fields E_y, E_z, and H_x then must have the form

$$X_n(x) = c_{3,n} \cosh\, [p_{3,n}(x - x_3)]. \tag{2.24}$$

For (E,M) and (E,E) solutions, the VPS represents an electric wall, thus E_y, E_z, and H_x must vanish at $x = x_3$. The x-dependence of the fields then reverses from the case for (M,E) and (M,M) solutions, with the x-dependence of the modal components being given by (2.23) for the fields E_y, E_z, and H_x and by (2.24) for the fields E_x, H_y, and H_z.

For (M,E) and (M,M) solutions, the series expansions for the fields of Region 3 then become

$$E_x^{(3)} = \sum_n A_{3,n} \frac{\sinh\,[p_{3,n}(x - x_3)]}{p_{3,n}} \cdot \begin{Bmatrix}\sin\\ \cos\end{Bmatrix} k_{3,n}\, y \tag{2.25a}$$

$$E_y^{(3)} = \sum_n B_{3,n} \cosh\,[p_{3,n}(x - x_3)] \cdot \begin{Bmatrix}\cos\\ \sin\end{Bmatrix} k_{3,n}\, y \tag{2.25b}$$

$$E_z^{(3)} = \sum_n j\, C_{3,n} \cosh\,[p_{3,n}(x - x_3)] \cdot \begin{Bmatrix}\sin\\ \cos\end{Bmatrix} k_{3,n}\, y \tag{2.25c}$$

$$H_x^{(3)} = \sum_n D_{3,n} \cosh\,[p_{3,n}(x - x_3)] \cdot \begin{Bmatrix}\cos\\ \sin\end{Bmatrix} k_{3,n}\, y \tag{2.25d}$$

$$H_y^{(3)} = \sum_n F_{3,n} \frac{\sinh\,[p_{3,n}(x - x_3)]}{p_{3,n}} \cdot \begin{Bmatrix}\sin\\ \cos\end{Bmatrix} k_{3,n}\, y \tag{2.25e}$$

$$H_z^{(3)} = \sum_n j\, G_{3,n} \frac{\sinh\,[p_{3,n}(x - x_3)]}{p_{3,n}} \cdot \begin{Bmatrix}\cos\\ \sin\end{Bmatrix} k_{3,n}\, y \tag{2.25f}$$

while for (E,E) and(E,M) solutions the fields are

$$E_x^{(3)} = \sum_n A_{3,n} \cosh\,[p_{3,n}(x - x_3)] \cdot \begin{Bmatrix}\sin\\ \cos\end{Bmatrix} k_{3,n}\, y \tag{2.26a}$$

$$E_y^{(3)} = \sum_n B_{3,n} \frac{\sinh\,[p_{3,n}(x - x_3)]}{p_{3,n}} \cdot \begin{Bmatrix}\cos\\ \sin\end{Bmatrix} k_{3,n}\, y \tag{2.26b}$$

$$E_z^{(3)} = \sum_n j\, C_{3,n} \frac{\sinh\,[p_{3,n}(x - x_3)]}{p_{3,n}} \cdot \begin{Bmatrix}\sin\\ \cos\end{Bmatrix} k_{3,n}\, y \tag{2.26c}$$

$$H_x^{(3)} = \sum_n D_{3,n} \frac{\sinh\,[p_{3,n}(x - x_3)]}{p_{3,n}} \cdot \begin{Bmatrix}\cos\\ \sin\end{Bmatrix} k_{3,n}\, y \tag{2.26d}$$

$$H_y^{(3)} = \sum_n F_{3,n} \cosh\,[p_{3,n}(x - x_3)] \cdot \begin{Bmatrix}\sin\\ \cos\end{Bmatrix} k_{3,n}\, y \tag{2.26e}$$

$$H_z^{(3)} = \sum_n j\, G_{3,n} \cosh\,[p_{3,n}(x - x_3)] \cdot \begin{Bmatrix}\cos\\ \sin\end{Bmatrix} k_{3,n}\, y. \tag{2.26f}$$

Analogous to the case for Region 1, the upper trigonometric function for the y-dependence is to be used for (M,E) and (E,E) solutions with

$$k_{3,n} = 2n\pi/d \tag{2.27a}$$

while the lower trigonometric function is to be used for (M,M) and (E,M) solutions with

$$k_{3,n} = (2n + 1)\,\pi/d. \tag{2.27b}$$

The separation equation for all solutions is given by

$$p_{3,n}^2 = \beta^2 + k_{3,n}^2 - \omega^2\mu_0\,\epsilon_0\,\epsilon_r \tag{2.27c}$$

where ϵ_r is the relative dielectric constant of the dielectric material.

The relationship between the amplitude coefficients of the modal components in the series expansion for the fields in Region 3 may be found in a manner similar to that of Region 1. For (M,E) and (M,M) solutions, (2.11) is applied to (2.25) on a term-by-term basis, with the results

$$(\beta^2 + k_{3,n}^2)\, C_{3,n} = -\beta\, A_{3,n} \mp k_{3,n}\, \omega\, \mu_0\, D_{3,n} \tag{2.28a}$$

$$(\beta^2 + k_{3,n}^2)\, B_{3,n} = \pm\, k_{3,n}\, A_{3,n} - \omega\, \mu_0\, \beta\, D_{3,n} \tag{2.28b}$$

$$(\beta^2 + k_{3,n}^2)\, F_{3,n} = \omega\, \epsilon_3\, \beta\, A_{3,n} \mp k_{3,n}\, p_{3,n}^2\, D_{3,n} \tag{2.28c}$$

$$(\beta^2 + k_{3,n}^2)\, G_{3,n} = \mp\, k_{3,n}\, \omega\, \epsilon_3\, A_{3,n} - \beta\, p_{3,n}^2\, D_{3,n} \tag{2.28d}$$

where $\epsilon_3 = \epsilon_r \epsilon_0$. For (E,E) and (E,M) solutions , the results of applying Eq. (2.11) to Eq. (2.26) are

$$(\beta^2 + k_{3,n}^2)\, C_{3,n} = -\beta\, p_{3,n}^2\, A_{3,n} \mp k_{3,n}\, \omega\, \mu_0\, D_{3,n} \tag{2.29a}$$

$$(\beta^2 + k_{3,n}^2)\, B_{3,n} = \pm\, k_{3,n}\, p_{3,n}^2\, A_{3,n} - \omega\, \mu_0\, \beta\, D_{3,n} \tag{2.29b}$$

$$(\beta^2 + k_{3,n}^2)\, F_{3,n} = \omega\, \epsilon_3\, \beta\, A_{3,n} \mp k_{3,n}\, D_{3,n} \tag{2.29c}$$

$$(\beta^2 + k_{3,n}^2)\, G_{3,n} = \mp\, k_{3,n}\, \omega\, \epsilon_3\, A_{3,n} - \beta\, D_{3,n}. \tag{2.29d}$$

Expressed in matrix form, Eqs. (2.28) and (2.29) are given by

$$\left[\begin{array}{c|c} \psi_3 & 0 \\ \hline 0 & \psi_3 \end{array}\right] \left(\begin{array}{c} \mathbf{C}_3 \\ \hline \mathbf{B}_3 \end{array}\right) = \left[\begin{array}{c|c} -\Phi & \pm K_3 \\ \hline \pm K_3 & \Phi \end{array}\right] \left[\begin{array}{c|c} W_A & 0 \\ \hline 0 & -\omega\mu_0 U \end{array}\right] \left(\begin{array}{c} \mathbf{A}_3 \\ \hline \mathbf{D}_3 \end{array}\right) \tag{2.30}$$

$$\left[\begin{array}{c|c} \psi_3 & 0 \\ \hline 0 & \psi_3 \end{array}\right] \left(\begin{array}{c} \mathbf{F}_3 \\ \hline \mathbf{G}_3 \end{array}\right) = -\left[\begin{array}{c|c} -\Phi & \pm K_3 \\ \hline \pm K_3 & \Phi \end{array}\right] \left[\begin{array}{c|c} \omega\epsilon_3 U & 0 \\ \hline 0 & W_D \end{array}\right] \left(\begin{array}{c} \mathbf{A}_3 \\ \hline \mathbf{D}_3 \end{array}\right) \tag{2.31}$$

where the vectors $\mathbf{C}_3$, $\mathbf{B}_3$, $\mathbf{F}_3$, $\mathbf{G}_3$, $\mathbf{A}_3$, and $\mathbf{D}_3$ are column vectors, with the elements of $\mathbf{C}_3$ being the ordered amplitude coefficients $C_{3,n}$, etc. The matrices ψ_3, K_3, and P_3^2 are diagonal matrices with elements

$$\{\psi_3\}_{m,n} = (\beta^2 + k_{3,n}^2 + \delta^0)\delta_{mn} \tag{2.32a}$$

$$\{K_3\}_{m,n} = k_{3,n}\delta_{mn} \tag{2.32b}$$

$$\{P_3^2\}_{m,n} = p_{3,n}^2\delta_{mn}. \tag{2.32c}$$

The matrix Φ is the same as for Region 1 and is given by (2.21). The matrices W_A and W_D are also diagonal, and for (M,E) and (M,M) solutions

$$W_A = U \tag{2.33a}$$

$$W_D = P_3^2 \tag{2.33b}$$

while for (E,E) and (E,M) solutions

$$W_A = P_3^2 \tag{2.34a}$$

$$W_D = U. \tag{2.34b}$$

The singular condition ($\delta^0 = 1$) in Region 3 is treated in a manner similar to that for Region 2. For $k_{3,n}$ equal to zero, then in the limit as β becomes small, from Eqs. (2.28)

$$\lim_{\beta \to 0} D_{3,0} = 0$$

$$\lim_{\beta \to 0} \frac{B_{3,0}}{G_{3,0}} = \frac{\omega\mu_0}{p_{3,0}^2}$$

for (M,E) solutions, while for (E,E) solutions, from Eqs. (2.29)

$$\lim_{\beta \to 0} D_{3,0} = 0$$

$$\lim_{\beta \to 0} \frac{B_{3,0}}{G_{3,0}} = \omega\mu_0.$$

Thus, for the matrix equations of Eqs. (2.30) and (2.31) to remain valid, the leading element of the vector $\mathbf{D}_3$ must be replaced as $-G_{3,0}/p_{3,0}^2$ for the singular condition in (M,E) solutions. For the singular condition in (E,E) solutions, the leading element of $\mathbf{D}_3$ must be $-G_{3,0}$. For the singular condition, the coefficients $A_{3,0}$, $C_{3,0}$, and $F_{3,0}$ are dummy coefficients; thus, the relationship between them is immaterial. In (E,M) and (M,M) solutions, the singular condition is not encountered since $k_{i,n}$ is nonzero for all n in each region, $i = 1, 2, 3$.

In Region 2, the x-dependence of each modal component in the series expansion for the fields will retain the general form given in Eq. (2.9) with two unknown amplitude coefficients. The fields of Region 2 are then given by

$$E_x^{(2)} = \sum_n [A_{2,n}^{(+)} \cosh(p_{2,n}x) + A_{2,n}^{(-)} \sinh(p_{2,n}x)/p_{2,n}] \cdot \begin{Bmatrix} \sin \\ \cos \end{Bmatrix} k_{2,n}y \tag{2.35a}$$

$$E_y^{(2)} = \sum_n [B_{2,n}^{(+)} \cosh(p_{2,n}x) + B_{2,n}^{(-)} \sinh(p_{2,n}x)/p_{2,n}] \cdot \begin{Bmatrix} \cos \\ \sin \end{Bmatrix} k_{2,n}y \tag{2.35b}$$

$$E_z^{(2)} = \sum_n j[C_{2,n}^{(+)} \cosh(p_{2,n}x) + C_{2,n}^{(-)} \sinh(p_{2,n}x)/p_{2,n}] \cdot \begin{Bmatrix} \sin \\ \cos \end{Bmatrix} k_{2,n}y \tag{2.35c}$$

$$H_x^{(2)} = \sum_n [D_{2,n}^{(+)} \cosh(p_{2,n}x) + D_{2,n}^{(-)} \sinh(p_{2,n}x)/p_{2,n}] \cdot \begin{Bmatrix} \cos \\ \sin \end{Bmatrix} k_{2,n}y \tag{2.35d}$$

$$H_y^{(2)} = \sum_n [F_{2,n}^{(+)} \cosh(p_{2,n}x) + F_{2,n}^{(-)} \sinh(p_{2,n}x)/p_{2,n}] \cdot \begin{Bmatrix} \sin \\ \cos \end{Bmatrix} k_{2,n}y \tag{2.35e}$$

$$H_z^{(2)} = \sum_n j[G_{2,n}^{(+)} \cosh(p_{2,n}x) + G_{2,n}^{(-)} \sinh(p_{2,n}x)/p_{2,n}] \cdot \begin{Bmatrix} \cos \\ \sin \end{Bmatrix} k_{2,n}y \tag{2.35f}$$

where the upper trigonometric function in the y-dependence is applicable for (M,E) and (E,E) solutions, with

$$k_{2,n} = 2n\pi/b \tag{2.36a}$$

and the lower trigonometric function is applicable for (E,M) and (M,M) solutions, with

$$k_{2,n} = (2n + 1)\pi/b \tag{2.36b}$$

and for all solutions the separation equation for Region 2 becomes

$$p_{2,n}^2 = \beta^2 + k_{2,n}^2 - \omega^2\mu_0\epsilon_2 \tag{2.36c}$$

where $\epsilon_2 = \epsilon_r \epsilon_0$. The superscript notation on the amplitude coefficients in this region is used to distinguish between these (unknown) constants. The choice of the (+) and (−) superscript notation was made to reflect the fact that the cosh (sinh) function may be expressed as the sum (difference) of two exponential functions.

Obtaining a relationship between amplitude coefficients in Region 2 is slightly more complicated than in Regions 1 or 3 because of the presence of both sinh and cosh terms in the x-dependence of each modal component in the series expansion of the fields. Upon application of Eqs. (2.11a) to (2.35) on a modal component, or term-by-term, basis

$$\psi_{2,n}[B_{2,n}^{(+)} \cosh(p_{2,n}x) + B_{2,n}^{(-)} \sinh(p_{2,n}x)/p_{2,n}] \cdot \begin{Bmatrix}\cos\\ \sin\end{Bmatrix} k_{2,n}y$$

$$= (\pm k_{2,n}p_{2,n})[A_{2,n}^{(+)} \sinh(p_{2,n}x) + A_{2,n}^{(-)} \cosh(p_{2,n}x)/p_{2,n}] \cdot \begin{Bmatrix}\cos\\ \sin\end{Bmatrix} k_{2,n}y$$

$$- \omega\mu_0\beta[D_{2,n}^{(+)} \cosh(p_{2,n}x) + D_2^{(-)} \sinh(p_{2,n}x)/p_{2,n}] \cdot \begin{Bmatrix}\cos\\ \sin\end{Bmatrix} k_{2,n}y \tag{2.37}$$

where

$$\psi_{2,n} = \omega^2\mu_0\epsilon_2 - p_{2,n}^2$$
$$= \beta^2 + k_{2,n}^2.$$

The function $p_{2,n} \sinh(p_{2,n}x)$ may be expressed as $p_{2,n}^2 \sinh(p_{2,n}x)/p_{2,n}$, and the function $p_{2,n} \cosh(p_{n,}x)/p_{2,n}$ expressed as $\cosh(p_{2,n}x)$, if the limiting definitions are used for $p_{2,n}$ equal to zero. Since Eq. (2.37) must hold for all points within the region, the coefficients of the cosh and sinh terms may be collected separately, with the results

$$(\beta^2 + k_{2,n}^2)B_{2,n}^{(+)} = \pm k_{2,n}A_{2,n}^{(-)} - \omega\mu_0\beta D_{2,n}^{(+)} \tag{2.38a}$$

$$(\beta^2 + k_{2,n}^2)B_{2,n}^{(-)} = \pm k_{2,n}p_{2,n}^2A_{2,n}^{(+)} - \omega\mu_0\beta D_{2,n}^{(-)}. \tag{2.38b}$$

In a similar fashion, the remaining equations of Eqs. (2.11) may be used with Eqs. (2.35) to give

$$(\beta^2 + k_{2,n}^2)C_{2,n}^{(+)} = -\beta A_{2,n}^{(-)} \mp k_{2,n}\omega\mu_0 D_{2,n}^{(+)} \tag{2.38c}$$

$$(\beta^2 + k_{2,n}^2)C_{2,n}^{(-)} = -\beta p_{2,n}^2 A_{2,n}^{(+)} \mp k_{2,n}\omega\mu_0 D_{2,n}^{(-)} \tag{2.38d}$$

$$(\beta^2 + k_{2,n}^2)F_{2,n}^{(+)} = \omega\epsilon_2\beta A_{2,n}^{(+)} \mp k_{2,n} D_{2,n}^{(-)} \tag{2.38e}$$

$$(\beta^2 + k_{2,n}^2)F_{2,n}^{(-)} = \omega\epsilon_2\beta A_{2,n}^{(-)} \mp k_{2,n}p_{2,n}^2 D_{2,n}^{(+)} \tag{2.38f}$$

$$(\beta^2 + k_{2,n}^2)G_{2,n}^{(+)} = \mp k_{2,n}\omega\epsilon_2 A_{2,n}^{(+)} - \beta D_{2,n}^{(-)} \tag{2.38g}$$

$$(\beta^2 + k_{2,n}^2)G_{2,n}^{(-)} = \mp k_{2,n}\omega\epsilon_2 A_{2,n}^{(-)} - \beta p_{2,n}^2 D_{2,n}^{(+)}. \tag{2.38h}$$

As for the case in Regions 1 and 3, the dual sign notation associated with the $k_{2,n}$ term arises as a consequence of the dual notation in the trigonometric representation for the y-dependence of the various modal components. For (M,E) and (E,E) solutions the upper sign is applicable, while the lower sign is applicable for (E,M) and (M,M) solutions.

The equations of (2.38) may be expressed in matrix form as

$$\left[\begin{array}{c|c} \psi_2 & 0 \\ \hline 0 & \psi_2 \end{array}\right] \left\{\begin{array}{c} \mathbf{C}_2^{(+)} \\ \hline \mathbf{B}_2^{(+)} \end{array}\right\} = \left[\begin{array}{c|c} -\Phi & \pm K_2 \\ \hline \pm K_2 & \Phi \end{array}\right] \left[\begin{array}{c|c} U & 0 \\ \hline 0 & -\omega\mu_0 U \end{array}\right] \left\{\begin{array}{c} \mathbf{A}_2^{(-)} \\ \hline \mathbf{D}_2^{(+)} \end{array}\right\} \tag{2.39}$$

$$\left[\begin{array}{c|c} \psi_2 & 0 \\ \hline 0 & \psi_2 \end{array}\right]\left(\begin{array}{c} \mathbf{C}_2^{(-)} \\ \hline \mathbf{B}_2^{(-)} \end{array}\right) = \left[\begin{array}{c|c} -\Phi & \pm K_2 \\ \hline \pm K_2 & \Phi \end{array}\right]\left[\begin{array}{c|c} P_2^2 & 0 \\ \hline 0 & -\omega\mu_0 U \end{array}\right]\left(\begin{array}{c} \mathbf{A}_2^{(+)} \\ \hline \mathbf{D}_2^{(-)} \end{array}\right) \tag{2.40}$$

$$\left[\begin{array}{c|c} \psi_2 & 0 \\ \hline 0 & \psi_2 \end{array}\right]\left(\begin{array}{c} \mathbf{F}_2^{(+)} \\ \hline \mathbf{G}_2^{(+)} \end{array}\right) = -\left[\begin{array}{c|c} -\Phi & \pm K_2 \\ \hline \pm K_2 & \Phi \end{array}\right]\left[\begin{array}{c|c} \omega\epsilon_2 U & 0 \\ \hline 0 & U \end{array}\right]\left(\begin{array}{c} \mathbf{A}_2^{(+)} \\ \hline \mathbf{D}_2^{(-)} \end{array}\right) \tag{2.41}$$

$$\left[\begin{array}{c|c} \psi_2 & 0 \\ \hline 0 & \psi_2 \end{array}\right]\left(\begin{array}{c} \mathbf{F}_2^{(-)} \\ \hline \mathbf{G}_2^{(-)} \end{array}\right) = -\left[\begin{array}{c|c} -\Phi & \pm K_2 \\ \hline \pm K_2 & \Phi \end{array}\right]\left[\begin{array}{c|c} \omega\epsilon_2 U & 0 \\ \hline 0 & P_2^2 \end{array}\right]\left(\begin{array}{c} \mathbf{A}_2^{(-)} \\ \hline \mathbf{D}_2^{(+)} \end{array}\right) \tag{2.42}$$

where the vectors are column vectors with each having elements corresponding to the ordered terms of the respective amplitude coefficients. The matrices ψ_2, K_2, and P_2^2 are diagonal matrices whose elements are

$$\{\psi_2\}_{m,n} = \left(\beta^2 + k_{2,n}^2 + \delta^0\right)\delta_{mn} \tag{2.43a}$$

$$\{K_2\}_{m,n} = k_{2,n}\delta_{mn} \tag{2.43b}$$

$$\{P_2^2\}_{m,n} = p_{2,n}^2\delta_{mn}. \tag{2.43c}$$

The matrix Φ is given by Eq. (2.21). The treatment of the singular condition in Region 2 is similar to that for Regions 1 and 3. From Eqs. (2.38)

$$\lim_{\beta\to 0} D_{2,0}^{(+)} = 0$$

$$\lim_{\beta\to 0} D_{2,0}^{(-)} = 0$$

$$\lim_{\beta\to 0} \frac{B_{2,0}^{(+)}}{G_{2,0}^{(-)}} = \frac{\omega\mu_0}{p_{2,0}^2}$$

$$\lim_{\beta\to 0} \frac{B_{2,0}^{(-)}}{G_{2,0}^{(+)}} = \omega\mu_0$$

for $k_{2,0} = 0$. Thus, the leading elements of the vectors $\mathbf{D}_2^{(+)}$ and $\mathbf{D}_2^{(-)}$ must be changed from $D_{2,0}^{(+)}$ and $D_{2,0}^{(-)}$ to $-G_{2,0}^{(-)}/p_{2,0}^2$ and $-G_{2,0}^{(+)}$, respectively, for the singular condition if the matrix equations of (2.39)-(2.42) are to remain valid. Analogous to the case in Regions 1 and 3, the amplitude coefficients $A_{2,0}^{(+)}$, $A_{2,0}^{(-)}$, $C_{2,0}^{(+)}$, $C_{2,0}^{(-)}$, $F_{2,0}^{(+)}$, and $F_{2,0}^{(-)}$ are dummy coefficients for the singular condition and the resulting relationships of these terms are immaterial.

In each region i, with $i = 1, 2, 3$, the matrix notation may be condensed somewhat with the following representation:

$$\Psi_i = \left[\begin{array}{c|c} \psi_i & 0 \\ \hline 0 & \psi_i \end{array}\right] \tag{2.44}$$

$$\Lambda_i = \left[\begin{array}{c|c} -\Phi & \pm K_i \\ \hline \pm K_i & \Phi \end{array}\right] \tag{2.45}$$

Simple matrix multiplication will show

$$\Lambda_i \Lambda_i = \Psi_i. \quad \text{for } i = 1, 2, 3. \tag{2.46}$$

It is apparent that Λ_i and Ψ_i each possess an inverse, with

$$\Lambda_i^{-1} = \Psi_i^{-1} \Lambda_i. \tag{2.47}$$

The need for the special treatment of the singular condition is obvious if inverse operations are to be made with these matrices.

While matrices in general do not commute, diagonal matrices do commute [62,63]. Thus, the matrix Ψ_i and its inverse Ψ_i^{-1} will commute with any matrix of the form $\left[\begin{array}{c|c} \phi_1 & \phi_2 \\ \hline \phi_3 & \phi_4 \end{array}\right]$ where each of the ϕ submatrices is a diagonal matrix (hence all are square matrices of the same size), and the matrix Λ_i will commute with any matrix of the form $\left[\begin{array}{c|c} \Gamma & 0 \\ \hline 0 & \Gamma \end{array}\right]$ where each submatrix Γ is diagonal, as may be shown by simple matrix manipulation. These commutation properties will be used in later stages of the analysis without further comment as to the validity of the commutation operation.

In each of the three regions for the waveguide analysis, the y-dependence functions $\sin k_{i,n} y$ and $\cos k_{i,n} y$ may be considered the basis functions for the series expansion of the fields [46,47,51]. These basis functions are orthogonal on the interval $-h/2 \leqslant y \leqslant h/2$, where h is the height of the particular region. For (E,M) and (M,M) solutions, with $k_{i,n} = (2n+1)\pi/h$

$$\int_{-h/2}^{h/2} \sin(k_{i,n} y) \sin(k_{i,m} y)\, dy = \begin{cases} 0 \text{ for } n \neq m \\ h/2 \text{ for } n = m \end{cases} \tag{2.48a}$$

$$\int_{-h/2}^{h/2} \cos(k_{i,n} y) \cos(k_{i,m} y)\, dy = \begin{cases} 0 \text{ for } n \neq m \\ h/2 \text{ for } n = m \end{cases} \tag{2.48b}$$

$$\int_{-h/2}^{h/2} \sin(k_{i,n} y) \cos(k_{i,m} y)\, dy = 0 \text{ for all } n, m. \tag{2.48c}$$

For (M,E) and (E,E) solutions, $k_{i,n}$ has the form $k_{i,n} = 2n\pi/h$, and the orthogonality of the basis functions is the same as for (E,M) and (M,M) solutions with the exception of n and m both equal to zero:

$$\int_{-h/2}^{h/2} \sin(k_{i,n} y) \sin(k_{i,m} y)\, dy = 0 \text{ for } n = m = 0 \tag{2.48d}$$

$$\int_{-h/2}^{h/2} \cos(k_{i,n} y) \cos(k_{i,m} y)\, dy = h \text{ for } n = m = 0. \tag{2.48e}$$

The interface between Regions 1 and 2 is the air-dielectric boundary at $x = -x_2$. The tangential components of the electric and magnetic fields must be continuous at this interface, thus

$$E_y^{(2)}\Big|_{x=-x_2} = E_y^{(1)}\Big|_{x=-x_2} \tag{2.49a}$$

$$E_z^{(2)}\Big|_{x=-x_2} = E_z^{(1)}\Big|_{x=-x_2} \tag{2.49b}$$

$$H_y^{(2)}\Big|_{x=-x_2} = H_y^{(1)}\Big|_{x=-x_2} \tag{2.49c}$$

$$H_z^{(2)}\Big|_{x=-x_2} = H_z^{(1)}\Big|_{x=-x_2}. \tag{2.49d}$$

For any given waveguide mode, symmetry considerations require the same effective wall type (electric or magnetic) for all regions at the HPS, $y = 0$. Since Region 1 and Region 2 each have a height b, $k_{1,n} = k_{2,n}$ for all n and all modes. The result of applying an integral operator $\int f(\xi)d\xi$ to a function $g(\xi)$ will be defined as $\int f(\xi)g(\xi)d\xi$, where any integration limits on the integral operator will reflect as limits in the resultant integral. The series expansions for the various fields may be substituted into Eq. (2.49). Subsequent application of the appropriate integral operator, either $\int_{-b/2}^{b/2} \sin(k_{1,m}y)dy$ or $\int_{-b/2}^{b/2} \cos(k_{1,m}y)dy$, dependent on the form of the basis functions for the particular field, to both sides of the equations will show that the equalities of (2.49) are valid on a modal component, or term-by-term basis. Thus,

$$B_{1,n} \sinh[p_{1,n}(x_1 - x_2)]/p_{1,n} = B_{2,n}^{(+)} \cosh(p_{2,n}x_2) - B_{2,n}^{(-)} \sinh(p_{2,n}x_2)/p_{2,n} \tag{2.50a}$$

$$C_{1,n} \sinh[p_{1,n}(x_1 - x_2)]/p_{1,n} = C_{2,n}^{(+)} \cosh(p_{2,n}x_2) - C_{2,n}^{(-)} \sinh(p_{2,n}x_2)/p_{2,n} \tag{2.50b}$$

$$F_{1,n} \cosh[p_{1,n}(x_1 - x_2)] = F_{2,n}^{(+)} \cosh(p_{2,n}x_2) - F_{2,n}^{(-)} \sinh(p_{2,n}x_2)/p_{2,n} \tag{2.50c}$$

$$G_{1,n} \cosh[p_{1,n}(x_1 - x_2)] = G_{2,n}^{(+)} \cosh(p_{2,n}x_2) - G_{2,n}^{(-)} \sinh(p_{2,n}x_2)/p_{2,n} \tag{2.50d}$$

where the y-dependence has been eliminated by virtue of the orthogonality of the basis functions. The relationships of Eqs. (2.50) may be expressed in matrix form as

$$\left[\begin{array}{c|c} \theta_1^{(E)} & 0 \\ \hline 0 & \theta_1^{(E)} \end{array}\right]\left(\begin{array}{c} \mathbf{C}_1 \\ \hline \mathbf{B}_1 \end{array}\right) = \left[\begin{array}{c|c} \theta_2^{(+)} & 0 \\ \hline 0 & \theta_2^{(+)} \end{array}\right]\left(\begin{array}{c} \mathbf{C}_2^{(+)} \\ \hline \mathbf{B}_2^{(+)} \end{array}\right) - \left[\begin{array}{c|c} \theta_2^{(-)} & 0 \\ \hline 0 & \theta_2^{(-)} \end{array}\right]\left(\begin{array}{c} \mathbf{C}_2^{(-)} \\ \hline \mathbf{B}_2^{(-)} \end{array}\right) \tag{2.51}$$

$$\left[\begin{array}{c|c} \theta_1^{(H)} & 0 \\ \hline 0 & \theta_1^{(H)} \end{array}\right]\left(\begin{array}{c} \mathbf{F}_1 \\ \hline \mathbf{G}_1 \end{array}\right) = \left[\begin{array}{c|c} \theta_2^{(+)} & 0 \\ \hline 0 & \theta_2^{(+)} \end{array}\right]\left(\begin{array}{c} \mathbf{F}_2^{(+)} \\ \hline \mathbf{G}_2^{(+)} \end{array}\right) - \left[\begin{array}{c|c} \theta_2^{(-)} & 0 \\ \hline 0 & \theta_2^{(-)} \end{array}\right]\left(\begin{array}{c} \mathbf{F}_2^{(-)} \\ \hline \mathbf{G}_2^{(-)} \end{array}\right) \tag{2.52}$$

where each of the θ matrices is diagonal with

$$\{\theta_1^{(E)}\}_{m,n} = \sinh[p_{1,n}(x_1 - x_2)]/p_{1,n}\delta_{mn} \tag{2.53a}$$

$$\{\theta_1^{(H)}\}_{m,n} = \cosh[p_{1,n}(x_1 - x_2)]\delta_{mn} \tag{2.53b}$$

$$\{\theta_2^{(+)}\}_{m,n} = \cosh(p_{2,n}x_2)\delta_{mn} \tag{2.54a}$$

$$\{\theta_2^{(-)}\}_{m,n} = \sinh(p_{2,n}x_2)/p_{2,n}\delta_{mn}. \tag{2.54b}$$

Further compactness for the matrix notation may be obtained by defining new matrices for the doubled θ matrices:

$$\Theta_1^{(E)} = \left[\begin{array}{c|c} \theta_1^{(E)} & 0 \\ \hline 0 & \theta_1^{(E)} \end{array}\right] \tag{2.55a}$$

$$\Theta_1^{(H)} = \left[\begin{array}{c|c} \theta_1^{(H)} & 0 \\ \hline 0 & \theta_1^{(H)} \end{array}\right] \tag{2.55b}$$

$$\Theta_2^{(+)} = \left[\begin{array}{c|c} \theta_2^{(+)} & 0 \\ \hline 0 & \theta_2^{(+)} \end{array}\right] \tag{2.55c}$$

$$\Theta_2^{(-)} = \left[\begin{array}{c|c} \theta_2^{(-)} & 0 \\ \hline 0 & \theta_2^{(-)} \end{array}\right]. \tag{2.55d}$$

Premultiplication of Eq. (2.51) by the matrix

$$\Theta_1^{(H)} \left[\begin{array}{c|c} \omega\epsilon_0 U & 0 \\ \hline 0 & U \end{array}\right] \Lambda_1$$

gives

$$\Theta_1^{(H)} \left[\begin{array}{c|c} \omega\epsilon_0 U & 0 \\ \hline 0 & U \end{array}\right] \Lambda_1 \Theta_1^{(E)} \left(\begin{array}{c} \mathbf{C}_1 \\ \hline \mathbf{B}_1 \end{array}\right) = \Theta_1^{(H)} \left[\begin{array}{c|c} \omega\epsilon_0 U & 0 \\ \hline 0 & U \end{array}\right] \Lambda_1 \left[\Theta_2^{(+)} \left(\begin{array}{c} \mathbf{C}_2^{(+)} \\ \hline \mathbf{B}_2^{(+)} \end{array}\right) - \Theta_2^{(-)} \left(\begin{array}{c} \mathbf{C}_2^{(-)} \\ \hline \mathbf{B}_2^{(-)} \end{array}\right)\right] \tag{2.56}$$

while Eq. (2.52) may be premultiplied by the matrix expression

$$-\Theta_1^{(E)} \left[\begin{array}{c|c} P_1^2 & 0 \\ \hline 0 & -\omega\mu_0 U \end{array}\right] \Lambda_1$$

to give

$$-\Theta_1^{(E)} \left[\begin{array}{c|c} P_1^2 & 0 \\ \hline 0 & -\omega\mu_0 U \end{array}\right] \Lambda_1 \Theta_1^{(H)} \left(\begin{array}{c} \mathbf{F}_1 \\ \hline \mathbf{G}_1 \end{array}\right)$$

$$= -\Theta_1^{(E)} \left[\begin{array}{c|c} P_1^2 & 0 \\ \hline 0 & -\omega\mu_0 U \end{array}\right] \Lambda_1 \left[\Theta_2^{(+)} \left(\begin{array}{c} \mathbf{F}_2^{(+)} \\ \hline \mathbf{G}_2^{(+)} \end{array}\right) - \Theta_2^{(-)} \left(\begin{array}{c} \mathbf{F}_2^{(-)} \\ \hline \mathbf{G}_2^{(-)} \end{array}\right)\right]. \tag{2.57}$$

But from Eqs. (2.16) and (2.47)

$$\Lambda_1 \left(\begin{array}{c} \mathbf{C}_1 \\ \hline \mathbf{B}_1 \end{array}\right) = \left[\begin{array}{c|c} P_1^2 & 0 \\ \hline 0 & -\omega\mu_0 U \end{array}\right] \left(\begin{array}{c} \mathbf{A}_1 \\ \hline \mathbf{D}_1 \end{array}\right) \tag{2.58}$$

while from Eqs. (2.17) and (2.47)

$$-\Lambda_1 \left(\begin{array}{c} \mathbf{F}_1 \\ \hline \mathbf{G}_1 \end{array}\right) = \left[\begin{array}{c|c} \omega\epsilon_0 U & 0 \\ \hline 0 & U \end{array}\right] \left(\begin{array}{c} \mathbf{A}_1 \\ \hline \mathbf{D}_1 \end{array}\right). \tag{2.59}$$

The commutation properties of the matrices may then be used to show that the left-hand sides of (2.56) and (2.57) are both equal to

$$\Theta_1^{(E)} \Theta_1^{(H)} \left[\begin{array}{c|c} \omega\epsilon_0 P_1^2 & 0 \\ \hline 0 & -\omega\mu_0 U \end{array}\right] \left(\begin{array}{c} \mathbf{A}_1 \\ \hline \mathbf{D}_1 \end{array}\right),$$

thus the right-hand sides of these two equations may be set equal. Substituting from Eqs. (2.39) to (2.42), the results are

$$\Theta_1^{(H)}\left[\begin{array}{c|c} \omega\epsilon_0 U & 0 \\ \hline 0 & U \end{array}\right]\Lambda_1\left\{\Theta_2^{(+)}\Psi_2^{-1}\Lambda_2\left[\begin{array}{c|c} U & 0 \\ \hline 0 & -\omega\mu_0 U \end{array}\right]\left[\begin{array}{c} \mathbf{A}_2^{(-)} \\ \hline \mathbf{D}_2^{(+)} \end{array}\right]\right.$$

$$\left.-\Theta_2^{(-)}\Psi_2^{-1}\Lambda_2\left[\begin{array}{c|c} P_2^2 & 0 \\ \hline 0 & -\omega\mu_0 U \end{array}\right]\left[\begin{array}{c} \mathbf{A}_2^{(+)} \\ \hline \mathbf{D}_2^{(-)} \end{array}\right]\right\}$$

$$= -\Theta_1^{(E)}\left[\begin{array}{c|c} P_1^2 & 0 \\ \hline 0 & -\omega\mu_0 U \end{array}\right]\Lambda_1\left\{-\Theta_2^{(+)}\Psi_2^{-1}\Lambda_2\left[\begin{array}{c|c} \omega\epsilon_2 U & 0 \\ \hline 0 & U \end{array}\right]\left[\begin{array}{c} \mathbf{A}_2^{(+)} \\ \hline \mathbf{D}_2^{(-)} \end{array}\right]\right.$$

$$\left.+\Theta_2^{(-)}\Psi_2^{-1}\Lambda_2\left[\begin{array}{c|c} \omega\epsilon_2 U & 0 \\ \hline 0 & P_2^2 \end{array}\right]\left[\begin{array}{c} \mathbf{A}_2^{(-)} \\ \hline \mathbf{D}_2^{(+)} \end{array}\right]\right\}. \tag{2.60}$$

The matrix Λ_1 commutes with the matrices $\Theta_2^{(+)}$ and $\Theta_2^{(-)}$, and since $\Lambda_1 = \Lambda_2$

$$\Lambda_1\Psi_2^{-1}\Lambda_2 = U.$$

With both sides of Eq. (2.60) premultiplied by

$$\left[\begin{array}{c|c} \omega\epsilon_0 U & 0 \\ \hline 0 & -\omega\mu_0 U \end{array}\right]^{-1}$$

collection of like terms will then give

$$\left\{\Theta_1^{(H)}\Theta_2^{(+)} + \left[\begin{array}{c|c} \epsilon_r P_1^2 & 0 \\ \hline 0 & P_2^2 \end{array}\right]\Theta_1^{(E)}\Theta_2^{(-)}\right\}\left[\begin{array}{c} \mathbf{A}_2^{(-)} \\ \hline \mathbf{D}_2^{(+)} \end{array}\right]$$

$$= \left\{\left[\begin{array}{c|c} \epsilon_r P_1^2 & 0 \\ \hline 0 & U \end{array}\right]\Theta_1^{(E)}\Theta_2^{(+)} + \left[\begin{array}{c|c} P_2^2 & 0 \\ \hline 0 & U \end{array}\right]\Theta_1^{(H)}\Theta_2^{(-)}\right\}\left[\begin{array}{c} \mathbf{A}_2^{(+)} \\ \hline \mathbf{D}_2^{(-)} \end{array}\right] \tag{2.61a}$$

The results of Eq. (2.61a) may be expressed as

$$Q_A^{(+)}\mathbf{A}_2^{(+)} = Q_A^{(-)}\mathbf{A}_2^{(-)} \tag{2.61b}$$

$$Q_D^{(+)}\mathbf{D}_2^{(+)} = Q_D^{(-)}\mathbf{D}_2^{(-)} \tag{2.61c}$$

where the diagonal Q matrices are given by

$$Q_A^{(+)} = \epsilon_r P_1^2 \theta_1^{(E)} \theta_2^{(+)} + P_2^2 \theta_1^{(H)} \theta_2^{(-)} \tag{2.62a}$$

$$Q_A^{(-)} = \epsilon_r P_1^2 \theta_1^{(E)} \theta_2^{(-)} + \theta_1^{(H)} \theta_2^{(+)} \tag{2.62b}$$

$$Q_D^{(+)} = \theta_1^{(H)} \theta_2^{(+)} + P_2^2 \theta_1^{(E)} \theta_2^{(-)} \tag{2.62c}$$

$$Q_D^{(-)} = \theta_1^{(E)} \theta_2^{(+)} + \theta_1^{(H)} \theta_2^{(-)}. \tag{2.62d}$$

With this Q matrix notation

$$\left[\begin{array}{c|c} Q_A^{(+)} & 0 \\ \hline 0 & Q_D^{(-)} \end{array}\right] \left(\begin{array}{c} \mathbf{A}_2^{(+)} \\ \hline \mathbf{D}_2^{(-)} \end{array}\right) = \left[\begin{array}{c|c} Q_A^{(-)} & 0 \\ \hline 0 & Q_D^{(+)} \end{array}\right] \left(\begin{array}{c} \mathbf{A}_2^{(-)} \\ \hline \mathbf{D}_2^{(+)} \end{array}\right). \tag{2.63}$$

The remaining boundary conditions to be satisfied are at the interface between Regions 2 and 3. This interface is the plane of the ridge wall, $x = 0$. Continuity of tangential magnetic field requires

$$H_y^{(2)}\Big|_{x=0} = H_y^{(3)}\Big|_{x=0} \tag{2.64a}$$

$$H_z^{(2)}\Big|_{x=0} = H_z^{(3)}\Big|_{x=0} \tag{2.64b}$$

for all $y \in \{Y_1\}$, where

$$\{Y_1\} = \{-d/2 \leqslant y \leqslant d/2\}.$$

The tangential electric field must also be continuous at this interface. In addition, the tangential electric field of Region 2 must vanish on the conducting surface of the ridge walls, thus

$$E_y^{(2)}|_{x=0} = \begin{cases} E_y^{(3)}|_{x=0} \text{ for } y \in \{Y_1\} \\ 0 \text{ for } x = 0,\ y \in \{Y_2\} \end{cases} \tag{2.65a}$$

$$E_z^{(2)}|_{x=0} = \begin{cases} E_z^{(3)}|_{x=0} \text{ for } y \in \{Y_1\} \\ 0 \text{ for } x = 0,\ y \in \{Y_2\} \end{cases} \tag{2.65b}$$

where

$$\{Y_2\} = \{-b/2 \leqslant y \leqslant -d/2,\ d/2 \leqslant y \leqslant b/2\}.$$

The requirements of Eqs. (2.65) ensure the condition that $H_x^{(2)}$ will also vanish on the surface $x = 0$, $y \in \{Y_2\}$ since $H_x^{(2)}$ may be expressed in terms of $E_y^{(2)}$ and $H_z^{(2)}$ by means of Maxwell's curl equation (2.2a).

It is apparent that an infinite number of terms must be used in the series expansion for the fields if the requirements of Eqs. (2.64) and (2.65) are to be completely fulfilled. If a numerical solution is to be obtained, the series must be truncated to some finite number of terms. The resulting error in the solution will depend on the number of terms used in the numerical calculations and on the convergence properties of the solution, i.e., how rapidly the solution converges with an increasing number of terms. The convergence properties will be discussed at a later stage of the analysis, and it will be shown that

accuracies of better than 1% may be obtained with as few as five or six terms in the series expansion for the fields.

At $x = 0$, the tangential field components in Region 2 reduce to

$$E_y^{(2)}|_{x=0} = \sum_{n=0}^{N_2} B_{2,n}^{(+)} \begin{Bmatrix}\cos\\ \sin\end{Bmatrix} k_{2,n}y$$

$$E_z^{(2)}|_{x=0} = j \sum_{n=0}^{N_2} C_{2,n}^{(+)} \begin{Bmatrix}\sin\\ \cos\end{Bmatrix} k_{2,n}y$$

$$H_y^{(2)}|_{x=0} = \sum_{n=0}^{N_2} F_{2,n}^{(+)} \begin{Bmatrix}\sin\\ \cos\end{Bmatrix} k_{2,n}y$$

$$H_z^{(2)}|_{x=0} = j \sum_{n=0}^{N_2} G_{2,n}^{(+)} \begin{Bmatrix}\cos\\ \sin\end{Bmatrix} k_{2,n}y$$

where the number of terms in the series expansion for the fields has been truncated to N_T terms, with

$$N_T = N_2 + 1.$$

In Region 3, the tangential fields at $x = 0$ are given by

$$E_y^{(3)}|_{x=0} = \sum_{n=0}^{N_2} \theta_{3,n}^{(E)} B_{3,n} \begin{Bmatrix}\cos\\ \sin\end{Bmatrix} k_{3,n}y$$

$$E_z^{(3)}|_{x=0} = j \sum_{n=0}^{N_2} \theta_{3,n}^{(E)} C_{3,n} \begin{Bmatrix}\sin\\ \cos\end{Bmatrix} k_{3,n}y$$

$$H_y^{(3)}|_{x=0} = \sum_{n=0}^{N_2} \theta_{3,n}^{(H)} F_{3,n} \begin{Bmatrix}\sin\\ \cos\end{Bmatrix} k_{3,n}y$$

$$H_z^{(3)}|_{x=0} = j \sum_{n=0}^{N_2} \theta_{3,n}^{(H)} G_{3,n} \begin{Bmatrix}\cos\\ \sin\end{Bmatrix} k_{3,n}y$$

where for (M,E) and (M,M) solutions

$$\theta_{3,n}^{(E)} = \cosh\,(p_{3,n}x_3) \tag{2.66a}$$

$$\theta_{3,n}^{(H)} = -\sinh\,(p_{3,n}x_3)/p_{3,n} \tag{2.66b}$$

while for (E,E) and (E,M) solutions

$$\theta_{3,n}^{(E)} = -\sinh\,(p_{3,n}x_3)/p_{3,n} \tag{2.67a}$$

$$\theta_{3,n}^{(H)} = \cosh\,(p_{3,n}x_3). \tag{2.67b}$$

Note that it is not necessary to truncate the number of terms for the series expansion of the fields in Region 3 to the same number of terms used in Regions 1 and 2. For this analysis, however, the fields in all regions will use the same number of terms in the series expansion to obtain numerical solutions.

To proceed further with the boundary conditions of Eqs. (2.64) and (2.65), it is necessary to distinguish between the two types of wall conditions, electric or magnetic, at the HPS. For an an electric wall at $y = 0$, the solutions are (M,E) and (E,E), and the upper trigonometric function in the y-dependence is used, with $k_{2,n} = 2n\pi/b$ and $k_{3,n} = 2n\pi/d$. Substitution of the truncated series for the fields into Eq. (2.64b) gives

$$\sum_{n=0}^{N_2} \theta_{3,n}^{(H)} G_{3,n} \cos\,(2n\pi y/d) = \sum_{n=0}^{N_2} G_{2,n}^{(+)} \cos\,(2n\pi y/b).$$

Applying to both sides of this equation the integral operator $\int_{-d/2}^{d/2} \cos(2m\pi y/d)\,dy$, where m takes the values 0, 1, 2, ..., N_2 then gives

$$d\theta_{3,0}^{(H)} G_{3,0} = dG_{2,0}^{(+)} + \sum_{n=1}^{N_2} G_{2,n}^{(+)} \int_{-d/2}^{d/2} \cos(2n\pi y/b)\,dy$$

and

$$\frac{d}{2}\,\theta_{3,m}^{(H)} G_{3,m} = G_{2,0}^{(+)} \int_{-d/2}^{d/2} \cos(2m\pi y/d)\,dy + \sum_{n=1}^{N_2} G_{2,n}^{(+)} \int_{-d/2}^{d/2} \cos(2n\pi y/b)\cos(2m\pi y/d)\,dy$$

for $m \geqslant 1$. But

$$\int_{-d/2}^{d/2} \cos(2n\pi y/b)\,dy = d\ \mathrm{sinc}\,(n\pi d/b)$$

$$\int_{-d/2}^{d/2} \cos(2m\pi y/d)\,dy = 0 \text{ for } m \geqslant 1$$

and using the mathematical identity

$$\cos\alpha\cos\beta = \frac{1}{2}[\cos(\alpha-\beta) + \cos(\alpha+\beta)]$$

the second summation integral may be evaluated as

$$\int_{-d/2}^{d/2} \cos(2n\pi y/b)\cos(2m\pi y/d)\,dy = \{\mathrm{sinc}\,[\pi(m - nd/b)] + \mathrm{sinc}\,[\pi(m + nd/b)]\}d/2$$

where the sinc function is given by

$$\mathrm{sinc}(\tau) = \frac{\sin(\tau)}{\tau}$$

With the height ratio defined as

$$r = d/b$$

then

$$\theta_{3,0}^{(H)} G_{3,0} = G_{2,0}^{(+)} + \sum_{n=1}^{N_2} \mathrm{sinc}\,(n\pi r) G_{2,n}^{(+)}$$

and

$$\theta_{3,m}^{(H)} G_{3,m} = \sum_{n=1}^{N_2} \{\mathrm{sinc}\,[\pi(m - nr)] + \mathrm{sinc}\,[\pi(m + nr)]\} G_{2,n}^{(+)}$$

for $m \geqslant 1$. In matrix form, the results are

$$\theta_3^{(H)}\mathbf{G}_3 = M_4\mathbf{G}_2^{(+)} \tag{2.68}$$

where the matrix $\theta_3^{(H)}$ is diagonal with

$$\{\theta_3^{(H)}\}_{m,n} = \theta_{3,n}^{(H)}\,\delta mn \tag{2.69}$$

and the matrix M_4 is given by

$$\{M_4\}_{m,n} = \begin{cases} 1 \text{ for } m = 0,\ n = 0 \\ \mathrm{sinc}\,(n\pi r) \text{ for } m = 0,\ n \neq 0 \\ 0 \text{ for } m \neq 0,\ n = 0 \\ \mathrm{sinc}\,[\pi(m - nr)] + \mathrm{sinc}\,[\pi(m + nr)] \text{ for } m \neq 0,\ n \neq 0. \end{cases} \tag{2.70}$$

Substitution of the truncated series representation for the fields $H_z^{(2)}$ and $H_z^{(3)}$ into Eq. (2.64a) gives

$$\sum_{n=0}^{N_2} \theta_{3,n}^{(H)} F_{3,n} \sin(2n\pi y/d) = \sum_{n=0}^{N_2} F_{2,n}^{(+)} \sin(2n\pi y/b).$$

Here the coefficients $F_{3,0}$ and $F_{2,0}^{(+)}$ are strictly dummy elements since the modal components in both regions corresponding to $n = 0$ are nonexistent. Applying to both sides of this equation, the integral operator $\int_{-d/2}^{d/2} \sin(2m\pi y/d)\,dy$ with $m = 1, 2, \ldots N_2$, and using the mathematical identity

$$\sin\alpha \sin\beta = \frac{1}{2}[\cos(\alpha - \beta) - \cos(\alpha + \beta)]$$

will yield

$$\theta_{3,m}^{(H)} F_{3,m} = \sum_{n=1}^{N_2} \{\text{sinc}\,[\pi(m - nr)] - \text{sinc}\,[\pi(m + nr)]\} F_{2,n}^{(+)}$$

for $m \geqslant 1$. The dummy elements $F_{3,0}$ and $F_{2,n}^{(+)}$ may be expressed as

$$\theta_{3,0}^{(H)} F_{3,0} = 0 \cdot F_{2,0}^{(+)}.$$

Thus, in matrix form

$$\theta_3^{(H)} \mathbf{F}_3 = M_3 \mathbf{F}_2^{(+)} \tag{2.71}$$

where the diagonal matrix $\theta_3^{(H)}$ is given by Eq. (2.69) and the matrix M_3 is given by

$$\{M_3\}_{m,n} = \begin{cases} 0 \text{ for } m = 0 \text{ or } n = 0 \\ \text{sinc}\,[\pi(m - nr)] - \text{sinc}\,[\pi(m + nr)] \text{ for } m \neq 0,\ n \neq 0 \end{cases} \tag{2.72}$$

The boundary conditions for $E_y^{(2)}$ and $E_y^{(3)}$ at $x = 0$ are given by Eq. (2.65a). Applying to both sides of this equation the integral operator $\int_{-d/2}^{d/2} \cos(2m\pi y/b)\,dy$ where $m = 0, 1, 2, \ldots, N_2$ gives

$$\int_{-d/2}^{d/2} E_y^{(2)}|_{x=0} \cos(2m\pi y/b)\,dy = \int_{-d/2}^{d/2} E_y^{(3)}|_{x=0} \cos(2m\pi y/b)\,dy.$$

Here the integration limits on the left may be extended to $\pm b/2$ since $E_y^{(2)}$ must vanish on the conducting side walls of the ridges at $x = 0$, $y \in \{Y_2\}$. Thus,

$$\int_{-b/2}^{b/2} E_y^{(2)}|_{x=0} \cos(2m\pi y/b)\,dy = \int_{-d/2}^{d/2} E_y^{(3)}|_{x=0} \cos(2m\pi y/b)\,dy. \tag{2.73}$$

Since a finite series representation for $E_y^{(2)}$ cannot be identically zero for all $y \in \{Y_2\}$ at $x = 0$, the approximation is apparent for the truncated series. With this approximation, substitution of the series representation for $E_y^{(2)}$ and $E_y^{(3)}$ into (2.73) will show that

$$B_{2,0}^{(+)} = r\theta_{3,0}^{(E)} B_{3,0}$$

$$B_{2,m}^{(+)} = 2r\,\text{sinc}\,(m\pi r)\theta_{3,0}^{(E)} B_{3,0} + r\sum_{n=1}^{N_2} \{\text{sinc}\,[\pi(n - mr)] + \text{sinc}\,[\pi(n + mr)]\}\theta_{3,n} B_{3,n} \text{ for } m \geqslant 1.$$

In matrix form these results may be expressed as

$$\mathbf{B}_2^{(+)} = M_2 \theta_3^{(E)} \mathbf{B}_3 \tag{2.74}$$

where the diagonal matrix $\theta_3^{(E)}$ is given by

$$\{\theta_3^{(E)}\}_{m,n} = \theta_{3,n}^{(E)}\,\delta_{mn} \tag{2.75}$$

and the matrix M_2 is given by

$$\{M_2\}_{m,n} = \begin{cases} r \text{ for } m = 0,\ n = 0 \\ 0 \text{ for } m = 0,\ n \neq 0 \\ 2r \operatorname{sinc}(m\pi r) \text{ for } m \neq 0,\ n = 0 \\ r\{\operatorname{sinc}[\pi(n - mr)] + \operatorname{sinc}[\pi(n + mr)]\} \text{ for } m \neq 0,\ n \neq 0. \end{cases} \tag{2.76}$$

The boundary conditions for $E_z^{(2)}$ and $E_z^{(3)}$ at $x = 0$ are given by Eq. (2.65b). Application to both sides of this equation of the integral operator $\int_{-d/2}^{d/2} \sin(2m\pi y/b)\,dy$, with $m = 1, 2, \ldots, N_2$, and extension of the integration limits in region 2 to $\pm b/2$ (since $E_z^{(2)}|_{x=0} = 0$ for $y \in \{Y_2\}$) gives

$$\int_{-b/2}^{b/2} E_z^{(2)}|_{x=0} \sin(2m\pi y/b)\,dy = \int_{-d/2}^{d/2} E_z^{(3)}|_{x=0} \sin(2m\pi y/b)\,dy.$$

Substitution of the truncated series representation for $E_z^{(2)}$ and $E_z^{(3)}$ and appropriate evaluation of the integrals will then yield

$$C_{2,m}^{(+)} = r \sum_{n=1}^{N_2} \{\operatorname{sinc}[\pi(n - mr)] - \operatorname{sinc}[\pi(n + mr)]\}\theta_{3,n} C_{3,n}.$$

The coefficients $C_{2,0}^{(+)}$ and $C_{3,0}$ are dummy elements and may be included in the matrix representation with

$$\mathbf{C}_2^{(+)} = M_1 \theta_3^{(E)} \mathbf{C}_3 \tag{2.77}$$

where the matrix M_1 is given by

$$\{M_1\}_{m,n} = \begin{cases} 0 \text{ for } m = 0 \text{ or } n = 0 \\ r\{\operatorname{sinc}[\pi(n - mr)]\} - \operatorname{sinc}[\pi(n + mr)]\} \text{ for } m \neq 0,\ n \neq 0. \end{cases} \tag{2.78}$$

The relationships developed thus far between amplitude coefficients of similar tangential fields in Regions 2 and 3 have been for (M,E) and (E,E) solutions. The dummy coefficients as described are included only as a convenience to simplify the notation. These dummy elements will later be discarded as they have no bearing on the numerical solution.

For (M,M) and (E,M) solutions, corresponding to a magnetic wall at $y = 0$, the lower trigonometric function of the y-dependence is used in the series expansion of the fields, with $k_{2,n} = (2n + 1)\pi/b$ and $k_{3,n} = (2n + 1)\pi/d$. For these solutions, the singular condition does not exist; i.e., neither $k_{2,n}$ or $k_{3,n}$ is zero for any value of n; thus, there are no dummy coefficients. The procedure for obtaining relationships between amplitude coefficients of similar tangential fields is similar to that used for (M,E) and (E,E) solutions. Application to Eqs. (2.64a) and (2.64b) of the integral operators $\int_{-d/2}^{d/2} \cos[(2m + 1)\pi y/d)\,dy$ and $\int_{-d/2}^{d/2} \sin[(2m + 1)\pi y/d]\,dy$, respectively, will yield upon substitution of the truncated series representation for the fields

$$\theta_{3,m}^{(H)} F_{3,m} = \sum_{n=0}^{N_2} \{\operatorname{sinc}\frac{\pi}{2}[(2m + 1) - (2n + 1)r] + \operatorname{sinc}\frac{\pi}{2}[(2m + 1) + (2n + 1)r]\} F_{2,n}^{(+)}$$

$$\theta_{3,m}^{(H)} G_{3,m} = \sum_{n=0}^{N_2} \{\operatorname{sinc}\frac{\pi}{2}[(2m + 1) - (2n + 1)r] - \operatorname{sinc}\frac{\pi}{2}[(2m + 1) + (2n + 1)r]\} G_{2,n}^{(+)}$$

for $m = 0, 1, 2, \ldots, N_2$. Application to Eqs. (2.65a) and (2.65b) of the integral operators $\int_{-d/2}^{d/2} \sin[(2m + 1)\pi y/b]\,dy$ and $\int_{-d/2}^{d/2} \cos[(2m + 1)\pi y/b]\,dy$, respectively, with the integration limits

extended to $\pm b/2$ for the tangential electric fields in Region 2, and subsequent substitution of the truncated series representation for these fields will yield

$$B_{2,m}^{(+)} = r\sum_{n=0}^{N_2} \{\text{sinc}\,\frac{\pi}{2}[(2n+1)-(2m+1)r] - \text{sinc}\,\frac{\pi}{2}[(2n+1)+(2m+1)r]\}\theta_{3,n}^{(E)}B_{3,n}$$

$$C_{2,m}^{(+)} = r\sum_{n=0}^{N_2} \{\text{sinc}\,\frac{\pi}{2}[(2n+1)-(2m+1)r] + \text{sinc}\,\frac{\pi}{2}[(2n+1)+(2m+1)r]\}\theta_{3,n}^{(E)}B_{3,n}$$

for $m = 0, 1, 2, \ldots, N_2$. In matrix form the results appear identical to those for (M,E) and (E,E) solutions, with

$$\mathbf{C}_2^{(+)} = M_1\theta_3^{(E)}\mathbf{C}_3 \tag{2.79a}$$

$$\mathbf{B}_2^{(+)} = M_2\theta_3^{(E)}\mathbf{B}_3 \tag{2.79b}$$

$$\theta_3^{(H)}\mathbf{F}_3 = M_3\mathbf{F}_2^{(+)} \tag{2.79c}$$

$$\theta_3^{(H)}\mathbf{G}_3 = M_4\mathbf{G}_2^{(+)} \tag{2.79d}$$

where, however, the matrices M_1, M_2, M_3, and M_4 are different. For (M,M) and (E,M) solutions

$$\{M_1\}_{m,n} = r\{\text{sinc}\,\frac{\pi}{2}[(2n+1)-(2m+1)r] + \text{sinc}\,\frac{\pi}{2}[(2n+1)+(2m+1)r]\} \tag{2.80a}$$

$$\{M_2\}_{m,n} = r\{\text{sinc}\,\frac{\pi}{2}[(2n+1)-(2m+1)r] - \text{sinc}\,\frac{\pi}{2}[(2n+1)+(2m+1)r]\} \tag{2.80b}$$

$$\{M_3\}_{m,n} = \text{sinc}\,\frac{\pi}{2}[(2m+1)-(2n+1)r] + \text{sinc}\,\frac{\pi}{2}[(2m+1)+(2n+1)r] \tag{2.80c}$$

$$\{M_4\}_{m,n} = \text{sinc}\,\frac{\pi}{2}[(2m+1)-(2n+1)r] - \text{sinc}\,\frac{\pi}{2}[(2m+1)+(2n+1)r]. \tag{2.80d}$$

The elements of the diagonal matrices $\theta_3^{(E)}$ and $\theta_3^{(H)}$ are given by Eqs. (2.66) or (2.67), dependent on the type of wall condition at the VPS, $x = x_3$.

With the matrix form of Eq. (2.79) valid for all solutions, the four separate matrix equations may be combined into a pair of matrix equations as

$$\begin{bmatrix} \mathbf{C}_2^{(+)} \\ \hline \mathbf{B}_2^{(+)} \end{bmatrix} = \mathrm{M}_{12}\Theta_3^{(E)} \begin{bmatrix} \mathbf{C}_3 \\ \hline \mathbf{B}_3 \end{bmatrix} \tag{2.81}$$

$$\Theta_3^{(H)} \begin{bmatrix} \mathbf{F}_3 \\ \hline \mathbf{G}_3 \end{bmatrix} = \mathrm{M}_{34} \begin{bmatrix} \mathbf{F}_2^{(+)} \\ \hline \mathbf{G}_2^{(+)} \end{bmatrix} \tag{2.82}$$

where

$$M_{12} = \left[\begin{array}{c|c} M_1 & 0 \\ \hline 0 & M_2 \end{array}\right] \tag{2.83a}$$

$$M_{34} = \left[\begin{array}{c|c} M_3 & 0 \\ \hline 0 & M_4 \end{array}\right] \tag{2.83b}$$

$$\Theta_3^{(E)} = \left[\begin{array}{c|c} \theta_3^{(E)} & 0 \\ \hline 0 & \theta_3^{(E)} \end{array}\right] \tag{2.84a}$$

$$\Theta_3^{(H)} = \left[\begin{array}{c|c} \theta_3^{(H)} & 0 \\ \hline 0 & \theta_3^{(H)} \end{array}\right]. \tag{2.84b}$$

From Eq. (2.30)

$$\left(\begin{array}{c} \mathbf{C}_3 \\ \hline \mathbf{B}_3 \end{array}\right) = \Psi_3^{-1}\,\Lambda_3 \left[\begin{array}{c|c} W_A & 0 \\ \hline 0 & -\omega\mu_0 U \end{array}\right] \left(\begin{array}{c} \mathbf{A}_3 \\ \hline \mathbf{D}_3 \end{array}\right)$$

while Eqs. (2.31) and (2.46) may be used to give

$$\left(\begin{array}{c} \mathbf{A}_3 \\ \hline \mathbf{D}_3 \end{array}\right) = -\left[\begin{array}{c|c} \omega\epsilon_3 U & 0 \\ \hline 0 & W_D \end{array}\right]^{-1} \Lambda_3 \left(\begin{array}{c} \mathbf{F}_3 \\ \hline \mathbf{G}_3 \end{array}\right),$$

thus

$$\left(\begin{array}{c} \mathbf{C}_3 \\ \hline \mathbf{B}_3 \end{array}\right) = -\,\Psi_3^{-1}\,\Lambda_3 \left[\begin{array}{c|c} \frac{1}{\omega\epsilon_3} W_A & 0 \\ \hline 0 & -\omega\mu_0 W_D^{-1} \end{array}\right] \Lambda_3 \left(\begin{array}{c} \mathbf{F}_3 \\ \hline \mathbf{G}_3 \end{array}\right). \tag{2.85}$$

This last result will be expressed as

$$\left(\begin{array}{c} \mathbf{C}_3 \\ \hline \mathbf{B}_3 \end{array}\right) = Z \left(\begin{array}{c} \mathbf{F}_3 \\ \hline \mathbf{G}_3 \end{array}\right) \tag{2.86}$$

where the matrix Z may be partitioned into submatrices as

$$Z = \left[\begin{array}{c|c} Z_{11} & Z_{12} \\ \hline Z_{21} & Z_{22} \end{array}\right].$$

Substitution of Eqs. (2.44) and (2.45) into Eq. (2.85) will show the submatrices of Z are diagonal with

$$Z_{11} = \psi_3^{-1}\left[-\frac{1}{\omega\epsilon_3}\Phi\, W_A \Phi + \omega\mu_0 K_3 W_D^{-1} K_3\right] \tag{2.87a}$$

$$Z_{12} = \pm K_3 \Phi \left[\frac{1}{\omega\epsilon_3}\, W_A - \omega\mu_0 W_D^{-1}\right] \psi_3^{-1} \tag{2.87b}$$

$$Z_{21} = Z_{12} \tag{2.87c}$$

$$Z_{22} = \psi_3^{-1}\left[-\frac{1}{\omega\epsilon_3}\, K_3 W_A K_3 + \omega\mu_0 \Phi\, W_D^{-1} \Phi\right]. \tag{2.87d}$$

The $\pm$ notation for the submatrices Z_{12} and Z_{21} is analogous to that for the individual regions, with the upper sign used for (M,E) and (E,E) solutions and the lower sign for (M,M) and (E,M) solutions.

Substitution of Eq. (2.86) into Eq. (2.81) will give

$$\begin{bmatrix} \mathbf{C}_2^{(+)} \\ \hdashline \mathbf{B}_2^{(+)} \end{bmatrix} = M_{12}\Theta_3^{(E)} Z \begin{bmatrix} \mathbf{F}_3 \\ \hdashline \mathbf{G}_3 \end{bmatrix}$$

which may be used with Eq. (2.82) to yield

$$\begin{bmatrix} \mathbf{C}_2^{(+)} \\ \hdashline \mathbf{B}_2^{(+)} \end{bmatrix} = M_{12}\Theta_3^{(E)} Z \left[\Theta_3^{(H)}\right]^{-1} M_{34} \begin{bmatrix} \mathbf{F}_2^{(+)} \\ \hdashline \mathbf{G}_2^{(+)} \end{bmatrix} \tag{2.88}$$

or

$$\begin{bmatrix} \mathbf{C}_2^{(+)} \\ \hdashline \mathbf{B}_2^{(+)} \end{bmatrix} = R \begin{bmatrix} \mathbf{F}_2^{(+)} \\ \hdashline \mathbf{G}_2^{(+)} \end{bmatrix} \tag{2.89}$$

where the matrix R is given by

$$R = M_{12}\Theta_3^{(E)} Z [\Theta_3^{(H)}]^{-1} M_{34}. \tag{2.90}$$

If R is partitioned as

$$R = \left[\begin{array}{c|c} R_{11} & R_{12} \\ \hdashline R_{21} & R_{22} \end{array}\right]$$

substitution of the appropriate lower order submatrices into Eq. (2.88) will show that each of the submatrices of R is a square matrix, with

$$R_{11} = M_1\Theta_3^{(E)} Z_{11} [\Theta_3^{(H)}]^{-1} M_3 \tag{2.91a}$$

$$R_{12} = M_1\Theta_3^{(E)} Z_{12} [\Theta_3^{(H)}]^{-1} M_4 \tag{2.91b}$$

$$R_{21} = M_2\Theta_3^{(E)} Z_{21} [\Theta_3^{(H)}]^{-1} M_3 \tag{2.91c}$$

$$R_{22} = M_2\Theta_3^{(E)} Z_{22} [\Theta_3^{(H)}]^{-1} M_4. \tag{2.91d}$$

Using Eqs. (2.44) and (2.45), Eq. (2.41) will show that

$$\begin{bmatrix} \mathbf{F}_2^{(+)} \\ \hdashline \mathbf{G}_2^{(+)} \end{bmatrix} = -\Psi_2^{-1}\Lambda_2 \left[\begin{array}{c|c} \omega\epsilon_2 U & 0 \\ \hdashline 0 & U \end{array}\right] \begin{bmatrix} \mathbf{A}_2^{(+)} \\ \hdashline \mathbf{D}_2^{(-)} \end{bmatrix} \tag{2.92}$$

while Eq. (2.39) will show that

$$\Lambda_2 \begin{bmatrix} \mathbf{C}_2^{(+)} \\ \hdashline \mathbf{B}_2^{(+)} \end{bmatrix} = \left[\begin{array}{c|c} U & 0 \\ \hdashline 0 & -\omega\mu_0 U \end{array}\right] \begin{bmatrix} \mathbf{A}_2^{(-)} \\ \hdashline \mathbf{D}_2^{(+)} \end{bmatrix}. \tag{2.93}$$

Premultiplication of Eq. (2.89) by Λ_2 with subsequent substitution of Eqs. (2.92) and (2.93) will give

$$\left[\begin{array}{c|c} U & 0 \\ \hline 0 & -\omega\mu_0 U \end{array}\right]\left(\begin{array}{c} \mathbf{A}_2^{(-)} \\ \hline \mathbf{D}_2^{(+)} \end{array}\right) = -\Lambda_2 R \Psi_2^{-1} \Lambda_2 \left[\begin{array}{c|c} \omega\epsilon_2 U & 0 \\ \hline 0 & U \end{array}\right]\left(\begin{array}{c} \mathbf{A}_2^{(+)} \\ \hline D_2^{(-)} \end{array}\right). \tag{2.94}$$

From Eq. (2.63)

$$\left[\begin{array}{c|c} Q_A^{(+)} & 0 \\ \hline 0 & Q_D^{(-)} \end{array}\right]\left(\begin{array}{c} \mathbf{A}_2^{(+)} \\ \hline \mathbf{D}_2^{(-)} \end{array}\right) = \left[\begin{array}{c|c} Q_A^{(-)} & 0 \\ \hline 0 & Q_D^{(+)} \end{array}\right]\left(\begin{array}{c} \mathbf{A}_2^{(-)} \\ \hline \mathbf{D}_2^{(+)} \end{array}\right)$$

thus premultiplication of Eq. (2.94) by

$$\left[\begin{array}{c|c} Q_A^{(-)} & 0 \\ \hline 0 & Q_D^{(+)} \end{array}\right]$$

will give

$$\left[\begin{array}{c|c} U & 0 \\ \hline 0 & -\omega\mu_0 U \end{array}\right]\left[\begin{array}{c|c} Q_A^{(+)} & 0 \\ \hline 0 & Q_D^{(-)} \end{array}\right]\left(\begin{array}{c} \mathbf{A}_2^{(+)} \\ \hline \mathbf{D}_2^{(-)} \end{array}\right) = -\left[\begin{array}{c|c} Q_A^{(-)} & 0 \\ \hline 0 & Q_D^{(+)} \end{array}\right]\Lambda_2 R \Psi_2^{-1} \Lambda_2 \left[\begin{array}{c|c} \omega\epsilon_2 U & 0 \\ \hline 0 & U \end{array}\right]\left(\begin{array}{c} \mathbf{A}_2^{(+)} \\ \hline \mathbf{D}_2^{(-)} \end{array}\right)$$

or

$$T\left(\begin{array}{c} \mathbf{A}_2^{(+)} \\ \hline \mathbf{D}_2^{(-)} \end{array}\right) = 0 \tag{2.95}$$

with the matrix T defined as

$$T = \left[\begin{array}{c|c} U & 0 \\ \hline 0 & -\omega\mu_0 U \end{array}\right]\left[\begin{array}{c|c} Q_A^{(+)} & 0 \\ \hline 0 & Q_D^{(-)} \end{array}\right] + \left[\begin{array}{c|c} Q_A^{(-)} & 0 \\ \hline 0 & Q_D^{(+)} \end{array}\right] S \left[\begin{array}{c|c} \omega\epsilon_2 U & 0 \\ \hline 0 & U \end{array}\right] \tag{2.96}$$

where the matrix S is given by

$$\begin{aligned} S &= \Lambda_2 R \Psi_2^{-1} \Lambda_2 \\ &= \Lambda_2 R \Lambda_2 \Psi_2^{-1}. \end{aligned} \tag{2.97}$$

Partitioning the matrix S as

$$S = \left[\begin{array}{c|c} S_{11} & S_{12} \\ \hline S_{21} & S_{22} \end{array}\right]$$

substitution of the appropriate lower order submatrices into Eq. (2.97) will show that the submatrices of S are square, with

$$S_{11} = \Phi R_{11} \Phi \mp \Phi R_{12} K_2 \mp K_2 R_{21} \Phi + K_2 R_{22} K_2 \tag{2.98a}$$

$$S_{12} = \mp \Phi R_{11} K_2 - \Phi R_{12} \Phi + K_2 R_{21} K_2 \pm K_2 R_{22} \Phi \tag{2.98b}$$

$$S_{21} = \mp K_2 R_{11} \Phi + K_2 R_{12} K_2 - \Phi R_{21} \Phi \pm \Phi R_{22} K_2 \tag{2.98c}$$

$$S_{22} = K_2 R_{11} K_2 \pm K_2 R_{12} \Phi \pm \Phi R_{21} K_2 + \Phi R_{22} \Phi. \tag{2.98d}$$

Again, the $(\pm)$ and $(\mp)$ symbolism is the result of the dual sign notation used to distinguish the type of wall condition at $y = 0$, with the upper sign to be used for (M,E) and (E,E) solutions and the lower sign for (M,M) and (E,M) solutions.

The expression of Eq. (2.95) represents an eigenvalue problem for which the eigenvalue is zero [51,63]. For a nontrivial solution to exist, the determinant of the matrix T must vanish:

$$\det [T] = 0.$$

All elements of T are determined uniquely for given values of radian frequency ω and propagation constant β when the type of solution; i.e., (M,E), (M,M), (E,M), or (E,E), is specified. Thus, the frequency may be fixed and β taken as the unknown, with

$$\det [T(\beta)] = 0$$

the requirement for a numerical solution for β, or the propagation constant may be fixed and ω taken as the unknown. In the latter case, only the cutoff frequency will be sought, with $\beta = 0$; thus

$$\det [T(\omega_c)] = 0$$

is the requirement for a numerical solution for cutoff for any mode.

The matrix T may be partitioned into square submatrices as

$$T = \left[\begin{array}{c|c} T_{11} & T_{12} \\ \hline T_{21} & T_{22} \end{array}\right]$$

where from Eq. (2.96)

$$\begin{aligned} T_{11} &= Q_4^{(+)} + \omega \epsilon_2 Q_4^{(-)} S_{11} \\ T_{12} &= Q_4^{(-)} S_{12} \\ T_{21} &= \omega \epsilon_2 Q_D^{(+)} S_{21} \\ T_{22} &= Q_D^{(+)} S_{22} - \omega \mu_0 Q_D^{(-)}. \end{aligned}$$

For the waveguide modes where the singular condition is not encountered; i.e., $k_{i,0} \neq 0$, examination of the matrix equations used to develop Eq. (2.95) will show that all elements of the matrices T_{12} and T_{21} vanish at the mode cutoff frequency where $\beta = 0$. Thus, when solving for the cutoff frequency of these modes,

$$\begin{aligned} \det [T] &= \det \left[\begin{array}{c|c} T_{11} & 0 \\ \hline 0 & T_{22} \end{array}\right] \\ &= \det [T_{11}] \cdot \det [T_{22}] \\ &= 0 \end{aligned}$$

and the requirement for the cutoff frequency is either

$$\det\,[T_{11}(\omega_c)] = 0 \tag{2.99a}$$

or

$$\det\,[T_{22}(\omega_c)] = 0. \tag{2.99b}$$

In the general case, both determinants will not be zero simultaneously, i.e., for the same frequency. For Eq. (2.95) to remain valid when $\det\,[T_{11}(\omega_c)] = 0$ but $\det\,[T_{22}(\omega_c)] \neq 0$, the vector $\mathbf{D}_2^{(-)}$ must vanish. If $\mathbf{D}_2^{(-)} = 0$, then from (2.61-c) $\mathbf{D}_2^{(+)} = 0$. Thus, the waveguide mode with cutoff frequency determined by Eq. (2.99a) has no x-directed component of magnetic field at cutoff, analogous to the condition for LSM modes in dielectric slab loaded rectangular waveguide (Appendix B), and will be referred to as a quasi-LSM, or QLSM mode.

If $\det\,[T_{22}(\omega_c)] = 0$, but $\det\,[T_{11}(\omega_c)] \neq 0$, then the vector $\mathbf{A}_2^{(+)}$ must vanish for Eq. (2.95) to remain valid. From Eq. (2.61b) $\mathbf{A}_2^{(-)} = 0$ if $\mathbf{A}_2^{(+)} = 0$, and the waveguide mode corresponding to the cutoff condition imposed by Eq. (2.99b) thus has no x-directed component of electric field at cutoff, analogous to the condition for LSE modes in dielectric slab loaded rectangular waveguide (Appendix B), and will be referred to therefore as a quasi-LSE, or QLSE mode.

Note that the QLSE and QLSM modes of the dielectric loaded ridged waveguide do possess x-directed components of electric field and magnetic field, respectively, at frequencies above cutoff. This is in contrast to the LSE and LSM modes of dielectric slab loaded rectangular waveguide, for which the x-directed components of electric field and magnetic field, respectively, maintain zero magnitude at frequencies above cutoff. Additional discussions of the QLSE and QLSM modes at frequencies above cutoff will be postponed until a more specific classification is formulated for the different waveguide modes.

For the waveguide modes where the singular condition exists at cutoff, i.e., $k_{i,0} = 0$ for $i = 1, 2, 3$, the vector element $A_{2,0}^{(+)}$ is a dummy element. To eliminate this dummy element, the eigenvalue problem of Eq. (2.95) must be modified to

$$T' \begin{bmatrix} \mathbf{A}_2'^{(+)} \\ \hdashline \mathbf{D}_2'^{(-)} \end{bmatrix} = 0 \tag{2.100}$$

where T' is the matrix formed by deleting the first row and first column of the matrix T. The vector $\mathbf{A}_2'^{(+)}$ is the vector $\mathbf{A}_2^{(+)}$ less the first, or dummy, element $A_{2,0}^{(+)}$. When solving for β at frequencies above cutoff, the vector $\mathbf{D}_2'^{(-)}$ is the same as the vector $\mathbf{D}_2^{(-)}$. When solving for the mode cutoff frequency, with $\beta = 0$, the vector $\mathbf{D}_2'^{(-)}$ is the vector $\mathbf{D}_2^{(-)}$, but with the leading element $D_{2,0}^{(-)}$ replaced as $-G_{2,0}^{(+)}$. The matrix T' may be partitioned as

$$[T'] = \left[\begin{array}{c|c} T_{11}' & T_{12}' \\ \hdashline T_{21}' & T_{22} \end{array}\right]$$

where T_{11}' is the matrix T_{11} less the first row and first column, T_{12}' is the matrix T_{12} less the first row, T_{21}' is the matrix T_{21} less the first column. The matrices T_{12}' and T_{21}' are nonsquare. It is straightforward to show that the eigenvalue problem of (2.100) is exactly the same as would have been obtained had the development not included the dummy elements to maintain a consistent notation for the mathematical analysis. The required condition for a numerical solution is thus

$$\det\,[T'(\omega,\beta)] = 0$$

where either ω or β may be treated as the unknown quantity. The only types of waveguide modes for which the singular condition exists, thus requiring modification of the matrix T to T' in the eigenvalue solution, are QLSE modes. This point will be clarified after the discussion of additional parameters which may be used to further specify the different waveguide modes.

Thus far in the analysis of the dielectric loaded double ridged waveguide, the specifications for the waveguide mode(s) have been the effective wall conditions, electric or magnetic, at the two planes of symmetry, with an additional classification of each mode as either QLSE or QLSM, dependent on the eigenvalue solution at the cutoff frequency. For each of the wall condition solution types, (M,E),(M,M),(E,E), and (E,M), there will exist an infinite number of both QLSE and QLSM waveguide modes. This situation is comparable to the infinite number of LSE and LSM modes that exist in dielectric slab loaded rectangular waveguide (Appendix B). In the case for the latter waveguide, an index integer pair is used to uniquely specify each of the LSE and LSM modes with any given mode characterized as the $\mathrm{LSE}_{m,n}$ mode or the $\mathrm{LSM}_{m,n}$ mode. The first index m refers to the number of half cyclic variations of each of the existing (nonzero) fields E_x, E_y, E_z, H_x, H_y, and H_z, as a function of x within the waveguide, i.e., from sidewall to sidewall. The second index n refers to the number of half cyclic variations of each field as a function of y, i.e., from topwall to bottomwall.

In the dielectric loaded ridged waveguide, the fields of every propagating mode consist of an infinite number of modal components. A single index integer pair may be used, however, to uniquely specify each mode, in a manner analogous to that for the LSE and LSM modes of dielectric slab loaded rectangular waveguide, if the integers refer to the number of half cyclic variations of the fields of the lowest order modal component present, i.e., the modal component with the smallest value of n. The y-dependence of the nth modal component in region i is

$$f_n^{(i)}(y) = \begin{Bmatrix}\sin\\ \cos\end{Bmatrix} k_{i,n}y \quad .$$

with the choice of the sin or cos function determined by the specific field. For (M,E) and (E,E) modes, with an effective electric wall at $y = 0$, in each region with height h_i

$$k_{i,n} = 2n\pi/h_i;$$

thus the number of half cyclic variations (topwall to bottomwall) of fields of the nth modal component is $2n$. For (M,M) and (E,M) modes, with an effective magnetic wall at $y = 0$, $k_{i,n} = (2n + 1)\pi/h_i$; thus the fields of the nth modal component have $2n + 1$ half cyclic variations from topwall to bottomwall. With each waveguide mode classified as $\mathrm{QLSE}_{m,n'}$ or $\mathrm{QLSM}_{m,n'}$, the lowest order modal component of the propagating mode is given by $n' = 2n$ for (M,E) and (E,E) modes, and by $n' = 2n + 1$ for (M,M) and (E,M) modes. In the series expansion of the fields, this represents a lower limit n_0 on the summation index n. For n' an even integer (corresponding to an electric wall at $y = 0$) the $\mathrm{QLSE}_{m,n'}$ and $\mathrm{QLSM}_{m,n'}$ modes have the lowest order field components with $n_0 = n'/2$, or $k_{i,n_0} = n'\pi/h_i$. For n' an odd integer (corresponding to a magnetic wall at $y = 0$), the $\mathrm{QLSE}_{m,n'}$ and $\mathrm{QLSM}_{m,n'}$ modes have the lowest order field components with $n_0 = (n' - 1)/2$, or $k_{i,n_0} = n'\pi/h_i$. With the lower limit set on the summation for all fields in each region, each of the matrices developed earlier in this section is thus dependent on this value for n_0. Some caution must be exercised when assigning the index notation for matrix and vector quantities in any computer program since most computer subroutines for matrix operations require a lowest order index of one.

For each propagating waveguide mode, the type of effective wall condition at the vertical plane of symmetry, $x = x_3$, will determine the symmetry aspects of each of the field components. With an effective magnetic wall at $x = x_3$, the tangential magnetic fields H_y and H_z and the normal electric field E_x must be antisymmetric about the VPS, while the tangential electric fields E_y and E_z and the normal magnetic field H_x must be symmetric about the VPS. For an effective electric wall at $x = x_3$, the symmetry conditions are reversed, with the fields E_y, E_z, and H_x antisymmetric and the fields H_y, H_z, and E_x symmetric about the VPS. The dependence of the field symmetry (antisymmetry) on the effective

wall type at the VPS is identical to that for the LSE and LSM modes of dielectric slab loaded rectangular waveguide (Appendix B). To maintain the analogy with the propagating modes of the latter waveguide, the first index of both the $QLSE_{m,n'}$ and $QLSM_{m,n'}$ modes of the dielectric loaded ridged waveguide will be an odd (even) integer for an effective magnetic (electric) wall at the VPS, $x = x_3$. The four combinations of effective wall conditions at the two planes (vertical, horizontal) of physical symmetry thus are reflected as restrictions on the index pair m,n' for either the $QLSE_{m,n'}$ mode or the $QLSM_{m,n'}$ mode with

Wall conditions		m	n'
(M,E)	$\rightarrow$	odd	even
(E,E)	$\rightarrow$	even	even
(M,M)	$\rightarrow$	odd	odd
(E,M)	$\rightarrow$	even	odd

(2.101)

In any propagating mode, the higher order modal components (terms of the series expansion for the fields with n larger than the lower limit n_0) will in general be evanescent with respect to x; i.e., the fields of these modal components will decay exponentially with distance from the ridge walls. For this reason, and to maintain an analogy with the index notation for modes of dielectric slab loaded rectangular waveguide, the first index m of both $QLSE_{m,n'}$ and $QLSM_{m,n'}$ modes will be used to describe the number of half cyclic variations (sidewall to sidewall) in the fields of the lowest order modal component, i.e., the field terms (with other than zero amplitude) corresponding to $n = n_0$ in the series expansions.

An equivalent but considerably more simplified description for the correlation between the field structure and the propagating mode designation may be obtained by viewing the modes of dielectric loaded ridged waveguide as the corresponding modes of dielectric slab loaded rectangular waveguide with fields that have been distorted due to the presence of the ridges. Thus, the $QLSX_{m,n'}$ mode, where m and n' are fixed integers and X denotes either E or M, would become the $LSX_{m,n'}$ mode if the ridges were to vanish, i.e., if the ridged waveguide was reduced to rectangular waveguide. Of course, the mode cutoff frequency and the propagation characteristics, as well as the exact field structure, would vary as the ridges were withdrawn.

The assumption of a lower limit n_0 other than zero for the summation index n in the series expansion for the fields of dielectric loaded ridged waveguide has an equivalent assumption if the corresponding waveguide mode is viewed as a distorted mode of dielectric slab loaded rectangular waveguide. The equivalent assumption is that the single modal component of the undistorted mode (in rectangular waveguide) remains as the lowest order modal component upon introduction of the ridges. As an example, the $LSE_{1,2}$ mode of dielectric slab loaded rectangular waveguide has fields that have a y-dependence $f(y) = \begin{pmatrix}\sin\\ \cos\end{pmatrix} 2\pi y/h$. Upon introduction of the ridges, the fields of this mode are distorted, with the mode becoming the $QLSE_{1,2}$ mode. Using the y-dependence to form the basis functions for a series expansion of the fields in each region i, with $f_{i,n} = \begin{pmatrix}\sin\\ \cos\end{pmatrix} 2n\pi y/h_i$ the assumption is that the lowest order modal component has $f_{i,n_0} = \begin{pmatrix}\sin\\ \cos\end{pmatrix} 2\pi y/h_i$, or that the lower limit on the summation index n is $n_0 = 1$.

The assumption of a lowest order modal component for the higher order waveguide modes is supported to some extent by numerical calculations made for several modes and several waveguide geometries. The cutoff frequency was calculated using the appropriate value for n_0 in the series expansions (thus setting the elements of the matrix for the eigenvalue solution) and compared with the cutoff frequency obtained when the lower limit was forced as $n_0 = 0$. For most waveguide modes and geometries tested, the agreement was excellent—less than 1% difference. Some comparisons were poor, possibly because of the difficulty in finding numerical solutions to the eigenvalue problem due to

the close proximity of poles and zeros of the determinant for the higher order modes. Such comparisons were made only for $QLSE_{m,n}$ and $QLSM_{m,n'}$ modes with $n' \geqslant 2$ since the lowest order modal component of modes with $n' = 0$ and $n' = 1$ correspond to the lower limit $n_0 = 0$. As discussed in the following paragraph, both the dominant mode and the first higher order mode will always have a lowest order modal component $n_0 = 0$. Since the primary objective of this investigation concerns the single mode bandwidth and field characteristics of the dominant mode, no further effort was made to rigorously justify the assumption of a lowest order modal component with $n_0 \neq 0$ for these higher order waveguide modes.

For the $QLSX_{m,n}$ mode (X = E or X = H) of dielectric loaded ridged waveguide, increasing either integer index will raise the cutoff frequency, analogous to the case for the modes of dielectric slab loaded rectangular waveguide. Also, by analogy with the latter waveguide, the first index of the $QLSE_{m,n}$ mode is restricted to nonzero positive integers, while the second index of the $QLSM_{m,n'}$ mode is restricted to nonzero positive integers. The possible propagating modes for dielectric loaded ridged waveguide are thus the $QLSE_{m,n}$ modes, with $m = 1, 2, 3, \ldots$ and $n' = 0, 1, 2, \ldots$, and the $QLSM_{m,n}$ modes, with $m = 0, 1, 2, \ldots$ and $n' = 1, 2, 3, \ldots$. As discussed earlier, the matrix of the eigenvalue problem is a function of each of these indices. A simple comparison of index pairs for the different modes will show that the two waveguide modes with the lowest cutoff frequencies, i.e., the dominant mode (lowest f_c) and the first higher order mode (second lowest f_c), must be a pair of modes from a group of four modes: the $QLSE_{1,0}$ mode, the $QLSE_{2,0}$ mode, the $QLSE_{1,1}$ mode, and the $QLSM_{0,1}$ mode. These four modes represent respectively the four mode types, (M,E),(E,E),(M,M), and (E,M), describing the effective wall conditions at the (vertical, horizontal) symmetry planes. For practical applications, the waveguide geometry usually will be chosen so that the $QLSE_{1,0}$ mode is the dominant mode.

Discussion on two issues raised earlier concerning certain properties of different waveguide modes may now be continued with greater clarity since the mode designation has been completed. Since the singular condition arises only at waveguide cutoff for modes with the lowest order modal component having $k_{i,0} = 0$ and thus occurs only for modes with the index $n' = 0$, and since $n' > 0$ for $QLSM_{m,n}$ modes, the singular condition exists only for QLSE modes, or more specifically the $QLSE_{m,0}$ modes, and then only at cutoff. The second issue is that of the x-directed electric and magnetic fields of the $QLSE_{m,n'}$ and $QLSM_{m,n'}$ modes where $n' \neq 0$. As pointed out earlier, $E_x = 0$ at cutoff for the $QLSE_{m,n'}$ mode but at frequencies above cutoff $E_x \neq 0$, while for the $QLSM_{m,n}$ mode $H_x = 0$ only at cutoff. If solving for the propagation constant β at some fixed frequency, the full determinant T must be used with

$$\det [T] = 0 \tag{2.102}$$

the requirement for a numerical solution. If the frequency is above the cutoff frequency of the $QLSE_{m,n}$ mode and that of the $QLSM_{m,n'}$ mode, where m and n' are fixed with $n' > 0$, separate roots to (2.102) will be found corresponding to the different values of β for the two waveguide modes. The lower root for β will normally (but not always) correspond to the mode with the larger cutoff frequency. The specific waveguide geometry will determine which mode has the larger cutoff frequency. By tracking the root(s) for β as a function of frequency from cutoff for each mode, and solving the eigenvector problem to determine amplitude coefficients of the various modal components, it is possible to compare the field magnitudes of the different modes. Such a procedure was used to compare the fields of the $QLSE_{1,1}$ mode with the fields of the $QLSM_{1,1}$ mode for several waveguide geometries. In each case, the most pronounced variation of any field component between the two modes at a frequency well above cutoff of either mode was in the relative magnitudes of the lowest order ($k_{i,0} = \pi/h_i$) modal component of E_x and H_x. With all fields normalized to unit power flow in the waveguide, the $QLSE_{1,1}$ mode had a consistently smaller magnitude for the lowest order term of E_x and a consistently higher magnitude for the lowest order term of H_x than the corresponding modal component amplitudes of the $QLSM_{1,1}$ mode. The amplitude difference between like fields varied from a factor of 3 to more than 2 orders of magnitude, dependent on the specific waveguide geometry and the

point where the comparison was made. For the $QLSE_{1,1}$ and $QLSM_{1,1}$ modes at least, this comparison lends additional credence to the nomenclature of quasi-LSE and quasi-LSM modes.

As discussed earlier, the $QLSE_{m,0}$ modes use the matrix T' in the eigenvalue solution, where the matrix T' is formed by deleting the first row and column of the matrix T of (2.96). This reduction of the matrix is necessary to eliminate the effects of the dummy vector coefficients—corresponding to the zero amplitudes of the $n = 0$ order modal components of E_x, E_z, and H_y—on the eigenvalue development. For any given frequency above cutoff, the requirement for a numerical solution is

$$\det [T'(\beta)] = 0.$$

When solving for the cutoff frequency of a $QLSE_{m,0}$ mode, the computational requirements may be reduced by partitioning the matrix T' as

$$T' = \left[\begin{array}{c|c} \tau_{11} & \tau_{12} \\ \hline \tau_{21} & \tau_{22} \end{array}\right].$$

If N_T terms were used in the series expansion for the fields, then the matrix T will be square, with size $2N_T \times 2N_T$. The matrix T' is square also, $(2N_T - 1) \times (2N_T - 1)$. The submatrices τ_{11} and τ_{22} are both square, where τ_{11} is $N_T \times N_T$ while τ_{22} is $(N_T - 1) \times (N_T - 1)$. While the submatrices τ_{12} and τ_{21} are both nonsquare, it is a straightforward procedure to show that each is a null matrix, i.e., all elements are zero, when $\beta = 0$. The requirement for a numerical solution for cutoff

$$\det [T'(\omega_c)] = 0 \tag{2.103}$$

may thus be reduced to

$$\det [\tau_{11}(\omega_c)] \cdot \det [\tau_{22}(\omega_c)] = 0.$$

With the matrix T' partitioned as described, the full eigenvalue problem for cutoff of a $QLSE_{m,0}$ mode is given by

$$\left[\begin{array}{c|c} \tau_{11} & 0 \\ \hline 0 & \tau_{22} \end{array}\right] \left\{\begin{array}{c} A_{2,1}^{(+)} \\ \vdots \\ A_{2,N_T}^{(+)} \\ -G_{2,0}^{(+)} \\ \hline D_{2,1}^{(-)} \\ \vdots \\ D_{2,N_T}^{(-)} \end{array}\right\} = 0 \tag{2.104}$$

where the coefficient $D_{2,0}^{(-)}$ has been replaced as $-G_{2,0}^{(+)}$ as discussed for the singular condition. If at some trial value of ω_c the determinant of the matrix τ_{22} were to vanish, but $\det [\tau_{11}] \neq 0$, then all of the lowest order ($n = 0$) model field components must vanish if (2.104) is to be satisfied, since $D_{2,0}^{(-)} = 0$ at cutoff. Thus, $\det [\tau_{22}] \neq 0$ for a $QLSE_{m,0}$ mode at cutoff, a fact confirmed by numerical evaluation of this determinant for a variety of waveguide geometries.

The requirement for waveguide cutoff of a $QLSE_{m,0}$ mode is thus

$$\det [\tau_{11}(\omega_c)] = 0. \tag{2.105}$$

Since $\det [\tau_{22}(\omega_c)] \neq 0$, then $H_x = 0$ to satisfy (2.104). This is in contrast to the cutoff of $QLSE_{m,n>0}$ modes, for which $E_x = 0$. However, the lowest order modal component of E_x, $E_{x,0}$, is zero for the $QLSE_{m,0}$ mode.

In addition to the null field features that have already been pointed out for cutoff conditions of the different waveguide modes, other features are readily seen upon examination of the relationships developed earlier between the x-directed electric and magnetic fields and the remained field components. For waveguide cutoff, the fields can be summarized for different modes:

$$\text{QLSM}_{m,n} \text{ modes} \begin{cases} E_z,\ H_x,\ H_y \equiv 0 \\ E_x,\ E_y,\ H_z \neq 0 \end{cases}$$

$$\underset{n\neq 0}{\text{QLSE}}_{m,n} \text{ modes} \begin{cases} E_x,\ E_y,\ H_z \equiv 0 \\ E_z,\ H_x,\ H_y \neq 0 \end{cases}$$

$$\text{QLSE}_{m,0} \text{ modes} \begin{cases} E_z,\ H_x,\ H_y \equiv 0 \\ E_y,\ H_z \neq 0 \\ E_{x,0} = 0 \\ E_{x,n>0} \neq 0. \end{cases}$$

Once the solution is obtained for a given waveguide mode, i.e., either the cutoff frequency ω_c (with $\beta = 0$) or the propagation term β (for a fixed frequency) is found to satisfy the null requirement of the appropriate determinant, conventional linear algebra techniques [51,62-65] may be used to calculate the eigenvector associated with the full matrix, from Eqs. (2.95) or (2.100). With the amplitude coefficients represented by the elements of the vectors $\mathbf{A}_2^{(-)}$ and $\mathbf{D}_2^{(+)}$ then known, calculation of the remaining field amplitudes in all regions may be accomplished in a straightforward manner.

For the purposes of this investigation, the only mode that requires numerical evaluation of the fields is the dominant mode. Because of practical considerations, only those waveguide geometries for which the dominant mode is the $\text{QLSE}_{1,0}$ mode will be considered. As with any waveguide, the operational frequency cannot be too close to cutoff because of greatly increased attenuation and dispersion. These considerations will normally limit the lowest frequency of operation to 15 to 20% above cutoff. Therefore, the details of the numerical determination of the fields will be given only for the $\text{QLSE}_{1,0}$ mode at frequencies above cutoff.

Once β is found for any given frequency $\omega > \omega_c$, i.e., det $[T'(\omega,\beta)] = 0$, the matrix T' is fixed and the vectors $\mathbf{A}_2^{(+)}$ and $\mathbf{D}_2^{(-)}$ may be calculated from Eq. (2.100). Because $A_{2,0}^{(+)}$ is effectively zero (since $k_{2,0} = 0$), the full vector $\mathbf{A}_2^{(+)}$ is thus known. The vectors $\mathbf{A}_2^{(-)}$ and $\mathbf{D}_2^{(+)}$ may be calculated from Eqs. (2.61b) and (2.61c):

$$\mathbf{A}_2^{(-)} = [Q_A^{(-)}]^{-1}\ Q_A^{(+)}\mathbf{A}_2^{(+)}$$
$$\mathbf{D}_2^{(+)} = [Q_D^{(+)}]^{-1}\ Q_D^{(-)}\mathbf{D}_2^{(-)}.$$

The remaining amplitude terms of Region 2 may then be found by using Eqs. (2.39) to (2.42), with

$$\mathbf{B}_2^{(+)} = [\psi_2]^{-1}[K_2\mathbf{A}_2^{(-)} - \omega\mu_0\beta\mathbf{D}_2^{(+)}]$$
$$\mathbf{B}_2^{(-)} = [\psi_2]^{-1}[K_2P_2^2\mathbf{A}_2^{(+)} - \omega\mu_0\beta\mathbf{D}_2^{(-)}]$$
$$\mathbf{C}_2^{(+)} = -[\psi_2]^{-1}[\beta\mathbf{A}_2^{(-)} + \omega\mu_0K_2\mathbf{D}_2^{(+)}]$$
$$\mathbf{C}_2^{(-)} = -[\psi_2]^{-1}[\beta P_2^2\mathbf{A}_2^{(+)} + \omega\mu_0K_2\mathbf{D}_2^{(-)}]$$
$$\mathbf{F}_2^{(+)} = [\psi_2]^{-1}[\omega\epsilon_2\beta\mathbf{A}_2^{(+)} - K_2\mathbf{D}_2^{(-)}]$$
$$\mathbf{F}_2^{(-)} = [\psi_2]^{-1}[\omega\epsilon_2\beta\mathbf{A}_2^{(-)} - K_2P_2^2\mathbf{D}_2^{(+)}]$$
$$\mathbf{G}_2^{(+)} = -[\psi_2]^{-1}[\omega\epsilon_2K_2\mathbf{A}_2^{(+)} + \beta\mathbf{D}_2^{(-)}]$$
$$\mathbf{G}_2^{(-)} = -[\psi_2]^{-1}[\omega\epsilon_2K_2\mathbf{A}_2^{(-)} + \beta P_2^2\mathbf{D}_2^{(+)}]$$

where the matrix Φ is replaced as βU for $\omega > \omega_c$ and the upper $(+)$ symbolism used for $\pm K_2$ since the $QLSE_{1,0}$ mode is a (M,E) mode. All of the vector elements may be calculated on a term-by-term basis in Region 2 since all of the matrices involved are diagonal.

A number of different methods could be used to find the coefficients of the field components in Region 3 once those of Region 2 are calculated. The method chosen was to first calculate $\mathbf{F}_3$ and $\mathbf{G}_3$. From Eq. (2.79c)

$$\mathbf{F}_3 = [\theta_3^{(H)}]^{-1} M_3 \mathbf{F}_2^{(+)}$$

while from Eq. (2.79d)

$$\mathbf{G}_3 = [\theta_3^{(H)}]^{-1} M_4 \mathbf{G}_2^{(+)}.$$

Determination of $\mathbf{F}_3$ and $\mathbf{G}_3$ requires matrix operations since neither M_3 or M_4 are diagonal matrices. Since $W_A = U$ and $W_D = P_3^2$ for a (M,E) mode, Eqs. (2.44) to (2.46) together with Eq. (2.31) will give

$$\mathbf{A}_3 = \frac{1}{\omega\epsilon_3}[\beta\mathbf{F}_3 - K_3\mathbf{G}_3]$$

$$\mathbf{D}_3 = -[P_3^2]^{-1}[K_3\mathbf{F}_3 + \beta\mathbf{G}_3].$$

Then Eq. (2.30) may be used to obtain

$$\mathbf{C}_3 = -[\psi_3]^{-1}[\beta\mathbf{A}_3 + \omega\mu_0 K_3\mathbf{D}_3]$$

$$\mathbf{B}_3 = [\psi_3]^{-1}[K_3\mathbf{A}_3 - \omega\mu_0\beta\mathbf{D}_3].$$

The elements of the vectors $\mathbf{A}_3$, $\mathbf{D}_3$, $\mathbf{C}_3$, and $\mathbf{B}_3$ may be calculated on a term-by-term basis since all of the matrices involved in calculating these vectors are diagonal.

The modal component coefficients of the fields in Region 1 may be found by matching tangential fields on a term-by-term basis at the air-dielectric interface, $x = -x_2$. With this procedure, terms of the form

$$a_n \cosh(p_{2,n}x_2) - b_n \sinh(p_{2,n}x_2)$$

will be encountered where the coefficients a_n and b_n approach the same value as n becomes large. For large n, the term $p_{2,n}$ is almost proportional to n, thus the cosh and sinh functions increase exponentially with n. With as few as five terms in the series expansion for the fields, significant errors can be caused by the numerical inaccuracy inherent in the calculation of the difference between two very large numbers [64]. Such computational errors may be avoided by matching the normal field components at $x = -x_2$. Using the matrix notation of Eq. (2.53),

$$\theta_1^{(H)}\mathbf{A}_1 = \epsilon_r[\theta_2^{(+)}\mathbf{A}_2^{(+)} - \theta_2^{(-)}\mathbf{A}_2^{(-)}] \tag{2.106}$$

$$\theta_1^{(E)}\mathbf{D}_1 = \theta_2^{(+)}\mathbf{D}_2^{(+)} - \theta_2^{(-)}\mathbf{D}_2^{(-)} \tag{2.107}$$

where the vector elements $A_{1,0}$, $A_{2,0}^{(+)}$ and $A_{2,0}^{(-)}$ are zero magnitude. Substitution of Eq. (2.61b) into Eq. (2.106) gives

$$\theta_1^{(H)}\mathbf{A}_1 = \epsilon_r[Q_A^{(-)}]^{-1}[Q_A^{(-)}\theta_2^{(+)} - Q_A^{(+)}\theta_2^{(-)}]\mathbf{A}_2^{(+)}.$$

Subsequent substitution for the matrices $Q_A^{(-)}$ and $Q_A^{(+)}$ from (2.62) and appropriate commutation of the diagonal matrices yields

$$\theta_1^{(H)}\mathbf{A}_1 = \epsilon_r[Q_A^{(-)}]^{-1}\{\epsilon_r P_1^2\theta_1^{(E)}[\theta_2^{(+)}\theta_2^{(-)} - \theta_2^{(+)}\theta_2^{(-)}] + \theta_1^{(H)}[\theta_2^{(+)}\theta_2^{(+)} - P_2^2\theta_2^{(-)}\theta_2^{(-)}]\}\mathbf{A}_2^{(+)}.$$

But

$$\theta_2^{(+)}\theta_2^{(+)} - P_2^2\theta_2^{(-)}\theta_2^{(-)} = U,$$

thus premultiplication by $[\theta_1^H]^{-1}$ yields

$$\mathbf{A}_1 = \epsilon_r [Q_A^{(-)}]^{-1} \mathbf{A}_2^{(+)}. \tag{2.108}$$

In a similar fashion, Eqs. (2.61c) and (2.62) may be used with Eq. (2.107) to show that

$$\mathbf{D}_1 = [Q_D^{(+)}]^{-1} \mathbf{D}_2^{(-)}. \tag{2.109}$$

The results of Eqs. (2.108) and (2.109) could also have been obtained by matching the tangential fields at $x = -x_2$ and using the relationships between the fields from Eqs. (2.16) and (2.17) to obtain cancellation of many terms. Such a procedure is straightforward but considerably more detailed than the method shown.

Once numerical quantities for the elements of $\mathbf{A}_1$ and $\mathbf{D}_1$ are found from Eqs. (2.108) and (2.109), calculation of the remaining field coefficients in Region 1 may be accomplished by using Eqs. (2.16) and (2.17) directly:

$$\mathbf{C}_1 = -[\psi_1]^{-1}[\beta P_1^2 \mathbf{A}_1 + \omega\mu_0 K_1 \mathbf{D}_1]$$

$$\mathbf{B}_1 = [\psi_1]^{-1}[K_1 P_1^2 \mathbf{A}_1 - \omega\mu_0 \beta \mathbf{D}_1]$$

$$\mathbf{F}_1 = [\psi_1]^{-1}[\omega\epsilon_0 \beta \mathbf{A}_1 - K_1 \mathbf{D}_1]$$

$$\mathbf{G}_1 = -[\psi_1]^{-1}[\omega\epsilon_0 K_1 \mathbf{A}_1 - \beta \mathbf{D}_1].$$

Since all matrices involved in the calculation of the amplitude vectors in Region 1 are diagonal, the coefficients may be determined on a term-by-term basis. The magnitude of any field may then be calculated at any point within the waveguide.

The number of terms N_T used in the series expansions of the fields affects the accuracy of the numerical solution. Numerical calculations for a variety of waveguide geometries indicated rapid convergence of solutions, for both ω_c and β. For all geometries tested, as few as five terms gave solutions within 0.5% of the numerical value obtained by using many more terms. Convergence characteristics of the cutoff frequencies for the four lowest order waveguide modes are shown in Table 1 for a typical waveguide geometry. The convergence characteristics for β of the $QLSE_{1,0}$ mode are shown in Table 2.

2.3 Peak Power Capacity

The peak power capacity of a waveguide is the maximum microwave power the waveguide will carry without arcing due to the large electric fields within the waveguide. The power level at which arcing occurs is referred to as the peak power breakdown level. The specified peak power capacity for some waveguides may include a safety factor; however, for purposes of this investigation the peak power capacity and the peak power breakdown level will be considered as equal unless otherwise noted.

The time-averaged power transmitted across any closed surface S is [40,41]

$$P = \frac{1}{2} \operatorname{Re} \iint_S \mathbf{E} \times \mathbf{H}^* \cdot d\mathbf{S}.$$

The coordinate system used in Section 2.2 will be used here also, with the waveguide axis in the $\mathbf{a}_z$ direction. Propagation again will be assumed to be in the positive $\mathbf{a}_z$ direction. The surface of integration is thus the interior cross section of the waveguide of Fig. 3, and with $d\mathbf{S} = \mathbf{a}_z dxdy$, then

$$(\mathbf{E} \times \mathbf{H}^*) \cdot d\mathbf{S} = (E_x H_y^* - E_y H_x^*) dxdy.$$

Advantage may be taken of the waveguide symmetry to limit the integration to the left half if a factor of 2 is included in the power calculations. The surface integration will be separated into three regions

Table 1 — Convergence Characteristics of Cutoff Frequencies for Different Modes

Waveguide geometry parameters:

$a = 1.0\ (2.54)$ $\quad s = 0.2\ (0.51)$

$b = 0.4\ (1.02)$ $\quad t = 0.4\ (1.02)$

$d = 0.15\ (0.38)$ $\quad \epsilon_r = 4.0$

Dimensions are in inches (cm)

Mode Cutoff Frequency in GHz

N_T	$QLSE_{1,0}$	$QLSE_{2,0}$	$QLSE_{1,1}$	$QLSM_{0,1}$
1	2.4528	9.6587	14.3651	12.3792
2	2.2497	8.8459	14.8782	12.3141
3	2.2478	8.8425	15.0177	12.3065
4	2.2392	8.8062	15.0146	12.3058
5	2.2353	8.7911	15.0555	12.2996
6	2.2352	8.7903	15.0611	12.2996
7	2.2329	8.7808	15.0667	12.2983
8	2.2327	8.7800	15.0782	12.2967
9	2.2321	8.7776	15.0776	12.2979
10	2.2313	8.7747	15.0831	12.2959
11	2.2315	8.7748	15.0862	12.2955
12	2.2310	8.7729	15.0862	12.2955
13	2.2308	8.7722	15.0899	12.2949
14	2.2308	8.7720	15.0903	12.2948
15	2.2304	8.7706	15.0915	12.2946
16	2.2304	8.7706	15.0935	12.2943

Table 2 — Convergence Characteristics of Waveguide Parameters for $QLSE_{1,0}$ Mode

Waveguide geometry parameters:

$a = 1.0\ (2.54)$ $s = 0.2\ (0.51)$

$b = 0.4\ (1.02)$ $t = 0.4\ (1.02)$

$d = 0.15\ (0.38)$ $\epsilon_r = 4.0$ $\tan\delta = 10^{-4}$

Dimensions are in inches (cm) Copper Walls

Frequency = 3.5 GHz $QLSE_{1,0}$ f_c = 2.23 GHz

N_T	β (°/cm)	Breakdown Power (kW)[1]	Breakdown Power (kW)[2]	α_c (dB/meter)	α_d (dB/meter)
1	365.89	6009.4	7195.8	0.1791	0.0818
2	395.17	2863.4	8984.8	0.1806	0.0768
3	395.48	2841.2	8957.5	0.1858	0.0768
4	396.65	2833.8	9120.1	0.1885	0.0766
5	397.18	2837.0	9187.4	0.1902	0.0765
6	397.21	2835.1	9188.9	0.1916	0.0765
7	397.54	2830.4	9221.6	0.1929	0.0765
8	397.56	2831.2	9225.3	0.1935	0.0765
9	397.61	2828.7	9232.6	0.1946	0.0765
10	397.54	2828.0	9242.6	0.1951	0.0765
11	397.54	2838.3	9242.0	0.1957	0.0765
12	397.76	2826.4	9248.7	0.1964	0.0765
13	397.81	2826.6	9250.9	0.1966	0.0764
14	397.81	2826.1	9251.5	0.1970	0.0764
15	397.84	2825.4	9255.6	0.1973	0.0764
16	397.84	2845.4	9321.3	0.1963	0.0768

Notes:

(1) Power for breakdown at air-dielectric interface

(2) Power for breakdown in dielectric

to conform with the region definition shown in Fig. 4. Since the expressions developed for the transverse fields E_x, E_y, H_x, and H_y are real, the power carried by the waveguide is

$$P = 2 \sum_{i=1}^{3} P_i \tag{2.110a}$$

with

$$P_i = \frac{1}{2} \int_x \int_y [E_x^{(i)} H_y^{(i)} - E_y^{(i)} H_x^{(i)}] dx dy \tag{2.110b}$$

where the i subscripts and superscripts denote the particular region and with the appropriate integration limits for each region.

The only propagating mode for which power breakdown is of interest for this investigation is the dominant, or $QLSE_{1,0}$ mode. For this mode, in each region the nth modal component of E_x and H_y has a y-dependence given by $\sin(2n\pi y/h)$, while the nth modal component of E_y and H_x has a y-dependence given by $\cos(2n\pi y/h)$, where h is the height of the region. Because of the orthogonality of these functions, the cross products generated by substitution of the series representation for the fields will vanish when the y integration is performed. Thus the expression for the power in each region may be reduced to

$$P_i = \frac{1}{2} \sum_n \int_x \int_y [E_{x,n}^{(i)} H_{y,n}^{(i)} - E_{y,n}^{(i)} H_{x,n}^{(i)}] dx dy \tag{2.111}$$

where the n subscript on each field quantity denotes the nth modal component for that field. For the dominant mode, the lower limit on n in the summation is zero. The upper limit is theoretically infinite, as in the analysis to determine the propagation characteristics; but as in the latter analysis, the number of terms must be truncated at some finite value for a numerical solution. The number of terms that can be used to find P_i is obviously limited by the number of terms N_T used in the propagation analysis, and for power breakdown calculations will be set equal to N_T. The effect of the series truncation on power breakdown determination will be discussed after the mathematical development has been completed.

In Region 1, substitution of the series representation for the fields from Eq. (2.12) into Eq. (2.111) gives

$$P_1 = \frac{1}{2} \sum_{n=1}^{N_2} \left\{ A_{1,n} F_{1,n} I_{1,n}^{cc} \int_{-b/2}^{b/2} \sin^2(2n\pi y/b) dy - B_{1,n} D_{1,n} I_{1,n}^{ss} \int_{-b/2}^{b/2} \cos^2(2n\pi y/b) dy \right\}$$

where

$$I_{1,n}^{cc} = \int_{-x_1}^{-x_2} \cosh^2[p_{1,n}(x + x_1)] dx$$

and

$$I_{1,n}^{ss} = \int_{-x_1}^{-x_2} \sinh^2[p_{1,n}(x + x_1)]/p_{1,n}^2 \, dx.$$

The mathematical identities

$$\cosh^2\theta = (\cosh 2\theta + 1)/2 \tag{2.112a}$$

$$\sinh^2\theta = (\cosh 2\theta - 1)/2 \tag{2.112b}$$

may be used to evaluate $I_{1,n}^{cc}$ and $I_{1,n}^{ss}$ as

$$I_{1,n}^{cc} = \{\cosh[p_{1,n}(x_1 - x_2)] \sinh[p_{1,n}(x_1 - x_2)]/p_{1,n} + (x_1 - x_2)\}/2$$

$$I_{1,n}^{ss} = \{\cosh[p_{1,n}(x_1 - x_2)] \sinh[p_{1,n}(x_1 - x_2)]/p_{1,n} - (x_1 - x_2)\}/2\, p_{1,n}^2.$$

After the y integration is performed, the expression for P_1 becomes

$$P_1 = -\frac{bB_{1,0}D_{1,0}}{2} I^{ss}_{1,0} + \frac{b}{4}\sum_{n=1}^{N_2} (A_{1,n}F_{1,n}I^{cc}_{1,n} - B_{1,n}D_{1,n}I^{ss}_{1,n}). \tag{2.113}$$

In Region 3, substitution of the series representation for the fields from Eq. (2.25) into Eq. (2.111) gives

$$P_3 = \frac{1}{2}\sum_{n=0}^{N_2}\left\{A_{3,n}F_{3,n}I^{ss}_{3,n}\int_{-d/2}^{d/2}\sin^2(2n\pi y/d)\,dy - B_{3,n}D_{3,n}I^{cc}_{3,n}\int_{-d/2}^{d/2}\cos^2(2n\pi y/d)\,dy\right\}$$

where

$$I^{ss}_{3,n} = \int_0^{x_3}\sinh^2[p_{3,n}(x - x_3)]/p^2_{3,n}\,dx$$

and

$$I^{cc}_{3,n} = \int_0^{x_3}\cosh^2[p_{3,n}(x - x_3)]\,dx.$$

The mathematical identities given in Eq. (2.112) may be used to evaluate $I^{ss}_{3,n}$ and $I^{cc}_{3,n}$ as

$$I^{ss}_{3,n} = [\cosh\,(p_{3,n}x_3)\,\sinh\,(p_{3,n}x_3)/p_{3,n} - x_3]/2p^2_{3,n}$$
$$I^{cc}_{3,n} = [\cosh\,(p_{3,n}x_3)\,\sinh\,(p_{3,n}x_3)/p_{3,n} + x_3]/2.$$

The y integration will then yield

$$P_3 = -\frac{dB_{3,0}D_{3,0}}{2} I^{cc}_{3,0} + \frac{d}{4}\sum_{n=1}^{N_2}(A_{3,n}F_{3,n}I^{ss}_{3,n} - B_{3,n}D_{3,n}I^{cc}_{3,n}) \tag{2.114}$$

In Region 2, the series representation of the fields from Eq. (2.35) is more complicated than in Regions 1 and 3, and substitution into Eq. (2.111) will give rise to additional terms:

$$P_2 = \frac{1}{2}\sum_{n=0}^{N_2}\left\{[A^{(+)}_{2,n}F^{(+)}_{2,n}I^{cc}_{2,n} + A^{(-)}_{2,n}F^{(-)}_{2,n}I^{ss}_{2,n} + (A^{(-)}_{2,n}F^{(+)}_{2,n} + A^{(+)}_{2,n}F^{(-)}_{2,n})I^{sc}_{2,n}]\int_{-b/2}^{b/2}\sin^2(2n\pi y/b)\,dy\right.$$
$$\left. - [B^{(+)}_{2,n}D^{(+)}_{2,n}I^{cc}_{2,n} + B^{(-)}_{2,n}D^{(-)}_{2,n}I^{ss}_{2,n} + (B^{(-)}_{2,n}D^{(+)}_{2,n} + B^{(+)}_{2,n}D^{(-)}_{2,n})I^{sc}_{2,n}]\int_{-b/2}^{b/2}\cos^2(2n\pi y/b)\,dy\right\}$$

where

$$I^{cc}_{2,n} = \int_{-x_2}^{0}\cosh^2(p_{2,n}x)\,dx$$

$$I^{ss}_{2,n} = \int_{-x_2}^{0}\sinh^2(p_{2,n}x)/p^2_{2,n}\,dx$$

$$I^{sc}_{2,n} = \int_{-x_2}^{0}\cosh\,(p_{2,n}x)\,\sinh\,(p_{2,n}x)/p_{2,n}\,dx.$$

Again, using the identities given in Eq. (2.112), the hyperbolic integrals may be evaluated as

$$I^{cc}_{2,n} = [\cosh\,(p_{2,n}x_2)\,\sinh\,(p_{2,n}x_2)/p_{2,n} + x_2]/2$$
$$I^{ss}_{2,n} = [\cosh\,(p_{2,n}x_2)\,\sinh\,(p_{2,n}x_2)/p_{2,n} - x_2]/2p^2_{2,n}$$
$$I^{sc}_{2,n} = -\,[\sinh\,(p_{2,n}x_2)/p_{2,n}]^2/2.$$

After performing the y integration

$$P_2 = -\frac{b}{2}[B_{2,0}^{(+)}D_{2,0}^{(+)}I_{2,0}^{cc} + B_{2,0}^{(-)}D_{2,0}^{(-)}I_{2,0}^{ss} + (B_{2,0}^{(-)}D_{2,0}^{(+)} + B_{2,0}^{(+)}D_{2,0}^{(-)})I_{2,0}^{sc}]$$
$$+ \frac{b}{4}\sum_{n=1}^{N_2}\Big\{[A_{2,n}^{(+)}F_{2,n}^{(+)} - B_{2,n}^{(+)}D_{2,n}^{(+)}]I_{2,n}^{cc} + [A_{2,n}^{(-)}F_{2,n}^{(-)} - B_{2,n}^{(-)}D_{2,n}^{(-)}]I_{2,n}^{ss}$$
$$+ [A_{2,n}^{(-)}F_{2,n}^{(+)} + A_{2,n}^{(+)}F_{2,n}^{(-)} - B_{2,n}^{(-)}D_{2,n}^{(+)} - B_{2,n}^{(+)}D_{2,n}^{(-)}]I_{2,n}^{sc}\Big\}. \tag{2.115}$$

Calculations using Eq. (2.115) directly will cause numerical errors when the number of terms N_T in the series expansion for the fields is large. These errors arise because Eq. (2.115) requires taking the difference between two very large numbers, analogous to the situation when calculating numerical values for the modal amplitudes in Region 1 as discussed in Section 2.2. Such numerical accuracy problems may be avoided in this case by using the elements of the Q matrices from Eq. (2.62) to reduce the expression given in Eq. (2.115). Using the notation of Eq. (2.54), with

$$\theta_{2,n}^{(+)} = \cosh\,(p_{2,n}x_2)$$
$$\theta_{2,n}^{(-)} = \sinh\,(p_{2,n}x_2)/p_{2,n}$$

then

$$I_{2,n}^{cc} = [\theta_{2,n}^{(+)}\theta_{2,n}^{(-)} + x_2]/2 \tag{2.116a}$$
$$I_{2,n}^{ss} = [\theta_{2,n}^{(+)}\theta_{2,n}^{(-)} - x_2]/2p_{2,n}^2 \tag{2.116b}$$
$$I_{2,n}^{sc} = -[\theta_{2,n}^{(-)}]^2/2. \tag{2.116c}$$

In Eq. (2.115) the notation

$$\phi_{2,n}^{AF} = A_{2,n}^{(+)}F_{2,n}^{(+)}I_{2,n}^{cc} + A_{2,n}^{(-)}F_{2,n}^{(-)}I_{2,n}^{ss} + [A_{2,n}^{(-)}F_{2,n}^{(+)} + A_{2,n}^{(+)}F_{2,n}^{(-)}]I_{2,n}^{sc} \tag{2.117}$$

and

$$\phi_{2,n}^{BD} = B_{2,n}^{(+)}D_{2,n}^{(+)}I_{2,n}^{cc} + B_{2,n}^{(-)}D_{2,n}^{(-)}I_{2,n}^{ss} + [B_{2,n}^{(-)}D_{2,n}^{(+)} + B_{2,n}^{(+)}D_{2,n}^{(-)}]I_{2,n}^{sc} \tag{2.118}$$

will be used for all values of n. Substitution of Eqs. (2.116) into (2.117) will yield

$$\phi_{2,n}^{AF} = x_2[A_{2,n}^{(+)}F_{2,n}^{(+)} - A_{2,n}^{(-)}F_{2,n}^{(-)}/p_{2,n}^2]/2$$
$$+ \theta_{2,n}^{(-)}F_{2,n}^{(+)}[\theta_{2,n}^{(+)}A_{2,n}^{(+)} - \theta_{2,n}^{(-)}A_{2,n}^{(-)}]/2 + \theta_{2,n}^{(-)}F_{2,n}^{(-)}[\theta_{2,n}^{(+)}A_{2,n}^{(-)}/p_{2,n}^2 - \theta_{2,n}^{(-)}A_{2,n}^{(+)}]/2.$$

From Eq. (2.61b)

$$Q_{A,n}^{(+)}A_{2,n}^{(+)} = Q_{A,n}^{(-)}A_{2,n}^{(-)}$$

thus,

$$\theta_{2,n}^{(+)}A_{2,n}^{(+)} - \theta_{2,n}^{(-)}A_{2,n}^{(-)} = [Q_{A,n}^{(-)}\theta_{2,n}^{(+)} - Q_{A,n}^{(+)}\theta_{2,n}^{(-)}]A_{2,n}^{(+)}/Q_{A,n}^{(-)} \tag{2.119}$$

$$\theta_{2,n}^{(+)}A_{2,n}^{(-)}/p_{2,n}^2 - \theta_{2,n}^{(-)}A_{2,n}^{(+)} = [Q_{A,n}^{(+)}\theta_{2,n}^{(+)}/p_{2,n}^2 - Q_{A,n}^{(-)}\theta_{2,n}^{(-)}]A_{2,n}^{(+)}/Q_{A,n}^{(-)}. \tag{2.120}$$

From Eqs. (2.62a) and (2.62b)

$$Q_{A,n}^{(+)} = \epsilon_r p_{1,n}^2\theta_{1,n}^{(E)}\theta_{2,n}^{(+)} + p_{2,n}^2\theta_{1,n}^{(H)}\theta_{2,n}^{(-)} \tag{2.121a}$$

$$Q_{A,n}^{(-)} = \epsilon_r p_{1,n}^2\theta_{1,n}^{(E)}\theta_{2,n}^{(-)} + \theta_{1,n}^{(H)}\theta_{2,n}^{(+)} \tag{2.121b}$$

where $\theta_{1,n}^{(E)}$ and $\theta_{1,n}^{(H)}$ are given by Eq. (2.53). Substitution of Eq. (2.121) into Eqs. (2.119) and (2.120), with proper rearrangement of terms and use of the mathematical identity

$$\cosh^2\zeta - \sinh^2\zeta = 1,$$

will yield

$$\theta_{2,n}^{(+)}A_{2,n}^{(+)} - \theta_{2,n}^{(-)}A_{2,n}^{(-)} = \theta_{1,n}^{(H)}A_{2,n}^{(+)}/Q_{A,n}^{(-)}$$

$$\theta_{2,n}^{(+)}A_{2,n}^{(-)}/p_{2,n}^2 - \theta_{2,n}^{(-)}A_{2,n}^{(+)} = \epsilon_r p_{1,n}^2\theta_{1,n}^{(E)}A_{2,n}^{(+)}/[p_{2,n}^2 Q_{A,n}^{(-)}.]$$

Thus, $\phi_{2,n}^{AF}$ may be expressed as

$$\phi_{2,n}^{AF} = \frac{1}{2}\left\{x_2[A_{2,n}^{(+)}F_{2,n}^{(+)} - A_{2,n}^{(-)}F_{2,n}^{(-)}/p_{2,n}^2] + \theta_{2,n}^{(-)}A_{2,n}^{(+)}[\theta_{1,n}^{(H)}F_{2,n}^{(+)} + \epsilon_r p_{1,n}^2\theta_{1,n}^{(E)}F_{2,n}^{(-)}/p_{2,n}^2]/Q_{A,n}^{(-)}\right\}. \quad (2.122)$$

In a similar fashion, substituting Eq. (2.116) into Eq. (2.118) and using Eqs. (2.61c), (2.62c), and (2.62d) will yield

$$\phi_{2,n}^{BD} = \frac{1}{2}\left\{x_2[B_{2,n}^{(+)}D_{2,n}^{(+)} - B_{2,n}^{(-)}D_{2,n}^{(-)}/p_{2,n}^2] + \theta_{2,n}^{(-)}D_{2,n}^{(-)}[\theta_{1,n}^{(E)}B_{2,n}^{(+)} + \theta_{1,n}^{(H)}B_{2,n}^{(-)}/p_{2,n}^2]/Q_{D,n}^{(+)}\right\}. \quad (2.123)$$

The expression for the power in Region 2 then becomes

$$P_2 = -\frac{b}{2}\phi_{2,0}^{BD} + \frac{b}{4}\sum_{n=1}^{N_2}(\phi_{2,n}^{AF} - \phi_{2,n}^{BD}). \quad (2.124)$$

If in both Eqs. (2.122) and (2.123), the quantities $\theta_{1,n}^{(H)}$ and $\theta_{1,n}^{(E)}$ are calculated as

$$\theta_{1,n}^{(H)} = \exp\,[p_{1,n}(x_1 - x_2)]\{1 + \exp\,[-2p_{1,n}(x_1 - x_2)]\}/2 \quad (2.125a)$$

$$\theta_{1,n}^{(E)} = \exp\,[p_{1,n}(x_1 - x_2)]\{1 - \exp\,[-2p_{1,n}(x_1 - x_2)]\}/2p_{1,n} \quad (2.125b)$$

and the common exponential term taken outside the brackets, the numerical computation does not require taking the difference between two very large numbers.

Calculations in all regions must consider the sign of $p_{i,n}^2$. For those modal components where $p_{i,n}^2$ is negative, the hyperbolic functions may be replaced by their trigonometric counterparts with

$$p_{i,n} = \sqrt{-p_{i,n}^2} \text{ for } p_{i,n}^2 < 0.$$

The power being carried by the waveguide, as calculated from Eq. (2.110) together with Eqs. (2.113), (2.114), and (2.124), is dependent on the magnitude of the (arbitrary) normalization constant used in solving for the eigenvector of amplitude coefficients in Eq. (2.100). Since the waveguide is a linear device, the power is proportional to the square of the electric field magnitude. Using a zero subscript to denote numerical quantities corresponding to the eigenvector normalization,

$$P/|\mathbf{E}|^2 = P_0/|\mathbf{E}_0|^2 \quad (2.126)$$

for a given waveguide geometry and fixed frequency. The equality is valid for the electric field at any point and in any direction as long as $\mathbf{E}$ and $\mathbf{E}_0$ are similarly defined.

Peak power breakdown in the dielectric loaded ridged waveguide of Fig. 3 will occur when either (1) the maximum electric field in the air region exceeds the electric breakdown strength of air, E_{air}^{BD}, or (2) the maximum electric field in the dielectric exceeds the electric breakdown strength of the dielectric, $E_{\text{dielectric}}^{BD}$. In any complete rigorous analysis, such as this approach with an infinite number of terms in the series expansion for the fields, a singularity in $\mathbf{E}$ will be found at the corners of the ridge [11,14,66]. Any ridged waveguide with perfectly square ridge corners would, in theory, break down at

vanishing small power levels. However, if the corners of the ridge are slightly rounded, as is done in practice [11], the **E** fields remain finite. The ratio of the maximum electric field intensity at the ridge corners, E_s, to that at the center of the ridge, E_c, is then a function of the corner radius [11]. Peak power breakdown will occur in the dielectric when $E_s > E^{BD}_{\text{dielectric}}$. Different dielectric materials have different breakdown strengths which in general will be dependent on several variables such as dielectric thickness and moisture content [25,26]. Rather than introduce additional parameters, the power breakdown aspect of this investigation will make the following assumptions unless otherwise noted: (1) the breakdown strength of the dielectric is 10 times that of dry air, and (2) the E_s/E_c ratio is 2.5. The basis for the first assumption is the dielectric strength of polystyrene, with $E^{BD} = 700$ volts/mil [25]. Other dielectrics such as polyethylene have substantially greater breakdown strengths [26]. The basis for the second assumption is the article by Hopfer on ridged waveguide [11] which shows a ratio of 2.5 for E_s/E_c to be a conservative value. For most configurations of the dielectric loaded ridged waveguide, air breakdown will occur at a much lower power level than that for breakdown in the dielectric, and the exact values of E_s/E_c and $E^{BD}_{\text{dielectric}}$ will not be relevant. If the waveguide is such that the actual value of either of these two parameters is sufficiently different from the assumed values—larger E_s/E_c or smaller $E^{BD}_{\text{dielectric}}$—so as to result in dielectric breakdown at a lower power level than that for air breakdown, appropriate corrections must be made for power breakdown.

At all points in the waveguide, the axially directed electric field E_z is small in comparison with the transverse electric field $\mathbf{E}_T$, where $\mathbf{E}_T = \mathbf{a}_x E_x + \mathbf{a}_y E_y$, for the dominant, or $\text{QLSE}_{1,0}$ mode at frequencies above cutoff. Since E_z is in phase quadrature with E_x and E_y, the maximum electric field will lie in the x-y plane. At the center of the waveguide E_x is zero for the $\text{QLSE}_{1,0}$ mode because of the effective magnetic wall at that plane; thus, the maximum electric field will be $|E_y|_{\max}$. From Eq. (2.25b), E_y at the waveguide center is

$$E_y|_{x=x_3} = \sum_{n=0}^{N_2} B_{3,n} \cos(2n\pi y/d).$$

Since the coefficients $B_{3,n}$ are a function of frequency and waveguide geometry, no rigorous procedure is available to find the maximum in terms of a general function of the coefficients. Investigation of numerous configurations, however, has shown the coefficients to alternate in sign. At the ridge surfaces, $y = \pm d/2$,

$$E_y|_{x=x_3} = \sum_{n=0}^{N_2} (-1)^n B_{3,n};$$

thus, the maximum value of E_y occurs at the ridge. Calculation of E_c as

$$E_c = \sum_{n=0}^{N_2} |B_{3,n}| \tag{2.127}$$

must then be a worst case condition since

$$|E_y(x = x_3)| \leqslant E_c \tag{2.128}$$

where the equality in Eq. (2.128) is valid at $y = \pm d/2$ for all of the many waveguide geometries that were checked. The maximum electric field within the dielectric will then be taken as 2.5 E_c with E_c calculated from Eq. (2.127). The peak power level for dielectric breakdown is thus

$$P^{BD}_{\text{dielectric}} = \frac{(10\, E^{BD}_{\text{air}})^2 P_0}{[2.5\Sigma|B_{3,n}|]^2}$$

or

$$P^{BD}_{\text{dielectric}} = 16\,(E^{BD}_{\text{air}})^2 P_0 \Big/ \left[\sum_{n=0}^{N_2} |B_{3,n}|\right]^2 \tag{2.129}$$

where the coefficients $B_{3,n}$ are the same used to calculate the normalized power P_0. Unless otherwise noted, the value for air breakdown will be taken [11,25] as

$$E_{\text{air}}^{BD} = 30{,}000 \text{ volts/cm}. \tag{2.130}$$

In the air region, the maximum electric field will occur at the air-dielectric interface, $x = -x_2$ in Fig. 4. At this plane, the fields are found from Eqs. (2.12)

$$E_x|_{x=-x_2} = \sum_{n=1}^{N_2} A_{1,n} \cosh\,[p_{1,n}(x_1 - x_2)] \sin\,(2n\pi y/b)$$

$$E_y|_{x=-x_2} = \sum_{n=1}^{N_2} B_{1,n} \sinh\,[p_{1,n}(x_1 - x_2)]/p_{1,n} \cos\,(2n\pi y/b).$$

The magnitude of the transverse field is

$$|\mathbf{E}_T| = (E_x^2 + E_y^2)^{1/2}.$$

Investigation of several waveguide geometries showed the point of maximum $|\mathbf{E}_T|$ to occur at varying distances from the horizontal plane of symmetry at $y = 0$, depending upon the thickness of the dielectric piece and the ridge gap. For large $(t - s)/d$ ratios, the maximum occurs at $y = 0$; as this ratio decreases the point of maximum $|\mathbf{E}_T|$ approaches $y = d/2$. Such behavior is to be expected when the fringing nature of the fields due to the ridge is considered. To determine the maximum electric field in the air region, $|\mathbf{E}_T|$ was calculated at $x = -x_2$ for 33 equally spaced points for y, from $y = 0$ to $y = d/2$, with $|\mathbf{E}_T|_{\max}$ taken as the maximum of these values. The peak power level for air breakdown is thus calculated as

$$P_{\text{air}}^{BD} = P_0(E_{\text{air}}^{BD})^2/|\mathbf{E}_T|_{\max}^2 \tag{2.131}$$

where the coefficients used to find $|\mathbf{E}_T|_{\max}$ are the same used to calculate the normalized power P_0.

Of course, the peak power capacity of the waveguide is the lesser of the two breakdown power levels, P_{air}^{BD} or $P_{\text{dielectric}}^{BD}$. As mentioned earlier, the power capacity will be limited by air breakdown for most of the configurations investigated. The distinction will be made apparent for those conditions where breakdown is in the dielectric rather than in the air.

Convergence characteristics of the numerical values calculated for power breakdown, both in air and in the dielectric, are shown in Table 2 for a typical waveguide geometry. While the calculated values for power do not converge as rapidly with increasing N_T as do the values for f_c or β, as few as four terms in the series expansion for the fields will generally yield a value within $\pm 2\%$ of that obtained using many more terms.

2.4 Attenuation Calculations from Perturbation of the Lossless Condition

Up until this point, the waveguide of Fig. 3 has been assumed to be lossless, with the complex propagation constant $\gamma = \alpha + j\beta$ having the loss term α equal to zero. This is a conventional assumption made when deriving the propagation characteristics of low loss transmission lines such as waveguide [1,2,16,41]. Of course, any physical transmission media has some finite loss. If the transmission loss is small, the conventional approach to theoretically determine the loss term is to assume that the perturbation of the actual (lossy) fields from the fields of the lossless condition is negligible. The lossless field distribution, together with parameters such as the conductivity of metallic conductors and the loss factor of dielectric materials, is then used to calculate the loss term [1,2]. Such an approach will be used to calculate the loss of the dielectric slab loaded ridged waveguide of this investigation.

For this attenuation analysis, the axis definition of Fig. 4 will be used and propagation in the positive $\mathbf{a}_z$ direction will be assumed. Each of the fields of the waveguide will vary as exp $(-\alpha z)$, thus the power will vary as exp $(-2\alpha z)$. If the power flow at a point z_0 is P_0, the power flow at a point incrementally removed from z_0, $z_0 + \Delta z$, is P_0 exp $(-2\alpha\Delta z)$. Thus,

$$P(z = z_0) - P(z = z_0 + \Delta z) = P_0[1 - \exp(-2\alpha\Delta z)].$$

If the increment Δz is small,

$$P(z = z_0) - P(z = z_0 + \Delta z) = W_L \Delta z$$

where W_L is the power lost per unit length of the waveguide. Thus,

$$P_0[1 - \exp(-2\alpha\Delta z)] = W_L \Delta z$$

and if the series expansion

$$\exp(-x) = 1 - x + x^2/2! - x^3/3! + \ldots$$

is used for the exponential term, then in the limit as Δz approaches zero

$$\alpha = W_L/2P_0. \tag{2.132}$$

For the purposes of this investigation, the power loss will be attributed to two factors only: (1) the imperfectly conducting metal walls of the waveguide, and (2) the finite resistivity of the dielectric material used in the center region of the waveguide. Such additional factors as radiation loss are not applicable. Loss in the air dielectric region will be neglected.

The power per unit length dissipated in the waveguide walls is given by [1,2]

$$W_c = \frac{R_s}{2}\oint_c |\mathbf{J}_s|^2 dl \tag{2.133}$$

where $\mathbf{J}_s$ is the surface current density and R_s is the surface resistivity of the metal. The contour integration is clockwise around the waveguide boundary. The surface current density is assumed to be that of the lossless waveguide, with [40,44]

$$\mathbf{J}_s = \mathbf{n} \times \mathbf{H}$$

where $\mathbf{n}$ is the unit vector normal to the conducting surface. Thus,

$$|\mathbf{J}_s|^2 = |\mathbf{H}_t|^2$$

where $\mathbf{H}_t$ is the tangential component of magnetic field at the surface. The surface resistance R_s is [2,45]

$$R_s = \sqrt{\pi f \mu/\sigma}$$

where f is the frequency in Hertz, μ is the permeability of the metal (usually $\mu = \mu_0$), and σ is the conductivity of the metal. The attenuation due to conductor losses then becomes

$$\alpha_c = \frac{R_s \oint_c |\mathbf{H}_t|^2 dl}{4P_0}. \tag{2.134}$$

The power flow P_0 in the waveguide has already been derived in Section 2.3 and will not be repeated here.

Advantage will be taken of the field symmetry to calculate the conductor losses. Defining the following surfaces of Fig. 4 as

$$S_1: \quad x = -x_1, -b/2 \leqslant y \leqslant b/2$$

$$S_2: \quad -x_1 \leqslant x \leqslant -x_2, y = b/2$$

$$S_3: \quad -x_2 \leqslant x \leqslant 0, y = b/2$$

$$S_4: \quad x = 0, d/2 \leqslant y \leqslant b/2$$

$$S_5: \quad 0 \leqslant x \leqslant x_3, y = d/2$$

and letting $W_c^{(i)}$ be the corresponding power per unit length dissipated at each surface, then

$$W_c = 2W_c^{(1)} + 4(W_c^{(2)} + W_c^{(3)} + W_c^{(4)} + W_c^{(5)}). \tag{2.135}$$

On the surface S_1

$$W_c^{(1)} = \frac{R_s}{2} \int_{-b/2}^{b/2} \left[|H_y^{(1)}|^2 + |H_z^{(1)}|^2\right]_{x=-x_1} dy.$$

Substituting the series expansion from Eqs. (2.12) for the fields $H_y^{(1)}$ and $H_z^{(1)}$ gives

$$W_c^{(1)} = \frac{R_s}{2} \sum_{n=0}^{N_2} \sum_{m=0}^{N_2} \left[F_{1,n}F_{1,m}\int_{-b/2}^{b/2} \sin(2n\pi y/b) \sin(2m\pi y/b)dy \right.$$
$$\left. + G_{1,n}G_{1,m}\int_{-b/2}^{b/2} \cos(2n\pi y/b) \cos(2m\pi y/b)dy\right].$$

Because of the orthogonality of the y-dependent functions on the interval $-b/2 \leqslant y \leqslant b/2$, the last equation reduces to

$$W_c^{(1)} = \frac{bR_s}{4}\left[2G_{1,0}^2 + \sum_{n=1}^{N_2} (F_{1,n}^2 + G_{1,n}^2)\right]. \tag{2.136}$$

On the surface S_2

$$W_c^{(2)} = \frac{R_s}{2} \int_{-x_1}^{-x_2} [|H_x^{(1)}|^2 + |H_z^{(1)}|^2]_{y=b/2} dx.$$

Substitution of the series expansion from Eqs. (2.12) for $H_x^{(1)}$ and $H_z^{(1)}$ then yields

$$W_c^{(2)} = \frac{R_s}{2} \sum_{n=0}^{N_2} \sum_{m=0}^{N_2} (-1)^{n+m} [D_{1,n}D_{1,m}\psi_{1,nm}^{ss} + G_{1,n}G_{1,m}\,\psi_{1,nm}^{cc}]$$

where the x integration is that for Region 1, with

$$\psi_{1,nm}^{ss} = \int_{-x_1}^{-x_2} \frac{\sinh[p_{1,n}(x + x_1)] \sinh[p_{1,m}(x + x_1)]}{p_{1,n}\,p_{1,m}}\, dx$$

and

$$\psi_{1,nm}^{cc} = \int_{-x_1}^{-x_2} \cosh[p_{1,n}(x + x_1)] \cosh[p_{1,m}(x + x_1)]dx.$$

These two integrals may be evaluated as

$$\psi_{1,nm}^{ss} = \{\cosh[p_{1,n}(x_1 - x_2)]\sinh[p_{1,m}(x_1 - x_2)]/p_{1,m} - \cosh[p_{1,m}(x_1 - x_2)]\sinh[p_{1,n}(x_1 - x_2)]/p_{1,n}\}/(p_{1,n}^2 - p_{1,m}^2) \qquad \text{for } n \neq m$$

$$\psi_{1,nm}^{ss} = \{\cosh[p_{1,n}(x_1 - x_2)]\sinh[p_{1,n}(x_1 - x_2)]/p_{1,n} - (x_1 - x_2)\}/2p_{1,n}^2 \qquad \text{for } n = m$$

$$\psi_{1,nm}^{cc} = \{p_{1,n}^2\cosh[p_{1,m}(x_1 - x_2)]\sinh[p_{1,n}(x_1 - x_2)]/p_{1,n} - p_{1,m}^2\cosh[p_{1,n}(x_1 - x_2)]\sinh[p_{1,m}(x_1 - x_2)]/p_{1,m}\}/(p_{1,n}^2 - p_{1,m}^2) \qquad \text{for } n \neq m$$

$$\psi_{1,nm}^{cc} = \{\cosh[p_{1,n}(x_1 - x_2)]\sinh[p_{1,n}(x_1 - x_2)]/p_{1,n} + (x_1 - x_2)\}/2 \text{ for } n = m.$$

On the surface S_3

$$W_c^{(3)} = \frac{R_s}{2}\int_{-x_2}^{0}\left[|H_x^{(2)}|^2 + |H_z^{(2)}|^2\right]_{y=b/2} dx.$$

Substitution of the series representation for the fields $H_x^{(2)}$ and $H_y^{(2)}$ from Eqs. (2.35) gives

$$W_c^{(3)} = \frac{R_s}{2}\sum_{n=0}^{N_2}\sum_{m=0}^{N_2}(-1)^{n+m}\left\{\psi_{2,nm}^{cc}\left[D_{2,n}^{(+)}D_{2,m}^{(+)} + G_{2,n}^{(+)}G_{2,m}^{(+)}\right] + \psi_{2,nm}^{cs}\left[D_{2,n}^{(+)}D_{2,m}^{(-)} + G_{2,n}^{(+)}G_{2,m}^{(-)}\right] + \psi_{2,nm}^{sc}\left[D_{2,n}^{(-)}D_{2,m}^{(+)} + G_{2,n}^{(-)}G_{2,m}^{(+)}\right] + \psi_{2,nm}^{ss}\left[D_{2,n}^{(-)}D_{2,m}^{(-)} + G_{2,n}^{(-)}G_{2,m}^{(-)}\right]\right\} \tag{2.138}$$

where the x integration is that for Region 2, with

$$\psi_{2,nm}^{cc} = \int_{-x_2}^{0}\cosh(p_{2,n}x)\cosh(p_{2,m}x)\,dx$$

$$\psi_{2,nm}^{cs} = \int_{-x_2}^{0}\cosh(p_{2,n}x)\sinh(p_{2,m}x)/p_{2,m}\,dx$$

$$\psi_{2,nm}^{sc} = \int_{-x_2}^{0}\cosh(p_{2,m}x)\sinh(p_{2,n}x)/p_{2,n}\,dx$$

$$\psi_{2,nm}^{ss} = \int_{-x_2}^{0}\frac{\sinh(p_{2,n}x)\sinh(p_{2,m}x)}{p_{2,n}p_{2,m}}\,dx.$$

After integrating with respect to x, these integrals are found to be

$$\psi_{2,nm}^{cc} = \{p_{2,n}^2\cosh(p_{2,m}x_2)\sinh(p_{2,n}x_2)/p_{2,n} - p_{2,m}^2\cosh(p_{2,n}x_2)\sinh(p_{2,m}x_2)/p_{2,m}\}/(p_{2,n}^2 - p_{2,m}^2) \qquad \text{for } n \neq m \tag{2.139a}$$

$$\psi_{2,nm}^{cc} = \{\cosh(p_{2,n}x_2)\sinh(p_{2,n}x_2)/p_{2,n} + x_2\}/2 \qquad \text{for } n = m \tag{2.139b}$$

$$\psi_{2,nm}^{cs} = \{\cosh(p_{2,n}x_2)\cosh(p_{2,m}x_2) - 1 - p_{2,n}^2\frac{\sinh(p_{2,n}x_2)\sinh(p_{2,m}x_2)}{p_{2,n}p_{2,m}}\}/(p_{2,n}^2 - p_{2,m}^2) \qquad \text{for } n \neq m \tag{2.139c}$$

$$\psi_{2,nm}^{cs} = \{1 - \cosh^2(p_{2,n}x_2)\}/2p_{2,n}^2 \qquad \text{for } n = m \tag{2.139d}$$

$$\psi_{2,nm}^{sc} = \{1 - \cosh(p_{2,n}x_2)\cosh(p_{2,m}x_2) + p_{2,m}^2\frac{\sinh(p_{2,n}x_2)\sinh(p_{2,m}x_2)}{p_{2,n}p_{2,m}}\}/(p_{2,n}^2 - p_{2,m}^2) \qquad \text{for } n \neq m \tag{2.139e}$$

$$\psi_{2,nm}^{sc} = \{1 - \cosh^2(p_{2,n}x_2)\}/2p_{2,n}^2 \qquad \text{for } n = m \tag{2.139f}$$

$$\psi^{ss}_{2,nm} = \{\cosh(p_{2,n}x_2)\sinh(p_{2,m}x_2)/p_{2,m} - \cosh(p_{2,m}x_2)\sinh(p_{2,n}x_2)/p_{2,n}\}/(p^2_{2,n} - p^2_{2,m}) \qquad \text{for } n \neq m \tag{2.139g}$$

$$\psi^{ss}_{2,nm} = \{\cosh(p_{2,n}x_2)\sinh(p_{2,n}x_2)/p_{2,n} - x_2\}/2p^2_{2,n} \qquad \text{for } n = m. \tag{2.139h}$$

The loss per unit length on the side of the ridge wall, or surface S_4, is

$$W_c^{(4)} = \frac{R_s}{2}\int_{b/2}^{d/2}\left[|H_y^{(2)}|^2 + |H_z^{(2)}|^2\right]_{x=0} dl.$$

The series representation for the fields may be substituted from Eqs. (2.35), and since $dl = -dy$ because of the clockwise contour integration

$$W_c^{(4)} = \frac{R_s}{2}\sum_{n=1}^{N_2}\sum_{m=1}^{N_2} F^{(+)}_{2,n}F^{(+)}_{2,m}\phi^{ss}_{nm} + \frac{R_s}{2}\sum_{n=0}^{N_2}\sum_{n=0}^{N_2} G^{(+)}_{2,n}\,G^{(+)}_{2,m}\,\phi^{cc}_{nm} \tag{2.140}$$

where

$$\phi^{ss}_{nm} = \int_{d/2}^{b/2}\sin(2n\pi y/b)\sin(2m\pi y/b)dy$$

$$\phi^{cc}_{nm} = \int_{d/2}^{b/2}\cos(2n\pi y/b)\cos(2m\pi y/b)dy.$$

These trigonometric integrals are evaluated as

$$\phi^{ss}_{nm} = \frac{d}{4}\{\text{sinc}[\pi(n+m)r] - \text{sinc}[\pi(n-m)r]\} \qquad \text{for } n \neq m$$

$$\phi^{ss}_{nm} = \{b - d + d\,\text{sinc}(2n\pi r)\}/4 \qquad \text{for } n = m$$

$$\phi^{cc}_{nm} = -\frac{d}{4}\{\text{sinc}[\pi(n+m)r] + \text{sinc}[\pi(n-m)r]\} \qquad \text{for } n \neq m$$

$$\phi^{cc}_{nm} = \{b - d - d\,\text{sinc}(2n\pi r)\}/4 \qquad \text{for } n = m \neq 0$$

$$\phi^{cc}_{nm} = (b-d)/2 \qquad \text{for } n = m = 0$$

where r is the height ratio, $r = d/b$.

Finally, on the surface S_5

$$W_c^{(5)} = \frac{R_s}{2}\int_0^{x_3}\left[|H_x|^2 + |H_z|^2\right]_{y=d/2} dx.$$

Substitution of the series representation for the fields from Eqs. (2.25) will yield

$$W_c^{(5)} = \frac{R_s}{2}\sum_{n=0}^{N_2}\sum_{m=0}^{N_2}(-1)^{n+m}\{D_{3,n}D_{3,m}\psi^{cc}_{3,nm} + G_{3,n}G_{3,m}\,\psi^{ss}_{3,nm}\} \tag{2.141}$$

where the x integration is that for Region 5, with

$$\psi^{cc}_{3,nm} = \int_0^{x_3}\cosh[p_{3,n}(x-x_3)]\cosh[p_{3,m}(x-x_3)]dx$$

$$\psi^{ss}_{3,nm} = \int_0^{x_3}\frac{\sinh[p_{3,n}(x-x_3)]\sinh[p_{3,m}(x-x_3)]}{p_{3,n}p_{3,m}}dx.$$

These hyperbolic integrals are easily evaluated as

$$\psi^{cc}_{3,nm} = \{(p^2_{3,n} \cosh (p_{3,m}x_3) \sinh (p_{3,n}x_3)/p_{3,n} - (p^2_{3,m} \cosh (p_{3,n}x_3) \sinh (p_{3,m}x_3)/p_{3,m}\}/(p^2_{3,n} - p^2_{3,m}) \quad \text{for } n \neq m \tag{2.142a}$$

$$\psi^{cc}_{3,nm} = \{\cosh (p_{3,n}x_3) \sinh (p_{3,n}x_3)/p_{3,n} + x_3\}/2 \quad \text{for } n = m \tag{2.142b}$$

$$\psi^{ss}_{3,nm} = \{\cosh(p_{3,n}x_3) \sinh (p_{3,m}x_3)/p_{3,m} - \cosh (p_{3,m}x_3) \sinh (p_{3,n}x_3)/p_{3,n}\}/(p^2_{3,n} - p^2_{3,m}) \quad \text{for } n \neq m \tag{2.142c}$$

$$\psi^{ss}_{3,nm} = \{\cosh (p_{3,n}x_3) \sinh (p_{3,n}x_3)/p_{3,n} - x_3\}/2p^2_{3,n} \quad \text{for } n = m. \tag{2.142d}$$

On the four surfaces where the double summation is required to obtain the loss, the contributing factors are symmetric; i.e., on each surface the loss term for $n = i$, $m = k$ is the same as the loss term for $n = k$, $m = i$. This fact is easily shown by examination of the various integration terms and may be used to reduce the number of computations required for numerical solutions. Having obtained the loss per unit length $W_c^{(i)}$ on each of the five surfaces S_i the total conductor loss per unit length W_c is found from Eq. (2.135), and the attenuation due to the finite conductivity of the metal walls is

$$\alpha_c = W_c/2P_0.$$

Of course, the set of modal component coefficients used to calculate W_c must be the same as that used to calculate P_0 as outlined in Section 2.3.

Any physical dielectric will absorb some energy when placed in a time varying electric field. In addition to conduction loss due to finite resistivity, there are a number of mechanisms which will generate loss in an imperfect dielectric [2,26,40]. The physics of dielectric loss is outside the scope of this investigation. The effects of such phenomena on the microwave properties of the subject waveguide may be included by expressing the dielectric constant as

$$\epsilon = \epsilon' - j\epsilon'' \tag{2.143}$$

where ϵ' is the $a-c$ capacitivity and all loss mechanisms are included in the dielectric loss factor ϵ'' [41]. A commonly used alternative expression to Eq. (2.143) is

$$\epsilon = |\epsilon| \exp (-j\delta_D)$$

where δ_D is the dielectric loss angle. Thus,

$$\epsilon''/\epsilon' = \tan \delta_D \tag{2.144}$$

where $\tan \delta_D$ is the dielectric loss tangent of the material. Good dielectrics have values of $\tan \delta_D$ in the $10^{-5} - 10^{-3}$ range [25,26].

For macroscopic properties, an equivalent conductance representing all losses in the dielectric [2] is

$$\sigma_e = \omega \epsilon''.$$

The power loss in the dielectric is given by

$$P_D = \iiint_{volume} \frac{1}{2}\omega\epsilon'' |\mathbf{E}|^2 dv.$$

The power loss per unit length along the z-axis due to imperfect dielectric is thus

$$W_d = \frac{\omega\epsilon''}{2} \iint_S \{|E_x|^2 + |E_y|^2 + |E_z|^2\} dx\, dy \tag{2.145}$$

where the surface integration is over the dielectric portion of the waveguide. Advantage may be taken of the waveguide symmetry to give

$$W_d = 2(W_d^{(2)} + W_d^{(3)}) \tag{2.146}$$

where $W_d^{(2)}$ and $W_d^{(3)}$ are the power loss per unit length in Regions 2 and 3, respectively, of Fig. 4. $W_d^{(2)}$ and $W_d^{(3)}$ are calculated from Eq. (2.145) using the fields and integration surface of the corresponding region. In each of the two regions, the integration in (2.145) may be done term-by-term, with

$$W_d^{(i)} = W_{d,x}^{(i)} + W_{d,y}^{(i)} + W_{d,z}^{(i)} \tag{2.147a}$$

for $i = 2, 3$, where

$$W_{d,\rho}^{(i)} = \frac{\omega\epsilon''}{2} \iint_{S_i} |E_\rho^{(i)}|^2 dx\, dy \tag{2.147b}$$

for $\rho = x, y, z$. Substitution of the series representation for $E_x^{(2)}$ from Eq. (2.35a) gives

$$W_{d,x}^{(2)} = \frac{\omega\epsilon''}{2} \int_{-x_2}^{0} \int_{-b/2}^{b/2} \left\{ \sum_{n=1}^{N_2} [A_{2,n}^{(+)} \cosh(p_{2,n}x) + A_{2,n}^{(-)} \sinh(p_{2,n}x)/p_{2,n}] \sin(2n\pi y/b) \right\}$$
$$\cdot \left\{ \sum_{m=1}^{N_2} [A_{2,m}^{(+)} \cosh(p_{2,m}x) + A_{2,m}^{(-)} \sinh(p_{2,m}x)/p_{2,m}] \sin(2m\pi y/b) \right\} dx\, dy. \tag{2.148}$$

Since the functions $\sin(2n\pi y/b)$ and $\sin(2m\pi y/b)$ are orthogonal on the interval $-b/2 \leqslant y \leqslant b/2$, the y integration will eliminate cross products of the different modal components and Eq. (2.148) reduces to

$$W_{d,x}^{(2)} = \frac{\omega\epsilon''}{2} \frac{b}{2} \sum_{n=1}^{N_2} \left\{ [A_{2,n}^{(+)}]^2 I_{2,n}^{cc} + 2A_{2,n}^{(+)} A_{2,n}^{(-)} I_{2,n}^{sc} + [A_{2,n}^{(+)}]^2 I_{2,n}^{ss} \right\}$$

where the x integration terms $I_{2,n}^{cc}$, $I_{2,n}^{sc}$ and $I_{2,n}^{ss}$ are the same as those used in the power analysis of Section 2.3, and the same as $\psi_{2,nm}^{cc}$, $\psi_{2,nm}^{sc}$ and $\psi_{2,nm}^{ss}$, respectively, of this section with $n = m$ and are evaluated in Eqs. (2.139b), (2.139f), and (2.139h).

The development of $W_{d,y}^{(2)}$ and $W_{d,z}^{(2)}$ is similar to that for $W_{d,x}^{(2)}$. With substitution of the series representation for the fields from Eqs. (2.35b) and (2.35c) into Eq. (2.147b)

$$W_{d,y}^{(2)} = \frac{\omega\epsilon''}{2} \frac{b}{2} \sum_{n=0}^{N_2} (1 + \delta_{n0}) \left\{ [B_{2,n}^{(+)}]^2 I_{2,n}^{cc} + 2B_{2,n}^{(+)} B_{2,n}^{(-)} I_{2,n}^{sc} + [B_{2,n}^{(-)}]^2 I_{2,n}^{ss} \right\}$$

$$W_{d,z}^{(2)} = \frac{\omega\epsilon''}{2} \frac{b}{2} \sum_{n=1}^{N_2} \left\{ [C_{2,n}^{(+)}]^2 I_{2,n}^{cc} + 2C_{2,n}^{(+)} C_{2,n}^{(-)} I_{2,n}^{sc} + [C_{2,n}^{(-)}]^2 I_{2,n}^{ss} \right\}.$$

In Region 3, the calculation of $W_d^{(3)}$ is similar to that for $W_d^{(2)}$ in Region 2. Using the series representation for the fields in Region 3 from Eq. (2.25) gives

$$W_{d,x}^{(3)} = \frac{\omega\epsilon''}{2} \frac{d}{2} \sum_{n=1}^{N_2} A_{3,n}^2 I_{3,n}^{ss}$$

$$W_{d,y}^{(3)} = \frac{\omega\epsilon''}{2} \frac{d}{2} \sum_{n=0}^{N_2} (1 + \delta_{n0}) B_{3,n}^2 I_{3,n}^{cc}$$

$$W_{d,z}^{(3)} = \frac{\omega\epsilon''}{2} \frac{d}{2} \sum_{n=1}^{N_2} C_{3,n}^2 I_{3,n}^{cc}$$

where the x integration terms $I^{ss}_{3,n}$ and $I^{cc}_{3,n}$ are the same as those of Section 2.3 and the same, respectively, as $\psi^{ss}_{3,nm}$ and $\psi^{cc}_{3,nm}$ of this section with $n = m$, and are evaluated in Eqs. (2.142b) and (2.142d).

Once the full loss per unit length W_d due to the imperfect dielectric is found from Eqs. (2.147) and (2.146) the dielectric attenuation constant is then calculated as

$$\alpha_d = W_d/2P_0 \tag{2.149}$$

where the amplitude coefficients of the fields are the same for numerical evaluation of both W_d and P_0. The total loss per unit length of the waveguide is $W_c + W_d$, thus the total attenuation factor due to conductor losses and imperfect dielectric is

$$\alpha = \alpha_c + \alpha_d. \tag{2.150}$$

Each of these attenuation terms is in nepers/unit length. To convert to the more conventional engineering terminology of dB/unit length, the relation is

$$\exp(-2\alpha_{nep} z) = 10^{-(\alpha_{dB} z)/10}$$

where α_{nep} = nepers/unit length and α_{dB} = dB/unit length, thus

$$\alpha_{dB} = 20\alpha_{nep}/\ln 10$$

or

$$\alpha_{dB} = 8.686\alpha_{nep}.$$

In calculating numerical values for both α_c and α_d, large errors may result when the number of terms N_T in the series expansion for the fields is large. This is due to the computational difficulty encountered for numerical evaluation of factors such as

$$a_n \cosh(p_n x) \sinh(p_m x) - b_m \cosh(p_m x) \sinh(p_n x) \tag{2.151}$$

when the hyperbolic terms are very large. Accuracy problems were found to be particularly troublesome when evaluating the quantity $W_c^{(3)}$ for determination of α_c and the quantity $W_d^{(2)}$ for determination of α_d. To avoid errors caused by such computational limitations, (2.61) and (2.62) may be used to reduce the various terms in the double summation equations to expressions where factors like those of Eq. (2.151) are not present. Such a technique is similar to that used in Section 2.2 for calculation of the coefficients $A_{1,n}$ and $D_{1,n}$.

Convergence characteristics for the attenuation terms α_c and α_d of the $QLSE_{1,0}$ mode as a function of N_T are shown in Table 2 for a typical waveguide geometry.

2.5 Computer Program Implementation

The mathematics of the theoretical analysis developed in the preceding sections of this chapter was incorporated in to the computer program DLDRWG to calculate numerical solutions for the dielectric loaded double ridged waveguide. Appendix E2 lists this program. The program is written in FORTRAN-10 and is designed for use on the DEC-10 timesharing computer.

Input parameters required for the program are the five physical dimensions (in inches) and the relative dielectric constant of the dielectric material (Fig. 3). The waveguide mode for which a solution is sought must be specified, as well as the number of terms N_T to be used in the series expansion for the fields. The cutoff frequency of the particular mode must be found first, then if desired the propagation term β may be found for any frequency $\omega > \omega_c$. When solving for a root, either ω_c or β, two modes of operations are available. The first is a search mode, for which the user must provide start, stop, and incremental values of the unknown quantity. This mode enables examination of the determinant value as a function of the unknown parameter and is useful to distinguish sign changes of the

determinant due to poles from those at the zeros (roots). The second operational mode is an automatic seek mode to find any root between specified limits. The seek mode uses a combination of the binary search method and Newton's method to obtain the root [64,65]. Because of the wide variation in the magnitude of the matrix determinant, the criterion used for root determination was that the unknown variable, ω_c or β, be within 0.001% of the actual determinant zero.

The program will calculate attenuation and power breakdown levels for the $QLSE_{1,0}$ mode only. If numerical values for these characteristics are requested, the user must supply additional parameter information: (1) the conductivity of the waveguide walls, normalized to that of copper; (2) the loss tangent of the dielectric materials; and (3) the electric breakdown strength, relative to that of dry air, of the dielectric material.

The program will also supply, if desired, the modal amplitude coefficients for the fields in each region of the waveguide.

In addition to the waveguide configuration of Fig. 3, program DLDRWG will provide numerical results for waveguides in which the dielectric width t is less than the ridge width s as shown in Fig. 5. The mathematical development of an analysis for such a waveguide geometry closely parallels the development presented for $t \geqslant s$, but the details will be omitted since the primary objective of this investigation concerns large power breakdown levels. The waveguide of Fig. 5 obviously is not appropriate for high peak power operation because of the large electric field intensity that would be present at the sides of the dielectric material.

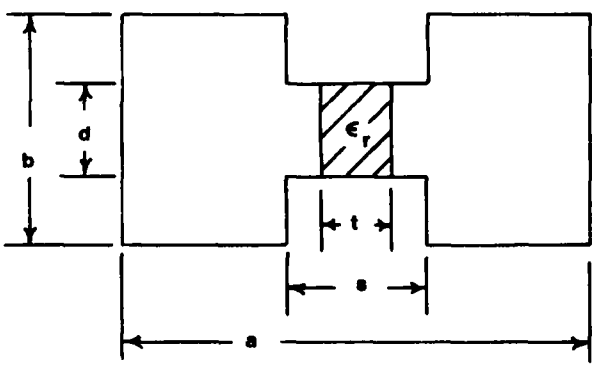

Fig. 5 — Dielectric loaded double ridged waveguide with $t < s$

Numerical solutions for dielectric loaded single ridged waveguide, Fig. 6, may be obtained with this theory by considering the waveguide as the top half of a dielectric loaded double ridged waveguide operating in a (M,E) or (E,E) mode, i.e., with an effective electric wall at the horizontal plane of symmetry. The modes of the waveguide of Fig. 6 thus would be the $QLSE_{m,n}$ and $QLSM_{m,n}$ modes, with n restricted to even integers, of the waveguide of Fig. 3 where all vertical dimensions of the latter waveguide are double those of the single ridged waveguide. The attenuation calculations for the double ridged waveguide, however, would not be valid for the single ridged waveguide.

Theoretical results obtained using program DLDRWG are presented in Fig. 7 for a typical dielectric loaded double ridged waveguide. Cutoff frequencies for the four lowest order waveguide modes are shown, while the power breakdown and propagation characteristics of the dominant $QLSE_{1,0}$ mode are plotted as functions of frequency. As with any waveguide, the phase term β and the power breakdown rapidly drop to zero as the frequency approaches cutoff, while the attenuation terms α_c (conductor loss) and α_d (dielectric loss) each display a minimum value as a function of frequency.

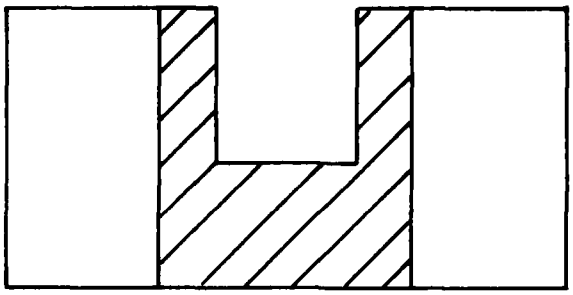

Fig. 6 — Cross section of dielectric loaded single ridged waveguide

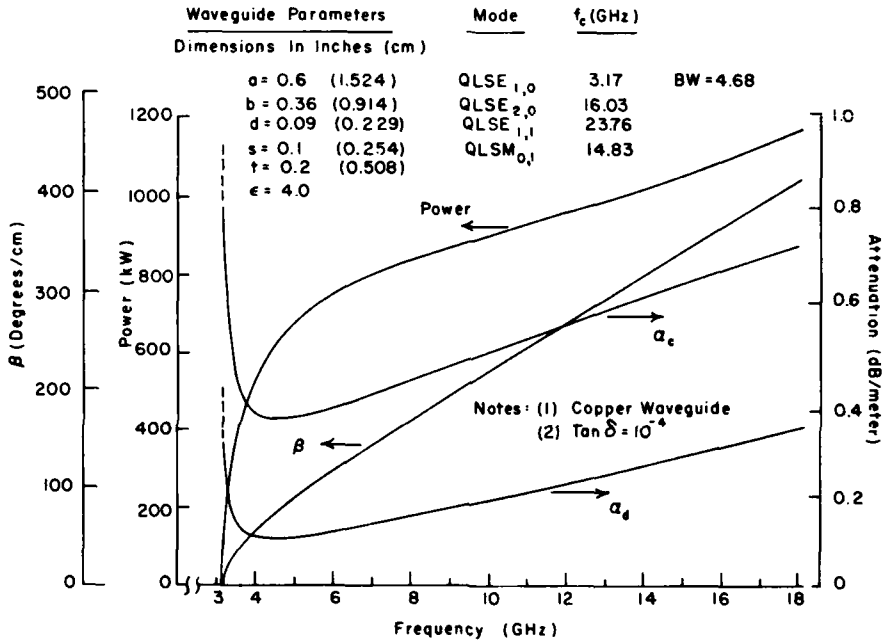

Fig. 7 — Typical waveguide characteristics for $QLSE_{1,0}$ mode

2.6 Comparison with Other Theory

Numerical results obtained from the theory presented in this chapter were compared with results obtained from other sources. For the reduction of the waveguide of Fig. 3 to empty rectangular waveguide, i.e., $d = b$ and $\epsilon_r = 1$, the results obtained from program DLDRWG—cutoff frequencies and propagation characteristics for all modes, as well as attenuation and power breakdown values for the dominant $TE_{1,0}$ mode—were identical to results obtained from conventional theory [1,2,41,42,67]. With the waveguide of Fig. 3 reduced to dielectric slab loaded rectangular waveguide, $d = b$, the results of this theory again were identical with other published results [3,18,20,23,68,69]. Such favorable comparison is expected, of course, since for both types of waveguide the mathematics of this theory reduce exactly to the corresponding mathematics of the conventional theory. This exact reduction is a consequence of the matrices M_1, M_2, M_3, and M_4 of Section 2.2 being diagonal when $d = b$, thus leading to a diagonal matrix for the eigenvalue problem.

Comparisons for empty double ridged waveguide ($\epsilon_r = 1$ but $d < b$ in Fig. 3) were made from several sources. Table 3 shows the agreement of this theory with results of Hopfer [11] for the normalized cutoff wavelength of the $TE_{1,0}(QLSE_{1,0})$ and $TE_{2,0}(QLSE_{2,0})$ modes. The attenuation results of this theory were between 2% (for $BW = 3$) and 18% (for $BW = 5$) less than the graphical results presented by Hopfer.

Table 3 — Comparison of Cutoff Frequencies with Results from Hopfer

Air-filled double ridged waveguide

s/a	d/b	λ_c/a $TE_{1,0}$ mode		λ_c/a $TE_{2,0}$ mode	
		This Theory	Hopfer	This Theory	Hopfer
0.1	0.1	4.104	4.11	0.911	0.91
0.1	0.3	2.863	2.89	0.935	0.93
0.1	0.5	2.414	2.43	0.956	0.96
0.3	0.1	5.160	5.15	0.823	0.82
0.3	0.3	3.257	3.26	0.927	0.93
0.3	0.5	2.623	2.62	0.960	0.97
0.5	0.1	5.395	5.40	1.113	1.12
0.5	0.3	3.324	3.33	1.132	1.12
0.5	0.5	2.657	2.67	1.090	1.09

Notes:
(1) $b/a = 0.5$
(2) $N_T = 6$
(3) Results from Hopfer [11] are graphical

Power and attenuation comparisons were made using published technical data for standard double ridged waveguide [67]. For all waveguide geometries tested, the results of this theory agreed within 8% of the listed values for both attenuation and power. For this comparison, the corner correction data from Hopfer [11] was used to correct for the increased electric field at the rounded ridge corners and the power safety factor of 4 included for this theory.

The only published data found in the open literature concerning higher order modes other than $TE_{m,0}$ modes for empty double ridged waveguide were calculated by Montgomery [14]. For the waveguide case with $\epsilon_r = 1$, the $QLSE_{m,0}$ mode designation of this theory may be replaced as a $TE_{m,0}$ mode since $E_z \equiv 0$; i.e., all modal components of E_z vanish for all frequencies. Also, all QLSM modes reduce to TE modes while all $QLSE_{m,n}$ modes (with $n > 0$) reduce to TM modes when $\epsilon_r = 1$. A comparison of cutoff frequencies for different TE modes obtained from this theory and those from [14] is shown in Table 4. The trough modes of Montgomery are cross-polarized to the hybrid modes; also, the trough modes occur in pairs which are almost degenerate, hence the one to two correspondence with the modal designation of this theory. No numerical results were given in [14] for TM modes corresponding to the $QLSE_{m,n}(n > 0)$ modes of this theory.

Table 4 — Comparison of Numerical Results with Those of Montgomery

Empty Double Ridged Waveguide

$a = 0.5$ (1.27) $d = 0.11$ (0.28)

$b = 0.4$ (1.02) $s = 0.1$ (0.25)

Dimensions in inches (cm)

This theory[1]		Montgomery	
Mode	f_c (GHz)	Mode	f_c (GHz)
$QLSE_{1,0}$	6.8907	$TE_{1,0}$ Hybrid	6.8570
$QLSE_{2,0}$	24.9308	$TE_{2,0}$ Hybrid	24.8582
$QLSE_{3,0}$	32.0311	$TE_{3,0}$ Hybrid	32.0246
$QLSM_{0,1}$	15.076	$TE_{1,0}$ Trough[2]	15.1046
$QLSM_{1,1}$	15.127		
$QLSM_{0,2}$	29.5737	$TE_{2,0}$ Trough[2]	29.5363
$QLSM_{1,2}$	29.5742		
$QLSM_{2,1}$	33.228	$TE_{1,1}$ Trough[2]	33.2723
$QLSM_{3,1}$	33.295		

Notes:
(1) With $N_T = 6$
(2) Trough modes are almost degenerate pairs

Magerl [27] had the only information found in the technical literature on dielectric loaded ridged waveguide, but the investigation was restricted to the case where the dielectric width was exactly equal to the ridge width ($t = s$ in Fig. 3). Although the analysis incorrectly assumed a true TE modal structure, the derivation of cutoff frequencies for modes corresponding to the $QLSE_{1,0}$ and $QLSE_{2,0}$ modes of this theory was valid [28] since E_z does vanish at cutoff for these modes. Within the limitations inherent in obtaining numerical values from the graphical data of [27], the results were found to be identical with those of this theory for cutoff of the $QLSE_{1,0}$ and $QLSE_{2,0}$ modes. Although a brief discussion of other waveguide modes was made in [27], no analysis was given.

3.0 COMPARISON OF EXPERIMENTAL DATA WITH THEORY

3.1 Propagation Characteristics

Measurements were made on experimental sections of partially dielectric loaded double ridged waveguide for comparison with the predicted performance of the theory based on the mathematical analysis derived in Section 2. Since the waveguide is a linear device, propagation characteristics are independent of power level. The propagation characteristics thus were measured at low-power levels due to the greater flexibility, increased accuracy and simplified hardware of a low-power measurement facility as opposed to that for a high-power facility.

All low-power measurements were made on a computer-aided automatic network analyzer (ANA), a Hewlett-Packard Model 8409B. This unit can measure complex transmission and reflection coefficients between 0.1 and 18 GHz of one and two port devices. The theory of operation and characteristics of this type of microwave measurement system are well documented [70-73] and need not be discussed further. Measurements were made in two bands, the first (low band) covering the 8 to 12 GHz range, and the second (high band) covering the 12 to 18 GHz range. This was necessary to allow transitions from the coax system of the ANA to the rectangular waveguide sections used to interface with the waveguide under test (WUT). The interfacing waveguide was standard X-band waveguide for the low band and standard K_u– band waveguide for the high band. These frequency bands were selected since precision waveguide calibration kits were available for both X and K_u waveguide; with the increased accuracy of the ANA calibration greater accuracy could be achieved in the measurements. Measurements were made in frequency increments of 0.5 GHz or less.

To obtain the propagation characteristics for a particular dielectric loaded double ridged waveguide, measurements were made on three different lengths of the waveguide, where each waveguide sample had the same cross-sectional geometry. Then at each measurement frequency, the three measured complex transmission coefficients were used, along with the measured physical lengths of the three samples, to correct for the inherent mismatch between WUT and the interfacing rectangular waveguides. The effect of the mismatch on the measured propagation characteristics is analyzed in detail in Appendix D, where the technique used for mismatch correction is derived as Method 3. The values of the propagation constant β that will be shown as experimental data thus are not direct measurement results, but are derived directly from the measured data. Discussion of the waveguide loss, or attenuation, term α will be made at a later stage in this section.

To allow measurements of waveguides with a variety of cross-sectional geometries, brass test fixtures were fabricated as shown in Fig. 8. For each length of waveguide the top and bottom wall sections were common for all cross-sectional geometries. The sidewall sections as well as the ridge sections were fabricated in pairs. Screws were used to assemble the complete structure, along with steel locating pins to minimize side play and allow accurate positioning when changing the geometry. While not a recommended construction method for an operational waveguide, this method of fabrication afforded a large degree of freedom in the choice of geometries for the waveguide. The three lengths of the waveguide used for the low-power tests were 1.25 in. (3.18 cm), 1.474 in. (3.74 cm), and 1.998 in. (5.07 cm). Corresponding lengths of H-shaped dielectric inserts were machined from polystyrene (ϵ_r =2.54) and from Emerson and Cummings Stycast K-12 (ϵ_r = 12) to mate with several housing geometries. Because of the slight imperfections in both the machining and assembly processes of the brass housing, it was necessary to make the dielectric inserts slightly undersize to allow assembly and disassembly of the complete waveguide test pieces.

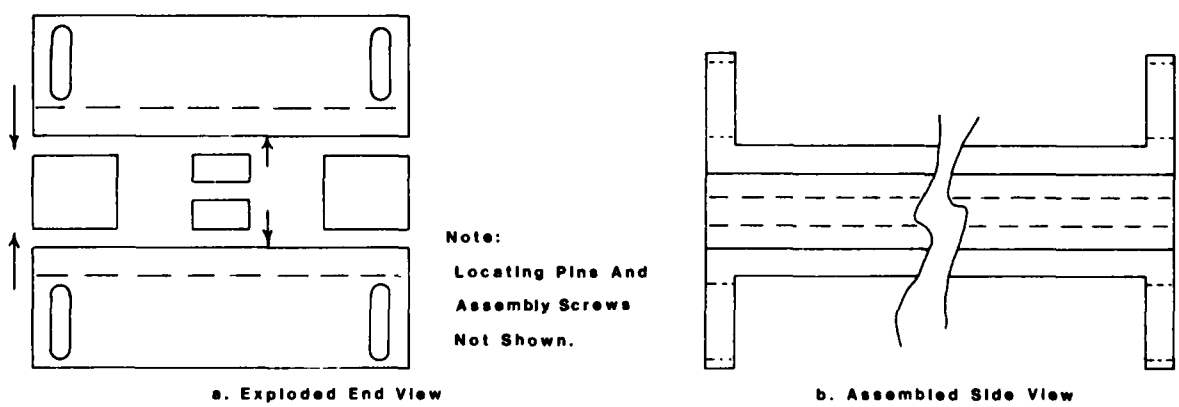

Fig. 8 — Low-power test housing

The first measurements were made on samples of dielectric slab loaded rectangular waveguide (DSLRWG) and air-filled double ridged waveguide (DRWG) as a check on the validity of the program used to correct for mismatch effects. For both waveguide types, the theory of this analysis has already been shown to agree quite closely with the results of other researches (exact agreement in the case of DSLRWG). Figure 9 shows the very close agreement between theoretical and measured values of β for DSLRWG operating in the dominant $TE_{1,0}$ mode. The agreement is good even for frequencies where higher order modes may propagate. The absence of an effect on propagation characteristics of the $TE_{1,0}$ mode by higher order modes may be due to the fact that the higher order modes are not present; i.e., although higher order modes may propagate, they are never launched by coupled energy from the dominant mode. Alternatively, the higher order modes could be present but with no frequencies for resonant conditions near the frequencies at which the measurements were taken, thus producing negligible effects. If higher order modes of significant magnitudes were present, they would cause abrupt spikes at resonant frequencies in the otherwise smooth trace of transmission (both magnitude and phase) through the sample waveguide when the measurement was made in the manual mode of operation for the ANA on a continuous swept frequency basis. Such a swept frequency measurement showed no discernible evidence of higher order modes up to 18 GHz for the waveguide of Fig. 9.

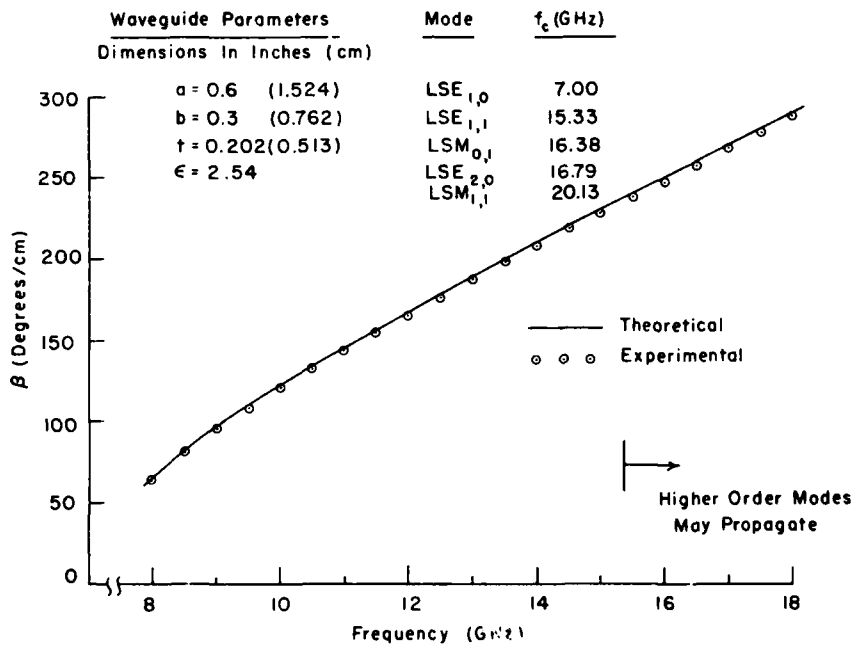

Fig. 9 — Comparison of theory with experimental data for dielectric slab loaded rectangular waveguide

The agreement between theoretical and measured β is shown as a function of frequency for the $TE_{1,0}$ mode of DRWG in Fig. 10. For this waveguide, the cutoff frequency of the first higher order mode is greater than 17 GHz. Any higher order modes would thus be very close to cutoff at the largest measurement frequency, 18 GHz, and the resultant attenuation so great as to preclude any effect on the $TE_{1,0}$ mode measurements.

The initial measurements on the first sample of dielectric loaded double ridged waveguide did not indicate good agreement with theory, as indicated by the triangular data values of β in Fig. 11. For these measurements, the actual volume of dielectric material was less than the theoretical volume

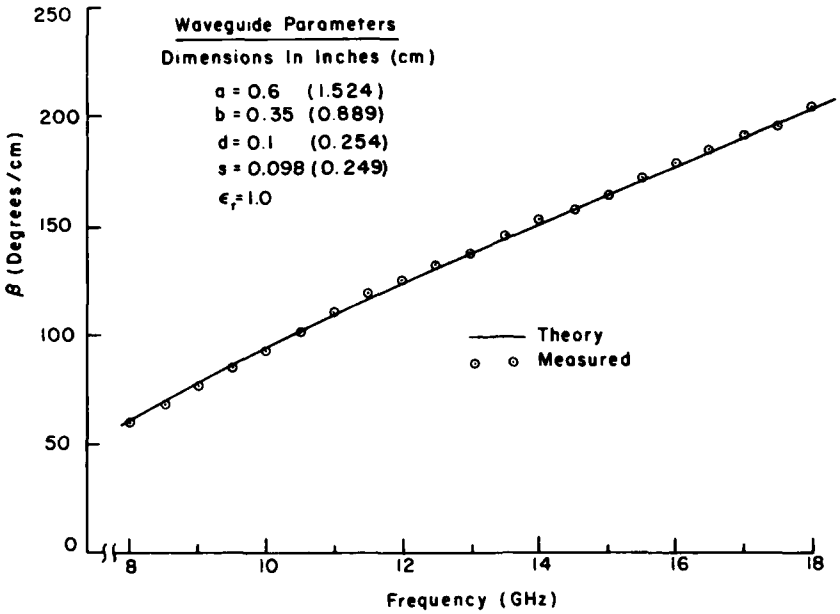

Fig. 10 — Comparison of theory with experimental data for empty double ridged waveguide

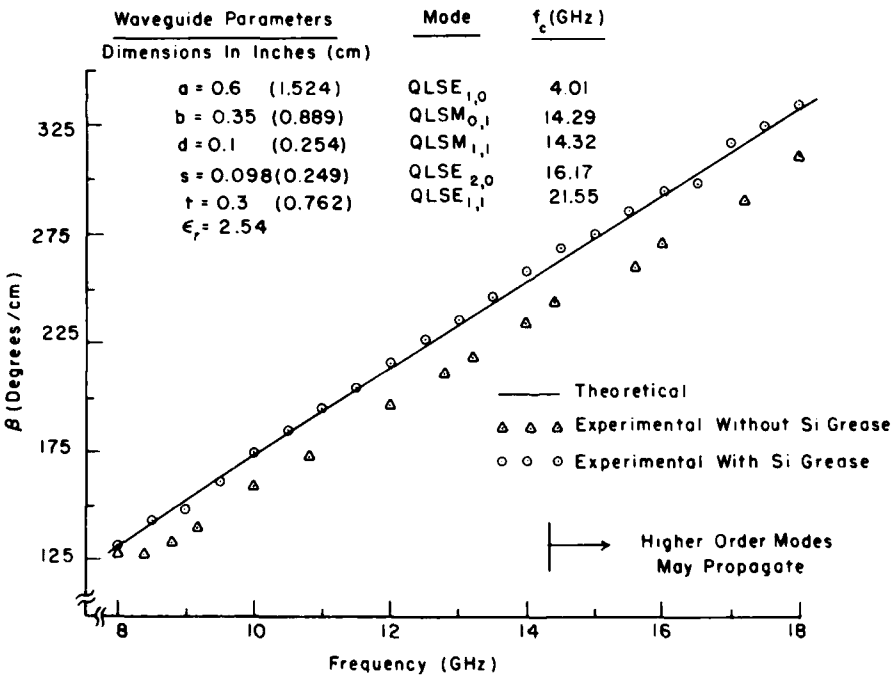

Fig. 11 — Comparison of theory with experimental data for DLDRWG with $QLSE_{1,0}$ f_c = 4 GHz

because of the required loose fit of the dielectric piece for assembly. An effective dielectric constant may be calculated on a volume basis as

$$\epsilon_{eff} = \frac{\epsilon_r V' + (V - V')}{V}$$

where V is the theoretical volume of the dielectric piece and V′ the actual volume of dielectric material. With $\epsilon_r = 2.54$ and V′ estimated to be 98% of V, ϵ_{eff} was calculated to have a value of 2.51. However, the initial measurements on this waveguide indicated a good fit for $\epsilon_{eff} = 2.2$. The possibility that the dielectric piece (polystyrene) might have some value other than the presumed $\epsilon_r = 2.54$ was considered as a cause for the discrepancy between theory and experiment. Sample pieces of polystyrene, machined from the same stock as the waveguide insert, were checked and found to have the expected $\epsilon_r = 2.54$, however. The conclusion was reached that correction for the air gaps at the interface between the dielectric material and the metal waveguide surfaces by a simple volume approximation to determine ϵ_{eff} was insufficient.

Rather than trying to derive a more sophisticated method to correct for air gaps, it was decided to simply eliminate the air gaps. Use of coil dope (polystyrene dissolved in toluene) was considered as a solution but rejected because of the need to disassemble the waveguide structure to change geometries. The method finally adapted was to fill the slots of the polystyrene piece with silicone grease prior to assembly. The relative dielectric constant of this material is slightly greater than that of polystyrene, with $\epsilon_r \approx 2.7$. Upon assembly of the waveguide structure the excess grease was forced out of the metal/dielectric interface volume, leaving no air gaps. Such assembly had to be performed slowly and with caution in order to give the excess grease time to flow and prevent cracking of the polystyrene due to a build up of hydraulic pressure. The slight difference between ϵ_r of the silicone grease and ϵ_r of the polystyrene was then ignored because of the relatively small volume of grease. Of course, the silicone grease did not harden as would have coil dope, and thus caused no problems with disassembly.

Using this silicone grease method for assembly, the measurements on the dielectric loaded double ridged waveguide were repeated. The agreement between the theoretical and measured values of β were excellent as indicated in Fig. 11. For frequencies above 14.3 GHz, swept frequency measurements gave no indication of the presence of propagating higher order modes.

All waveguides using polystyrene as the dielectric material were then assembled with silicone grease. The agreement between theoretical and measured values of β(QLSE$_{1,0}$ mode) as a function of frequency is shown in Fig. 12 for a waveguide similar to that of Fig. 11, but with an increased waveguide width. Swept frequency measurements on the waveguide of Fig. 12 gave definite indications of the presence of some higher order mode(s) for frequencies above 16 GHz. The large deviation of the measured β (corrected from the raw data) from theory is due to these higher order mode(s) since the mismatch correction assumes a single mode to be propagating in the sample waveguide (Appendix D). A similar situation existed for another waveguide with a different geometry as shown in Fig. 13. For this waveguide, agreement between theory and experiment was good also until higher order modes began to propagate.

By using the same brass housings, similar experiments using $\epsilon_r = 12$ dielectric material were attempted, although it was recognized that because of the heavy dielectric loading most of the single mode bandwidth would lie below 8 GHz. An assembly method similar to the silicone grease method was used, but using a material with $\epsilon_r \approx 12$ rather than silicone grease. For such a material it was decided to use the filler portion of a two-part castable dielectric epoxy with $\epsilon_r = 12.5$, without adding the hardening agent. Two such experiments were made, but both gave poor agreement with theory. In both cases, one or more of the dielectric pieces was found to be badly cracked when the waveguide housing was disassembled. This failure of the dielectric material was attributed to two causes. First, the material from which the dielectric insert was machined was old; experience has shown that dielectric materials of this type tend to become brittle with age. Secondly, the dielectric epoxy used to fill the air

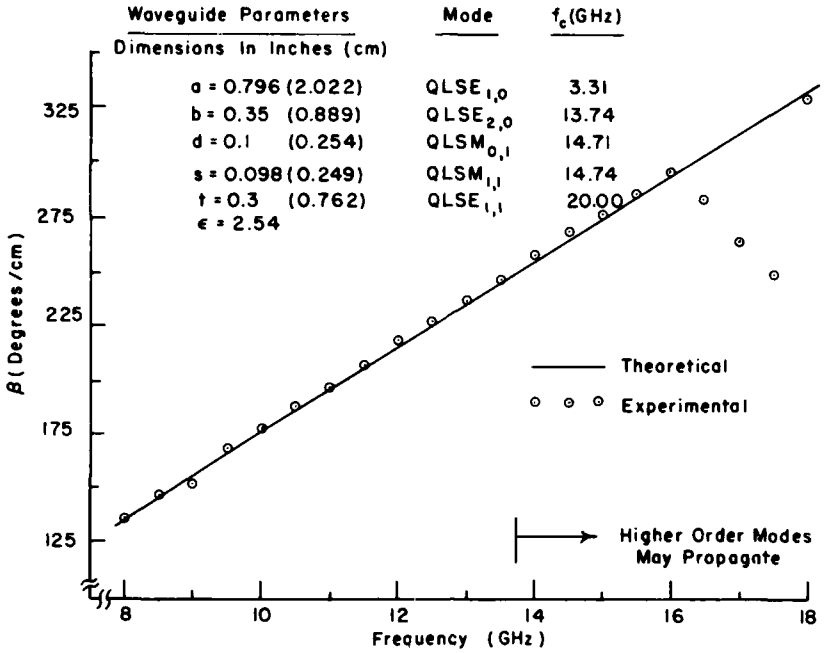

Fig. 12 — Comparison of theory with experimental data for DLDRWG with $QLSE_{1,0}$ f_c = 3.3 GHz

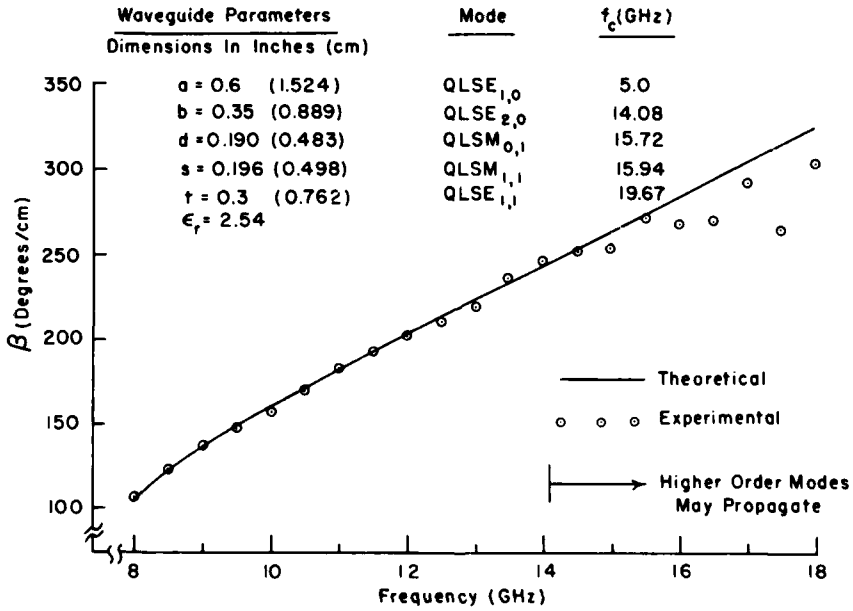

Fig. 13 — Comparison of theory with experimental data for DLDRWG with $QLSE_{1,0}$ f_c = 5 GHz

gap was considerably more viscous than silicone grease; the hydraulic pressure encountered during assembly split the dielectric. With the poor agreement between experiment and theory attributed to the cracked dielectric insert, no further experimental attempts were made using a high ϵ_r material; the excellent agreement for the $\epsilon_r = 2.54$ waveguide configurations was felt to constitute sufficient experimental verification of the propagation aspects of the theory for the phase term β.

By using the waveguides with polystyrene dielectrics, the actual cutoff frequencies for the $QLSE_{1,0}$ mode were confirmed directly. This was done by operating the ANA in a swept frequency mode to find the frequency at which the transmission through the waveguide rapidly approached zero. For this measurement, the interfacing waveguide had to be large enough to propagate at the cutoff frequency of the sample waveguide, and conventional S-band rectangular waveguide was used. For some measurements, the S-band waveguide was operated at frequencies where the $TE_{2,0}$ mode could propagate; in this case, however, overmoding of the interfacing waveguide was immaterial since the sample waveguide would still have infinite attenuation at its cutoff frequency. Since the interior size of the S-band waveguide was larger than the brass housing of the sample waveguide, aluminum foil and conductive copper tape was used to seal the gap between the waveguides and prevent coupling of the two interfacing waveguide sections via radiation. Dielectric slugs were glued to either end of the sample waveguide to increase the coupling between it and the adjacent sections of S-band waveguide, i.e., to form crude matching transformers. Such matching transformers, of course, had no effect on the cutoff frequency of the sample waveguide and were employed to partially overcome the huge discontinuity resulting from the drastic change in cross section.

Although the accuracy of such an elementary method to measure f_c of the sample waveguide is considerably less than the accuracy of the method used to measure β for $f > f_c$, the measurements resulted in values of cutoff for the dominant mode that were within 6% of the theoretical value for all waveguide geometries tested. Comparable deviations of measured values of f_c from theory were found when rectangular waveguide was used as a sample, and when the cutoff frequency was known exactly.

Attempts were made to compare the propagation characteristics of some of the higher order modes as determined from experimental data with the theoretical values, using resonance conditions for the propagating higher order modes in a manner similar to that used by Tsandoulas et al. [24]. At frequencies where any higher order mode could propagate in the WUT, a sharp spike in the transmission loss indicated that a significant degree of coupling existed between the dominant mode and the higher order mode, with a high Q resonant cavity being formed by the WUT for this higher order mode since such a mode could not propagate in the adjoining rectangular waveguide. Thus, at the frequency of the transmission loss spike, the WUT represents to the higher order mode a transmission line with an effective electrical length equal to an integral number of half wavelengths. The effective length includes the phase term of the reflection coefficient seen by the higher order mode at either end of the WUT as well the product $\beta_{HOM}L$. With an analysis similar to that developed for the dominant mode in Appendix D, resonant conditions for any higher order mode occur at frequencies where

$$\beta L - \phi_{22} = n\pi, \text{ for } n = 1, 2, 3, \ldots \tag{3.1}$$

with ϕ_{22} the phase of the reflection coefficient at either end of the WUT. Of course, the frequency dependence of both β and ϕ_{22} is determined by the particular higher order mode.

The waveguide geometry described in Fig. 12 was chosen for the higher order mode measurements. Determination of the higher order mode causing the resonant cavity effect was essential for comparison of experimental results with theory, and two techniques were tried to deliberately launch the $QLSE_{2,0}$ mode since the $QLSE_{2,0}$ mode was the higher order mode with the lowest cutoff frequency. The first technique used a small rectangular dielectric piece, $\epsilon_r = 13$, in the input section of K_u waveguide adjacent to the front face of the WUT and lined up with one arm of the H-shaped polystyrene insert. The generation of an asymmetrical component of electric field, due to the off-center dielectric in the input K_u waveguide, was quite effective in launching the $QLSE_{2,0}$ mode in the WUT as

evidenced by the appearance of spikes in the measured dominant mode transmission loss. However, this technique did not lead to good agreement between experiment and theory for β of the $QLSE_{2,0}$ mode. It was determined that the addition of the dielectric piece in the K_u waveguide effectively increased the length of the WUT for this mode since the $LSE_{2,0}$ mode could propagate in the short length of dielectric slab loaded (off center) rectangular waveguide thus formed.

The second technique tried to deliberately launch the $QLSE_{2,0}$ mode in the WUT consisted of a simple shift, or offset, of the input K_u waveguide (no dielectric loading) relative to the front face of the WUT. With this offset, the incident field pattern seen by the WUT was nonsymmetrical about its vertical plane of symmetry, thus increasing the coupling to the $QLSE_{2,0}$ mode for which the E_y fields are asymmetrical about the vertical plane of symmetry. This technique also proved effective in launching the $QLSE_{2,0}$ mode, as evidenced by the spikes in the measured transmission loss at frequencies close to the theoretical cutoff frequency of this mode. The magnitude of these loss spikes was reduced as the waveguide offset was decreased, and vanished when no offset was used. Other transmission spikes remained at higher frequencies, but were determined probably to be due to modes other than the $QLSE_{2,0}$ mode. Only the transmission spikes produced by the waveguide offset were used to obtain experimental verification of the propagation characteristics for a higher order mode since these spikes could be attributed to a given mode—the $QLSE_{2,0}$ mode—with a high degree of confidence.

The change of the phase term ϕ_{22} with the offset of the input K_u waveguide was immaterial since this phase quantity could not be measured directly under any circumstances. The condition for higher order mode resonance given by Eq. (3.1) remains valid if ϕ_{22} is taken as the average of the phase angles of the reflection coefficients at either end of the WUT for the higher order mode. Since the quantity ϕ_{22} is some unknown function of frequency, the following approach was used to determine β for the $QLSE_{2,0}$ mode. With equal amounts of waveguide offset on the input end of the WUT, each of the three lengths of the waveguide described in Fig. 12 was measured for transmission loss on the ANA using the manual swept frequency mode. For each length, the frequencies at which transmission loss spikes occurred—due to the waveguide offset—were recorded, and the value of ϕ_{22} was then calculated and plotted using Eq. (3.1) and the theoretical value of β for the $QLSE_{2,0}$ mode. For the short lengths used for the WUT, determination of the integer value for n was straightforward. Since ϕ_{22} was independent of the length of the WUT, the plotted values of ϕ_{22} were used to construct a best fit linear dependence of ϕ_{22} as a function of frequency between 14.05 and 16.15 GHz. The theoretical cutoff frequency of the $QLSE_{2,0}$ mode was 13.74 GHz for this waveguide geometry. The lowest frequency transmission loss spike, at f = 14.05 GHz, occurred in the shortest length sample, corresponding to n = 1 in Eq. (3.1). The lowest frequency spike for each of the two longer samples occurred at frequencies corresponding to n = 2. The absence of spikes at frequencies corresponding to n = 1 for these longer samples was disconcerting initially. However, when an extension of the assumed linear frequency dependence of ϕ_{22} was used to calculate the frequencies at which transmission loss spikes would be predicted for n = 1, such frequencies were found to be very close to the theoretical cutoff frequency. For frequencies very close to cutoff, the attenuation of the $QLSE_{2,0}$ mode would be very large, and the cavity formed by the WUT for this mode would have such a low Q as to preclude a spike in the transmission loss of the dominant mode.

Loss spikes due to the waveguide offset were indicated at frequencies above 16.15 GHz, but were ignored because of the erratic measured transmission loss at these frequencies—due to unknown higher order modes—that existed with no offset. The linear approximation of ϕ_{22} varied from $-38°$ at $f = 14.05$ GHz to $-78°$ at $f = 16.15$ GHz, with the calculated values of ϕ_{22} having a maximum deviation of $\pm 5°$ from the linear approximation. With the values of $\phi_{22}(f)$ taken from the linear best fit curve, calculations for β using Eq. (3.1) gave values within 3% of the theoretical value for all frequencies where spikes were noted in the measured transmission loss. It is recognized that this comparison is of limited value because of (1) the assumption of a linear dependence of ϕ_{22} on frequency, and (2) the use of theoretical β to calculate the points of ϕ_{22} (f) from which the linear best fit curve was derived. A more accurate determination of β as a function of frequency for this or any higher order mode would

require either a continuously variable length WUT—ideal, but obviously impossible from a fabrication standpoint—or a very large number of different lengths of the same waveguide geometry, in order to have multiple measurements (different lengths) at each spike frequency and thus be able to eliminate ϕ_{22} as an unknown in Eq. (3.1). With the three lengths of WUT used, two did have transmission spikes at one frequency, f = 15.2 GHz. Using Eq. (3.1), ϕ_{22} was eliminated and β calculated directly as β = 94.7°/cm. This value compares favorably with the value β = 94.5°/cm as determined using the linear approximation of $\phi_{22}(f)$ and the theoretical value β = 95.8°/cm for the $QLSE_{2,0}$ mode at this frequency, thus tending to justify the bootstrap calculations used to compare the theoretical and experimentally derived propagation characteristics at other frequencies for this higher order waveguide mode.

The approach of Method 3 of Appendix D used to correct for mismatch effects yields an attenuation factor, or loss term α, as well as the phase term β for the dominant waveguide mode. However, this method was found to be unsuitable for calculating α from the measured data. Using the measured complex transmission coefficient of three different length samples resulted in wild fluctuations of calculated α as a function of frequency, even calculating α as a negative quantity (waveguide gain rather than loss) in some instances. This was determined to be a result of the sensitivity of the mismatch correction program to variations of α in the three different length samples. With the construction technique used for the waveguide housing—with six separate metal pieces held together with screws—the conductor losses were greatly affected by the effective extra resistance formed at the metal-to-metal interfaces, although such imperfections had only a negligible effect on the phase term β. Sizable variations in attenuation (loss/unit length) thus were not unexpected since the nature of the metal-to-metal contacts could not be controlled. The effect of variations in actual α between sample lengths on the calculated values of α and β was checked for a variety of conditions. In each case, the complex transmission coefficient t_{21} of three lengths of an imaginary waveguide was computed, assuming a fixed β and fixed values for the S-parameters representing the discontinuity at either end of the WUT. Only α was changed for the three different lengths. Then using the approach of Method 3 incorporated into program CROOT3, these computed values of t_{21}, along with the three assumed lengths, were used to calculate the "measured" values for α and β. In all cases, β was calculated to be within 1% of the presumed value, but in general the calculated value of α was far removed from the average of the three presumed values.

The method that was used to experimentally determine the attenuation of the dominant mode for comparison with the theoretical value was the approach of Method 4 described in Appendix D. With this method, only one length of WUT was required, and the loss term α was calculated at frequencies where the measured transmission loss was minimum, or equivalently where $|t_{21}|$ was maximum. At these frequencies, with $|t_{21}|_{max} = T$,

$$T = \frac{(1 - |s_{11}|^2)\exp(-\alpha L)}{1 - |s_{11}|^2 \exp(-2\alpha L)} \tag{3.2a}$$

from which

$$\alpha(\text{nepers/length}) = -(\ln X)/L \tag{3.2b}$$

where

$$X = \left\{[(1 - |s_{11}|^2)^2 + 4T^2|s_{11}|^2] + |s_{11}|^2 - 1\right\}/(2T|s_{11}|^2). \tag{3.2c}$$

The 5.07 cm length sample of the waveguide described in Fig. 12 had minimum transmission loss at frequencies f_1 = 8.34 GHz, f_2 = 10.52 GHz, and f_3 = 11.85 GHz, with measured losses of 0.35 dB ($|t_{21}|$ = 0.961), 0.5 dB ($|t_{21}|$ = 0.944), and 0.55 dB ($|t_{21}|$ = 0.939), respectively. Using resistive film loading of the WUT as described in Appendix C, the value of $|s_{11}|$ at these three frequencies was then measured as 0.776, 0.750, and 0.724, respectively. With α(dB/m) = α(Np/m) · 20/ln10, the attenuation was calculated from (3.2) as $\alpha(f_1)$ = 1.74 dB/m, $\alpha(f_2)$ = 2.83 dB/m, and $\alpha(f_3)$ = 3.47 dB/m.

From the theory, taking the conductivity of brass as $\sigma = 1.41 \times 10^7$ mhos/m [74] and the dielectric loss tangent of polystyrene as $\tan \delta = 4.3 \times 10^{-4}$ [26], the total loss term, $\alpha = \alpha_c + \alpha_d$, was predicted to have values of $\alpha(f_1) = 1.15$ dB/m, $\alpha(f_2) = 1.37$ dB/m, and $\alpha(f_3) = 1.50$ dB/m. At each frequency, the conductor loss term was slightly more than the dielectric loss term. In a ratio comparison, the ratio (in dB/m) of measured loss to theoretical loss was 1.51 at f_1, 2.07 at f_2, and 2.31 at f_3. Measurements of other waveguide geometries resulted in similar ratios of measured/theoretical attenuation; in all cases the discrepancy was attributed to the multisection design of the waveguide housing for which the added resistance at the joints was not taken into account by the theory. Previous experience with sectioned experimental waveguide housings has indicated discrepancies of similar magnitudes between theoretical and measured attenuation values.

3.2 Peak Power Breakdown

The peak power breakdown level was measured for one sample of dielectric loaded double ridged waveguide to give a comparison with the theoretically determined value. The fabrication of this waveguide was different than that used for low-power tests. A two-piece housing was machined from aluminum, with the ridges being direct extensions of the top and bottom waveguide walk to prevent possible arcing at the joints between the walls and separate ridge sections. Repeated assembly and disassembly was not a consideration, and a fabrication method was sought that would ensure the complete absence of air gaps at the metal/dielectric interface. With polystyrene chosen as the dielectric material, an *H*-shaped insert was machined to form a loose fit in the assembled aluminum housing. The polystyrene surfaces that would mate with the metal surfaces of the housing were then deposited with a thin ($\approx$3000 Å) evaporated gold film. The complete waveguide section was then assembled using silver epoxy to fill any voids between the metal walls and the plated surfaces of the polystyrene. When the high-power tests were made, breakdown occurred in the dielectric rather than in air at the dielectric side walls although the theory predicted a power breakdown level for the dielectric more than five times that for air breakdown. It was determined that the dielectric breakdown was due to the rough surface left by the milling operation at the bottom of the slot in the polystyrene, where the evaporated gold film effectively formed a *conducting surface* with very sharp protrusions and irregular features. The conflict with the theory was attributed to the extreme buildup of electric field intensity at these sharp points, since the theoretical analysis assumed smooth wall surfaces (Section 2.3). To avoid arcing within the dielectric due to rough surface conditions, the metal evaporation technique was abandoned in favor of the construction method which was finally used for the high power test. This method used coil dope to fill the space between the smooth metal surfaces and the solid polystyrene *H*-shaped insert as shown in Fig. 14, analogous to the use of silicone grease for the low-power tests. The waveguide was assembled using screws and steel locating pins, and then baked at 90°C in an oven to drive out the toluene from the coil dope. A rectangular steel insert was then used to remove any last traces of coil dope from the top and bottom walls at the junction with the polystyrene insert. One end of this waveguide was shorted by an aluminum plate screwed to the end of the housing. The other end had a flange to mate with X-band waveguide (not shown in Fig. 14).

The physical length of the waveguide sample (WUT) was chosen to that at a frequency $f = 9.368$ GHz (the frequency of the high-power measurement facility) the electrical length would be such that the front face of the sample waveguide would be close to a voltage null position of the standing wave pattern caused by the short circuit. This aspect of the high-power measurement was necessary to ensure that power breakdown (arcing) would first occur within the WUT rather than in air at the interface of the WUT and the X-band waveguide of the high-power system. The WUT was fabricated with an initial length longer than necessary. A brass plunger, U-shaped with rectangular arms machined to fill the air region of WUT, was then inserted into the WUT to form an adjustable quasi-short circuit. Using the ANA in the swept frequency mode, the position of the quasi-short was adjusted to a position where the front face of the WUT represented a near short circuit to the adjoining section of X-band waveguide. The insertion depth of the plunger was measured, and a corresponding length then removed from the backside of the WUT by machining. Addition of the aluminum plate to form the

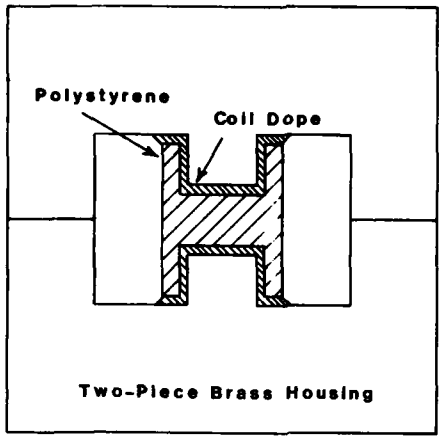

Note: Coil Dope Thickness Exaggerated For Illustration

Fig. 14 — High-power test housing

backside short circuit then completed the fabrication. The dimensions of the waveguide used for the high-power measurement were: a = 0.600 in. (1.524 cm), b = 0.250 in. (0.635 cm), d = 0.150 in. (0.381 cm), s = 0.100 in. (0.254 cm), t = 0.200 in. (0.508 cm), and a length L = 1.587 in. (4.031 cm). With the polystyrene used as the dielectric material, $\epsilon_r = 2.54$.

Because of the standing wave within the WUT set up by the short circuit, points of maximum voltage occur at distances equal to an odd number of quarter wavelengths from the short. At these points, the voltage is twice that due to the wave traveling in either direction. (The small amount of loss in the short length of the WUT was neglected.) Such voltage peaks thus are equal to the voltage that would be produced by a single unidirectional wave carrying four times the amount of power carried by either wave forming the standing wave pattern (Appendix D). Peak power breakdown of the waveguide occurs when, at any point, the electric field intensity (proportional to the voltage in the equivalent transmission line circuit) exceeds the breakdown strength of the medium (either air or dielectric) at that point. Since the power-handling capability of the waveguide has been assumed to be the peak power breakdown level of the waveguide when propagating energy in a single direction, the power quantity of interest in the high-power measurement will be the maximum voltage effective power, or P_{MVE}, equal to four times the power carried by each of the waves forming the standing wave pattern in the WUT.

Because the actual power levels within the WUT could not be measured directly, it was necessary to calculate P_{MVE} in terms of power incident on the front face of the WUT since the latter power could be measured. From Appendix D, Eq. (D14)

$$P_{\mathrm{MVE}} = \frac{4(1 - |s_{22}|^2)}{1 + |s_{22}|^2 + 2|s_{22}| \cos \zeta} P_i \tag{3.3}$$

$$\zeta = \phi_{22} - 2\beta L \tag{3.4}$$

where P_i is the peak power incident on the front face of the WUT and s_{22} is the complex reflection coefficient of the discontinuity formed at the junction of the WUT and the X-band waveguide, as seen from the side of the WUT, with

$$s_{22} = |s_{22}| \exp (j\phi_{22}).$$

Prior to the high-power testing, measurements of the WUT were made at low power using the ANA to determine the necessary parameters required to calculate P_{MVE} using Eq. (3.3). Using resistive film to load the WUT (Appendix C), the complex reflection coefficient of the junction discontinuity, as seen from the side of the X-band waveguide, was measured as a return loss of 4.4 dB with a phase angle of 176 deg, or equivalently

$$s_{11} = 0.6 \angle 176°.$$

From Appendix C, $|s_{22}| = |s_{11}|$, thus

$$|s_{22}| = 0.6. \tag{3.5}$$

After removing the resistive film, the complex reflection coefficient of the shorted WUT was measured as t_{11}. At the frequency $f_0 = 9.368$ GHz,

$$t_{11}|_{f=f_0} = 0.999 \angle -165°,$$

thus verifying that the front face of the WUT would present an approximate short circuit to the X-band waveguide. Return loss maximums (minimum $|t_{11}|$) were found at frequencies of $f_1 = 8.775$ GHz and $f_2 = 10.76$ GHz. The procedure outlined as Method 5 in Appendix D was then used to calculate ϕ_{22}. From (D16)

$$\phi_{22}|_{f=f_i} = (2n + 1)\pi + \beta_i L, \quad i = 1, 2 \tag{3.6}$$

where β_i is the propagation constant of the WUT at the frequency f_i. Using Eq. (3.4), ϕ_{22} for the frequencies f_1 and f_2 were computed as 33.2° and 31.8°, respectively. From (D17), linear interpolation was used to determine

$$\phi_{22}|_{f=f_0} = 32.5°.$$

Then from Eq. (3.4)

$$\zeta = 67.6° \text{ (modulo } 360°) \tag{3.7}$$

at the frequency f_0. With the values given by Eqs. (3.5) and (3.7), the relationship expressed in Eq. (3.1) was calculated to be

$$P_{\text{MVE}} = 1.409\ P_i \tag{3.8}$$

at the high power frequency f_0. Of course, the numerical constant in Eq. (3.8) would change if either the length or geometry of the WUT were different.

Peak power breakdown was measured using a pulsed high-power source. The experimental facility used is depicted schematically in Fig. 15. The high-power modulator, an FXR 1 Megawatt Test Modulator, was triggered from a 1 kHz pulse generator and powered a Raytheon QK-172 X-band magnetron. The pulsed output from the magnetron was at an RF frequency of 9.368 GHz, with a repetition rate of 1 kHz and a pulse width adjustable from 0.1 to 1.0 μs. The pulse width was set to 0.8 μs for the high-power measurement. Maximum peak power available from the magnetron was 100 kW. The motor driven power divider was not used and locked into the low loss state. The high voltage from the modulator was set to achieve maximum power from the magnetron. Peak power incident on the WUT was controlled by manually adjusting the ganged waveguide sliding shorts, which together with the short slot 3 dB hybrid coupler and the folded magic tees formed a high-power attenuator, with the excess power from the magnetron being absorbed by a high-power waveguide load. The coupling between the main RF line and the thermistor head was measured independently at low-power levels on the ANA for accuracy in determining the power level incident on the WUT. The total coupling was measured as −49.8 dB at $f = f_0$, equivalent to a power ratio of 1.05×10^{-5}. The power in the RF pulse was flat within the 0.8 μs pulsewidth as measured by the crystal detector output on the oscilloscope. The peak power incident on the WUT was thus calculated as

$$P_i = \frac{\text{Pulse width}}{(\text{Repetition rate})(\text{power coupling})} P_1$$

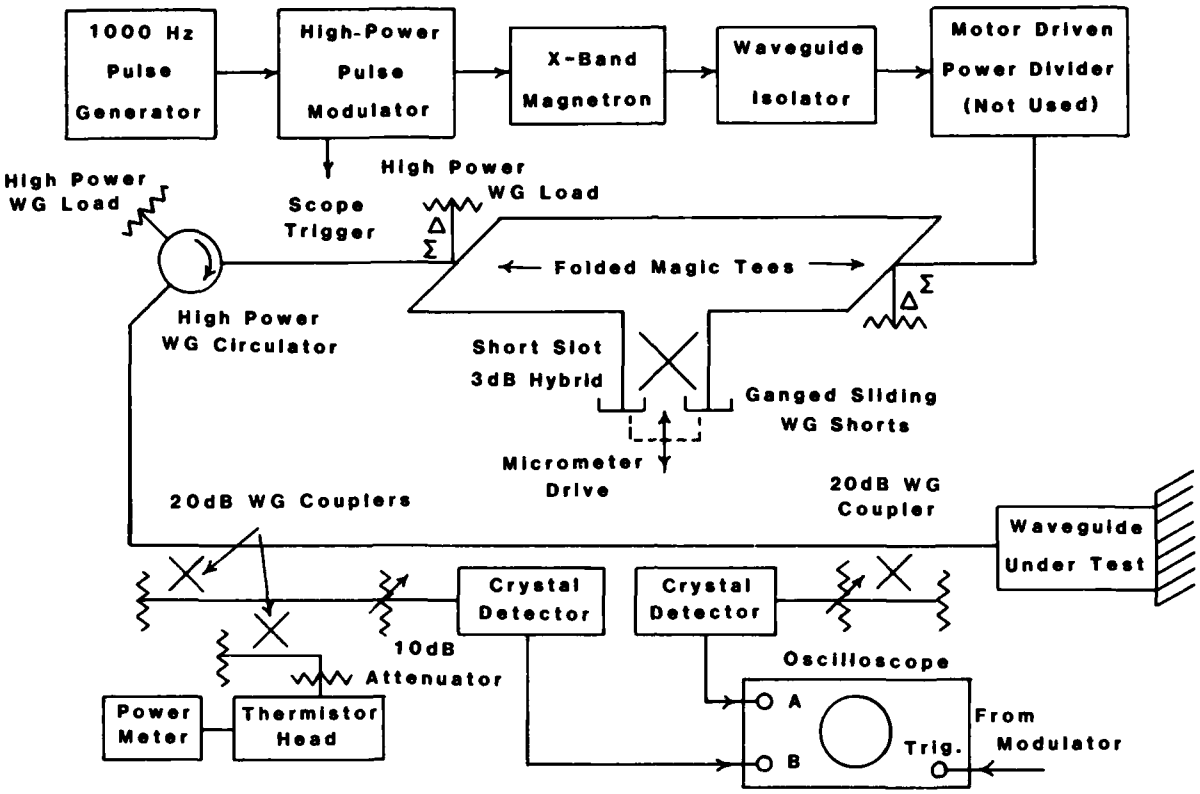

Fig. 15 — High-power test circuit

where P_1 was the average power measured at the thermistor head. With the appropriate numerical values,

$$P_i(\text{kW}) = 119\ P_1(\text{mW}).$$

A peak power meter was used as a check for the power measurement, using a crystal detector in place of the thermistor, and showed agreement within 2% of the peak power as calculated from the average power reading. The crystal detector shown connected to channel B of the oscilloscope in Fig. 15 was used to monitor the shape of the high-power pulse incident on the WUT, while the detector shown connected to channel A was used to monitor the reflected power pulse.

In the test to measure the peak power breakdown, the power level was slowly increased from zero while carefully monitoring the reflected pulse displayed on the oscilloscope and listening for any sounds of arcing within the WUT with the aid of a stethoscope. The first evidence of breakdown was a sudden onset of strong jitter in the reflected pulse, accompanied by the sudden and distinctly audible arcing noise. This first breakdown occurred at an average power of 0.58 mW as measured by the average power meter, corresponding to an incident peak power level of 69 kW incident on the WUT. Because of the accumulation of carbon deposits in the WUT, subsequent measurements yielded decreasing power breakdown levels. After the high-power measurements were concluded, the WUT was disassembled. As expected, the arcing, as evidenced by the carbon buildup, was at regular intervals along the sides of the polystyrene insert. These intervals corresponded to a half wavelength in the WUT, with the arcing closest to the short occurring approximately one quarter wavelength from the short and having the greatest degree of carbon buildup. There was a very slight trace of arcing within the polystyrene, but the majority of breakdown was at the air dielectric interface as predicted by the theory. There was evidence of arcing at the front face of the WUT also, between corners of the ridge, as evidenced by carbon paths across the end of the polystyrene insert. This arcing at the interface of the

WUT with the X-band waveguide was attributed to a shift in the position of the maximum in the standing wave pattern. Prior to the initial breakdown, an approximate voltage null was located at the interface. When the power level was increased sufficiently to cause arcing at a point $\lambda_g/4$ from the short, such arcing effectively produced a short circuit at that point during the short interval of the arc, thus shifting a near maximum of the standing wave pattern to the front face of the WUT and producing the arcing at that point.

From Eq. (3.8), the incident peak power of 69 kW for the initial power breakdown measurement corresponds to an equivalent unidirectional power level of $P_{\mathrm{MVE}} = 97.2$ kW. With the voltage breakdown strength of air taken as 30 kV/cm, a peak power breakdown value of $P_{BD} = 696$ kW is predicted by the theory. The discrepancy between the peak power breakdown level predicted by the theory and that determined experimentally was attributed to three factors. First, a power safety factor of 4 is commonly utilized in practice for peak power ratings [67]. With this safety factor included, equivalent to reducing the breakdown strength of air to 15 kV/cm, the theoretical power breakdown of the WUT reduces to $P_{BD} = 174$ kW. The second factor was the presence of small but sharp protrusions of hardened coil dope left at the junction of the top and bottom waveguide walls with the sidewalls of the polystyrene insert. Such protrusions were the result of using the metal mandrel to attempt to remove all of the excess coil dope from the waveguide. Just as at sharp corners of conducting surfaces, extreme buildup of electric field intensity can occur at sharp dielectric corners [66]. The theoretical analysis did not take into account such possible electric field enhancement caused by a flawed assembly technique. The third factor was the unknown effects of heating within the polystyrene insert. At peak power breakdown, the average power carried by each wave forming the standing wave within the WUT was 20 W. Using the theoretical value of dielectric loss, power dissipation within the dielectric was calculated as 0.5 W. Since the thermal conductivity of polystyrene is very low and the power level was raised gradually, it is quite possible that the heating caused portions of the dielectric to weaken or even melt, forming irregularities on the otherwise smooth sidewalls, thus sharply increasing the electric field intensity at some points. Thermal effects caused by average power heating were not considered in the waveguide analysis of this investigation.

4.0 WAVEGUIDE PERFORMANCE CHARACTERISTICS

4.1 Discussion of General Waveguide Characteristics and Parameters

For the purposes of this investigation, the primary waveguide characteristics of concern are the single mode bandwidth and the peak power handling capability. Attenuation is also an important factor but will be considered secondary to the primary characteristics. All results presented in this chapter are based on the theoretical analysis derived in Section 2.

Material properties such as metal wall conductivity, dielectric breakdown strength, and dielectric loss tangent will affect the waveguide performance. However, these material properties will not be considered as design parameters, but will be assumed constant as discussed in Section 2. The wall conductivity and dielectric loss tangent affect only the waveguide attenuation; corrections to the calculated attenuation must be made as outlined in Section 2.4 to account for deviation from these assumed parameter values. The exact value for the dielectric breakdown strength will not affect the peak power breakdown calculation for most waveguide configurations since breakdown will occur in the air region rather than in the dielectric. For those cases where the power level for dielectric breakdown is less than that for air breakdown, or where the actual dielectric strength is significantly less than the assumed value, corrections to the waveguide power handling capability must be made as discussed in Section 2.3.

The design parameters will consist of the five waveguide dimensions shown in Fig. 3 and the relative dielectric constant of the dielectric loading material. The six waveguide design parameters are thus (1) the width a, (2) the height b, (3) the gap height d, (4) the ridge width s, (5) the dielectric width t, and (6) ϵ_r. For many design purposes, the number of variable parameters may be reduced to five by

normalizing all dimensional quantities to the waveguide width. Conventional frequency scaling techniques [8] are applicable for such a normalization process. The power-handling capability and attenuation also may be normalized. Since these waveguide characteristics are of interest for the $QLSE_{1,0}$, or dominant, mode only, they will be normalized to the corresponding characteristics of an empty rectangular waveguide operating in its dominant ($TE_{1,0}$) mode and at the same frequency. The normalized power will thus be calculated as

$$P_{BD}\,(\text{normalized}) = \frac{P_{BD}}{P_{BD}\,(\text{reference WG})}$$

while the normalized attenuation due to conductor loss will be calculated as

$$\alpha_c\,(\text{normalized}) = \frac{\alpha_c}{\alpha_c\,(\text{reference WG})}.$$

For each configuration of the dielectric loaded double ridged waveguide (DLDRWG), the corresponding reference waveguide is conventional rectangular waveguide with the necessary width to give a $TE_{1,0}$ mode cutoff frequency equal to f_c for the $QLSE_{1,0}$ mode of the DLDRWG. The reference waveguide will use an aspect ratio (height/width) of 0.5 regardless of the aspect ratio of the DLDRWG, and will assume copper walls and an air voltage breakdown of 30 kV/cm. Since the reference waveguide has no dielectric loss, the dielectric loss of the DLDRWG will be normalized to the conductor loss as

$$\alpha_d\,(\text{normalized}) = \frac{\alpha_d\,(\text{frequency (GHz)})^{1/2}}{\alpha_c\,(\text{reference WG})}.$$

The added factor of $f^{1/2}$ is necessary because of the difference in frequency dependence of α_c and α_d (Section 2.4).

Even with the number of design parameters reduced to five, it is obviously impossible to present complete design information, either in graphical form or otherwise. However, sufficient theoretical results will be displayed to show typical characteristics for the DLDRWG, and more detailed results will be presented for a specific dielectric material.

Figures 16 and 17 emphasize the fact that the first higher order mode that may propagate in DLDRWG is dependent on the exact waveguide geometry. For the fixed parameter ratios given in Fig. 16(a), the first higher order mode (FHOM) is the $QLSE_{1,1}$ mode for values of $d/b > 0.73$, but is the $QLSE_{2,0}$ mode for smaller values of d/b. With the fixed parameter ratios changed slightly, Fig. 16(b) shows the FHOM to be the $QLSE_{1,1}$ mode for $d/b > 0.82$ but the $QLSM_{0,1}$ mode for smaller values of d/b. In Fig. 17, the parameter ratio s/a is treated as the variable, with the ratio t/a maintained as $t/a = s/a + 0.1$ and with the other parameters fixed. The FHOM is the $QLSM_{0,1}$ mode for $s/a < 0.2$ and the $QLSE_{2,0}$ mode for $s/a \geqslant 0.2$.

For dielectric slab loaded rectangular waveguide with an aspect ratio of 0.5, the $LSE_{1,1}$ mode is normally the FHOM. The corresponding $QLSE_{1,1}$ mode in DLDRWG was found never to be the FHOM for a variety of geometries where $b/a = 0.5$ and $d/b < 0.5$. The elimination of the quasi-$LSE_{1,1}$ mode as the FHOM is the principal reason that the DLDRWG can achieve large single mode bandwidths without having to reduce the waveguide aspect ratio.

4.2 Variation of Performance About a Fixed Geometry

To demonstrate some of the characteristics of DLDRWG, a fixed (normalized) geometry was chosen, with $b/a = 0.5$, $d/b = 0.3$, $s/a = 0.3$, $t/a = 0.4$, and $\epsilon_r = 6$. Each of these quantities was then treated separately as a variable, with the remaining quantities held constant, and the resulting change in normalized waveguide performance plotted. The attenuation and power breakdown levels were calculated at a frequency $f = \sqrt{3}\,f_c$, where f_c is the $QLSE_{1,0}$ mode cutoff frequency for the corresponding waveguide geometry.

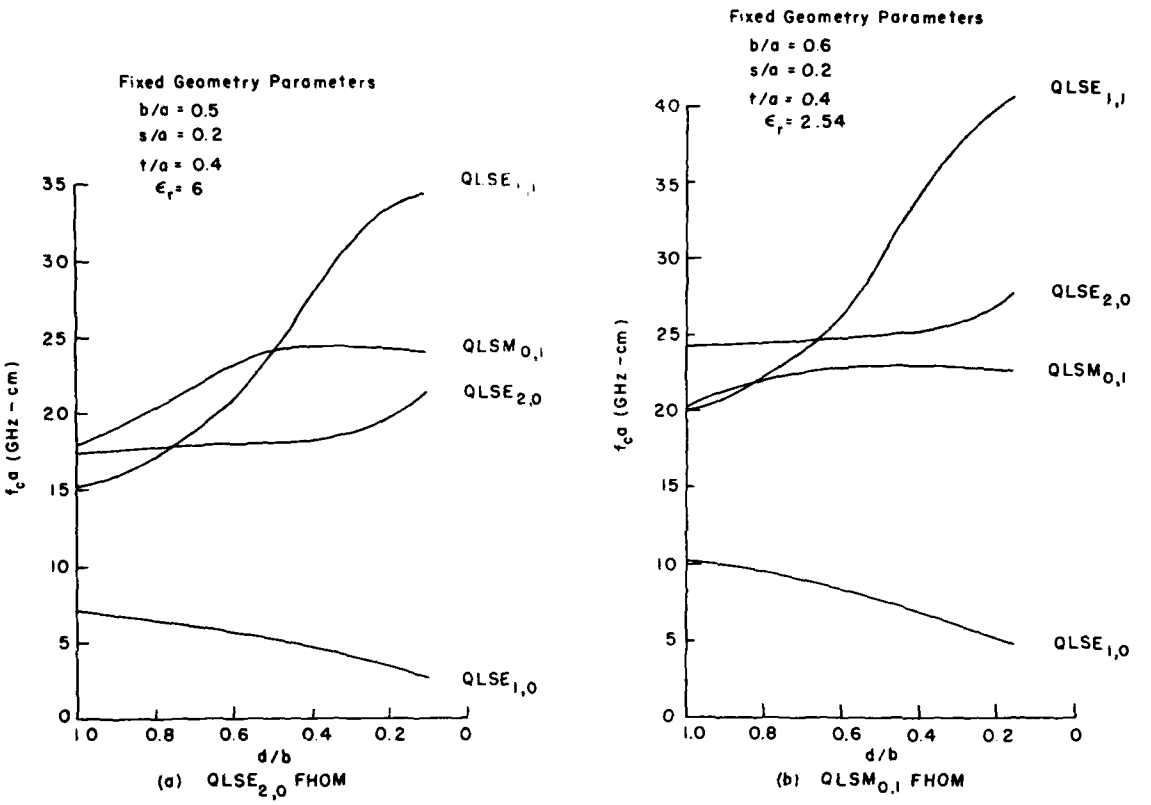

Fig. 16 — Variation of f_c as a function of d/b for different modes; (a) $QLSE_{2,0}$ FHOM and (b) $QLSM_{0,1}$ FHOM

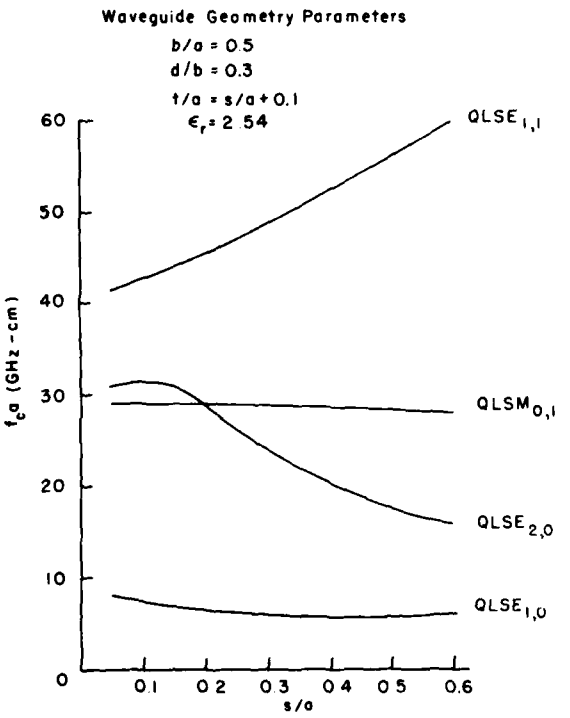

Fig. 17 — Variation of f_c as a function of s/a for different modes

In Fig. 18, the waveguide performance is plotted as a function of the ratio d/b. The dashed portion of the bandwidth curve represents a condition where the $QLSE_{1,1}$ mode is the FHOM, and the solid portion, the condition where the $QLSE_{2,0}$ mode limits the single mode bandwidth. A decreasing value of d/b provides an increasing bandwidth, but also results in a decreasing power breakdown level and an increasing attenuation due to conductor loss. Note that most of the increase in bandwidth arises as a consequence of the lowered cutoff frequency of the dominant $QLSE_{1,0}$ mode rather than an increase in the cutoff frequency of the FHOM. For this particular geometry, as d/b is varied from unity to a value of 0.1, the cutoff frequency of the $QLSE_{1,0}$ mode is reduced by a factor of 2.65, while the cutoff frequency of the FHOM increases by a factor of 1.41. The size of the reference waveguide used to normalize the power and attenuation characteristics of the DLDRWG is determined by the cutoff frequency of the $QLSE_{1,0}$ mode, and thus increases with bandwidth. With increased size, the reference waveguide will have greatly increased P_{BD} and decreased α_c, thus the variations of normalized P_{BD} and α_c of the DLDRWG with d/b are accentuated relative to the variations of the corresponding nonnormalized values.

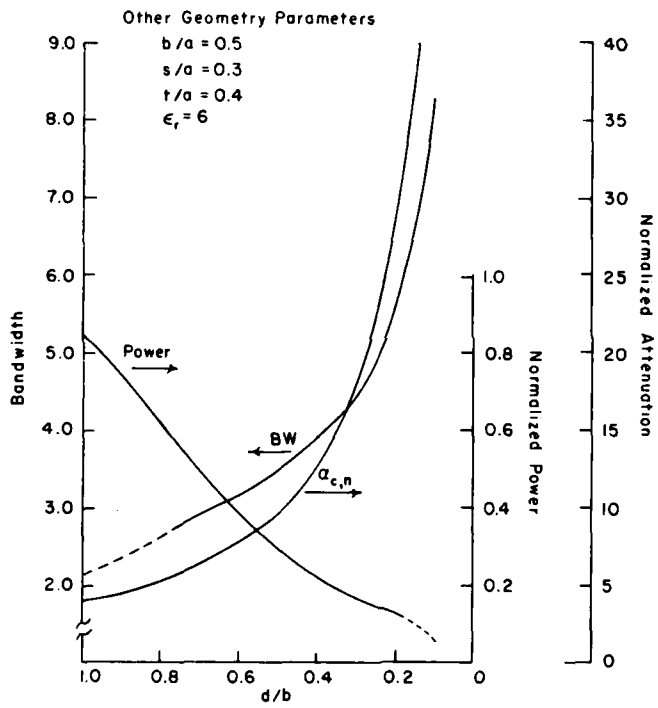

Fig. 18 — Waveguide performance as a function of d/b variation about a fixed geometry

The normalized dielectric loss as a function of d/b was essentially constant, with $\alpha_{d,n} = 10.2$ for $d/b = 1$ and $\alpha_{d,n} = 11$ for $d/b = 0.1$. The solid portion of the power breakdown curve represents voltage breakdown in air, while the dashed portion denotes breakdown of the dielectric material. A similar convention for plotting power breakdown will be used henceforth.

The parameter ratio of s/a is treated as the variable in Fig. 19. The FHOM was the $QLSE_{2,0}$ mode for all values of s/a. The bandwidth peaks for $s/a = 0.17$, whereas the power peaks at $s/a = 0.07$. Any design must therefore consider some trade-off between bandwidth and power. Such trade-off considerations will be required to determine most parameters. Here the variation of attenuation is small, but in other cases the change of attenuation may be large and thus be a factor in determining a

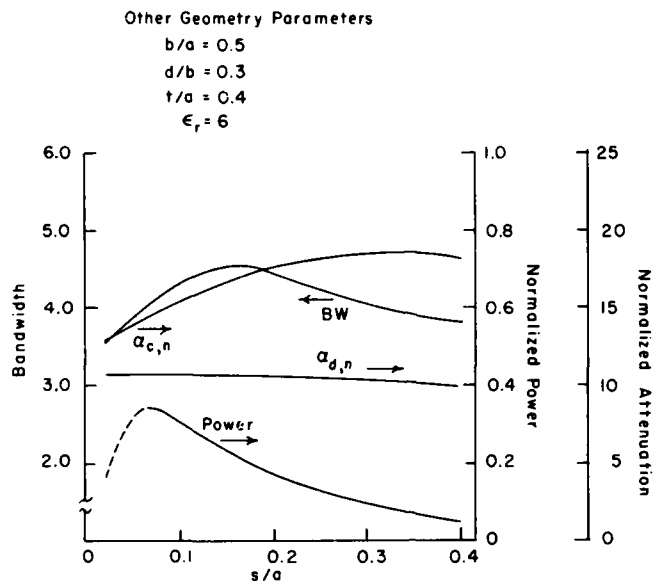

Fig. 19 — Waveguide performance as a function of s/a variation about a fixed geometry

final waveguide geometry. The rapid drop in P_{BD} as s/a becomes small is due to dielectric breakdown because of the increased electric fields in the gap region. As the ridge width approaches the dielectric width, $s/a \rightarrow t/a$, more of the fringing fields from the ridge gap extend into the air region, thus lowering P_{BD}.

In Fig. 20, the variable is the ratio t/a. Again the $QLSE_{2,0}$ mode is the FHOM. The trade-off between bandwidth and power is even more pronounced than in Fig. 19. As the width of the dielectric increases, more and more of the propagating energy is contained in the dielectric, thus dielectric breakdown becomes the limiting factor for power handling capability.

In Fig. 21, the ratio of b/a is taken as the variable quantity. Both power and bandwidth are weak functions of b/a, and attenuation from dielectric loss is almost constant. Conductor loss is strongly dependent on the height, however, increasing rapidly as b/a becomes small. A good design philosophy would incorporate as large an aspect ratio as practical, making up lost power and bandwidth by varying other parameters which would not lead to such drastic increases in attenuation.

Since the ratio d/b is fixed, small values of b/a result in small gap spacing, and the consequential dielectric breakdown is apparent. The solid portion of the bandwidth curve denotes the $QLSE_{2,0}$ mode as the FHOM, while the dashed portion denotes the $QLSM_{0,1}$ mode as the FHOM. For this geometry, the $QLSM_{0,1}$ mode will remain the FHOM for $b/a > 0.76$, and the bandwidth will start to drop sharply for larger values of b/a. As for any geometry, sufficiently large values of b/a will cause the $QLSM_{0,1}$ mode to become the dominant mode. The practical upper limit on b/a for a good design would be the value at which the bandwidth starts to degrade rapidly.

In Fig. 22, the waveguide performance is plotted with the relative dielectric constant ϵ_r as the variable. Low values of dielectric result in the $QLSM_{0,1}$ mode as the FHOM (dashed portion of the bandwidth curve), while larger values of ϵ_r have the $QLSE_{2,0}$ mode as the FHOM. For values of $\epsilon_r > 4$, the increase in bandwidth is negligible with further increase of ϵ_r, while the power is dropping and the attenuation is increasing rapidly. The curves of Fig. 22, as well as investigation of other waveguide geometries, dictate that a good design should use the minimum value of ϵ_r required to achieve the

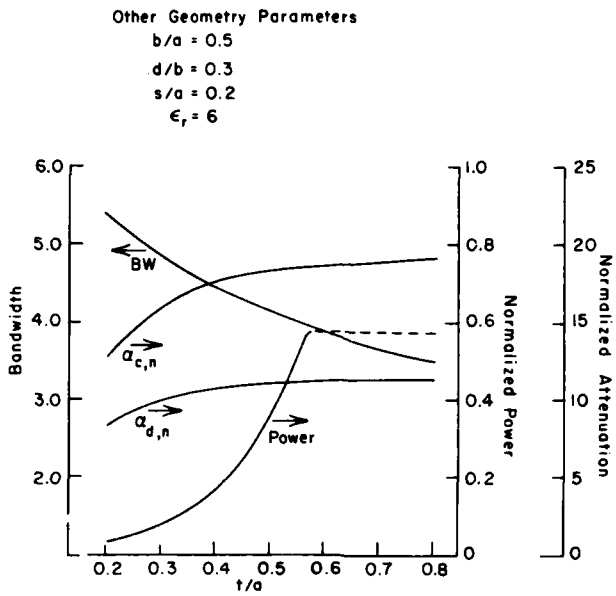

Fig. 20 — Waveguide performance as a function of t/a variation about a fixed geometry

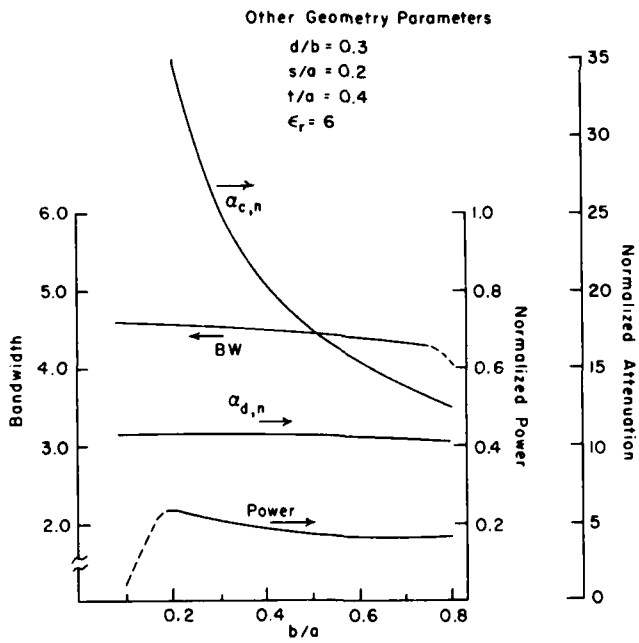

Fig. 21 — Waveguide performance as a function of b/a variation about a fixed geometry

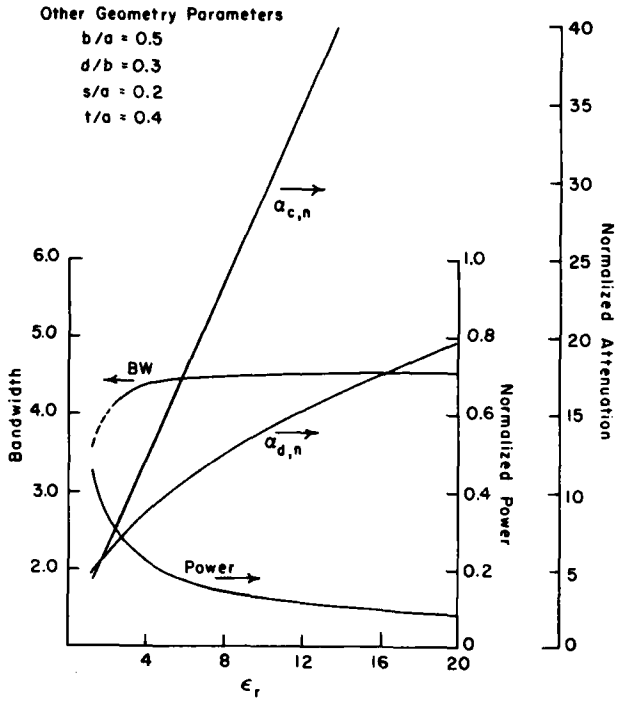

Fig. 22 — Waveguide performance as a function of ϵ_r variation about a fixed geometry

required power and bandwidth. Of course, there will still be performance trade-offs to be made in any design, and dielectrics with very low values of ϵ_r will generally have lower breakdown values than that assumed.

Any number of geometries could be chosen as the fixed geometry and plots made analogous to those depicted in Figs. 18 to 22. The resulting variation of waveguide performance with each parameter will depend on the initial geometry. It is obviously impossible to describe all of the combinations of performance variations, but certain consistent design aspects stand out: (1) decreasing the value of d/b will result in larger bandwidths, but will also result in reduced power and increased attenuation; (2) both bandwidth and power will have peaks as a function of the parameter ratio s/a, usually at different values of the variable; (3) as the parameter ratio t/a is increased, the power increases until dielectric breakdown occurs, and the bandwidth will normally decrease but may peak for certain geometries; (4) bandwidth and power are relatively weak functions of the ratio b/a if the $QLSE_{2,0}$ mode is the FHOM, but attenuation becomes large as b/a is decreased; and (5) best overall waveguide performance will normally be achieved with the lowest practical value of ϵ_r.

4.3 Design Information for $\epsilon_r = 2.54$

Since low values of ϵ_r will normally give the best waveguide performance characteristics, more detailed design information will be presented for a dielectric with $\epsilon_r = 2.54$. This value of ϵ_r is typical for a dielectric material such as polystyrene [25,26]. A loss tangent of $\tan \delta = 10^{-4}$ and a dielectric breakdown strength of 300 kV/cm again will be assumed.

In Fig. 23, bandwidth is plotted as a function of s/a for different values of d/b. The ratio t/a is not fixed but varies as s/a, with $t/a = s/a + 0.1$. The rationale for maintaining such a relationship between t/a and s/a is to have the high strength dielectric extend out far enough to prevent air breakdown due to fringing fields from the gap, yet not so far as to greatly reduce the bandwidth. The ratio differential constant of 0.1 thus represents a design trade-off between power and bandwidth.

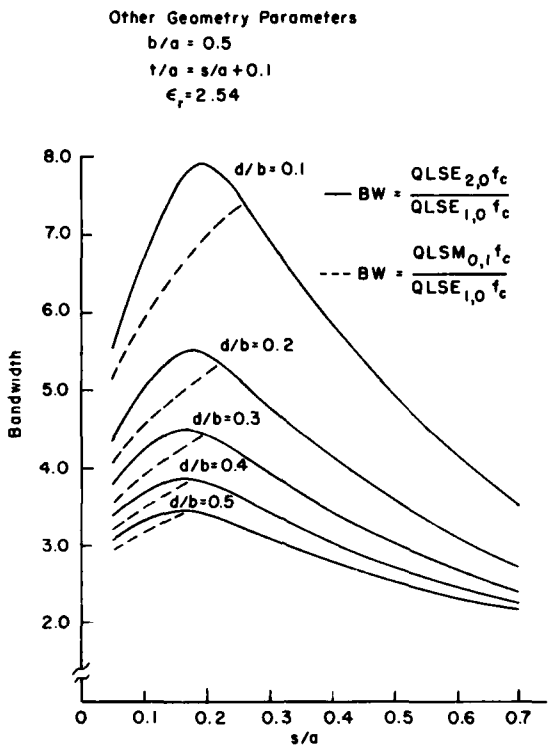

Fig. 23 — Bandwidth as a function of s/a for $\epsilon_r = 2.54$

The FHOM is seen to be the $QLSM_{0,1}$ mode for low values of s/a, thus the dashed portion of the bandwidth curves must be used to define the single mode bandwidth. The bandwidth as defined by the ratio of cutoff frequencies of the $QLSE_{2,0}$ and $QLSE_{1,0}$ modes is included for low values of s/a to emphasize the fact that the FHOM is dependent on the specific geometry. If the ratio of b/a were reduced (at the expense of increased attenuation), f_c for the $QLSM_{0,1}$ mode could be raised above f_c for the $QLSE_{2,0}$ mode for all s/a, and while both solid and dashed curves would be modified they would not intersect.

In Fig. 24, the normalized waveguide performance at a frequency $f = \sqrt{3} f_c$ is plotted as a function of s/a for $d/b = 0.5$, 0.3, and 0.1. Again t/a is maintained as $t/a = s/a + 0.1$. For all d/b values, P_{BD} increases with s/a, whereas bandwidth peaks for $s/a \approx 0.2$ (from Fig. 23), and the power/bandwidth trade-off is encountered once again.

In Fig. 25, the ratio s/a is held fixed and normalized waveguide performance plotted as a function of t/a for $d/b = 0.5$, 0.3, and 0.1. Bandwidth is also plotted to show the effects of variations of t/a on this characteristic. In all cases, the power breakdown level is minimum for $t/a = s/a$. Such a condition is to be expected since the fringing fields from the gap extend into the air region. The increase of P_{BD} with t/a is dependent on the value of d/b, with lower values of d/b giving a sharper rise of power. This is a predictable characteristic, since the smaller gaps will have fringing fields which do not extend out from the ridge walls as far as those of larger gaps.

Breakdown is seen to occur in the dielectric rather than in air for progressively lower values of t/a as d/b becomes smaller. This is to be expected since lower values of d/b result in increased concentration of the propagating energy in the gap region.

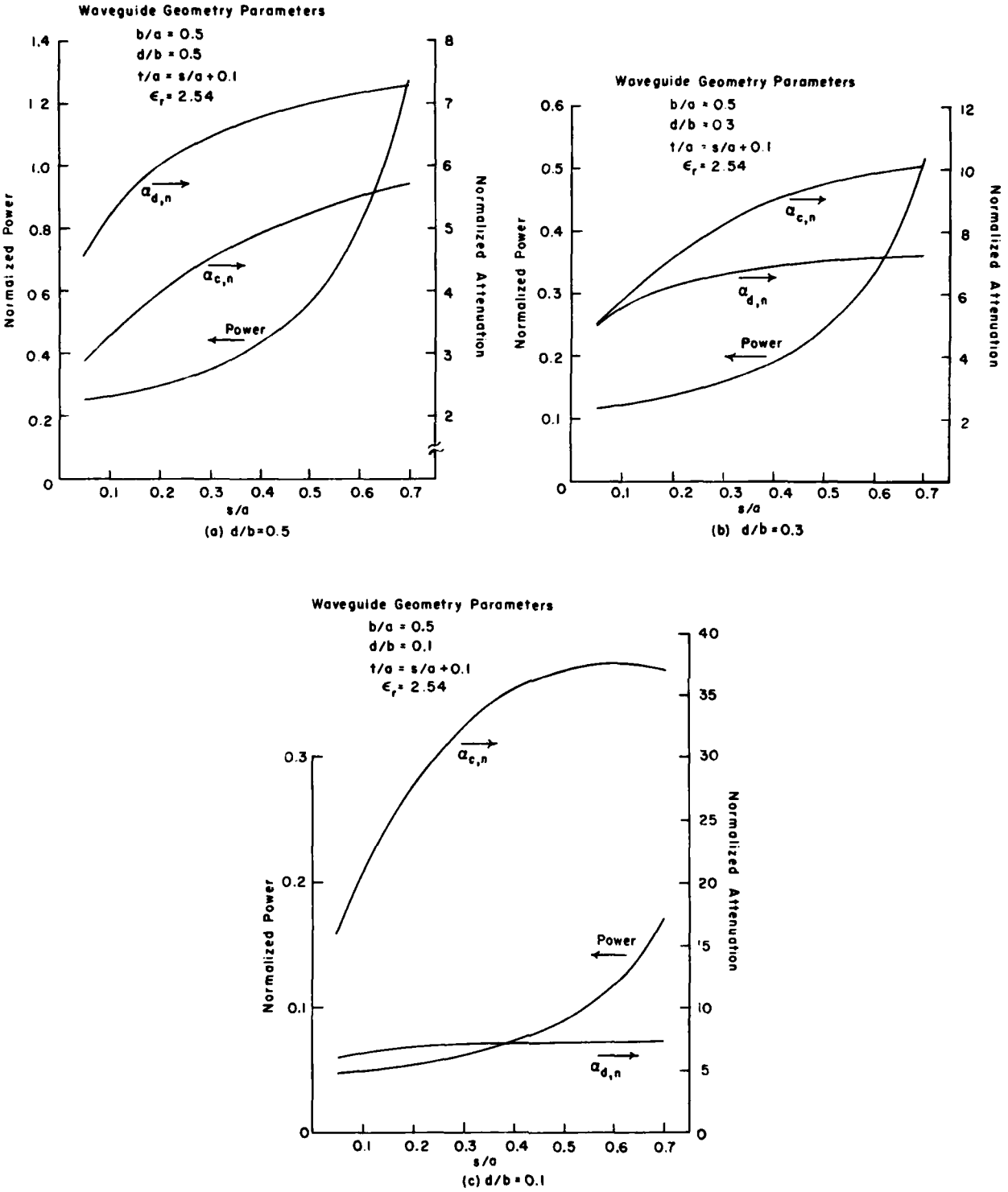

Fig. 24 — Waveguide performance as a function of s/a for $\epsilon_r = 2.54$; (a) $d/b = 0.5$; (b) $d/b = 0.3$; (c) $d/b = 0.1$

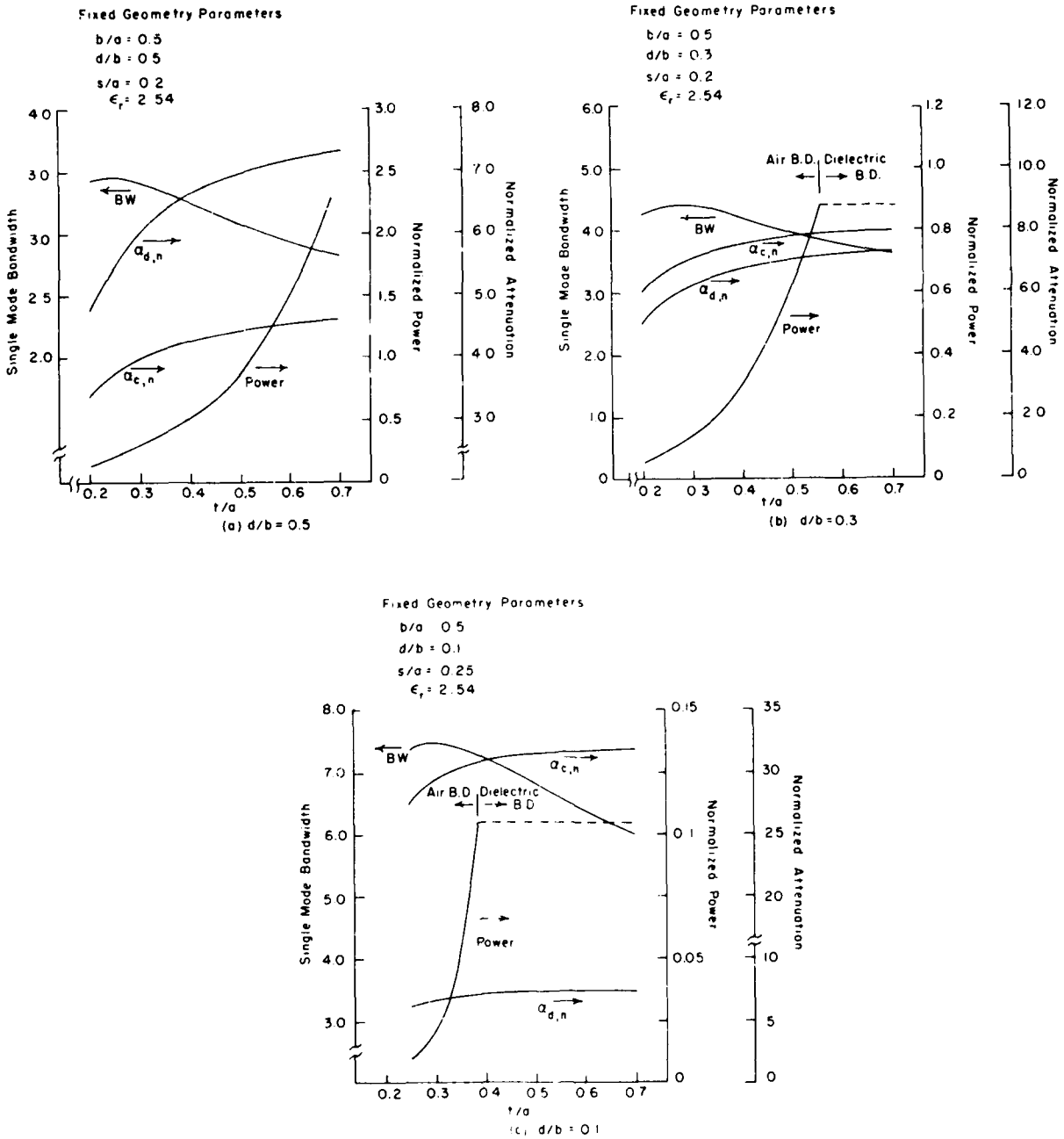

Fig. 25 — Waveguide performance as a function of t/a for $\epsilon_r = 2.54$; (a) $d/b = 0.5$; (b) $d/b = 0.3$; (c) $d/b = 0.1$

The bandwidth is essentially flat for low values of t/a, and decreasing moderately as t/a increases to larger values. A maximum power-bandwidth product would set t/a as $t/a = s/a + \Delta$, where Δ would have to be determined for the remaining values of parameters. In general, Δ would decrease as d/b decreases, and typically would have a range from 0.1 to 0.35.

The performance characteristics shown in Figs. 23 to 25 are not intended to provide a complete design procedure, since even for a fixed value of ϵ_r there remain too many variables to plot all characteristics. The depicted characteristics are intended to enable one to obtain an initial design geometry, and to provide an insight on how to fine-tune the design parameters to achieve the optimum waveguide performance.

4.4 Performance Comparison With Other Waveguide Types

The performance characteristics of a dielectric loaded ridged waveguide can be compared with those of other types of waveguide. For a fair comparison, the other waveguides should have a single mode bandwidth equal to that of the DLDRWG. The waveguides for which the comparison is made are the dielectric slab loaded rectangular waveguide (DSLRWG) and empty double ridged waveguide (DRWG). All waveguides are assumed to have copper walls, and all dielectric materials assume the values $\tan\delta = 10^{-4}$ and $E^{BD}_{dielectric} = 300$ kV/cm.

The design information presented by Findakly and Haskel [23] and Gardiol [68] for DSLRWG was used to achieve the optimum design for that waveguide, but with the aspect ratio reduced to force the $TE_{2,0}$ ($LSE_{2,0}$) mode to be the FHOM. The design information of Hoppfer [11] was used to achieve the optimum design for the DRWG. Performance characteristics of both waveguide types were calculated with the same program used in the calculations for DLDRWG.

The first comparison is for waveguides with a single mode bandwidth equal to 4.0 and a dominant mode cutoff frequency $f_c = 4.0$ GHz. For the DSLRWG, the minimum value of ϵ_r needed for BW = 4 was found to be $\epsilon_r = 18$. The remaining parameters used for the DSLRWG were: $a = 0.649$ (1.648), $b = 0.114$ (0.290), and $t = 0.071$ (0.180). Dimensional values are given in inches (centimeters). For the DRWG, the parameters were: $a = 0.833$ (2.116), $b = 0.416$ (1.057), $d = 0.098$ (0.249), $s = 0.221$ (0.561), and $\epsilon_r = 1$. Parameters for the DLDRWG were selected as: $a = 0.645$ (1.638), $b = 0.322$ (0.818), $d = 0.106$ (0.268), $s = 0.129$ (0.328), $t = 0.258$ (0.655), and $\epsilon_r = 2.54$. With these parameters, all three waveguide types have $f_c = 4.0$ GHz for the dominant mode and $f_c = 16.0$ GHz for the FHOM. The FHOM is the $TE_{2,0}$ mode for DSLRWG, the $TE_{2,0}$ mode for DRWG, and the $QLSE_{2,0}$ mode for DLDRWG.

Figure 26 shows the difference in the propagation constant β for the three different types of waveguides. As should be expected, the DSLRWG has the largest β for frequencies above cutoff because of the large dielectric loading with $\epsilon_r = 18$, while the DRWG has the lowest β since $\epsilon_r = 1$.

Figure 27 compares the attenuation characteristics of the three waveguide types. The large attenuation of the DSLRWG is due primarily to the reduced aspect ratio required to maintain the cutoff frequency of the $LSE_{1,1}$ mode above that of the $TE_{2,0}$ mode and achieve the single mode bandwidth. As with any waveguide, the attenuation increase for all three types as $f \rightarrow f_c$ is due to the rapid increase of dispersion.

Figure 28 compares power breakdown. The difference in power of the DLDRWG and that of the DRWG is actually greater than depicted since no corrections were made for corner effects in the latter waveguide. Such corrections were not required for the DLDRWG since breakdown in air occurred at a considerably lower power level than that for dielectric breakdown.

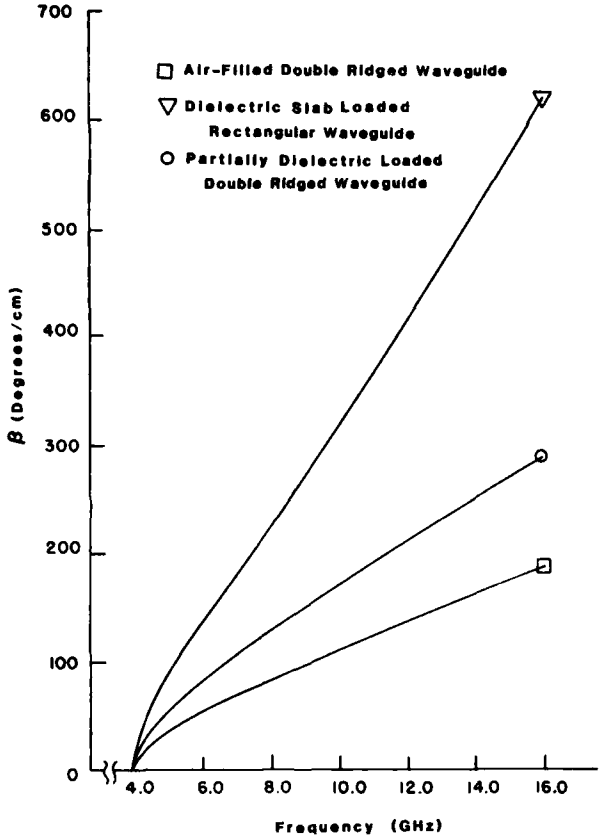

Fig. 26 — Comparison of propagation characteristics for waveguide types with $BW = 4$

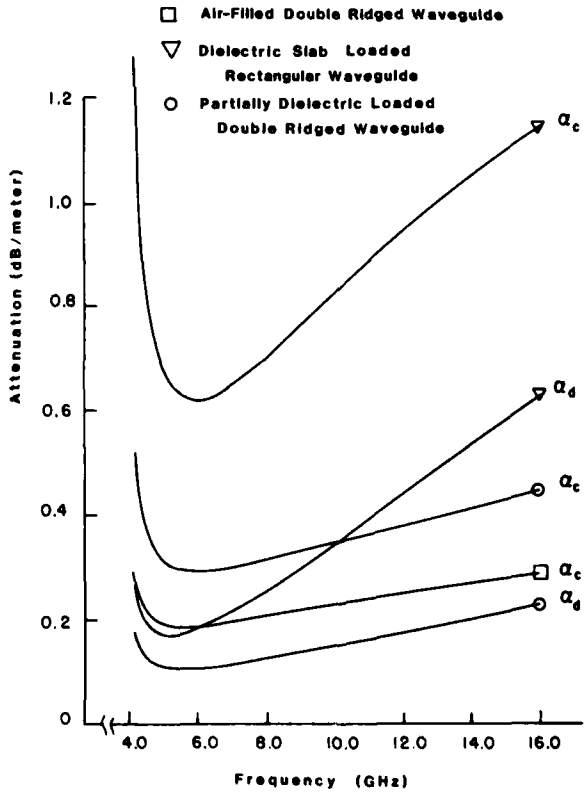

Fig. 27 — Comparison of loss characteristics for waveguide types with $BW = 4$

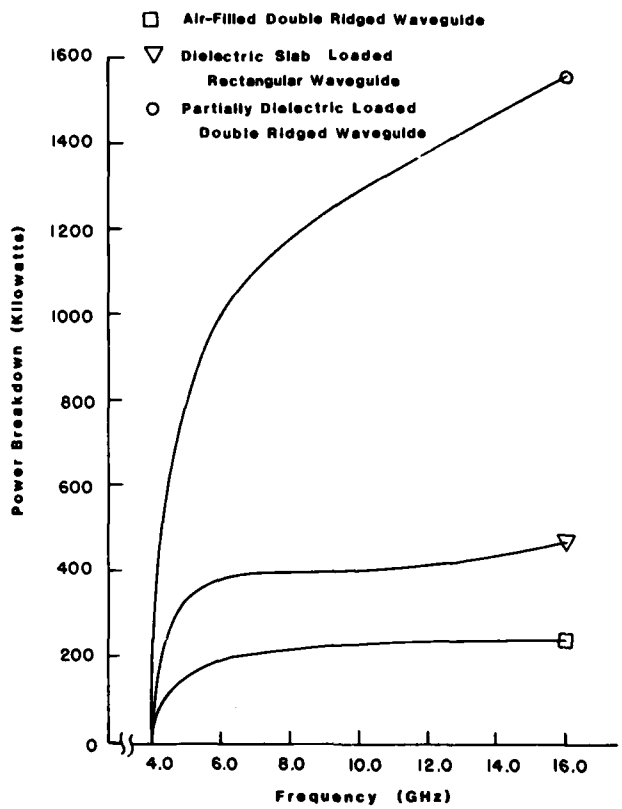

Fig. 28 — Comparison of power breakdown characteristics for waveguide types with $BW = 4$

Similar comparisons are made of the three waveguide types for each having a single mode bandwidth equal to 5.0 in Figs. 29 to 31. The parameters used for the DSLRWG were: $a = 1.056$ (2.682), $b = 0.119$ (0.302), $t = 0.076$ (0.193), and $\epsilon_r = 42$ (the minimum value of ϵ_r needed for BW = 5). An even smaller aspect ratio is required to prevent the $LSE_{1,1}$ mode from being the FHOM than in the case where BW = 4. The parameters used for the DRWG were: $a = 1.396$ (3.546), $b = 0.698$ (1.773), $d = 0.108$ (0.274), $s = 0.378$ (0.960), and $\epsilon_r = 1$. For the DLDRWG, the parameters were chosen as: $a = 1.046$ (2.657), $b = 0.522$ (1.326), $d = 0.105$ (0.267), $s = 0.209$ (0.531), $f = 0.450$ (1.143), and $\epsilon_r = 2.54$. For each type of waveguide, the dominant mode cutoff frequency is 2.0 GHz while the FHOM has $f_c = 10$ GHz. The FHOM for DSLRWG and DRWG is the $TE_{2,0}$ mode, but is the $QLSM_{0,1}$ mode for DLDRWG.

The propagation constant β is shown as a function of frequency for each of the waveguide types in Fig. 29. Because of the larger degree of dielectric loading in the DSLRWG, where $\epsilon_r = 42$, the difference between β of this waveguide and β of the other waveguides is more pronounced than for the BW = 4 case where $\epsilon_r = 18$.

Comparison of Fig. 30 with Fig. 27 will show that the attenuation difference between the DSLRWG and the other waveguide types to be more pronounced for the BW = 5 case than for the BW = 4 case. This is due to the smaller aspect ratio required for BW = 5.

In Fig. 31, the power breakdown levels are shown as a function of frequency for each waveguide. The increase in power breakdown of the DLDRWG over that of the other waveguide types is considerably more pronounced than for the BW = 4 comparison. The DLDRWG does have dielectric breakdown near the upper end of the design band.

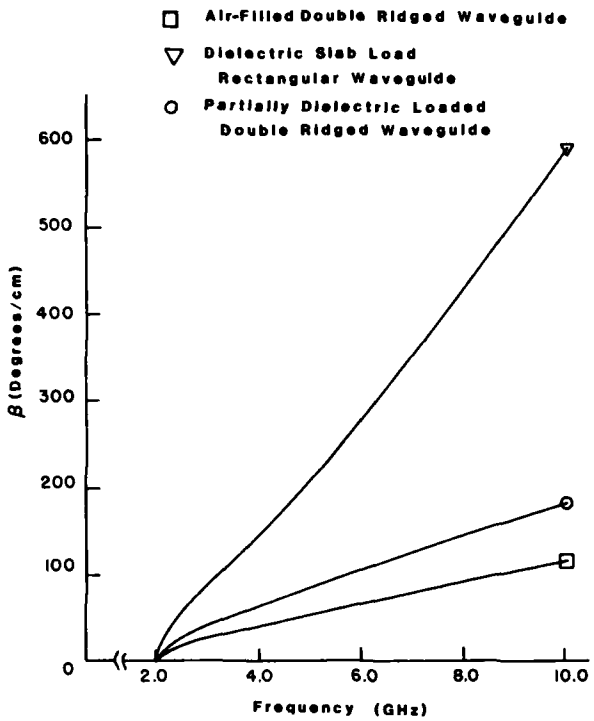

Fig. 29 — Comparison of propagation characteristics for waveguide types with $BW = 5$

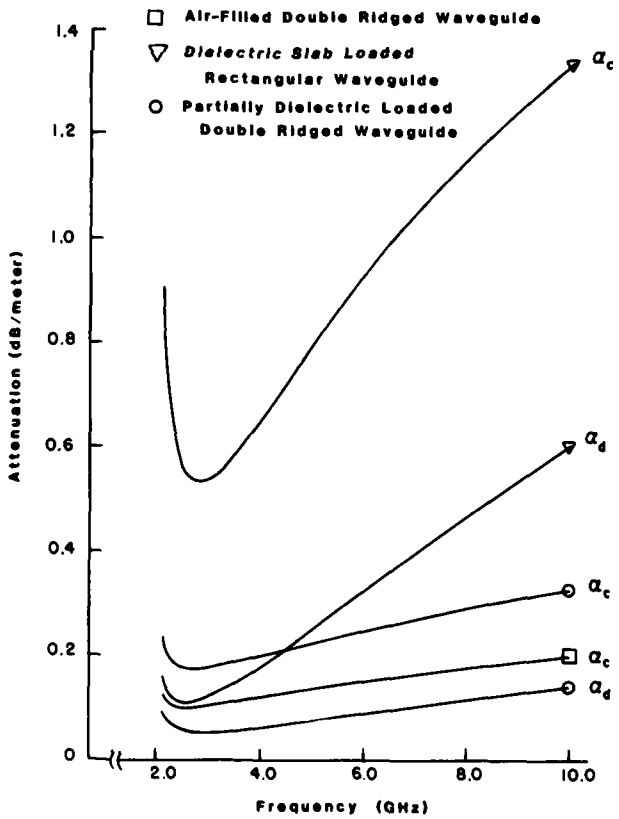

Fig. 30 — Comparison of attenuation characteristics for waveguide types with $BW = 5$

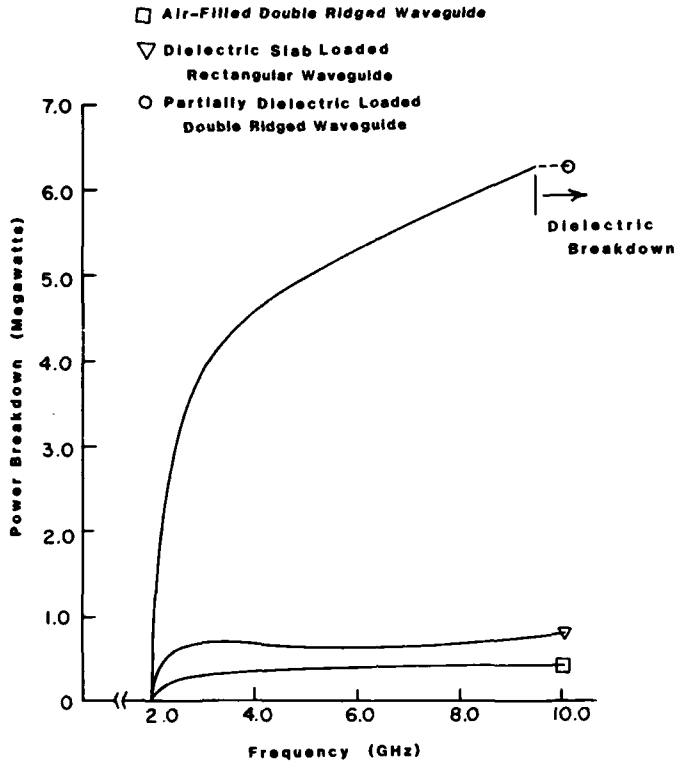

Fig. 31 — Comparison of power breakdown characteristics for waveguide types with $BW = 5$

An interesting feature of the DLDRWG is the behavior of the power breakdown level as a function of frequency. Unlike the power breakdowns of DSLRWG and DRWG, which essentially flatten out with frequency, the P_{BD} of DLDRWG increases monotonically with frequency until dielectric breakdown occurs, and is constant for higher frequencies.

When waveguide performance comparisons are made with DSLRWG, it should be noted that the aspect ratio of this waveguide need not be reduced to maintain the $TE_{2,0}$ mode as the FHOM. The cutoff frequency and dispersion characteristics of the $TE_{1,0}$ mode are independent of height, while the power breakdown level is directly proportional to the height. Also, the attenuation decreases with increased height. Although f_c for the $TE_{2,0}$ mode is independent of the waveguide height as well, the cutoff frequency of the $LSE_{1,1}$ mode is not, but decreases rapidly with increasing height, thus restricting the single mode bandwidth. As an example, for the DSLRWG with BW = 5 used for comparison in Figs. 29 to 31, the aspect ratio was taken as $b/a = 0.113$. With this aspect ratio, the cutoff frequency of the $LSE_{1,1}$ mode was the same as that of the $TE_{2,0}$ mode, 10 GHz. If the height is increased to give $b/a = 0.189$, the cutoff frequency of the $LSE_{1,1}$ mode is reduced to 6.99 GHz (BW = 3.5), and if the height is increased to give $b/a = 0.5$ f_c for the $LSE_{1,1}$ mode is reduced to 3.82 GHz (BW = 1.9). Of course, the optimum values of t/a and ϵ_r to achieve a given bandwidth would be different if consideration were given to the fact that the $QLSE_{1,1}$ mode was the FHOM. However, for large single mode bandwidths, the superior design must maintain an aspect ratio to keep the $TE_{2,0}$ mode as the FHOM because the drop in bandwidth as the aspect ratio is increased is much greater than the corresponding increase in power breakdown. Waveguide performance comparisons with DSLRWG were thus confined to the condition that the aspect ratio of this waveguide have equal cutoff frequencies for the $LSE_{1,1}$ and $TE_{2,0}$ modes.

The conclusions that may be reached after comparing the theoretical performance characteristics of the three waveguide types are apparent. For a given single mode bandwidth, the peak power handling capability of the DLDRWG is superior to that of either DSLRWG or DRWG, with the power advantage of DLDRWG increasing with bandwidth. The price paid for the greater power breakdown of the DLDRWG is increased attenuation over that of the DRWG. Expressed in terms of percentages, however, the increased attenuation is far less than the increased power breakdown level. Also, with attenuation calculated in terms of loss/wavelength rather than loss/unit length, the percentage change of attenuation between waveguide types is even less, as shown in Table 5. The same waveguides described earlier in this section were used for this comparison. The DLDRWG is superior to DSLRWG from the viewpoint of both power and attenuation, with the added advantage of not requiring very large dielectric constant materials to achieve large single mode bandwidths. From a practical viewpoint, some cost effective manufacturing method must be found for DLDRWG to achieve the theoretical performance. The peak power breakdown would be particularly sensitive to any flaws in the waveguide structure.

Table 5 — Comparison of Attenuation in dB/λ_g for Different Waveguide Types

Waveguide Type	
WGT1	#1—Air-filled double ridged waveguide
WGT2	#2—Dielectric slab loaded rectangular waveguide
WGT3	#3—Partially dielectric loaded double ridged waveguide

(a) Waveguides with single mode bandwidth = 4 and dominant mode cutoff frequency = 4 GHz

Attenuation term	Waveguide type	Attenuation (dB/λ_g)		
		f = 5 GHz	f = 8 GHz	f = 10 GHz
α_c	#1	0.0194	0.0090	0.0055
	#2	0.0284	0.0113	0.0067
	#3	0.0205	0.0088	0.0056
α_d	#2	0.0071	0.0041	0.0036
	#3	0.0071	0.0035	0.0029

(b) Waveguides with single mode bandwidth = 5 and dominant mode cutoff frequency = 2 GHz

Attenuation term	Waveguide type	Attenuation (dB/λ_g)		
		f = 2.5 GHz	f = 4 GHz	f = 10 GHz
α_c	#1	0.0205	0.0107	0.0061
	#2	0.0373	0.0161	0.0081
	#3	0.0227	0.0112	0.0065
α_d	#2	0.0074	0.0045	0.0037
	#3	0.0074	0.0035	0.0028

5.0 REFERENCES

1. R.E. Collin, *Field Theory of Guided Waves* (McGraw-Hill, New York, 1960).

2. S. Ramo, J.R. Whinnery, and T. Van Duzer, *Fields and Waves in Communications Electronics* (John Wiley and Sons, New York, 1965).

3. G.N. Tsandoulas, D.H. Temme, and F.G. Willwerth, "Longitudinal Section Mode Analysis of Dielectrically Loaded Rectangular Waveguides with Application to Phase Shifter Design," *IEEE Trans. Microwave Theory Tech.* **MTT-18**, 88-95 (1970).

4. W.L. Barrow, *Proc. IRE* **24**, 1298 (1936).

5. J.R. Carson, S.P. Mead, and S.A. Schelkunoff, *Bell System Tech. J.* **15**, 310 (1936).

6. L.J. Chu and W.L. Barrow, *Proc. IRE*, **26**, 1520 (1938).

7. N. Marcuvitz, *Waveguide Handbook* (McGraw-Hill, New York, 1951).

8. J.L. Altman, *Microwave Circuits* (Van Nostrand, Princeton, NJ, 1964).

9. S.B. Cohn, "Properties of Ridge Wave Guides," *Proc. IRE* **35**, 783-788 (1947).

10. J.R. Pyle, "The Cutoff Wavelength of the TE_{10} Mode in Ridged Rectangular Waveguide of any Aspect Ratio," *IEEE Trans. Microwave Theory Tech.* **MTT-14**, 175-183 (1966).

11. S. Hopfer, "The Design of Ridged Waveguide," *IRE Trans. Microwave Theory Tech.* **MTT-3**, 20-29 (1955).

12. T.S. Chen, "Calculation of the Parameters of Ridge Waveguides," *IRE Trans. Microwave Theory Tech.* **MTT-5** (1957).

13. W.J. Getsinger, "Ridge Waveguide Field Description and Application to Directional Couplers," *IRE Trans. Microwave Theory Tech.* **MTT-10**, 41-50 (1962).

14. J.P. Montgomery, "On the Complete Eigenvalue Solution of Ridged Waveguide," *IEEE Trans. Microwave Theory Tech.* **MTT-19**, 547-555 (1971).

15. L. Pincherle, "Electromagnetic Waves in Metal Tubes Filled Longitudinally with Two Dielectrics," *Phys. Rev.* **66**, 118-130 (1944).

16. C.G. Montgomery, R.H. Dicke, and E.M. Purcell, *Principles of Microwave Circuits*, MIT Radiation Lab Series No. 8 (McGraw-Hill, New York, 1948).

17. G.F. Bland and A.G. Franco, "Phase-shift Characteristics of Dielectric Loaded Waveguide," *IRE Trans. Microwave Theory Tech.* **MTT-10**, 492-496 (1962).

18. P.H. Vartanian, W.P. Ayers, and A.L. Helgesson, "Propagation in Dielectric Slab Loaded Rectangular Waveguide," *IRE Trans. Microwave Theory Tech.* **MTT-6**, 215-222 (1958).

19. F.E. Gardiol, "Comment on 'On the Design of Dielectric Loaded Waveguides,'" *IEEE Trans. Microwave Theory Tech.* **MTT-25**, 624-625 (1977).

AD-A167 269 AN INVESTIGATION OF DIELECTRIC LOADED RIDGED WAVEGUIDE 2/2
(U) NAVAL RESEARCH LAB WASHINGTON DC C W YOUNG
31 MAR 86 NRL-8917

UNCLASSIFIED F/G 9/1 NL

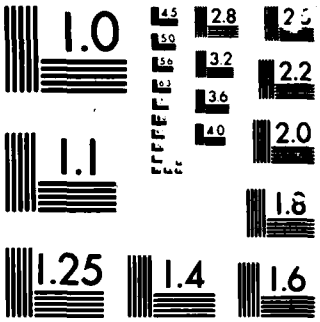

MICROCOPY CHART

20. R. Seckelmann, "Propagation of TE Modes in Dielectric Loaded Waveguides," *IEEE Trans. Microwave Theory Tech.* **MTT-14**, 518-527 (1966).

21. F. Gauthier, M. Besse, and Y. Garault, "Analysis of an Inhomogeneously Loaded Rectangular Waveguide with Dielectric and Metallic Losses," *IEEE Trans. Microwave Theory Tech.* **MTT-25**, 904-907 (1977).

22. S. Halevy, S. Raz, and H. Cory, "Bandwidth Optimization by Dielectric Loading," *IEEE Trans. Microwave Theory Tech.* **MTT-26**, 406-412 (1978).

23. T.K. Findakly and H.M. Haskal, "On the Design of Dielectric Loaded Waveguides," *IEEE Trans. Microwave Theory Tech.* **MTT-24**, 39-43 (1976).

24. F.N. Tsandoulas, F.G. Willwerth, and W. J. Ince, "LSE_{20}-mode Characteristics in Phase-shifter Parametrization," *IEEE Trans. Microwave Theory Tech.* **MITT-20**, 253-258 (1972).

25. *Reference Data for Radio Engineers* (Howard W. Sams and Co., New York, 1975).

26. A.R. Von Hippel, *Dielectric Materials and Applications* (MIT Press, Cambridge, MA, 1954).

27. G. Magerl, "Ridged Waveguides with Inhomogeneous Dielectric-slab Loading," *IEEE Trans. Microwave Theory Tech.* **MTT-26**, 413-416 (1978).

28. C.W. Young, Jr., "Comments on 'Ridged Waveguides with Inhomogeneous Dielectric-slab Loading,'" *IEEE Trans. Microwave Theory and Tech.* **MTT-26**, 919 (1978).

29. L. Lewin, "On the Resolution of a Class of Waveguide Discontinuity Problems by the Use of Singular Integral Equations," *IRE Trans. Microwave Theory Tech.* **MTT-9**, 321-332 (1961).

30. J.B. Davies, "Review of Methods for Numerical Solution of the Hollow Waveguide Problem," *Proc. IEE* **119**, 33-37 (1972).

31. F.L. Ng, "Tabulation of Methods for the Numerical Solution of the Hollow-Waveguide Problem," *IEEE Trans. Microwave Theory and Tech.* **MTT-22**, 322-329 (1974).

32. S.K. Chatterjee and R. Chatterjee, "Dielectric Loaded Waveguides—A Review of Theoretical Solutions: Part I. Mathematical Methods," *The Radio and Electronic Engineer*, 145-160 (1965).

33. J.R. Whinnery and H.W. Jamieson, "Equivalent Circuits for Discontinuities in Transmission Lines," *Proc. IRE* **32**, 98-114 (1944).

34. L. Spruch and R. Bartram, "Bounds on the Elements of the Equivalent Network for Scattering in Waveguides, I. Theory," *J. Applied Physics* **31**, 905-912 (1960).

35. R. Bartram and L. Spruch, "Bounds on the Elements of the Equivalent Network for Scattering in Waveguides, II. Application to Dielectric Obstacles," *J. Applied Physics* **31**, 913-917 (1960).

36. C.T.M Chang, "Equivalent Circuit for Partially Dielectric-filled Rectangular Waveguide Junctions," *IEEE Trans. Microwave Theory Tech.* **MTT-21**, 403-411 (1973).

37. W.K. McRitchie and M.M.Z. Kharadly, "Properties of Interface between Homogeneous and Inhomogeneous Waveguides," *Proc. IEE* **121**, 1367-1374 (1974).

38. L. Lewin, *Theory of Waveguides* (Wiley, New York, 1975).

39. J. Schwinger and D.S. Saxon, *Discontinuities in Waveguides* (Gordon and Breach, New York, 1968).

40. R.E. Collin, *Foundations for Microwave Engineering* (McGraw-Hill, New York, 1966).

41. R.F. Harrington, *Time-Harmonic Electromagnetic Fields* (McGraw-Hill, New York, 1961).

42. H.A. Atwater, *Introduction to Microwave Theory* (McGraw-Hill, New York, 1962).

43. J.A. Stratton, *Electromagnetic Theory* (McGraw-Hill, New York, 1941).

44. P. Moon and D.E. Spencer, *Foundations of Electrodynamics* (Van Nostrand, Princeton, NJ, 1960).

45. R.N. Ghose, *Microwave Circuit Theory and Analysis* (McGraw-Hill, New York, 1963).

46. F.B. Hildebrand, *Methods of Applied Mathematics*, 2nd ed. (Prentice-Hall, Englewood Cliffs, NJ, 1965).

47. R.F. Harrington, *Field Computation by Moment Methods* (MacMillan, New York, 1968).

48. R. Mittra and S.W. Lee, *Analytical Techniques in the Theory of Guided Waves* (MacMillan, New York, 1971).

49. I. Aronson, K. Kalikstein, C.J. Kleinman, and L. Spruch, "Variational Bound Principle for Scattering of Electromagnetic Waves by Obstacles in a Waveguide," *IEEE Trans. Microwave Theory Tech.* **MTT-18**, 725-731 (1970).

50. B.E. Spielman, and R.F. Harrington, "Waveguides of Arbitrary Cross Section by Solution of a Nonlinear Integral Eigenvalue Equation," *IEEE Trans. Microwave Theory Tech.* **MTT-20**, 578-585 (1972).

51. J. Mathews and R.L. Walker, *Mathematical Methods of Physics* (W.A. Benjamin, Inc., New York, 1964).

52. R.M. Bulley and J.B. Davies, "Computation of Approximate Polynomial Solutions to TE Modes in an Arbitrarily Shaped Waveguide," *IEEE Trans. Microwave Theory Tech.* **MTT-17**, 440-446 (1969).

53. R.M. Bulley, "Analysis of the Arbitrarily Shaped Waveguide by Polynomial Approximation," *IEEE Trans. Microwave Theory Tech.* **MTT-18**, 1022-1028 (1970).

54. V.H. Rumsey, "Reaction Concept in Electromagnetic Theory," *Phys. Rev.* **94**(6), 1483-1491 (1954).

55. M.J. Beaubien and A. Wexler, "An Accurate Finite-difference Method for Higher Order Waveguide Modes," *IEEE Trans. Microwave Theory Tech.* **MTT-16**, 1007-1017 (1968).

56. D.J. Richards and A. Wexler, "Finite-element Solutions within Curved Boundaries," *IEEE Trans. Microwave Theory Tech.* **MTT-20**, 650-657 (1972).

57. P. Silvester, "A General High-order Finite-element Waveguide Analysis Program," *IEEE Trans. Microwave Theory Tech.* **MTT-17**, 204-210 (1969).

58. A. Wexler, "Solution of Waveguide Discontinuities by Modal Analysis," *IEEE Trans. Microwave Theory Tech.* **MTT-15**, 508-517 (1967).

59. Z.J. Csendes and P. Silvester, "Numerical Solution of Dielectric Loaded Waveguides: II—Modal Approximation Technique," *IEEE Trans. Microwave Theory Tech.* **MTT-19**, 504-509 (1971).

60. Z.J. Csendes and P. Silvester, "Numerical Solution of Dielectric Loaded Waveguides: I—Finite-element Analysis," *IEEE Trans. Microwave Theory Tech.* **MTT-18**, 1124-1131 (1970).

61. R.V. Churchill, *Fourier Series and Boundary Value Problems*, 2nd ed. (McGraw-Hill, New York, 1963).

62. P. Hlawiczka, *Matrix algebra for Electronic Engineers* (Hayden, New York, 1965).

63. J.A. Eisele and R.M. Mason, *Applied Matrix and Tensor Analysis* (Wiley-Interscience, New York, 1970).

64. Forman S. Acton, *Numerical Methods That Work* (Harper & Row, New York, 1970).

65. A. Jennings, *Matrix Computation for Engineers and Scientists* (John Wiley and Sons, New York, 1977).

66. Josef Meixner, "The Behavior of Electromagnetic Fields at Edges," Research Report No. EM-72, Courant Institute of Mathematical Sciences, Division of Electromagnetic Research, New York University, Dec. 1954.

67. A.F. Harvey, *Microwave Engineering* (Academic Press, New York, 1963).

68. F.E. Gardiol, "Higher-order Modes in Dielectrically Loaded Rectangular Waveguides," *IEEE Trans. Microwave Theory Tech.* **MTT-16**, 919-924 (1968).

69. W.P. Clark, K.H. Hering, and D.A. Charlton, "TE-mode Solutions for Partially Ferrite-filled Rectangular Waveguide Using ABCD Matrices," *IEEE International Convention Record* **14**(5), 39-48 (1966).

70. G.F. Engen, "Advances in Microwave Measurement Science," *Proc. IEEE* **66**, 374-384 (1978).

71. S.F. Adam, "Automatic Microwave Network Measurements," *Proc. IEEE* **66**, 384-391 (1978).

72. R.A. Hackborn, "An Automatic Network Analyzer System," *Microwave J.* **11**, 45-52 (1968).

73. S.F. Adam, "A New Precision Automatic Microwave Measurement System," *IEEE Trans. Instrum. Meas.* **IM-17**, 308-313 (1968).

74. *Handbook of Chemistry and Physics* (CRC Press, Cleveland, OH, 1974).

75. W.C. Johnson, *Transmission Lines and Networks* (McGraw-Hill, New York, 1950).

76. N. Balabanian and T.A. Bickart, *Electrical Network Theory* (John Wiley and Sons, Inc., New York, 1969).

77. S.F. Adam, *Microwave Theory and Applications* (Prentice-Hall, Englewood Cliffs, NJ, 1969).

78. R.V. Churchill, *Complex Variables and Applications*, 2nd ed. (McGraw-Hill, New York, 1960).

Appendix A

TRANSVERSE RESONANCE METHOD ANALYSIS

If the assumption is made that an electromagnetic wave propagating in a waveguide with cross-section as shown in Fig. 3 is a $TE_{m,0}$ mode, then a solution for the propagation constant β can be obtained by a straightforward extension of the transverse resonance method used [9,11] to obtain solutions for the homogeneous ridged waveguide. Because of the symmetrical configuration of the waveguide, the resonance condition for the transverse component of the propagation wave will result in an infinite impedance at the center for m odd and zero impedance for m even in the equivalent transmission line circuit. Equivalently, this condition can be represented by a magnetic wall (m odd) or an electric wall (m even) placed at the vertical plane of symmetry of the waveguide. The equivalent circuit to be solved then reduces to that of Fig. A1a for m odd or Fig. A1b for m even. The capacitive susceptance B_c is the lumped element term to represent the waveguide height discontinuity. Within each region, where the regions are defined from Fig. 4, Z_{0i} is the characteristic impedance, $Y_{0i} = 1/Z_{0i}$ is the characteristic admittance, and θ_i is the product of the physical transverse dimension of the region and γ_{xi}, the complex x-directed propagation constant. For the lossless model, γ_{xi}, and therefore θ_i, will be either real or imaginary.

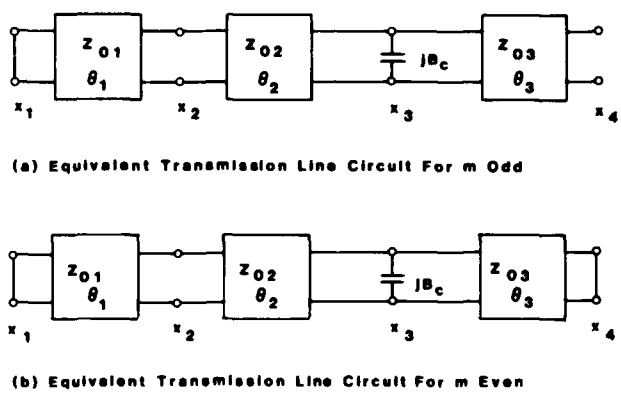

Fig. A1 — Equivalent circuit for transverse resonance method analysis of $TE_{m,0}$ modes (a) m odd; (b) m even

The reflected impedance Z presented by a load impedance Z_L terminating a transmission line of characteristic impedance Z_0 with propagating constant γ and length L is [75]

$$Z = Z_0 \frac{(Z_L + Z_0)\exp(\gamma L) + (Z_L - Z_0)\exp(-\gamma L)}{(Z_L + Z_0)\exp(\gamma L) - (Z_L - Z_0)\exp(-\gamma L)}. \tag{A1}$$

For the circuit of Fig. A1a the open circuit at x_4 will reflect back to x_3 as

$$Z_{4-3} = Z_{03} \coth \theta_3 \tag{A2}$$

or

$$Y_{4-3} = Y_{03} \tanh \theta_3 \tag{A3}$$

The short circuit at x_1 will reflect back to x_2 as

$$Z_{1-2} = Z_{01} \tanh \theta_1 \cdot \tag{A4}$$

Equation (A1) may be expressed as

$$Z = Z_0 \frac{Z_L \cosh \gamma L + Z_0 \sinh \gamma L}{Z_L \sinh \gamma L + Z_0 \cosh \gamma L}. \tag{A5}$$

Since Z_{1-2} terminates Region 2, the short at x_1 will reflect to x_3 as

$$Z_{1-3} = Z_{02} \frac{Z_{1-2} \cosh \theta_2 + Z_{02} \sinh \theta_2}{Z_{1-2} \sinh \theta_2 + Z_{02} \cosh \theta_2}. \tag{A6}$$

Substitution of Eq.(A4) into Eq.(A6) yields

$$Z_{1-3} = Z_{02} \frac{Z_{01} \sinh \theta_1 \cosh \theta_2 + Z_{02} \cosh \theta_1 \sinh \theta_2}{Z_{01} \sinh \theta_1 \sinh \theta_2 + Z_{02} \cosh \theta_1 \cosh \theta_2} \tag{A7}$$

or

$$Y_{1-3} = Y_{02} \frac{Z_{01} \sinh \theta_1 \sinh \theta_2 + Z_{02} \cosh \theta_1 \cosh \theta_2}{Z_{01} \sinh \theta_1 \cosh \theta_2 + Z_{02} \cosh \theta_1 \sinh \theta_2}. \tag{A8}$$

Since the equivalent circuit is a composite, dissipationless, passive line matched at both ends, it must be matched at all points [2]. Therefore, the sum of the admittances at the point x_3 must equal zero,

$$Y_{1-3} + jB_c + Y_{4-3} = 0. \tag{A9}$$

Substitution from Eqs. (A3) and (A8) gives

$$\frac{Y_{03}}{Y_{02}} \tanh \theta_3 + j \frac{B_c}{Y_{02}} + \frac{\sinh \theta_1 \sinh \theta_2 + \dfrac{Z_{02}}{Z_{01}} \cosh \theta_1 \cosh \theta_2}{\sinh \theta_1 \cosh \theta_2 + \dfrac{Z_{02}}{Z_{01}} \cosh \theta_1 \sinh \theta_2} = 0. \tag{A10}$$

Since Region 2 and Region 3 have the same dielectric loading, $\gamma_{x2} = \gamma_{x3}$, and the impedances are proportional to the heights:

$$\frac{Z_{03}}{Z_{02}} = \frac{Y_{02}}{Y_{03}} = \frac{d}{b} \cdot \tag{A11}$$

Region 1 and Region 2 have the same heights, and since the transverse wave is TE the impedance ratio is

$$\frac{Z_{02}}{Z_{01}} = \frac{\gamma_{x1}}{\gamma_{x2}}. \tag{A12}$$

The left side of Eq. (A10) may be expressed as a single fraction. All terms in the denominator are finite, so the numerator may be equated to zero. With substitution of Eqs. (A11) and (A12), the resultant expression is

$$(\gamma_{x2} \sinh \theta_1 \cosh \theta_2 + \gamma_{x1} \cosh \theta_1 \sinh \theta_2)\left(\frac{b}{d} \sinh \theta_3 + j\frac{B_c}{Y_{02}} \cosh \theta_3\right) \tag{A13}$$
$$+ \cosh \theta_3 (\gamma_{x2} \sinh \theta_1 \sinh \theta_2 + \gamma_{x1} \cosh \theta_1 \cosh \theta_2) = 0 \cdot$$

Within each region

$$\gamma_{xi}^2 + \gamma_{yi}^2 + \gamma_{zi}^2 = -\omega^2 \mu_0 \epsilon_i \quad \text{for } i = 1, 2, 3$$

with

$$\epsilon_1 = \epsilon_0 \quad \text{and} \quad \epsilon_2 = \epsilon_3 = \epsilon_r \epsilon_0 \cdot$$

For $TE_{m,0}$ modes $\gamma_{yi} = 0$ and $\gamma_{zi} = j\beta$ for all regions; β is the longitudinal propagation constant (above cutoff) for the waveguide configuration. Substituting into Eq. (A13)

$$\begin{aligned} \gamma_{xi} &= \sqrt{\beta^2 - \omega^2 \mu_0 \epsilon_i} \quad \text{for} \quad \omega^2 \mu_0 \epsilon_i < \beta^2 \\ &= j\sqrt{\omega^2 \mu_0 \epsilon_i - \beta^2} \quad \text{for} \quad \omega^2 \mu_0 \epsilon_i \geqslant \beta^2 \end{aligned} \tag{A14}$$

and $\theta_i = \gamma_{xi} L_i$ with $L_1 = (a - t)/2$, $L_2 = (t - s)/2$, and $L_3 = s/2$, where a, t, and s are the dimensions from Fig. 3, then defines the transcendental equation that must be solved to obtain solutions for the $TE_{m,0}$ modes for m odd. When solving for the cutoff frequency, $\beta = 0$ and frequency is the unknown quantity, with the smallest root of (A13) the solution for ω_c of the $TE_{1,0}$ mode, the second root ω_c of the $TE_{3,0}$ mode, etc. If the frequency is fixed and the propagation term β is taken as the unknown, the solution (actually in terms of β^2 rather than β) to (A13) will yield multiple roots of β^2 if the frequency is greater than cutoff of the $TE_{3,0}$ mode. The first root represents β for the $TE_{3,0}$ mode, the second root β for the $TE_{1,0}$ mode.

For $TE_{m,0}$ modes with m even, the effective short circuit at x_4 in Fig. A1b will reflect back to x_3 as

$$Z_{4-3} = Z_{03} \tanh \theta_3.$$

The resultant transcendental equation (with either ω or β the unknown) that must be solved for $TE_{even,0}$ mode solutions is given by (A13) with the terms $\cosh \theta_3$ and $\sinh \theta_3$ interchanged.

For all $TE_{m,0}$ modes, m even or odd, the impedance ratio B_c/Y_{02} may be calculated as [7,39]

$$\frac{B_c}{Y_{02}} = \frac{2b}{\lambda_x}\left\{\ln\left(\frac{1 - r^2}{4r}\right) + \frac{1}{2}\left(r + \frac{1}{r}\right) \ln\left(\frac{1 + r}{1 - r}\right) + 2\,\frac{A + A' + 2C}{AA' - C^2}\right.$$
$$\left. + \left(\frac{b}{4\lambda_x}\right)^2 \left(\frac{1 - r}{1 + r}\right)^{4r} \left(\frac{5r^2 - 1}{1 - r^2} + \frac{4}{3}\,\frac{r^2 C}{A}\right)\right\} \tag{A15}$$

where

$$A = \left(\frac{1+r}{1-r}\right)^{2r} \frac{1+[1-(b/\lambda_x)^2]^{1/2}}{1-[1-(b/\lambda_x)^2]^{1/2}} - \frac{1+3r^2}{1-r^2}$$

$$A' = \left(\frac{1+r}{1-r}\right)^{2/r} \frac{1+[1-(d/\lambda_x)^2]^2}{1-[1-(d/\lambda_x)^2]^2} + \frac{3+r^2}{1-r^2}$$

$$C = \left(\frac{4r}{1-r^2}\right)^2$$

with r the height ratio, $r = d/b$. The wavelength λ_x is the transverse wavelength, $\lambda_x = 2\pi/\beta_x$, where the transverse propagation term β_x is that for Regions 2 and 3, with

$$\gamma_{x2} = \gamma_{x3} = j\beta_x$$

since $\omega^2\mu_0\epsilon_0\epsilon_r \geqslant \beta^2$ for any propagating mode.

The computer program TRMWG incorporates the mathematics of this Appendix and may be used to calculate solutions for the $TE_{m,0}$ modes of dielectric loaded ridged waveguide. Since true TE modes do not exist in this waveguide, the accuracy of the solutions is limited by the deviation of the actual modal structure ($QLSE_{m,0}$ or $QTE_{m,0}$ modes) from that of the presumed TE mode.

Program TRMWG also may be used for calculating $TE_{m,0}$ mode solutions (with accuracy limitations already noted) for the waveguide where the dielectric width t is less than the ridge width s (Fig. 5). The analysis for this waveguide structure is similar to that for the case where $t > s$, with one important difference. For large values of ϵ_r, the waveguide of Fig. 5 will have the propagating energy concentrated in the dielectric at some frequencies above cutoff, with fields transversely evanescent in the vicinity of the ridge wall. For $\omega > \omega_0$, where $\omega_0 > \omega_c$, $\omega^2\mu_0\epsilon_0 < \beta^2$ thus $\gamma_{x1}(=\gamma_{x2})$ will be real. The definition of wavelength at these frequencies then loses meaning, and (A15) may not be used to calculate a numerical value of the shunt susceptance term in an equivalent circuit for the transverse wave. For these conditions, program TRMWG assumes a value $B_c = 0$. This assumption is equivalent to ignoring the effects of the ridge, but since the transverse wave is evanescent at the ridge wall for $\omega > \omega_0$, the assumption is reasonable for a first order approximation.

The FORTRAN listing for program TRMWG is given in Appendix E1.

Appendix B

DIELECTRIC CENTER LOADED RECTANGULAR WAVEGUIDE

In the analysis of dielectric loaded rectangular waveguide (Fig. 2), most authors [1,3,18,68] correctly point out that propagating modes may be divided into two classes: (1) the LSE (Longitudinal Section Electric) modes, which have no electric field component normal to the air-dielectric interface, and (2) the LSM (Longitudinal Section Magnetic) modes, which have no magnetic field component normal to the air-dielectric interface. The propagation analysis is based on this *a priori* knowledge of the wave structure. Identical results may be achieved by a more rigorous analysis, similar to that used in the main body of this investigation, in which all field components are assumed to exist until proven to be nonexistent.

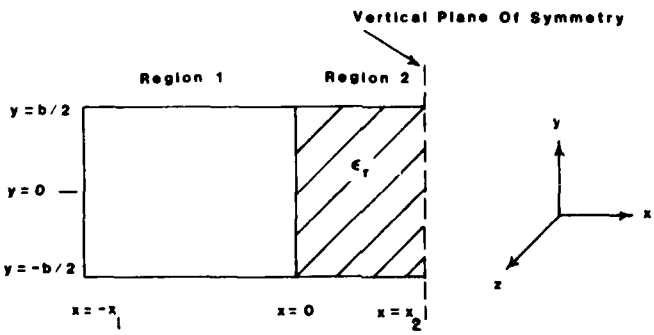

Fig. B1 — Model for analysis of dielectric slab loaded rectangular waveguide

If only the symmetric waveguide configuration is considered, the model for analysis may be reduced to a half-waveguide cross section with either a magnetic or electric wall located at the vertical plane of symmetry (Fig. B1). For this waveguide configuration, locating the $y=0$ plane at the top or bottom wall of the waveguide would simplify the analysis somewhat; however, in order to maintain similarity with the analysis of the ridged waveguide, the $y=0$ plane will be located at the horizontal plane of symmetry. The derivations (from Maxwell's equations and the wall boundary conditions) for the form of the field components in each region are exactly as for the ridged waveguide configuration; the results are repeated here for clarity. In Region 1

$$E_x^{(1)} = \sum_n A_{1,n} \cosh\,[p_{1,n}(x + x_1)] \cdot \begin{Bmatrix}\sin\\ \cos\end{Bmatrix} k_{1,n}y \tag{B1a}$$

$$E_y^{(1)} = \sum_n B_{1,n} \sinh\,[p_{1,n}(x + x_1)]/p_{1,n} \cdot \begin{Bmatrix}\cos\\ \sin\end{Bmatrix} k_{1,n}y \tag{B1b}$$

$$E_z^{(1)} = \sum_n jC_{1,n} \sinh\,[p_{1,n}(x + x_1)]/p_{1,n} \cdot \begin{Bmatrix}\sin\\ \cos\end{Bmatrix} k_{1,n}y \tag{B1c}$$

$$H_x^{(1)} = \sum_n D_{1,n} \sinh\,[p_{1,n}(x + x_1)]/p_{1,n} \cdot \begin{Bmatrix}\cos\\ \sin\end{Bmatrix} k_{1,n}y \tag{B1d}$$

$$H_y^{(1)} = \sum_n F_{1,n} \cosh\,[p_{1,n}(x + x_1)] \cdot \begin{Bmatrix}\sin\\ \cos\end{Bmatrix} k_{1,n}y \tag{B1e}$$

$$H_z^{(1)} = \sum_n jG_{1,n} \cosh\,[p_{1,n}(x + x_1)] \cdot \begin{Bmatrix}\cos\\ \sin\end{Bmatrix} k_{1,n}y \tag{B1f}$$

with the separation equation given by

$$\beta^2 + k_{1,n}^2 - p_{1,n}^2 = \omega^2 \mu_0 \epsilon_0 \tag{B2}$$

for all n. For (M,E) and (M,M) solutions, corresponding to a magnetic wall at the VPS, the fields of Region 2 are given by

$$E_x^{(2)} = \sum_n A_{2,n} \sinh [p_{2,n}(x - x_2)]/p_{2,n} \cdot \begin{Bmatrix}\sin\\ \cos\end{Bmatrix} k_{2,n}y \tag{B3a}$$

$$E_y^{(2)} = \sum_n B_{2,n} \cosh [p_{2,n}(x - x_2)] \cdot \begin{Bmatrix}\cos\\ \sin\end{Bmatrix} k_{2,n}y \tag{B3b}$$

$$E_z^{(2)} = \sum_n jC_{2,n} \cosh [p_{2,n}(x - x_2)] \cdot \begin{Bmatrix}\sin\\ \cos\end{Bmatrix} k_{2,n}y \tag{B3c}$$

$$H_x^{(2)} = \sum_n D_{2,n} \cosh [p_{2,n}(x - x_2)] \cdot \begin{Bmatrix}\cos\\ \sin\end{Bmatrix} k_{2,n}y \tag{B3d}$$

$$H_y^{(2)} = \sum_n F_{2,n} \sinh [p_{2,n}(x - x_2)]/p_{2,n} \cdot \begin{Bmatrix}\sin\\ \cos\end{Bmatrix} k_{2,n}y \tag{B3e}$$

$$H_z^{(2)} = \sum_n jG_{2,n} \sinh [p_{2,n}(x - x_2)]/p_{2,n} \cdot \begin{Bmatrix}\cos\\ \sin\end{Bmatrix} k_{2,n}y \tag{B3f}$$

with the separation equation given by

$$\beta^2 + k_{2,n}^2 - p_{2,n}^2 = \omega^2 \mu_0 \epsilon_0 \epsilon_r \tag{B4}$$

for all n. For (E,E) and (E,M) solutions, corresponding to an electric wall at the VPS, the fields of Region 2 are given by Eq. (B3) with the functions $\cosh [p_{2,n}(x - x_2)]$ and $\sinh [p_{2,n}(x - x_2)]/p_{2,n}$ interchanged. In both regions, $k_{1,n} = k_{2,n} = n\pi/b$ and the upper trigonometric function for the y-dependence, with n restricted to even integers, is used where an electric wall is located at the HPS, i.e., (M,E) and (E,E) solutions. The lower trigonometric function for the y-dependence, with n restricted to odd integers, is used for the (M,M) and (E,M) solutions which have a magnetic wall at the HPS.

The remaining boundary condition to be satisfied is at the air-dielectric interface, $x = 0$. Since the heights of the two regions are the same, the basis functions which form the y-dependence of the modal components are orthogonal on the interval $-b/2 \leqslant y \leqslant b/2$. Equating the tangential fields of **E** and **H** of the two regions at $x = 0$ will then show

$$B_{1,n} \sinh (p_{1,n}x_1)/p_{1,n} = B_{2,n} \cosh (p_{2,n}x_2) \tag{B5a}$$

$$C_{1,n} \sinh (p_{1,n}x_1)/p_{1,n} = C_{2,n} \cosh (p_{2,n}x_2) \tag{B5b}$$

$$F_{1,n} \cosh (p_{1,n}x_1) = -F_{2,n} \sinh (p_{2,n}x_2)/p_{2,n} \tag{B5c}$$

$$G_{1,n} \cosh (p_{1,n}x_1) = -G_{2,n} \sinh (p_{2,n}x_2)/p_{2,n} \tag{B5d}$$

for (M,E) and (M,M) solutions. For (E,E) and (E,M) solutions Eq. (B5) will be valid if the functions $\cosh (p_{2,n}x_2)$ and $-\sinh (p_{2,n}x_2)/p_{2,n}$ are interchanged. In matrix form, Eq. (B5) becomes

$$\left[\begin{array}{c|c} \theta_1^{(E)} & 0 \\ \hline 0 & \theta_1^{(E)} \end{array}\right] \left(\begin{array}{c} \mathbf{C}_1 \\ \hline \mathbf{B}_1 \end{array}\right) = \left[\begin{array}{c|c} \theta_2^{(E)} & 0 \\ \hline 0 & \theta_2^{(E)} \end{array}\right] \left(\begin{array}{c} \mathbf{C}_2 \\ \hline \mathbf{B}_2 \end{array}\right) \tag{B6}$$

$$\left[\begin{array}{c|c} \theta_1^{(H)} & 0 \\ \hline 0 & \theta_1^{(H)} \end{array}\right]\left\{\begin{array}{c} \mathbf{F}_1 \\ \hline \mathbf{G}_1 \end{array}\right\} = \left[\begin{array}{c|c} \theta_2^{(H)} & 0 \\ \hline 0 & \theta_2^{(H)} \end{array}\right]\left\{\begin{array}{c} \mathbf{F}_2 \\ \hline \mathbf{G}_2 \end{array}\right\} \tag{B7}$$

where the matrices are diagonal with

$$\{\theta_1^{(E)}\}_{m,n} = \sinh\,(p_{1,n}x_1)/p_{1,n}\,\delta_{mn} \tag{B8a}$$

$$\{\theta_1^{(H)}\}_{m,n} = \cosh\,(p_{1,n}x_1)\,\delta_{mn} \tag{B8b}$$

and for (M,E) and (M,M) solutions

$$\{\theta_2^{(E)}\}_{m,n} = \cosh\,(p_{2,n}x_2)\delta_{mn} \tag{B8c}$$

$$\{\theta_2^{(H)}\}_{m,n} = -\sinh\,(p_{2,n}x_2)/p_{2,n}\delta_{mn} \tag{B8d}$$

while for (E,E) and (E,M) solutions

$$\{\theta_2^{(E)}\}_{m,n} = -\sinh(p_{2,n}x_2)/p_{2,n}\,\delta_{mn} \tag{B8e}$$

$$\{\theta_2^{(H)}\}_{m,n} = \cosh\,(p_{2,n}x_2)\,\delta_{mn}. \tag{B8f}$$

The relationships between modal components coefficients within a given region have been derived in the main body of this analysis. Expressed in matrix form, they are repeated here for clarity:

$$\left[\begin{array}{c|c} \psi_1 & 0 \\ \hline 0 & \psi_1 \end{array}\right]\left\{\begin{array}{c} \mathbf{C}_1 \\ \hline \mathbf{B}_1 \end{array}\right\} = \left[\begin{array}{c|c} -\Phi & \pm K_1 \\ \hline \pm K_1 & \Phi \end{array}\right]\left[\begin{array}{c|c} P_1^2 & 0 \\ \hline 0 & -\omega\mu_0\,U \end{array}\right]\left\{\begin{array}{c} \mathbf{A}_1 \\ \hline \mathbf{D}_1 \end{array}\right\} \tag{B9}$$

$$\left[\begin{array}{c|c} \psi_1 & 0 \\ \hline 0 & \psi_1 \end{array}\right]\left\{\begin{array}{c} \mathbf{F}_1 \\ \hline \mathbf{G}_1 \end{array}\right\} = -\left[\begin{array}{c|c} -\Phi & \pm K_1 \\ \hline \pm K_1 & \Phi \end{array}\right]\left[\begin{array}{c|c} \omega\epsilon_0\,U & 0 \\ \hline 0 & U \end{array}\right]\left\{\begin{array}{c} \mathbf{A}_1 \\ \hline \mathbf{D}_1 \end{array}\right\} \tag{B10}$$

$$\left[\begin{array}{c|c} \psi_2 & 0 \\ \hline 0 & \psi_2 \end{array}\right]\left\{\begin{array}{c} \mathbf{C}_2 \\ \hline \mathbf{B}_2 \end{array}\right\} = \left[\begin{array}{c|c} -\Phi & \pm K_2 \\ \hline \pm K_2 & \Phi \end{array}\right]\left[\begin{array}{c|c} W_A & 0 \\ \hline 0 & -\omega\mu_0\,U \end{array}\right]\left\{\begin{array}{c} \mathbf{A}_2 \\ \hline \mathbf{D}_2 \end{array}\right\} \tag{B11}$$

$$\left[\begin{array}{c|c} \psi_2 & 0 \\ \hline 0 & \psi_2 \end{array}\right]\left\{\begin{array}{c} \mathbf{F}_2 \\ \hline \mathbf{G}_2 \end{array}\right\} = -\left[\begin{array}{c|c} -\Phi & \pm K_2 \\ \hline \pm K_2 & \Phi \end{array}\right]\left[\begin{array}{c|c} \omega\epsilon_3\,U & 0 \\ \hline 0 & W_D \end{array}\right]\left\{\begin{array}{c} \mathbf{A}_2 \\ \hline \mathbf{D}_2 \end{array}\right\} \tag{B12}$$

where the indicated matrices are diagonal with

$$\{K_1\}_{m,n} = (n\pi/b)\,\delta_{mn}$$

$$\{\Phi\}_{m,n} = (\beta + \delta^*)\delta_{mn}$$

$$\{\psi_1\}_{m,n} = [\beta^2 + (n\pi/b)^2 + \delta^*]\,\delta_{mn}$$
$$\{P_1^2\}_{m,n} = p_{1,n}^2\delta_{mn}$$
$$\{P_2^2\}_{m,n} = p_{2,n}^2\delta_{mn}$$
$$K_2 = K_1$$
$$\psi_2 = \psi_1$$
$$\delta^* = \begin{cases} 1 \text{ for } \beta = 0,\ n = 0 \\ 0 \text{ otherwise.} \end{cases}$$

For (M,E) and (M,M) solutions

$$W_A = U$$
$$W_D = P_2^2$$

while for (E,E) and (E,M) solutions

$$W_A = P_2^2$$
$$W_D = U.$$

The $\pm$ notation on the K matrices corresponds to n being $\begin{pmatrix} even \\ odd \end{pmatrix}$ integers.

Premultiplying (B6) and (B7) by the matrix $\left[\begin{array}{c|c} \psi_1 & 0 \\ \hline 0 & \psi_1 \end{array}\right]$ and then substituting from (B9 - B12) yields

$$\left[\begin{array}{c|c} \theta_1^{(E)} & 0 \\ \hline 0 & \theta_1^{(E)} \end{array}\right]\left[\begin{array}{c|c} -\Phi & \pm K_1 \\ \hline \pm K_1 & \Phi \end{array}\right]\left[\begin{array}{c|c} P_1^2 & 0 \\ \hline 0 & -\omega\mu_0\, U \end{array}\right]\left(\begin{array}{c} \mathbf{A}_1 \\ \hline \mathbf{D}_1 \end{array}\right)$$

$$= \left[\begin{array}{c|c} \theta_2^{(E)} & 0 \\ \hline 0 & \theta_2^{(E)} \end{array}\right]\left[\begin{array}{c|c} -\Phi & \pm K_2 \\ \hline \pm K_2 & \Phi \end{array}\right]\left[\begin{array}{c|c} W_A & 0 \\ \hline 0 & -\omega\mu_0\, U \end{array}\right]\left(\begin{array}{c} \mathbf{A}_2 \\ \hline \mathbf{D}_2 \end{array}\right) \tag{B13}$$

$$\left[\begin{array}{c|c} \theta_1^{(H)} & 0 \\ \hline 0 & \theta_1^{(H)} \end{array}\right]\left[\begin{array}{c|c} -\Phi & \pm K_1 \\ \hline \pm K_1 & \Phi \end{array}\right]\left[\begin{array}{c|c} \omega\epsilon_0\, U & 0 \\ \hline 0 & U \end{array}\right]\left(\begin{array}{c} \mathbf{A}_1 \\ \hline \mathbf{D}_1 \end{array}\right)$$

$$= \left[\begin{array}{c|c} \theta_2^{(H)} & 0 \\ \hline 0 & \theta_2^{(H)} \end{array}\right]\left[\begin{array}{c|c} -\Phi & \pm K_2 \\ \hline \pm K_2 & \Phi \end{array}\right]\left[\begin{array}{c|c} \omega\epsilon_3\, U & 0 \\ \hline 0 & W_D \end{array}\right]\left(\begin{array}{c} \mathbf{A}_2 \\ \hline \mathbf{D}_2 \end{array}\right) \tag{B14}$$

after noting that diagonal matrices commute and $\psi_2 = \psi_1$. Since $K_2 = K_1$, and since the matrix $\left[\begin{array}{c|c} -\Phi & \pm K_i \\ \hline \pm K_i & \Phi \end{array}\right]$ commutes with any diagonal matrix of the form $\left[\begin{array}{c|c} \theta & 0 \\ \hline 0 & \theta \end{array}\right]$, (B13) and (B14) may be premultiplied by $\left[\begin{array}{c|c} -\Phi & \pm K_1 \\ \hline \pm K_1 & \Phi \end{array}\right]^{-1}$ to give

$$\left[\begin{array}{c|c} \theta_1^{(E)} & 0 \\ \hline 0 & \theta_1^{(E)} \end{array}\right]\left[\begin{array}{c|c} P_1^2 & 0 \\ \hline 0 & -\omega\mu_0 U \end{array}\right]\left(\begin{array}{c} \mathbf{A}_1 \\ \hline \mathbf{D}_1 \end{array}\right) = \left[\begin{array}{c|c} \theta_2^{(E)} & 0 \\ \hline 0 & \theta_2^{(E)} \end{array}\right]\left[\begin{array}{c|c} W_A & 0 \\ \hline 0 & -\omega\mu_0 U \end{array}\right]\left(\begin{array}{c} \mathbf{A}_2 \\ \hline \mathbf{D}_2 \end{array}\right) \tag{B15}$$

$$\left[\begin{array}{c|c} \theta_1^{(H)} & 0 \\ \hline 0 & \theta_1^{(H)} \end{array}\right]\left[\begin{array}{c|c} \omega\epsilon_0 U & 0 \\ \hline 0 & U \end{array}\right]\left(\begin{array}{c} \mathbf{A}_1 \\ \hline \mathbf{D}_1 \end{array}\right) = \left[\begin{array}{c|c} \theta_2^{(H)} & 0 \\ \hline 0 & \theta_2^{(H)} \end{array}\right]\left[\begin{array}{c|c} \omega\epsilon_3 U & 0 \\ \hline 0 & W_D \end{array}\right]\left(\begin{array}{c} \mathbf{A}_2 \\ \hline \mathbf{D}_2 \end{array}\right). \tag{B16}$$

If (B15) is now premultiplied by $\left[\begin{array}{c|c} \theta_1^{(H)} & 0 \\ \hline 0 & \theta_1^{(H)} \end{array}\right]\left[\begin{array}{c|c} U & 0 \\ \hline 0 & \frac{1}{\omega\mu_0} U \end{array}\right]$ and (B.16) premultiplied by $\left[\begin{array}{c|c} \theta_1^{(E)} & 0 \\ \hline 0 & \theta_1^{(E)} \end{array}\right]\left[\begin{array}{c|c} \frac{1}{\omega\epsilon_0} P_1^2 & 0 \\ \hline 0 & -U \end{array}\right]$, the left-hand sides of the two resulting equations will both be equal to

$$\left[\begin{array}{c|c} \theta_1^{(E)} & 0 \\ \hline 0 & \theta_1^{(E)} \end{array}\right]\left[\begin{array}{c|c} \theta_1^{(H)} & 0 \\ \hline 0 & \theta_1^{(H)} \end{array}\right]\left[\begin{array}{c|c} P_1^2 & 0 \\ \hline 0 & -U \end{array}\right]\left(\begin{array}{c} \mathbf{A}_1 \\ \hline \mathbf{D}_1 \end{array}\right).$$

Equating the right-hand sides of these equations then yields

$$\left[\begin{array}{c|c} \theta_1^{(H)} & 0 \\ \hline 0 & \theta_1^{(H)} \end{array}\right]\left[\begin{array}{c|c} \theta_2^{(E)} & 0 \\ \hline 0 & \theta_2^{(E)} \end{array}\right]\left[\begin{array}{c|c} W_A & 0 \\ \hline 0 & -U \end{array}\right]\left(\begin{array}{c} \mathbf{A}_2 \\ \hline \mathbf{D}_2 \end{array}\right) = \left[\begin{array}{c|c} \theta_1^{(E)} & 0 \\ \hline 0 & \theta_1^{(E)} \end{array}\right]\left[\begin{array}{c|c} \theta_2^{(H)} & 0 \\ \hline 0 & \theta_2^{(H)} \end{array}\right]\left[\begin{array}{c|c} \epsilon_r P_1^2 & 0 \\ \hline 0 & -W_D \end{array}\right]\left(\begin{array}{c} \mathbf{A}_2 \\ \hline \mathbf{D}_2 \end{array}\right).$$

This last equation may be expressed as

$$\left[\begin{array}{c|c} \xi_1 & 0 \\ \hline 0 & \xi_2 \end{array}\right]\left(\begin{array}{c} \mathbf{A}_2 \\ \hline \mathbf{D}_2 \end{array}\right) = 0 \tag{B17}$$

where the matrices ξ_1 and ξ_2 are diagonal with

$$\xi_1 = \theta_1^{(H)}\theta_2^{(E)} W_A - \epsilon_r P_1^2 \theta_1^{(E)}\theta_2^{(H)} \tag{B18a}$$

$$\xi_2 = \theta_1^{(E)}\theta_2^{(H)} W_D - \theta_1^{(H)}\theta_2^{(E)}. \tag{B18b}$$

The expression of Eq. (B17) represents an eigenvalue problem, $[M]\mathbf{V} = \lambda\mathbf{V}$, for the special case where $\lambda = 0$. For Eq. (B17) to be valid, the determinant of the matrix must vanish:

$$\mathrm{Det}\left[\begin{array}{c|c} \xi_1 & 0 \\ \hline 0 & \xi_2 \end{array}\right] = 0.$$

Since the determinant in question is diagonal,

$$\mathrm{Det}\left[\begin{array}{c|c} \xi_1 & 0 \\ \hline 0 & \xi_2 \end{array}\right] = \prod_n \{\xi_1\}_{n,n} \{\xi_2\}_{n,n},$$

thus the determinant is zero whenever any diagonal term is zero. For the general case, the functions forming the diagonal elements of the matrix in Eq. (B17) will have separate roots (zeros). For a given diagonal matrix element equal to zero (whether as a function of ω or β), all vector components other than the one which is multiplied by the given matrix element must have zero magnitude in order for Eq. (B17) to remain valid. Thus, any solution for a single propagating mode will have either $H_x = 0$ (LSM modes) or $E_x = 0$ (LSE modes). Furthermore, the field structure will consist entirely of modal components corresponding to a single value of n.

From Eq. (B18) the individual diagonal components of the matrices ξ_1 and ξ_2 are

$$\{\xi_1\}_{n,n} = \cosh(p_{1,n}x_1)\cosh(p_{2,n}x_2) + \epsilon_r p_{1,n}\sinh(p_{1,n}x_1)\sinh(p_{2,n}x_2)/p_{2,n} \tag{B19a}$$

$$\{\xi_2\}_{n,n} = -\cosh(p_{1,n}x_1)\cosh(p_{2,n}x_2) - p_{2,n}\sinh(p_{2,n}x_2)\sinh(p_{1,n}x_1)/p_{1,n} \tag{B19b}$$

for (M,E) and (M,M) solutions, while for (E,E) and (E,M) solutions they are

$$\{\xi_1\} = -p_{2,n}\cosh(p_{1,n}x_1)\sinh(p_{2,n}x_2) - \epsilon_r p_{1,n}\sinh(p_{1,n}x_1)\cosh(p_{2,n}x_2) \tag{B20a}$$

$$\{\xi_2\}_{n,n} = \cosh(p_{2,n}x_2)\sinh(p_{1,n}x_1)/p_{1,n} + \cosh(p_{1,n}x_1)\sinh(p_{2,n}x_2/p_{2,n}. \tag{B20b}$$

For a solution with the expression of Eq. (B19a) equal to zero, the resulting mode is LSM, with the **H** field antisymmetric about the VPS, and hence is called an antisymmetric LSM mode. A similar definition may be made for modes corresponding to Eqs. (B19b), (B20a) and (B20b) being zero; in summary,

Eq. (B19a) = 0 ==> LSM modes, antisymmetric **H**
Eq. (B19b) = 0 ==> LSE modes, symmetric **E**
Eq. (B20a) = 0 ==> LSM modes, symmetric **H**
Eq. (B20b) = 0 ==> LSE modes, antisymmetric **E** .

The expression (solutions) of Eqs. (B19) and (B20) are easily shown to be equivalent to the solutions obtained by others [3,18,20,68].

A short discussion of homogeneous rectangular waveguide is appropriate before the question of index assignments is addressed. The field structure of homogeneous rectangular waveguide is normally characterized in terms of degenerate modes, $TE_{m,n}$ and $TM_{m,n}$ were $E_z = 0$ for TE modes and $H_z = 0$ for TM modes [1,2,8,42]. The index pair m,n represents the number of half sinusoidal cycles the

fields of **E** and **H** make within the waveguide in the x and y directions, respectively. For $TE_{m,n}$ modes, both indices may not be zero, while for $TM_{m,n}$ modes neither index may equal zero. For $TE_{0,n}$ modes, all fields are independent of x, while for $TE_{m,0}$ modes all fields are independent of y. For any given index pair, the propagation characteristics of the $TE_{m,n}$ mode are identical to those of the $TM_{m,n}$ mode, and any linear combination of the two degenerate modes constitutes a propagating mode. Of course, if $m = 0$ or $n = 0$, the corresponding $TM_{m,n}$ mode does not exist, and the field structure of the TE mode is unique.

The homogeneous rectangular waveguide alternatively may be characterized by $LSE_{m,n}$ and $LSM_{m,n}$ modes [41] with any single propagating mode consisting of the appropriate linear combination of these two modes. The index pair has exactly the same interpretation as for the TE and TM modes. For a given index pair with $m \neq 0$ and $n \neq 0$, the $LSE_{m,n}$ mode and the $LSM_{m,n}$ mode have identical propagation characteristics (equal to those for the $TE_{m,n}$ and $TM_{m,n}$ modes). Since E_y and E_z must be zero at the waveguide sidewalls, there must be a minimum of one half cycle for the fields in the x direction if any fields are to exist for LSE modes where $E_x = 0$; i.e., $m \geqslant 1$ for the $LSE_{m,n}$ mode. The index n will equal zero for $E_z = 0$, thus the $LSE_{m,0}$ mode is identical to the $TE_{m,0}$ mode. For LSM modes, H_x is zero everywhere, and H_y must vanish at the top and bottom walls. Therefore, there must be a minimum of one half cycle variation in H_y (and hence in the other nonzero fields) in the y direction since no propagating mode can exist with only an axial component of magnetic field. All fields may be independent of x only if E_y and E_z vanish everywhere; thus, the $LSM_{0,m}$ mode is identical to the $TE_{0,m}$ mode.

Of course, in the homogeneous waveguide there is no air-dielectric interface to define the "normal" direction. The $\mathbf{a}_x$ unit vector was chosen to replace the normal unit vector of the dielectric slab loaded waveguide to maintain similarity with that analysis. Had $\mathbf{a}_y$ been chosen instead, the roles of LSE and LSM would simply be interchanged, corresponding to a 90° rotation of the axis system in the x-y plane.

For the dielectric slab loaded rectangular waveguide, the $TE_{m,0}$ and the $LSE_{m,0}$ modes are identical. No other TE or TM modes exist, thus the reason for the $LSE_{m,n}$ and $LSM_{m,n}$ analysis. The index n for these modes still represents the number of half sinusoidal cycles made by the nonzero field components in the y direction within the waveguide. Although the fields within any homogeneous region may have a sinusoidal x-dependence, the variation with x over the full waveguide may be greatly distorted from a simple sinusoidal form [1-3,18,41]. However, the index m may still be used to represent the number of distorted half cycles the fields make in the x-direction if the definition of a cyclic function is extended to include any function which is either (1) antisymmetric about the VPS with $\partial/\partial x = 0$ at the waveguide side walls, or (2) symmetric about the VPS and zero at the waveguide sidewalls. The only questionable aspect of this definition of the index m arises for LSM modes, which in this analysis will have index assignments $m = 0, 1, 2, 3, \ldots$ and $n = 1, 2, 3, \ldots$ which is in contrast to Ref. 3 where the lowest index value for m is one. The $LSM_{m,n}$ mode of Ref. 3 is the $LSM_{m-1,n}$ mode of this report.

There are several reasons for having $m = 0$ as the lowest order index for the LSM modes:

(1) The dielectric loading may be considered a perturbation of the homogeneous condition. As the dielectric loading is reduced ($\epsilon_r \rightarrow 1$), the field pattern of the waveguide must approach that of the corresponding mode of the homogeneous waveguide. Since a $LSM_{0,n}(TE_{0,n})$ mode exists for the homogeneous case, it is logical to refer to the perturbed mode as $LSM_{0,n}$ rather than $LSM_{1,n}$.

(2) A large change in the width ("a" dimension) of the waveguide has only a second order effect on the propagation characteristics of the $LSM_{0,n}$ modes, analogous to the $LSM_{0,n}(TE_{0,n})$ modes of the homogeneous waveguide for which the propagation characteristics are completely independent of the width.

(3) The fields H_y and H_z may not vanish at the waveguide sidewalls if any fields are to exist. For a LSM mode with symmetric **H** fields ((E,M) and (E,E) solutions), these fields must possess an even number of half cycles as a function of x, and with the definition used here m must be even (m is odd in [3]). For a LSM mode with antisymmetric **H** fields ((M,E) and (M,M) solutions), these fields must undergo an odd number of half cycles as a function of x, thus m is odd (m is even in Ref. 3).

(4) Any LSM mode of dielectric slab loaded waveguide will have fields which are dependent on the x variable. The LSM modes which have fields with the least dependence on x (corresponding to the lowest order of m) are for (E,M) and (E,E) solutions and will have tangential **E** fields (E_y and E_z) for which the x-dependence function has two half cycles. However, the x-dependence function of the remaining fields, E_x, H_y, and H_z, will not be cyclic; it will be nonzero for all x and may be thought of as a perturbed constant. The next highest order LSM mode with (E,M) and (E,E) solutions will have all fields with x-dependence functions which undergo two half cyclic variations (m = 2). Therefore, the index assignment $m = 0$ will describe those lowest order LSM modes.

In summary, the dielectric slab loaded rectangular waveguide has two types of modal structures, LSE modes with $E_x = 0$, and LSM modes with $H_x = 0$. For (E,M) and (E,E) solutions, the modes are $\mathrm{LSE}_{m,n}$ with $m = 2, 4, 6, 8, \ldots, n = 0, 1, 2, 3, \ldots$ and $\mathrm{LSM}_{m,n}$ with $m = 0, 2, 4, 6, \ldots, n = 1, 2, 3, 4, \ldots$. For (M,M) and (M,E) solutions, the modes are $\mathrm{LSE}_{m,n}$ with $m = 1, 3, 5, 7, \ldots, n = 0, 1, 2, 3, \ldots$ and $\mathrm{LSM}_{m,n}$ with $m = 1, 3, 5, 7, \ldots, n = 1, 2, 3, 4, \ldots$. The characteristic equations for these modes are given by

$$\mathrm{LSE}_{\mathrm{odd},n} \text{ modes:} \quad \cosh\phi_{1,n}\cosh\phi_{2,n} + p_{2,n}\sinh\phi_{2,n}\sinh\phi_{1,n}/p_{1,n} = 0$$

$$\mathrm{LSE}_{\mathrm{even},n} \text{ modes:} \quad \cosh\phi_{2,n}\sinh\phi_{1,n}/p_{1,n} + \cosh\phi_{1,n}\sinh\phi_{2,n}/p_{2,n} = 0$$

$$\mathrm{LSM}_{\mathrm{odd},n} \text{ modes:} \quad \cosh\phi_{1,n}\cosh\phi_{2,n} + \epsilon_r p_{1,n}\sinh\phi_{1,n}\sinh\phi_{2,n}/p_{2,n} = 0$$

$$\mathrm{LSM}_{\mathrm{even},n} \text{ modes:} \quad p_{2,n}\cosh\phi_{1,n}\sinh\phi_{2,n} + \epsilon_r p_{1,n}\sinh\phi_{1,n}\cosh\phi_{2,n} = 0$$

where

$$\phi_{i,n} = p_{i,n}x_i$$

$$p_{i,n} = [\beta^2 + (n\pi/b)^2 - \omega^2\mu_0\epsilon_i]^{1/2}, \quad i = 1,2.$$

For a given m,n index pair, the $\mathrm{LSE}_{m,n}$ and $\mathrm{LSM}_{m,n}$ modes will have different cutoff frequencies and different propagation characteristics, in contrast to the homogeneous waveguide, and thus are not degenerate modes. Also, in contrast to homogeneous waveguide, for which knowledge of the cutoff frequency of any mode may be used to immediately obtain the propagation constant β for frequencies above cutoff [1,2,42], there is no simple formula to describe the dispersion characteristics for the dielectric slab loaded waveguide; the transcendental equation appropriate for the desired mode must be solved at each different frequency.

Appendix C

SCATTERING MATRIX PROPERTIES OF LOSSLESS WAVEGUIDE JUNCTIONS

Two different waveguides, each with a uniform cross section, may be joined together along a common axis of propagation. The resultant cross-sectional discontinuity will excite higher order modes in both waveguides. Assuming the frequency is such that only the dominant mode will propagate in each waveguide, the fields of these higher order modes will decay exponential in both axial directions from the discontinuity. At distances sufficiently far from the discontinuity, the fields of the higher order modes will have decayed to negligible magnitudes, and only the single (dominant) mode need be considered for circuit analysis if a suitable equivalent circuit is included to account for the coupling between the dominant mode and the higher order evanescent modes caused by the discontinuity. Such an equivalent circuit may be represented as a T-network of lumped elements as shown in Fig. C1 [1,2,8]. Alternatively, a Π network could be used. If the waveguide is lossless, as will be presumed, each element in the equivalent circuit must be reactive, either inductive or capacitive, as shown. In general, each reactive element will be a function of frequency and the cross-sectional geometry of both waveguides. In the equivalent circuit, the reactive elements represent the energy stored in the higher order evanescent modes. The dominant mode impedance of the waveguide on either side of the discontinuity is reflected as the characteristic impedance of the corresponding transmission line in the equivalent circuit.

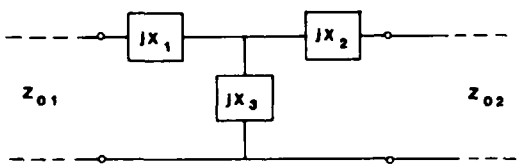

Fig. C1 — Lumped element representation of waveguide discontinuity

The scattering matrix representation [8,42,45] for the two-port network of Fig. C1 is shown in Fig. C2. Each term of the two by two scattering matrix [S] may be found in terms of the parameters of Fig. C1. The importance of the S-parameter representation is twofold: (1) circuit analysis may be greatly simplified by the use of S-parameter notation, and (2) the results of microwave measurements are usually expressed in terms of S-parameters.

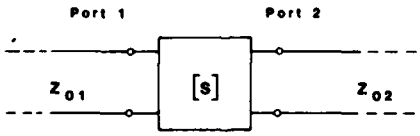

Fig. C2 — S-parameter representation of waveguide discontinuity

If the composite waveguide is assumed to be lossless, the normalized scattering matrix of the equivalent circuit must be unitary [40,42,45] with $S\,\tilde{S}^* = U$. Thus,

$$\begin{bmatrix} s_{11} & s_{12} \\ s_{21} & s_{22} \end{bmatrix} \begin{bmatrix} s_{11}^* & s_{21}^* \\ s_{12}^* & s_{22}^* \end{bmatrix} = \begin{bmatrix} 1 & 0 \\ 0 & 1 \end{bmatrix}$$

or

$$s_{11}s_{11}^* + s_{12}s_{12}^* = 1 \tag{C1a}$$

$$s_{11}s_{21}^* + s_{12}s_{22}^* = 0 \tag{C1b}$$

$$s_{21}s_{11}^* + s_{22}s_{12}^* = 0 \tag{C1c}$$

$$s_{21}s_{21}^* + s_{22}s_{22}^* = 1. \tag{C1d}$$

The unitary property of the scattering matrix alternatively may be expressed as $\tilde{S}^*\,S = U$, yielding the additional relationships:

$$s_{11}^*s_{11} + s_{21}^*s_{21} = 1 \tag{C2a}$$

$$s_{12}^*s_{12} + s_{22}^*s_{22} = 1. \tag{C2b}$$

When Eqs. (C1a), (C1d), (C2a), and (C2b) are combined, the following equalities are found:

$$|s_{11}|^2 + |s_{21}|^2 = 1 \tag{C3a}$$

$$|s_{22}|^2 + |s_{12}|^2 = 1 \tag{C3b}$$

$$|s_{11}| = |s_{22}| \tag{C3c}$$

$$|s_{12}| = |s_{21}|. \tag{C3d}$$

Expressing the elements of the scattering matrix as

$$s_{11} = |s_{11}|e^{j\phi_{11}}$$

$$s_{12} = |s_{12}|e^{j\phi_{12}}$$

$$s_{21} = |s_{21}|e^{j\phi_{21}}$$

$$s_{22} = |s_{22}|e^{j\phi_{22}}$$

and substituting into Eqs. (C1b) and (C1c) yields the following relationship between the phase terms:

$$\exp\,[j(\phi_{11} - \phi_{21})] + \exp\,[j(\phi_{12} - \phi_{22})] = 0$$

or equivalently

$$\exp\,[j(\phi_{11} + \phi_{22})] = -\exp\,[j(\phi_{12} + \phi_{21})] \tag{C4}$$

The properties of the scattering matrix found thus far have depended only on the loss free requirement. Since the waveguide junction is reciprocal, the scattering matrix for the equivalent circuit must be symmetric [76]: $s_{12} = s_{21}$, or $\phi_{12} = \phi_{21}$. With this additional requirement, the determinant of the scattering matrix is Det [S] $= s_{11}s_{22} - s_{12}s_{21}$, where

$$s_{11}s_{22} - s_{12}s_{21} = |s_{11}|^2 e^{j(\phi_{11} + \phi_{22})} - |s_{21}|^2 e^{j(\phi_{21} + \phi_{21})}$$

Since $\phi_{12} = \phi_{21}$, Eq. (C4) together with Eq. (C3a) gives

$$s_{11}s_{22} - s_{12}s_{21} = e^{j(\phi_{11} + \phi_{22})} \quad . \tag{C5}$$

For the lossless reciprocal two-port circuit of Fig. (C1), all properties of the 2 × 2 scattering matrix derived up to this stage are easily shown to be valid regardless of the numerical values of the parameters.

For many types of discontinuities in homogeneous waveguide, the corresponding equivalent circuit will have a reactive network containing only a shunt element ($X_1 = 0$ and $X_2 = 0$ in Fig. C1). Examples are a change in width or a change in height of rectangular waveguide, for which the shunt reactance is inductive or capacitive, respectively [1,7,33]. Numerical values of the reactance (normalized to one of the transmission line impedances) for both of the latter discontinuities, as well as for many other discontinuities which may be represented by an equivalent circuit containing only a shunt reactance, have been obtained by several different analysis methods [1,2,7,38,39]. The scattering matrix for such an equivalent circuit is of special interest because a relationship may be found between the phase of s_{11} and the phase of s_{22}. If the shunt reactance in Fig. C1 is $X_3 = X$, with $X_1 = 0$ and $X_2 = 0$, the scattering matrix elements are given by

$$s_{11} = \left[jX(Z_{02} - Z_{01}) - Z_{01}Z_{02}\right] / \left[jX(Z_{02} + Z_{01}) + Z_{01}Z_{02}\right]$$

$$s_{12} = s_{21} = j2X\sqrt{Z_{01}Z_{02}} / \left[jX(Z_{02} + Z_{01}) + Z_{01}Z_{02}\right]$$

$$s_{22} = \left[-jX(Z_{02} - Z_{01}) - Z_{01}Z_{02}\right] / \left[jX(Z_{02} + Z_{01}) + Z_{01}Z_{02}\right].$$

For this circuit, the relation between s_{11} and s_{22} may be expressed as

$$s_{22} = -s_{11}^{*}(1 + s_{11})/(1 + s_{11}^{*}). \tag{C6}$$

The validity of Eq. (C6) is easily proven by substitution for s_{22} and s_{11} in terms of the circuit elements. An alternative way of stating the relation between s_{11} and s_{22} is

$$|s_{11}| = |s_{22}|$$

$$\phi_{22} = -\phi_{11} + \pi + 2\tan^{-1}\left[|s_{11}| \sin\phi_{11}/(1 + |s_{11}| \cos\phi_{11})\right].$$

For an equivalent circuit containing only a series reactance (where $X_2 = 0$ and $X_3 = \infty$ in Fig. C1), the relation between s_{11} and s_{22} is given by

$$s_{22} = -s_{11}^{*}(1 - s_{11})/(1 - s_{11}^{*}) \tag{C7}$$

or alternatively

$$|s_{22}| = |s_{11}|$$

$$\phi_{22} = -\phi_{11} + \pi + 2\tan^{-1}\left[|s_{11}| \sin\phi_{11}/(1 - |s_{11}| \cos\phi_{11})\right].$$

For any discontinuity which can be represented by an equivalent circuit containing only one reactance, either series or shunt, inductive or capacitive, the full scattering matrix may be found if the phase and amplitude of either s_{11} or s_{22} is known.

For the general representation of the discontinuity as shown in Fig. (C1), no fixed relationship exists between the phases of s_{11} and s_{22}, as may be shown by example. In the limiting case of $X_3 \to 0$, the phase of s_{11} is determined entirely by the ratio X_1/Z_{01}, while the phase of s_{22} is determined entirely

by the ratio X_3/Z_{02}; thus the two phases of this (extreme) example are completely independent of each other. Of course, if quantitative values for the equivalent circuit are known, all complex S-parameters may be calculated.

The discontinuity of interest for this investigation occurs at the junction of the homogeneous rectangular waveguide used in the microwave test facility and the dielectric slab loaded (inhomogeneous) double ridged waveguide to be measured. The overall discontinuity is thus a simultaneous combination of different types of simple discontinuities: (1) change of width in rectangular waveguide, (2) change of height in rectangular waveguide, (3) abrupt transition from rectangular to ridged waveguide, and (4) abrupt transition from homogeneous to inhomogeneous (dielectric slab loaded) waveguide. Each of the first three types of discontinuities has a dominant mode equivalent circuit containing only a shunt reactance [7,38,39]. The equivalent circuit for the last type of discontinuity has been shown [36,37] to be the general circuit of Fig. C1. For this equivalent circuit, X_1 and X_2 have opposite signs; i.e., one is capacitive and the other is inductive, while the shunt element X_3 is inductive and is normally the major contributor to reflection among the three elements of the reactance junction network [36].

No specific equivalent circuit to represent the composite discontinuity was found in the technical literature. Since three of the four simple discontinuities which form the composite discontinuity have equivalent circuits containing only a shunt element, and the fourth simple discontinuity has an equivalent circuit in which the shunt element predominates, the equivalent circuit for the composite discontinuity may be approximated by a single shunt element for many applications.

If in Fig. C2, port 1 represents the waveguide of the test facility while port 2 represents the waveguide under test, the complex parameter s_{11} may be measured directly by terminating the WUT with its characteristic impedance. This latter condition may be approximated by inserting tapered resistive film in the plane of maximum electric field inside the WUT to absorb the microwave energy with minimum reflection. Since this technique does not provide a perfect matched load to the WUT, there will be a small amount of ripple in both magnitude and phase of measured s_{11} as a function of frequency. However, if the assumption is made that s_{11} is not varying rapidly with frequency, s_{11} may be determined by constructing a smooth curve through frequency plots of measured $|s_{11}|$ and ϕ_{11}. The desirability of having an equivalent circuit with only a shunt reactive term to represent the discontinuity is apparent, even if the quantitative value is unknown. With s_{11} determined experimentally, s_{22} may be calculated using Eqs. (C6), then (C3) and (C4) used to find s_{12} and s_{21}.

The only element of the scattering matrix that can be obtained directly by measurement of a single WUT is s_{11}. For those applications where the approximation of the discontinuity equivalent circuit as a single reactive element is not applicable, and the equivalent circuit is that of Fig. C1, only the relationships between S-parameters based upon the lossless and reciprocal properties of the circuit may be used:

$$|s_{11}| = |s_{22}|$$

$$s_{12} = s_{21}$$

$$|s_{11}|^2 + |s_{21}|^2 = 1$$

$$s_{11}s_{22} - s_{12}s_{21} = e^{j(\phi_{11} + \phi_{22})}.$$

For some calculations, it may be necessary to consider the loss factor in the WUT. For waveguides with loss, the scattering matrix to represent the waveguide discontinuity is no longer unitary. However, if the WUT has reasonably low loss (little attenuation) the effect on the scattering matrix is small and will be neglected. The loss factor will be used only to determine attenuation of signals traversing the length of the sample, and the scattering matrix of waveguide discontinuities will be assumed unitary.

Appendix D

EFFECTS OF STANDING WAVE PATTERNS ON SAMPLE MEASUREMENTS

Microwave measurements of any component will be affected by the standing wave pattern resulting from the interaction of two or more mismatches caused by discontinuities within the measurement system [40,45,75,77]. For the measurements to be made in this investigation, the only applicable mismatches to be considered are at the junctions between the standard waveguide used in the measurement facility and each end of the sample waveguide section to be measured; any mismatches in the remaining portions of the measurement system are corrected for in the calibration procedure when using a computer-aided automatic network analyzer [71-73].

Properties of the dominant mode scattering matrix for the discontinuity formed by the junction of different waveguides are derived in Appendix C. The relevant transmission line circuit to be analyzed to determine the effects of standing waves within the waveguide under test (WUT), and to correct for these effects, is shown in Fig. D1. The initial analysis will consider the discontinuities, and therefore the representative scattering matrices, at either end of the WUT to be different. Each scattering matrix will use the port designation indicated within the box representing the equivalent circuit for the discontinuity, as shown in Fig. D1. Each of the different traveling waves indicated will be normalized to the square root of the characteristic impedance of the transmission line which the wave is traveling; i.e., the power carried by a given wave is one half the square of the absolute value of the amplitude coefficient. This wave normalization and the use of normalized S-parameters is a conventional procedure [1,8,16,45,76]. The wave $a_1^{(+)}$ is the wave in the standard waveguide (SWG) traveling in the $+x$ direction and incident on the front face, or port 1, of the WUT. The wave $a_1^{(-)}$ is the wave in the SWG traveling in the $-x$ direction from port 1 of the WUT. Both $a_1^{(+)}$ and $a_1^{(-)}$ will use port 1 as the reference position. Using port 2, or the back face, of the WUT as a reference position, $a_2^{(+)}$ is the wave transmitted through the WUT and traveling in SWG in the $+x$ direction. The SWG on the back side of the WUT may be considered to be terminated in a matched load; thus there is no incident wave on the back face. Within the WUT, $b^{(+)}$ is the wave traveling in the $+x$ direction and will be referenced to port 1 of the WUT, while $b^{(-)}$ is the wave traveling in the $-x$ direction and will be referenced to port 2 of the WUT. At any point within the WUT, the total wave will be the sum of the two traveling waves

$$b = b^{(+)} \exp(-\gamma x) + b^{(-)} \exp \gamma(x - L) \tag{D1}$$

where L is the physical length of the WUT and γ is the complex propagation constant, $\gamma = \alpha + j\beta$, with α being the attenuation factor and β being the phase factor. The time dependence $\exp(j\omega t)$ is implicit.

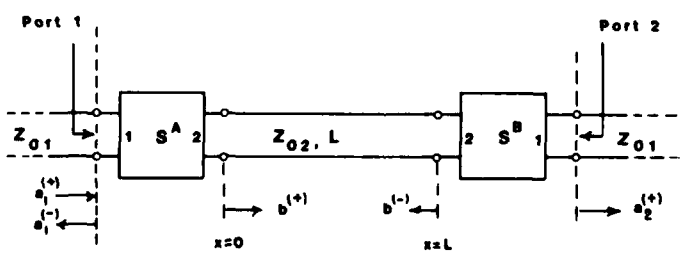

Fig. D1 — Equivalent transmission line circuit for analysis of standing wave effects in WUT

In Fig. D1 the transmission line with characteristic impedance Z_{01} represents the SWG, while the transmission line with characteristic impedance Z_{02} represents the WUT. The equivalent circuits representing the waveguide discontinuities at either end of the WUT are composed of lumped elements and thus have no associated lengths. For this analysis, the following assumptions are made: (1) the SWG and the WUT will each support only a single (dominant) propagating mode, (2) the WUT is of sufficient length such that there is negligible coupling between the discontinuities at either end via higher order evanescent modes generated by the discontinuities, and (3) the equivalent circuit for each discontinuity is lossless; i.e., the corresponding normalized scattering matrix is unitary [Appendix C].

At port 2 in Fig. D1, the wave traveling in the $+x$ direction will be

$$b^{(+)}\Big|_{x=L} = b^{(+)} \exp(-\gamma L).$$

Since there is no incident wave on port 2 in the $-x$ direction,

$$b^{(-)} = s_{22}^{B} b^{(+)} \exp(-\gamma L). \tag{D2}$$

At port 1 the wave traveling in the $-x$ direction is

$$b^{(-)}\Big|_{x=0} = b^{(-)} \exp(-\gamma L)$$

thus

$$b^{(+)} = s_{21}^{A} a_1^{(+)} + s_{22}^{A} b^{(-)} \exp(-\gamma L).$$

Substituting for $b^{(-)}$ from Eq. (D2) gives

$$b^{(+)} = s_{21}^{A} a_1^{(+)} + s_{22}^{A} s_{22}^{B} b^{(+)} \exp(-2\gamma L)$$

or

$$b^{(+)} = s_{21}^{A} a_1^{(+)} / [1 - s_{22}^{A} s_{22}^{B} \exp(-2\gamma L)]. \tag{D3}$$

The wave $a_1^{(-)}$ is given by

$$a_1^{(-)} = s_{11}^{A} a_1^{(+)} + s_{12}^{A} b^{(-)} \exp(-\gamma L).$$

Substitution from Eqs. (D2) and (D3) then yields

$$a_1^{(-)} = s_{11}^{A} a_1^{(+)} + \frac{s_{12}^{A} s_{21}^{A} s_{22}^{B} \exp(-2\gamma L)}{1 - s_{22}^{A} s_{22}^{B} \exp(-2\gamma L)} a_1^{(+)}. \tag{D4}$$

The wave $a_2^{(+)}$ is given by

$$a_2^{(+)} = s_{12}^{B} b^{(+)} \exp(-\gamma L)$$

which becomes, upon substitution from Eq. (D3),

$$a_2^{(+)} = \frac{s_{21}^{A} s_{12}^{B} \exp(-\gamma L) a_1^{(+)}}{1 - s_{22}^{A} s_{22}^{B} \exp(-2\gamma L)}. \tag{D5}$$

Measurements made on the network analyzer will have results expressed in terms of the normalized scattering matrix for the complete WUT. This scattering matrix will be designated as T, with elements t_{ik}. For transmission measurements, the SWG will be the same at each end of the WUT; thus, the waveguide interface discontinuities are identical, and with the S matrix port designations indicated $S^A = S^B$. From symmetry considerations, $t_{11} = t_{22}$ and $t_{12} = t_{21}$, with $t_{11} = a_1^{(-)}/a_1^{(+)}$ and $t_{21} = a_2^{(+)}/a_1^{(+)}$. For transmission measurements, only t_{21} is of importance. Letting $S = S^A$, Eq. (D5) becomes

$$t_{21} = \frac{s_{12} s_{21} \exp(-\gamma L)}{1 - s_{22}^{2} \exp(-2\gamma L)}. \tag{D6}$$

If the elements of the scattering matrix S were known, it would be a simple exercise in algebra to calculate γ from the measured complex transmission term t_{21}. Since quantitative knowledge of the discontinuity equivalent circuit is not generally available, the elements of S may not be obtained directly from theory. With certain approximations, measured s_{11} may be used to calculate the three remaining terms of S, as discussed in Appendix C. Before this latter approach is considered, it is instructive to examine closely the quantitative effects of the discontinuity mismatches on the measured transmission term t_{21}.

All four elements of the scattering matrix S are determined uniquely at any given frequency by the discontinuity at the waveguide interface and are independent of the length of the WUT. If the denominator term in Eq. (D6) could be ignored, measurements on two different lengths of the sample waveguide could be used to eliminate the quantity $s_{12}s_{21}$ and easily calculate γ. Unfortunately, the denominator term cannot be ignored for short lengths of the WUT. Expressing the various scattering matrix parameters in terms of magnitude and phase,

$$\left.\begin{aligned} s_{ik} &= |s_{ik}| \exp(j\phi_{ik}) \\ t_{ik} &= |t_{ik}| \exp(j\theta_{ik}) \end{aligned}\right\} i, k = 1, 2,$$

shows that

$$\theta_{21} = \phi_{12} + \phi_{21} - \beta L - \psi$$

where ψ is the phase of the denominator

$$\psi = \tan^{-1}\left[\frac{-|s_{22}|^2 \exp(-2\alpha L) \sin 2(\phi_{22} - \beta L)}{1 - |s_{22}|^2 \exp(-2\alpha L) \cos 2(\phi_{22} - \beta L)}\right].$$

The measured phase θ_{21} is seen to be basically linear with length but with a periodic perturbation. The period of the phase perturbation is $L = \pi/\beta$ while the peak phase deviation from the linear case is easily shown by inspection of a phasor diagram to be

$$\Delta\psi_{max} = \pm \sin^{-1}[|s_{22}|^2 \exp(-2\alpha L)].$$

If the small variations with frequency of the elements of S are ignored, the same phase ripple in θ_{21} will occur for a fixed length WUT with changing frequency. For a waveguide discontinuity with a 5:1 VSWR, and assuming zero loss in the WUT ($\alpha = 0$), the phase error caused by the standing wave set up between the ends of the WUT could be as much as $\pm 26.4°$, or 7.3% in a sample one wavelength long. If the attenuation of the WUT is small, the phase error will be reduced only slightly.

The standing wave pattern will also affect the loss measurement. From Eq. (D6)

$$|t_{21}| = \frac{|s_{12}s_{21}| \exp(-\alpha L)}{|1 - |s_{22}|^2 \exp(-2\alpha L) \exp j2(\phi_{22} - \beta L)|}.$$

The measured loss also has a periodic component, with period $L = \pi/\beta$. The extremes of $|t_{21}|$ occur when

$$\phi_{22} - \beta L = \pm n\pi/2.$$

Since $|s_{12}s_{21}| = 1 - |s_{22}|^2$ for a unitary scattering matrix S, the extremes of $|t_{21}|$ are given by

$$|t_{21}|_{max} = \frac{(1 - |s_{22}|^2) \exp(-\alpha L)}{1 - |s_{22}|^2 \exp(-2\alpha L)} \tag{D7a}$$

and

$$|t_{21}|_{min} = \frac{(1 - |s_{22}|^2) \exp(-\alpha L)}{1 + |s_{22}|^2 \exp(-2\alpha L)}. \tag{D7b}$$

For $|s_{22}| > 0$ and $\alpha > 0$

$$\frac{(1 - |s_{22}|^2)}{1 - |s_{22}|^2 \exp(-2\alpha L)} < 1$$

thus even the minimum measured loss, $|t_{21}|_{max}$, will be greater (in dB) than the actual loss in the WUT, $\exp(-\alpha L)$. For a sample waveguide with a loss of 0.2 dB and a 5:1 VSWR mismatch at each face, the measured extremes in loss, also expressed in dB, will be $|t_{21}|_{max} =$ 0.51 dB loss and $|t_{21}|_{min} =$ 8.38 dB loss. These large variations in loss may be viewed as a cavity effect [2,40-42] where the WUT forms the cavity.

Errors in the transmission measurement t_{21} caused by the standing wave pattern within the WUT will decrease rapidly as the match between the WUT and the SWG is improved. For a perfect match ($s_{22} = 0$), the standing wave will vanish as will the measurement errors for both phase and magnitude. A perfect match is impossible to achieve other than at a single frequency, and fabrication of matching structures may be impractical, especially for measurements covering a large frequency bandwidth and involving a number of different geometries for the WUT, because of the very low mismatch required before the standing wave effects on the transmission measurements may be neglected. However, there are a number of approaches that may be utilized to correct for the standing wave effects, even when the mismatches at the waveguide interfaces are large.

In the approach that will be referred to as Method 1, the exact equivalent circuit for the waveguide discontinuity is used to calculate the elements of the dominant mode scattering matrix S. The complex propagation constant γ for a particular sample waveguide is then found from Eq. (D6) using the measured transmission coefficient t_{21} for a single length of the WUT. If only the general form of the equivalent circuit is known for the waveguide discontinuity, this method is not applicable.

In Method 2, the equivalent circuit to represent the waveguide discontinuity is assumed to consist only of a shunt element with unknown numerical value. With this assumption, the scattering matrix elements s_{12}, s_{21}, and s_{22} are found from the measured value of s_{11} as described in Appendix C. Then, Eq. (D6) may be used to calculate γ directly from the measured transmission coefficient t_{21} of a single length sample.

Other methods for obtaining the propagation constant of the waveguide from measured data were investigated, including those which assumed the WUT to be lossless ($\alpha = 0$) with the phase term β the desired quantity. None offered any real advantage over the approach which will be referred to as Method 3. This method requires the measurement of the complex transmission coefficient t_{21} from three different lengths of sample waveguide, each with the same cross-sectional geometry. The advantage of this method is that it requires no knowledge, either measured or theoretical, of the waveguide discontinuity equivalent circuit or the associated S matrix. For the WUT with length L_i, let the corresponding measured transmission coefficient t_{21} be represented by

$$t_{21}(L = L_i) = \tau_i, \; i = 1,2,3.$$

Then Eq. (D6) may be written as

$$\tau_i e^{\gamma L_i} - \tau_i e^{-\gamma L_i} s_{22}^2 = s_{12}s_{21}$$

Since the quantity $s_{12}s_{21}$ is independent of the length of the WUT,

$$\tau_i e^{\gamma L_i} - \tau_i e^{-\gamma L_i} s_{22}^2 = \tau_k e^{\gamma L_k} - \tau_k e^{-\gamma L_k} s_{22}^2$$

for any combination of lengths i, k = 1,2,3. This last equation may be rearranged to yield

$$\frac{\tau_i e^{\gamma L_i} - \tau_k e^{\gamma L_k}}{\tau_i e^{-\gamma L_i} - \tau_k e^{-\gamma L_k}} = s_{22}^2. \tag{D8}$$

Since s_{22}^2 is also independent of the length of the WUT, Eq. (D8) is valid for any combination of i,k, thus

$$\frac{\tau_3 e^{\gamma L_3} - \tau_1 e^{\gamma L_1}}{\tau_3 e^{-\gamma L_3} - \tau_1 e^{-\gamma L_1}} = \frac{\tau_2 e^{\gamma L_2} - \tau_1 e^{\gamma L_1}}{\tau_2 e^{-\gamma L_2} - \tau_1 e^{-\gamma L_1}}$$

from which

$$\begin{aligned} &\tau_3\tau_2 e^{\gamma(L_3 - L_2)} - \tau_3\tau_1 e^{-\gamma(L_1 - L_3)} - \tau_1\tau_2 e^{-\gamma(L_2 - L_1)} + \tau_1^2 \\ &= \tau_3\tau_2 e^{-\gamma(L_3 - L_2)} - \tau_3\tau_1 e^{\gamma(L_1 - L_3)} - \tau_1\tau_2 e^{\gamma(L_2 - L_1)} + \tau_1^2. \end{aligned}$$

Expressing the length differences as

$$L_i - L_k = \Delta_{ik}, \quad i,k = 1,2,3$$

then

$$\tau_3\tau_2 \sinh(\gamma\Delta_{32}) + \tau_2\tau_1 \sinh(\gamma\Delta_{21}) + \tau_1\tau_3 \sinh(\gamma\Delta_{13}) = 0 \quad . \tag{D9}$$

Thus, the unknown elements of S have been eliminated by utilizing the measured complex transmission term t_{21} of three different lengths of the WUT. Of course, Eq. (D9) must be solved at each frequency for which γ is sought using the corresponding measured data.

The left-hand side of Eq. (D9) is a complex function of a complex variable,

$$F(\gamma) = F(\alpha + j\beta)$$

and for the value $\gamma_0 = \alpha_0 + j\beta_0$ at which the function is zero, its real and imaginary parts may be equated to zero separately:

$$R(\alpha_0,\beta_0) = 0 \tag{D10a}$$

$$I(\alpha_0,\beta_0) = 0 \tag{D10b}$$

where $R(\alpha,\beta) = \mathrm{Re}\,[F(\alpha + j\beta)]$ and $I(\alpha,\beta) = \mathrm{Im}\,[F(\alpha + j\beta)]$. Use of the mathematical identity

$$\sinh(x + jy) = \sinh x \cos y + j \cosh x \sin y$$

will show that

$$\begin{aligned} R(\alpha,\beta) &= X_{32}P_{32} - Y_{32}Q_{32} + X_{21}P_{21} - Y_{21}Q_{21} + X_{13}P_{13} - Y_{13}Q_{13} \\ I(\alpha,\beta) &= X_{32}Q_{32} + Y_{32}P_{32} + X_{21}Q_{21} + Y_{21}P_{21} + X_{13}Q_{13} + Y_{13}P_{13} \end{aligned}$$

where

$$\begin{aligned} X_{ik} &= \mathrm{Re}\,[\tau_i\tau_k] \\ Y_{ik} &= \mathrm{Im}[\tau_i\tau_k] \\ P_{ik} &= \sinh(\alpha\Delta_{ik}) \cos(\beta\Delta_{ik}) \\ Q_{ik} &= \cosh(\alpha\Delta_{ik}) \sin(\beta\Delta_{ik}) \end{aligned}$$

for the index pair $ik = 32,21,13$. Newton's method in two dimensions [64] may be used to find a solution to Eq. (D10). With $\gamma_1 = \alpha_1 + j\beta_1$ used as an initial estimate for γ_0,

$$\begin{aligned} R(\alpha_1,\beta_1) &= R_1 \\ I(\alpha_1,\beta_1) &= I_1. \end{aligned}$$

With $\alpha_0 = \alpha_1 + \Delta\alpha$ and $\beta_0 = \beta_1 + \Delta\beta$,

$$\begin{aligned} R(\alpha_1 + \Delta\alpha,\beta_1 + \Delta\beta) &= 0 \\ I(\alpha_1 + \Delta\alpha,\beta_1 + \Delta\beta) &= 0. \end{aligned}$$

Approximating each of the functions $R(\alpha,\beta)$ and $I(\alpha,\beta)$ by a first order Taylor series [51,78] then gives

$$R_1 + \frac{\partial R}{\partial \alpha}\Delta\alpha + \frac{\partial R}{\partial \beta}\Delta\beta\bigg|_{\alpha_1,\beta_1} = 0$$

$$I_1 + \frac{\partial I}{\partial \alpha}\Delta\alpha + \frac{\partial I}{\partial \beta}\Delta\beta\bigg|_{\alpha_1,\beta_1} = 0$$

or in matrix form

$$\begin{bmatrix} \partial R/\partial\alpha & \partial R/\partial\beta \\ \partial I/\partial\alpha & \partial I/\partial\beta \end{bmatrix}_{\alpha_1,\beta_1} \begin{bmatrix} \Delta\alpha \\ \Delta\beta \end{bmatrix} = -\begin{bmatrix} R_1 \\ I_1 \end{bmatrix}.$$

Since the function $F(\gamma)$ is an entire function, i.e., $\partial F/\partial\gamma$ exists at all points in the complex γ plane, advantage may be taken from the Cauchy-Riemann condition [78], with

$$\partial R/\partial\alpha = \partial I/\partial\beta$$

$$\partial R/\partial\beta = -\partial I/\partial\alpha$$

to show that

$$\Delta\alpha = -\left\{\left(\frac{\partial R}{\partial\alpha}R_1 - \frac{\partial R}{\partial\beta}I_1\right) \Big/ \left[\left(\frac{\partial R}{\partial\alpha}\right)^2 + \left(\frac{\partial R}{\partial\beta^2}\right)^2\right]\right\}_{\alpha_1,\beta_1} \tag{D11a}$$

$$\Delta\beta = -\left\{\left(\frac{\partial R}{\partial\beta}R_1 + \frac{\partial R}{\partial\alpha}I_1\right) \Big/ \left[\left(\frac{\partial R}{\partial\alpha}\right)^2 + \left(\frac{\partial R}{\partial\beta^2}\right)^2\right]\right\}_{\alpha_1,\beta_1}. \tag{D11b}$$

The derivatives are given by

$$\partial R/\partial\alpha = \Delta_{32}\left(X_{32}U_{32} - Y_{32}V_{32}\right) + \Delta_{21}\left(X_{21}U_{21} - Y_{21}V_{21}\right) + \Delta_{13}\left(X_{13}U_{13} - Y_{13}V_{13}\right)$$

$$\partial R/\partial\beta = -\Delta_{32}\left(X_{32}V_{32} + Y_{32}U_{32}\right) - \Delta_{21}\left(X_{21}V_{21} + Y_{21}U_{21}\right) - \Delta_{13}\left(X_{13}V_{13} + Y_{13}U_{13}\right)$$

where

$$U_{ik} = \cosh(\alpha\Delta_{ik})\cos(\beta\Delta_{ik})$$

$$V_{ik} = \sinh(\alpha\Delta_{ik})\sin(\beta\Delta_{ik})$$

for the index pair $ik = 32,21,13$.

The function $F(\gamma)$ is a relatively simple function possessing no poles or singularities, and Newton's method, via repeated iterations of Eq. (D11), will quickly converge on the root γ_0. The computer program CROOT3 utilizes this approach (Method 3) to solve for the complex propagation constant γ when provided with the measured complex transmission coefficient t_{21} of three different lengths of the WUT. A FORTRAN listing for this program is given in Appendix E3.

The loss term α of the complex propagation constant may be found independently of the phase term β at frequencies where the measured transmission loss of the WUT is minimum. This may be accomplished by measuring s_{11}, as described in Appendix C, at the frequencies where $|t_{21}|$ is maximum. Since $|s_{22}| = |s_{11}|$, then from Eq. (D7a)

$$|t_{21}|_{max} = \frac{(1-|s_{11}|^2)\exp(-\alpha L)}{1 - |s_{11}|^2\exp(-2\alpha L)}.$$

This last equation is quadradic in $\exp(-\alpha L)$ and is easily solved. With $X = \exp(-\alpha L)$ and $T = |t_{21}|_{max}$

$$X = \{[(1 + |s_{11}|^2)^2 + 4T^2|s_{11}|^2]^{1/2} + |s_{11}|^2 - 1\}/(2T|s_{11}|^2) \tag{D12a}$$

$$\alpha = -\ln X/L. \tag{D12b}$$

This technique for obtaining the loss term α of a given WUT will be referred to as Method 4. The number of points at which $|t_{21}|$ will be maximum will depend on the length of the WUT and on the frequency band for the measurements. As with the other methods, this technique is valid only if a single mode propagates in the WUT.

A similar development to find α at frequencies where $|t_{21}|$ is minimum is possible; however, this procedure is not recommended for the following reasons. First, the measured value of $|t_{21}|$ will have a minimum that is much less sharply defined than is the maximum as can be seen by examination of Eq. (D6) or as can be shown by experiment. A second and more important reason is that the sensitivity of calculated α to measurement errors in both $|s_{11}|$ and $|t_{21}|$ is much greater when $|t_{21}|$ is minimum than when $|t_{21}|$ is maximum. Thus, Method 4 will ignore the minima of $|t_{21}|$ and calculate α only at frequencies where the transmission magnitude is maximum, or equivalently, where the transmission loss is minimum.

Up to this point, the effects of the standing wave within the WUT on the reflected signal have been ignored since the emphasis has been on the measured transmission t_{21} through the effective two-port network, with little or no additional knowledge of γ to be found from the measured reflection coefficient t_{11}. If one port of the WUT is terminated, the effective circuit becomes a one-port network and reflection is the only measurement possible. In particular, if port 2 of the WUT is terminated with a short circuit, then in Fig. D1 $s_{22}^B = -1$. From Eq. (D3), with $S^A = S$.

$$b^{(+)} = s_{21}a_1^{(+)}/[1 + s_{22}\exp(-2\gamma L)].$$

The power contained in the wave traveling in the +x direction within the WUT is given by

$$P^{(+)}|_{x=0} = P_i \frac{|s_{21}|^2}{|1 + s_{22}\exp(-2\gamma L)|^2} \tag{D13}$$

where P_i is the power incident on the front face, or port 1, of the WUT. Like $b^{(+)}$, the power $P^{(+)}$ is referenced to port 1 of the WUT, but will drop off as $\exp(-2\alpha x)$. If the attenuation of the WUT is small, and if the length L is only a few wavelengths, $\exp(-2\alpha L)$ may be approximated as unity (equivalent to assuming $\alpha = 0$) for calculations to determine the peak voltage within the WUT. With this approximation, from Eq. (D2)

$$b^{(-)} = -b^{(+)}\exp(-j\beta L).$$

Then, from Eq. (D1) the total voltage at any point within the WUT is

$$b(x) = b^{(+)}[\exp(-j\beta x) - \exp(j\beta x - j2\beta L)]$$

or

$$|b(x)| = 2|b^{(+)}\sin[\beta(L - x)]|.$$

The total voltage will be maximum

$$|b(x)|_{max} = 2|b^{(+)}|$$

when $\sin[\beta(L - x)] = \pm 1$, or equivalently, when

$$L - x = (2n + 1)\lambda_g/4,\ n = 0,1,2,\ldots$$

where the guide wavelength λ_g is given by

$$\lambda_g = 2\pi/\beta.$$

Since power is proportional to the square of the voltage magnitude, the voltage maximum is the same that would be produced by a single wave, traveling in either direction, with a power four times that of either wave forming the standing wave pattern. This power will be referred to as the maximum voltage equivalent power, or P_{MVE}. Thus, from Eq. (D13)

$$P_{MVE} = 4P_i \frac{|s_{21}|^2}{|1 + s_{22} \exp(-j2\beta L)|^2}.$$

Since $|s_{21}|^2 = 1 - |s_{22}|^2$

$$P_{MVE} = \frac{4(1 - |s_{22}|^2)P_i}{1 + |s_{22}|^2 + 2|s_{22}| \cos \xi} \tag{D14a}$$

where

$$\xi = \phi_{22} - 2\beta L. \tag{D14b}$$

Peak power breakdown in a waveguide occurs when the electric field intensity at any point exceeds the electric breakdown strength of the dielectric medium at that point, thus causing arcing to occur. With a WUT terminated at one end with a short circuit, points of maximum E field thus will be located at odd multiples of quarter wavelengths from the short. The equivalent unidirectional power P_{MVE} at breakdown may be calculated in terms of the power incident on the WUT from Eq. (D14). Even if the phase term β is known, the phase and magnitude of s_{22} must be found for accurate calculation of P_{MVE}. As in the case for determination of the propagation constant γ from measured transmission through the WUT, quantitative knowledge of the discontinuity equivalent circuit will not be available for most geometries of the WUT, thus Method 1 is not applicable for finding s_{22}. Assumption of an equivalent circuit containing only a shunt element to calculate s_{22} from measured s_{11} (Method 2) may be applicable for some geometries of the WUT, but in general will give rise to some error in the calculated phase (ϕ_{22}) of s_{22}. As the calculation of P_{MVE} from Eq. (D14) may be very sensitive to errors in ϕ_{22}, a more reliable method to determine ϕ_{22} is indicated.

A method analogous to Method 3 is possible to determine peak power breakdown. This method would require testing three sample waveguides, each with the same cross-sectional geometry but with different lengths, to their respective breakdown levels of incident power. Using Eq. (D14) together with the three measured power levels, s_{22} could be eliminated as an unknown and P_{MVE} calculated. This approach was rejected because of two major practical deficiencies: (1) the actual peak power breakdown levels of the three different length samples could vary significantly because of slight differences in construction, and (2) the length of the WUT must be such that the standing wave pattern produces a electric field null at the interface of the WUT and the SWG. The latter condition is required to prevent arcing at the interface and is discussed in greater detail in the section on peak power measurements in Section 3.

The technique that was chosen to calculate P_{MVE} from measured incident peak power at breakdown will be referred to as Method 5. The phase factor β will be assumed known as a function of frequency (either from theory or from measurement). For a single WUT with length L, the measured reflection, $t_{11} = a_1^{(-)}/a_1^{(+)}$, from the front face, with the back face shorted, from Eq. (D4) is

$$t_{11} = s_{11} - \frac{s_{12}s_{21} \exp(-2\gamma L)}{1 + s_{22} \exp(-2\gamma L)}$$

or

$$t_{11} = \frac{s_{11} + (s_{11}s_{22} - s_{12}s_{21}) \exp(-2\gamma L)}{1 + s_{22} \exp(-2\gamma L)}.$$

From Appendix C

$$s_{11}s_{22} - s_{12}s_{21} = e^{j(\phi_{11}+\phi_{22})}$$

thus

$$t_{11} = e^{j\phi_{11}} \frac{|s_{11}| + e^{-2\alpha L} e^{j(\phi_{22} - 2\beta L)}}{1 + |s_{22}| e^{-2\alpha L} e^{j(\phi_{22} - 2\beta L)}} .$$

Letting

$$|s_{22}| = |s_{11}| = G$$
$$e^{-2\alpha L} = X$$
$$\phi_{22} - 2\beta L = \xi$$

then

$$|t_{11}| = \left| \frac{G + Xe^{j\xi}}{1 + GXe^{j\xi}} \right|$$

and

$$|t_{11}|^2 = \frac{G^2 + X^2 + 2GX \cos \xi}{1 + G^2X^2 + 2GX \cos \xi}. \tag{D15}$$

If the WUT is lossless, then $\alpha = 0$, $X = 1$, and $|t_{11}| = 1$. However, even a small amount of loss will have a pronounced effect on the magnitude of the reflected signal. The extremes in reflection will occur when $\partial\, |t_{11}|^2 / \partial\, \xi = 0$. From Eq. (D15)

$$\frac{\partial}{\partial \xi} |t_{11}|^2 = \frac{2GX(G^2 + X^2 - G^2X^2 - 1)}{(1 + G^2X^2 + 2GX \cos \xi)^2} \sin \xi .$$

Since

$$G^2 + X^2 - G^2X^2 - 1 = (G^2 - 1)\,(1 - X^2) \neq 0$$

the extremes of $|t_{11}|^2$ occur when $\sin \xi = 0$ or, equivalently, $\cos \xi = \pm 1$. Return loss will be minimum ($|t_{11}|^2$ maximum) for $\cos \xi = 1$, or

$$\xi = 2n\pi,\ n = 0, 1, 2, \ldots$$

and return loss will be maximum ($|t_{11}|^2$ minimum) for $\cos \xi = -1$, or

$$\xi = (2n + 1)\pi, \quad n = 0, 1, 2, \ldots$$

as may be shown either from (1) calculating $\partial^2 |t_{11}|^2 / \partial \xi^2$ as negative or positive, respectively, for $\sin \xi = 0$, or (2) direct inspection of Eq. (D15) for $\cos \xi = \pm\ 1$.

When measured on a swept frequency basis, $|t_{11}|^2$ will display a broad maximum but a very sharp minimum. If the peak power breakdown test is to be run at a frequency f_0, then the frequencies of the first minima on either side of f_0, $f_1 < f_0$ and $f_2 > f_0$, may be accurately measured. The phase of s_{22} may then be calculated at each of these frequencies

$$\phi_{22}|_{f_i} = (2n + 1)\pi + \beta_i L, \quad i = 1,2 \tag{D16}$$

since $\beta_i = \beta(f_i)$ is known. The ambiguity of n in Eq. (D16) is easily resolved since $-\pi \leqslant \phi_{22} \leqslant \pi$. A linear interpolation is then used to find ϕ_{22} at the desired frequency f_0:

$$\phi_{22}|_{f_0} = \phi_{22}|_{f_1} + (f_0 - f_1)\ \frac{\phi_{22}|_{f_2} - \phi_{22}|_{f_1}}{f_2 - f_1}. \tag{D17}$$

The accuracy of the linear interpolation will depend on (1) the dependence of the phase ϕ_{22} on frequency, and (2) the spacing of the frequency points f_1 and f_2. The latter factor is dependent on the length of the WUT, with a greater length yielding closer spacing, hence greater accuracy in the calculation of ϕ_{22} at f_0. If the difference in phase between the two measurement frequency points is less than a few degrees, the error in the calculated value of ϕ_{22} at f_0 due to linear interpolation will be negligible. The magnitude of s_{22} at f_0 is found by measurement of s_{11} as described in Appendix C, with $|s_{22}| = |s_{11}|$.

All measurements to determine the phase and magnitude of s_{22} may be accomplished at low power levels since the WUT is a linear device. However, these low-power measurements must be done prior to the actual high-power breakdown test since any arcing may leave conducting paths of carbon build-up which could affect subsequent low-power measurements. Once s_{22} at the frequency of the high-power test is determined, the WUT (with a short circuit on the back face) may be subjected to increasing levels of peak power until breakdown, i.e., arcing within the WUT is detected. The final step of Method 5 is then to calculate from Eq. (D14) the effective, or undirectional, peak power breakdown level using the known phase term β and the measured incident power at which breakdown occurred.

Appendix E

COMPUTER PROGRAMS

E1 PROGRAM TRMWG
E2 PROGRAM DLDRWG
E3 PROGRAM CROOT3

PROGRAM TRMWG

```
00100   C THIS IS PROGRAM TRMWG.FOR - CWY -OCT 80
00200   C THIS PROGRAM USES A TRANSVERSE RESONANCE METHOD TO
00300   C SOLVE FOR SOLUTIONS OF SYMMETRICAL DIELECTRIC LOADED
00400   C DOUBLE RIDGED WAVEGUIDE. WAVEGUIDE MODES ARE PRESUMED
00500   C TO BE TE(M,0) MODES.
00600           INTEGER RIK
00700           PI=3.1415927
00800           C=2.997925E+08
00900           R1=39.37008
01000           R2=2.0*R1
01100           RRMDI=180.0/(PI*R1)
01200           C1=(2.0E+09*PI/C)**2
01300           NEWRUN=0
01400           TYPE 100
01500   100     FORMAT (//// PROGRAM TRMWG/CWY/OCT 80')
01600   105     TYPE 110
01700   110     FORMAT(/// WAVEGUIDE DIMENSIONS IN INCHES - A,B,D,S: '$)
01800           READ(5,*)A,B,D,S
01900   115     TYPE 120
02000   120     FORMAT (// RELATIVE DIELECTRIC CONSTANT OF CENTER
02100         1 LOADING: '$)
02200           READ(5,*)EPSR
02300           TYPE 125
02400   125     FORMAT (' WIDTH IN INCHES OF CENTER LOADING: '$)
02500           READ(5,*)T
02600   128     TYPE 130
02700   130     FORMAT(' WAVEGUIDE MODE - TE(1,0) [1] OR TE(2,0) [2] -
02800         1 1 OR 2? '$)
02900           ACCEPT 133,ITE12
03000   133     FORMAT(I1)
03100           IF(ITE12.NE.1.AND.ITE12.NE.2)GO TO 128
03200           IFTGS=0
03300           IF(T.GT.S)IFTGS=1
03400   140     TYPE 145
03500   145     FORMAT (/// DRWGDL PARAMETERS ------- DIMENSIONS IN
03600         1 INCHES'/8X' A'9X'B'9X'D'9X'S'12X'T'6X4HEPS')
03700           TYPE 150,A,B,D,S,T,EPSR
03800   150     FORMAT (4F10.4,F13.4,F10.3)
03900           R=D/B
04000           RS=R**2
04100           IFR=0
04200           IF(ABS(R-1.0).LT.1.0E-06)IFR=1
04300           W1=(1-IFTGS)*(A-S)/R2+IFTGS*(A-T)/R2
04400           W2=(1-IFTGS)*(S-T)/R2+IFTGS*(T-S)/R2
04500           W3=(1-IFTGS)*T/R2+IFTGS*S/R2
04600           ATRY=1.5*A*(1.0+1.0/R+(EPSR-1.0)*T/A)
04700           IF(ITE12.EQ.2)ATRY=2.5*A
04800   C THE ABOVE QUANTITIES ARE TO BE USED FOR CALCULATING
04900   C APPROXIMATE STARTING VALUES OF CUTOFF FREQUENCIES
05000           IBC=1
05100           FREQ=C*R1/(ATRY*2.0E+09)
05200           XXDEL=1.5*FREQ
05300           BY=0.0
05400           GO TO 215
05500   160     IF(NEWRUN.LT.2)GO TO 165
05600           IF(FSTART.GT.FCGHZ)GO TO 180
05700   165     CONTINUE
05800           IF(ITE12.EQ.2)GO TO 480
05900           TYPE 167
06000   167     FORMAT(' WISH TE(1,0) PROPAGATION CONSTANTS? '$)
06100           ACCEPT 133,IBETA
06200           IF(IBETA.NE.1)GO TO 480
06300   169     TYPE 170
06400   170     FORMAT (// FREQUENCIES IN GHZ - START,STOP,INCREMENT: '$)
06500           READ(5,*)FSTART,FSTOP,DELF
06600   175     FORMAT (F9.3,1X,F9.3,1X,F9.3)
```

```
06700   180     IF(FSTART.LT.1.0E-13)GO TO 480
06800           IF(FSTART.GT.FCGHZ)GO TO 190
06900           TYPE 185
07000   185     FORMAT(' FREQUENCY MUST BE GREATER THAN CUTOFF')
07100           GO TO 165
07200           IF(FSTOP.LT.1.0E-13)FSTOP=FSTART-1.0
07300   190     TYPE 195
07400   195     FORMAT (/4X4HFREQ8X4HBETA9X3HGWL7X5HRATIO8X5HGXAIR/
07500         1 5X3HGHZ6X6HDEG/IN6X6HINCHES4X8HGWL/FSWL7X6HR OR I/)
07600           FREQ=FSTART
07700           BY=0.1
07800   C THIS IS A FIRST TRY FOR BETA
07900           XXDEL=10.0*FREQ
08000   210     CONTINUE
08100   215     CONTINUE
08200           IBTRY=0
08300           IRST=2
08400   220     C1F=C1*FREQ**2
08500           C1FEP=C1F*EPSR
08600   225     IBTRY=IBTRY+1
08700           IF(IBTRY.LT.26)GO TO 235
08800           TYPE 230
08900   230     FORMAT (' MORE THAN 25 TRIES AT ROOT')
09000           GO TO 420
09100   235     BYSQ=BY**2
09200           GX3SQ=C1FEP-BYSQ
09300           GX1SQ=C1F-BYSQ
09400           GX3=SQRT(ABS(GX3SQ))
09500           GX1=SQRT(ABS(GX1SQ))
09600           IF(GX3SQ)240,250,250
09700   240     CHS3=SINH(GX3*W3)
09800           CHC3=COSH(GX3*W3)
09900           IRGX3=1
10000           GO TO 260
10100   250     CHS3=SIN(GX3*W3)
10200           CHC3=COS(GX3*W3)
10300           IRGX3=-1
10400   260     CONTINUE
10500           IF(GX1SQ)270,280,280
10600   270     CHS1=SINH(GX1*W1)
10700           CHC1=COSH(GX1*W1)
10800           GXAIR=GX1
10900           RIK=1HP
11000           IRGX1=1
11100           GO TO 285
11200   280     CHC1=SIN(GX1*W1)
11300           CHC1=COS(GX1*W1)
11400           IRGX1=-1
11500           GXAIR=GX1*RPMDI
11600           RIK=1HI
11700   285     CONTINUE
11800           IF(IFTGS.EQ.1)GO TO 290
11900           IRGX2=(IRGX1+1)/2
12000           GX2=GX1
12100           GO TO 300
12200   290     IRGX2=(IRGX3+1)/2
12300           GX2=GX3
12400   300     CHS2=IRGX2*SINH(GX2*W2)+(1-IRGX2)*SIN(GX2*W2)
12500           CHC2=IRGX2*COSH(GX2*W2)+(1-IRGX2)*COS(GX2*W2)
12600   310     BOY=0.0
12700           IF(IFR.EQ.1)GO TO 320
12800           IF(IRGX2.EQ.1)GO TO 320
12900   C CALCULATE B/Y TERM
13000           P=(1+R)/(1-R)
13100           GL=2.0*PI/GX2
13200           P2ARG=1.0-(B/(R1*GL))**2
13300           P3ARG=1.0-(D/(R1*GL))**2
13400           IF(P2ARG.LE.0.0)P2ARG=0.0
13500           IF(P3ARG.LE.0.0)P3ARG=0.0
```

```
      P2=SQRT(P2ARG)
      P3=SQRT(P3ARG)
      PA=P**(2.0*R)*(1.0+P2)/(1.0-P2)-(1.0+3.0*RS)/(1.0-RS)
      PAP=P**(2.0/R)*(1.0+P3)/(1.0-P3)+(3.0*RS)/(1.0-RS)
      PC=((4.0*R)/(1.0-R2))**2
      PT1=ALOG((1.0-RS)/(4.0*R)*P**(0.5*(R+1.0/R)))
      PT2=2.0*(PA+PAP+2.0*PC)/(PA*PAP-PC**2)
      PT3=(B/(R1*4.0*GL))**2*(1.0/P)**(4.0*R)*((5.0*PC
     1 -1.0)/(1.0-RS)+4.0*RS*PC/(3.0*PA))**2
      BOY=2.0*B*(PT1+PT2+PT3)/(R1*GL)
320    CONTINUE
C CALCULATE F(BETA)
      IF(ITE12.EQ.2)GO TO 324
      FR3N=CHS3
      FR3D=CHC3
      GO TO 326
324   FR3N=CHC3
      FR3D=CHS3
326   CONTINUE
      ONEPM=IRGX3
      IF(ITE12.EQ.2)ONEPM=1.0
      IF(IFTGS.EQ.1)GO TO 330
      FBETA=P*(-BOY*CHS1+CHC1)*(GX2*FR3D*CHC2
     1 +ONEPM*GX3*FR3N*CHS2)+CHS1*(IRGX1*GX2*FR3D*CHS2
     2 +ONEPM*GX3*FR3N*CHC2)
      GO TO 340
330   FBETA=FR3D*(IRGX3*GX2*CHS1*CHS2+GX1*CHC1*CHC2)
     1 +(ONEPM*FR3N/P-BOY*FR3D)*(GX2*CHS1*CHC2+GX1*CHC1*CHS2)
340   IF(IBC.EQ.1)XX=FREQ
      IF(IBC.EQ.2)XX=BY
C ROOT SEARCH ROUTINE
      IF(IBTRY.GT.1)GO TO 350
345   XXNEW=XX+XXDEL
      GO TO 390
350   KROS=1
      IF(FBETA*FBOLD.LT.0.0)KROS=-1
      IF(IRST.EQ.1)GO TO 355
      IF(KROS.GT.0)GO TO 345
      IRST=1
      XXU=XX
      XXL=XXOLD
      GO TO 380
355   IF(ABS(FBETA).LT.1.0E-04.AND.ABS(XX-XXOLD).LT.
     1 0.001)GO TO 420
360   IF(KROS.LT.0)GO TO 365
      IF(XX.GT.XXOLD)GO TO 370
      GO TO 375
365   IF(XX.GT.XXOLD)GO TO 375
370   XXL=XX
      GO TO 380
375   XXU=XX
380   XXNEW=XX-FBETA*(XX-XXOLD)/(FBETA-FBOLD)
      IF(XXNEW.GT.XXL.AND.XXNEW.LT.XXU)GO TO 390
      XXNEW=0.5*(XXL+XXU)
390   FBOLD=FBETA
      XXOLD=XX
      XX=XXNEW
      IF(IBC.EQ.1)GO TO 395
      BY=XX
      GO TO 225
395   FREQ=XX
      GO TO 220
C ROOT NOW KNOWN
420   IF(IBC.EQ.2)GO TO 450
      FCGHZ=FREQ
      TYPE 430,ITE12,FCGHZ,BOY
430   FORMAT(/' TE('I1',0) MODE CUTOFF FREQUENCY IN GHZ = 'F7.4'
     1     B/Y = 'F7.3)
```

```
20400            IRC=2
20500            GO TO 160
20600   440      CONTINUE
20700   450      BYDI=BY*RRMDI
20800            GWL=360.0/BYDI
20900            FSWL=R1*C/(FREQ*1.0E+09)
21000            RGLFS=GWL/FSWL
21100   460      TYPE 470,FREQ,BYDI,GWL,RGLFS,GNAIP,RIK
21200   470      FORMAT (1X,F7.3,2X,F8.2,3X,F9.4,4X,F8.4,3X,F8.2,1X,A1)
21300            IF(FREQ.GE.FSTOP)GO TO 480
21400   C SET FIRST TRY BETA FOR NEW FREQUENCY
21500            FNEW=FREQ+DELF
21600            BY=0.5*BY*SQRT((FNEW**2-FCGHZ**2)/(FREQ**2-FCGHZ**2))
21700            XXDEL=BY
21800            FREQ=FNEW
21900            GO TO 210
22000   480      TYPE 490
22100   490      FORMAT (/// WISH NEW PARAMETERS? NONE=0, ALL=1,
22200         1 CENTER LOADING=2, FREQ=3, MODE=4 : '$)
22300            ACCEPT 133,NEWRUN
22400            GO TO(500,105,115,169,128,480)NEWRUN+1
22500   500      CONTINUE
22600            END
```

PROGRAM DLDRWG

```
00100   C THIS IS PROGRAM DLDRWG.FOR - C. W. YOUNG JR. - SEPT 1983
00200   C THIS PROGRAM USES A SERIES MODAL EXPANSION FOR THE
00300   C FIELDS,ALONG WITH APPROPPIATE BOUNDARY CONDITIONS, TO
00400   C CALCULATE CUTOFF FREQUENCIES AND PROPAGATION VALUES AT
00500   C FREQUENCIES ABOVE CUTOFF FOR DIFFERENT WAVEGUIDE MODES
00600   C IN DOUBLY SYMMETRIC DIELECTRIC SLAB LOADED RIDGED
00700   C WAVEGUIDE (LOSSLESS APPROXIMATION). IF DESIRED, POWER
00800   C BREAKDOWN LEVELS AND ATTENUATION FACTORS MAY BE
00900   C CALCULATED FOR THE OLSE(1,0) MODE.
01000            DIMENSION GY1(16),GY1SQ(16),GY3(16),GY3SQ(16),P1(16)
01100            DIMENSION P1SQ(16),P2(16),P2SQ(16),P3(16),P3SQ(16)
01200            DIMENSION GNX1SQ(16),GNX3SQ(16),HC1(16),HC2(16),HE3(16)
01300            DIMENSION HSP1(16),HSP2(16),HH3(16),TMATX(32,32)
01400            DIMENSION Z11(16),Z12(16),Z22(16),TZ11(16,16)
01500            DIMENSION TZ12(16,16),TZ21(16,16),TZ22(16,16)
01600            DIMENSION XXA(16),XXV(16),QAM(16),QAP(16)
01700            DIMENSION SMEY(16,16),SMEZ(16,16),SMHY(16,16)
01800            DIMENSION SMHZ(16,16),CAM(32,32),QDM(16),QDP(16)
01900            DIMENSION WKAREA(70),VVEC(32)
02000            DIMENSION A1(16),B1(16),C1(16),D1(16),F1(16),G1(16)
02100            DIMENSION A2P(16),A2M(16),B2P(16),B2M(16)
02200            DIMENSION C2P(16),C2M(16),D2P(16),D2M(16)
02300            DIMENSION F2P(16),F2M(16),G2P(16),G2M(16)
02400            DIMENSION A3(16),B3(16),C3(16),D3(16),F3(16),G3(16)
02500            DIMENSION EXADI(16),EYADI(16),EZADI(16),HXADI(16)
02600            DIMENSION HYADI(16),HZADI(16),A3R(16),B3R(16)
02700            DIMENSION C3R(16),D3R(16),F3R(16),G3R(16)
02800            DIMENSION PXN1(16),PXN2(16),PXN3(16)
02900            TYPE 100
03000   100      FORMAT(//// PROGRAM DLDRWG.FOR - NOV 1983')
03100   110      NREPUN=0
03200            TYPE 121
03300   121      FORMAT(// ALL DIMENSIONS ARE IN INCHES'/)
03400   124      TYPE 125
03500   125      FORMAT(' "A" DIMENSION = '$)
03600            READ(5,*)ADIM
03700            IF(NREPUN.EQ.2)GO TO 144
03800   128      TYPE 129
03900   129      FORMAT(' "B" DIMENSION = '$)
04000            READ(5,*)BDIM
04100            IF(NREPUN.EQ.3)GO TO 144
```

```
04200   132     TYPE 133
04300   133     FORMAT(' "D" DIMENSION = '$)
04400           READ(5,*)DDIM
04500           IF(NRERUN.EQ.4)GO TO 144
04600   136     TYPE 137
04700   137     FORMAT(' "S" DIMENSION = '$)
04800           READ(5,*)SDIM
04900           IF(NRERUN.EQ.5)GO TO 144
05000   140     TYPE 141
05100   141     FORMAT(' "T" DIMENSION = '$)
05200           READ(5,*)TDIM
05300   144     DBR=DDIM/BDIM
05400           SAR=SDIM/ADIM
05500           IF(DBR.GT.1.0E-6.AND.DBR.LE.1.0)GO TO 146
05600           TYPE 162
05700           GO TO 150
05800   146     IF(SAR.GE.0.0.AND.SAR.LT.1.0)GO TO 152
05900           TYPE 167
06000   150     TYPE 151
06100   151     FORMAT(' RESUBMIT DIMENSIONS')
06200           GO TO (124,124,124,128,132,136)NRERUN+1
06300   152     IF(NRERUN.NE.0)GO TO 203
06400           GO TO 175
06500   162     FORMAT(' D/B RATIO MUST BE POSITIVE AND UNITY OR LESS')
06600   167     FORMAT(' S/A RATIO MUST BE POSITIVE AND LESS THAN ONE')
06700   175     TYPE 176
06800   176     FORMAT(' RELATIVE DIELECTRIC CONSTANT = '$)
06900           READ(5,*)RDC
07000   190     TYPE 191
07100   191     FORMAT(' DESIRED WAVEGUIDE MODE -- OLS(E OR M),M,N( '$)
07200           ACCEPT 192,EMMODE,MMODE,NMODE
07300   192     FORMAT(A1,2I1)
07400           IF(EMMODE.NE.'E'.AND.EMMODE.NE.'M')GO TO 195
07500           IF(EMMODE.EQ.'E')MEH=1
07600           IF(EMMODE.EQ.'M')MEH=2
07700           IF(MEH.EQ.1.AND.MMODE.GE.1.AND.MMODE.LE.2.AND.NMODE
07800         1 .GE.0.AND.NMODE.LE.3)GO TO 197
07900           IF(MEH.EQ.2.AND.MMODE.GE.0.AND.MMODE.LE.1.AND.NMODE
08000         1 .GE.1.AND.NMODE.LE.4)GO TO 197
08100   195     TYPE 196
08200   196     FORMAT(' ALLOWED MODES ARE OLSE(1,0 THRU 2,3) AND
08300         1 OLSM(0,1 THRU 1,4)')
08400           GO TO 190
08500   197     NED=(-1)**NMODE
08600           MED=(-1)**MMODE
08700           IF(NRERUN.EQ.9)GO TO 230
08800   200     TYPE 201
08900   201     FORMAT(' NUMBER OF HIGHER ORDER MODES TO BE USED IN
09000         1 ANALYSIS? '$)
09100           READ(5,*)NHOM
09200           IF(NHOM.GE.0.AND.NHOM.LE.15)GO TO 203
09300           TYPE 202
09400   202     FORMAT(' NUMBER OF HIGHER ORDER MODES MUST BE POSITIVE
09500         1 AND IS LIMITED TO 15')
09600           GO TO 200
09700   203     TYPE 204
09800   204     FORMAT(' WISH TO CHANGE ANY PARAMETERS? NO=0, YES=1
09900         1 ?:'$)
10000           ACCEPT 210,IFCP
10100   210     FORMAT(I1)
10200           IF(IFCP.EQ.1)GO TO 110
10300           NTERMS=NHOM+1
10400           HR=DDIM/BDIM
10500           HRI=1.0/HR
10600           JTTYPE=1
10700           IF(TDIM.LE.SDIM)JTTYPE=-1
10800           IF(JTTYPE.GT.0)GO TO 220
10900           A11=0.5*(ADIM-SDIM)
```

```
11000          AX2=0.5*(SDIM-TDIM)
11100          AX3=0.5*TDIM
11200          GO TO 230
11300   220    AX1=0.5*(ADIM-TDIM)
11400          AX2=0.5*(TDIM-SDIM)
11500          AX3=0.5*SDIM
11600   C SET FREQUENCY INDEPENDENT TERMS
11700   230    DO 240 I=1,NTERMS,1
11800          IARG=2*(I-1)+NMODE
11900          GY1(I)=IARG*3.141593/BDIM
12000          GY3(I)=GY1(I)/HR
12100          GY1SQ(I)=GY1(I)**2
12200          GY3SQ(I)=GY3(I)**2
12300   235    DO 240 J=1,NTERMS,1
12400          JARG=2*(J-1)+NMODE
12500          SMEZ(I,J)=HR*SINC(-NED,0,JARG,IARG,HR)
12600          SMEY(I,J)=HR*SINC(NED,2,JARG,IARG,HR)
12700          SMHY(I,J)=SINC(-NED,0,IARG,JARG,HR)
12800   240    SMHZ(I,J)=SINC(NED,1,IARG,JARG,HR)
12900   C SOLVE FIRST FOR CUTOFF FREQUENCY
13000   245    IFFC=0
13100          TYPE 249
13200   249    FORMAT(/' WISH CUTOFF FREQ SEARCH(0) OR FIX(1)? '$)
13300          ACCEPT 210,MRSF
13400          IF(MRSF.EQ.1)GO TO 255
13500          TYPE 251
13600   251    FORMAT(' CUTOFF FREQ (GHZ) - - START,STOP,INCREMENT: '$)
13700          READ(5,*)XX1,XX2,XDEL
13800          FREQ=XX1
13900          GO TO 260
14000   255    TYPE 256
14100   256    FORMAT(' SET LIMITS FOR FIXING CUTOFF FREQ(GHZ)'/'
14200        1 LOWER, UPPER: '$)
14300          READ(5,*)XLL,XUL
14400          FREQ=XLL
14500   260    BDG=0.0
14600          BDGSQ=0.0
14700   265    CONTINUE
14800          IF(MRSF.EQ.1)GO TO 275
14900          TYPE 270
15000   270    FORMAT(5X'FREQ'5X'BETA'10X'DET  I3'5X'P3SQ(1)'
15100        1 5X'P2SQ(1)'6X'HH3(1)')
15200   275    NCOUNT=0
15300          KFC=0
15400          IF(NMODE.EQ.0.AND.IFFC.EQ.0)KFC=1
15500   C START FREQUENCY LOOP
15600   290    OMEGA=6.283185E+09*FREQ
15700          WEFS=2.249005E-13*OMEGA
15800          WER=WEFS*RDC
15900          WU=3.191864E-08*OMEGA
16000          GDSSQ=WER*WU
16100          GFSSQ=WEFS*WU
16200   295    BETA=BDG/57.29578
16300   C START BETA LOOP
16400          BETASQ=BETA*BETA
16500          BDLS=SQRT(GFSSQ*RDC)
16600          ZDLS=376.73/SQRT(RDC)
16700          NCOUNT=NCOUNT+1
16800          IF(NCOUNT.LT.26)GO TO 310
16900          TYPE 301
17000   301    FORMAT(/' MORE THAN 25 TRIES AT ROOT')
17100          GO TO 245
17200   310    CONTINUE
17300   C SET MATRIX VALUES FOR K, P, HC, HSP, RO
17400   320    DO 530 J=1,NTERMS,1
17500          GNX1SQ(J)=BETASQ+GY1(J)**2
17600          GNX3SQ(J)=BETASQ+GY3(J)**2
17700          P1SQ(J)=GNX1SQ(J)-GFSSQ
```

```
17800          P2SQ(J)=GNX1SQ(J)-GDSSQ
17900          IF(JTTYPE.LT.0)P2SQ(J)=GNX3SQ(J)-GFSSQ
18000          P3SQ(J)=GNX3SQ(J)-GDSSQ
18100          P1(J)=SQRT(ABS(P1SQ(J)))
18200          P2(J)=SQRT(ABS(P2SQ(J)))
18300          P3(J)=SQRT(ABS(P3SQ(J)))
18400          ARG=P1(J)*AX1
18500          IF(P1SQ(J))344,346,348
18600    344   HC1(J)=COS(ARG)
18700          HSP1(J)=SIN(ARG)/P1(J)
18800          PXN1(J)=1.0
18900          GO TO 350
19000    346   HC1(J)=1.0
19100          HSP1(J)=AX1
19200          PXN1(J)=1.0
19300          GO TO 350
19400    348   PXN1(J)=0.5*EXP(ARG)
19500          HC1(J)=COSH(ARG)
19600          HSP1(J)=SINH(ARG)/P1(J)
19700    350   ARG=P2(J)*AX2
19800          IF(P2SQ(J))354,356,358
19900    354   HC2(J)=COS(ARG)
20000          HSP2(J)=SIN(ARG)/P2(J)
20100          PXN2(J)=1.0
20200          GO TO 360
20300    356   HC2(J)=1.0
20400          HSP2(J)=AX2
20500          PXN2(J)=1.0
20600          GO TO 360
20700    358   PXN2(J)=0.5*EXP(ARG)
20800          HC2(J)=COSH(ARG)
20900          HSP2(J)=SINH(ARG)/P2(J)
21000    360   ARG=P3(J)*AX3
21100          IF(P3SQ(J))362,364,366
21200    362   HC3=COS(ARG)
21300          HSP3=-SIN(ARG)/P3(J)
21400          PXN3(J)=1.0
21500          GO TO 368
21600    364   HC3=1.0
21700          HSP3=-AX3
21800          PXN3(J)=1.0
21900          GO TO 368
22000    366   PXN3(J)=0.5*EXP(ARG)
22100          HC3=COSH(ARG)
22200          HSP3=-SINH(ARG)/P3(J)
22300    368   CONTINUE
22400          IF(MEQ.GT.0)GO TO 435
22500          HE3(J)=HC3
22600          HH3(J)=HSP3
22700          XXA(J)=1.0
22800          XXV(J)=P3SQ(J)
22900          GO TO 440
23000    435   HE3(J)=HSP3
23100          HH3(J)=HC3
23200          XXA(J)=P3SQ(J)
23300          XXV(J)=1.0
23400    440   CONTINUE
23500          IF(P2SQ(J).GT.0.0)GO TO 445
23600          TX2P=HC2(J)
23700          TX2M=HSP2(J)
23800          GO TO 450
23900    445   EP2X2=EXP(-2.0*P2(J)*AX2)
24000          TX2P=1.0+EP2X2
24100          TX2M=(1.0-EP2X2)/P2(J)
24200    450   CONTINUE
24300          IF(JTTYPE.LT.0)GO TO 465
24400          IF(P1SQ(J).GT.0.0)GO TO 455
24500          TX1H=HC1(J)
```

```
24600          TX1E=HSP1(J)
24700          GO TO 460
24800   455    EP1X1=EXP(-2.0*P1(J)*AX1)
24900          TX1H=1.0+EP1X1
25000          TX1E=(1.0-EP1X1)/P1(J)
25100   460    QAP(J)=RDC*P1SQ(J)*TX1E*TX2P+P2SQ(J)*TX1H*TX2M
25200          QAM(J)=RDC*P1SQ(J)*TX1E*TX2M+TX1H*TX2P
25300          QDP(J)=TX1H*TX2P+P2SQ(J)*TX1E*TX2M
25400          QDM(J)=TX1E*TX2P+TX1H*TX2M
25500          GO TO 500
25600   465    CONTINUE
25700          IF(P3SQ(J).GT.0.0)GO TO 470
25800          HC3N=HC3
25900          HSP3N=HSP3
26000          GO TO 475
26100   470    EP3X3=EXP(-2.0*P3(J)*AX3)
26200          HC3N=1.0+EP3X3
26300          HSP3N=-(1.0-EP3X3)/P3(J)
26400   475    CONTINUE
26500          IF(MED.GT.0)GO TO 480
26600          TX3E=HC3N
26700          TX3H=HSP3N
26800          GO TO 490
26900   480    TX3E=HSP3N
27000          TX3H=HC3N
27100   490    QAP(J)=TX3E*TX2P*XXA(J)-RDC*P2SQ(J)*TX3H*TX2M
27200          QAM(J)=RDC*TX3H*TX2P-TX3E*TX2M*XXA(J)
27300          QDP(J)=TX3H*TX2P*XXV(J)-TX3E*TX2M*P2SQ(J)
27400          QDM(J)=TX3E*TX2P-TX3H*TX2M*XXV(J)
27500   500    CONTINUE
27600          KD1=0
27700          IF(KFC.EQ.1.AND.J.EQ.1)KD1=1
27800          BS1=BETA+KD1
27900          BS1SQ=BS1**2
28000          IF(JTTYPE.LT.0)GO TO 510
28100          ZR=-XXA(J)/WER
28200          ZS=WU/XXV(J)
28300          GYK=GY3(J)
28400          GYKSQ=GY3SQ(J)
28500          DENOMZ=GNX3SQ(J)+KD1
28600          GO TO 520
28700   510    ZR=-WEFS/P1SQ(J)
28800          ZS=1.0/WU
28900          GYK=GY1(J)
29000          GYKSQ=GY1SQ(J)
29100          DENOMZ=GNX1SQ(J)+KD1
29200   520    Z11(J)=(BS1SQ*ZR+GYKSQ*ZS)/DENOMZ
29300          Z12(J)=NED*GYK*BS1*(-ZR+ZS)/DENOMZ
29400          Z22(J)=(GYKSQ*ZR+BS1SQ*ZS)/DENOMZ
29500   530    CONTINUE
29600          P3AVG=SQRT(P3(1)*P3(NTERMS))
29700          IF(P3AVG.LT.1.0)P3AVG=1.0
29800   C MATRIX VALUES FIXED
29900   540    DO 550 J=1,NTERMS,1
30000          DO 550 I=1,NTERMS,1
30100          TZ11(I,J)=0.0
30200          TZ12(I,J)=0.0
30300          TZ21(I,J)=0.0
30400          TZ22(I,J)=0.0
30500          DO 550 K=1,NTERMS,1
30600          IF(JTTYPE.LT.0)GO TO 545
30700          RHEHH=HE3(K)/HH3(K)
30800          TZ11(I,J)=TZ11(I,J)+SMEZ(I,K)*RHEHH*Z11(K)*SMHY(K,J)
30900          TZ12(I,J)=TZ12(I,J)+SMEZ(I,K)*RHEHH*Z12(K)*SMHZ(K,J)
31000          TZ21(I,J)=TZ21(I,J)+SMEY(I,K)*RHEHH*Z12(K)*SMHY(K,J)
31100          TZ22(I,J)=TZ22(I,J)+SMEY(I,K)*RHEHH*Z22(K)*SMHZ(K,J)
31200          GO TO 550
31300   545    RHHHE=HC1(K)/HSP1(K)
31400          TZ11(I,J)=TZ11(I,J)+SMHY(I,K)*RHHHE*Z11(K)*SMEZ(K,J)
```

```
      TZ12(I,J)=TZ12(I,J)+SMHY(I,K)*RHHHE*Z12(K)*SMEY(K,J)
      TZ21(I,J)=TZ21(I,J)+SMHZ(I,K)*RHHHE*Z12(K)*SMEZ(K,J)
      TZ22(I,J)=TZ22(I,J)+SMHZ(I,K)*RHHHE*Z22(K)*SMEY(K,J)
550   CONTINUE
      MCAMP=0
560   DO 585 I=1,NTERMS,1
      BSI=BETA
      IF(KFC.EQ.1.AND.I.EQ.1)BSI=1.0
      GKI=NED*GY1(I)
      IF(JTTYPE.LT.0)GKI=NED*GY3(I)
      DO 585 J=1,NTERMS,1
      BSJ=BETA
      IF(KFC.EQ.1.AND.J.EQ.1)BSJ=1.0
      KDIJ=0
      IF(I.EQ.J)KDIJ=1
      Q11=TZ11(I,J)
      Q12=TZ12(I,J)
      Q21=TZ21(I,J)
      Q22=TZ22(I,J)
      GKJ=NED*GY1(J)
      IF(JTTYPE.LT.0)GKJ=NED*GY3(J)
      PSI=GNX1SO(J)
      IF(JTTYPE.LT.0)PSI=GNX3SO(J)
      IF(KFC.EQ.1.AND.J.EQ.1)PSI=1.0
      TQ11=BSI*Q11*BSJ-BSI*Q12*GKJ-GKI*Q21*BSJ+GKI*Q22*GKJ
      TQ12=-BSI*Q11*GKJ-BSI*Q12*BSJ+GKI*Q21*GKJ+GKI*Q22*BSJ
      TQ21=-GKI*Q11*BSJ+GKI*Q12*GKJ-BSI*Q21*BSJ+BSI*Q22*GKJ
      TQ22=GKI*Q11*GKJ+GKI*Q12*BSJ+BSI*Q21*GKJ+BSI*Q22*BSJ
      IF(JTTYPE.LT.0)GO TO 580
      TMATX(I,J)=(QAM(I)*TQ11*WER/PSI+KDIJ*QAP(J))/(20*FREQ)
      TMATX(I,J+NTERMS)=QAM(I)*TQ12/(PSI*SQRT(WU/WER)*20*FREQ)
      TMATX(I+NTERMS,J)=QDP(I)*TQ21*WER/PSI
      TMATX(I+NTERMS,J+NTERMS)=(QDP(I)*TQ22/PSI-KDIJ*WU
     1 *QDM(J))/SQRT(WU/WER)
      GO TO 585
580   TMATX(I,J)=QAP(I)*TQ11/PSI+KDIJ*QAM(I)*WEFS
      TMATX(I,J+NTERMS)=-WU*QAP(I)*TQ12/PSI
      TMATX(I+NTERMS,J)=QDM(I)*TQ21/PSI
      TMATX(I+NTERMS,J+NTERMS)=-WU*QDM(I)*TQ22/PSI
     1 +KDIJ*QDP(I)
C MATRIX FOR CONDITION OF TDIM LESS THAN SDIM IS NOT
C NORMALIZED. IF A LARGE NUMBER OF MODAL TERMS IS REQUIRED
C THIS MATRIX SHOULD BE NORMALIZED BY A POSITIVE
C DEFINITE MATRIX TO AVOID NUMERICAL INSTABILITIES.
585   CONTINUE
      IF(MCAMP.EQ.1)GO TO 600
      DO 590 I=1,NTERMS,1
      DO 590 J=1,NTERMS,1
      TN11=1.0/P3AVG
      TN12=P3(J)/P3AVG
      TN21=P3(NTERMS-I+1)/P3AVG
      TN22=P3(NTERMS-I+1)*P3(J)/P3AVG
      TMATX(I,J)=TMATX(I,J)*TN11
      TMATX(I,J+NTERMS)=TMATX(I,J+NTERMS)*TN12
      TMATX(I+NTERMS,J)=TMATX(I+NTERMS,J)*TN21
590   TMATX(I+NTERMS,J+NTERMS)=TMATX(I+NTERMS,J+NTERMS)*TN22
C DETERMINANT OF TMATX = ZERO FOR SOLUTION
600   IF(IFFC.GT.0)GO TO 625
      MXSIZE=NTERMS
      IF(MEH.EQ.2)GO TO 650
      KMFC=1
      IF(NMODE.NE.0)KMFC=NTERMS
610   DO 620 I=1,MXSIZE,1
      DO 620 J=1,MXSIZE,1
620   TMATX(I,J)=TMATX(I+KMFC,J+KMFC)
      GO TO 650
625   IF(NMODE.NE.0)GO TO 640
      MXSIZE=NTERMS+NHOM
      DO 630 I=1,MXSIZE,1
```

```
      DO 630 J=1,MXSIZE,1
630   TMATX(I,J)=TMATX(I+1,J+1)
      GO TO 650
640   MXSIZE=2*NTERMS
650   IF(MCAMP.NE.1)GO TO 800
      MVSIZE=MXSIZE-1
      A2P(1)=0.0
      A2M(1)=0.0
      DO 665 I=1,NHOM,1
      VVEC(I)=TMATX(I,NTERMS)
      VVEC(I+NHOM)=TMATX(I+NTERMS,NTERMS)
      DO 665 J=1,NHOM,1
      CAM(I,J)=TMATX(I,J)
      IF(IFFC.EQ.0)GO TO 665
      CAM(I,J+NHOM)=TMATX(I,J+NTERMS)
      CAM(I+NHOM,J)=TMATX(I+NTERMS,J)
      CAM(I+NHOM,J+NHOM)=TMATX(I+NTERMS,J+NTERMS)
665   CONTINUE
      DD1=1.0
      CALL LINV3F(CAM,VVEC,2,MVSIZE,32,DD1,DD2,WKAREA,IER)
      D2NORM=1.0/SQRT(WU/WER)
      D2M(1)=-D2NORM
      D2P(1)=D2M(1)*QDM(1)/QDP(1)
      DO 675 I=2,NTERMS,1
      A2P(I)=VVEC(I-1)
      A2M(I)=QAP(I)*A2P(I)/QAM(I)
      IF(IFFC.EQ.0)GO TO 670
      D2M(I)=D2NORM*VVEC(I-1+NHOM)
      D2P(I)=QDM(I)*D2M(I)/QDP(I)
      GO TO 675
670   D2P(I)=0.0
      D2M(I)=0.0
675   CONTINUE
680   DO 685 I=1,NTERMS,1
      ZONE=0.0
      IF(KFC.EQ.1.AND.I.EQ.1)ZONE=1.0
      PHI=BETA+ZONE
      PSI=GNX1SQ(I)+ZONE
      GY2=NED*GY1(I)
      C2P(I)=(-PHI*A2M(I)-WU*GY2*D2P(I))/PSI
      B2P(I)=(GY2*A2M(I)-WU*PHI*D2P(I))/PSI
      F2P(I)=(PHI*WEP*A2P(I)-GY2*D2M(I))/PSI
      G2P(I)=(-WEP*GY2*A2P(I)-PHI*D2M(I))/PSI
      C2M(I)=(-PHI*P2SQ(I)*A2P(I)-WU*GY2*D2M(I))/PSI
      B2M(I)=(GY2*P2SQ(I)*A2P(I)-WU*PHI*D2M(I))/PSI
      F2M(I)=(WEP*PHI*A2M(I)-GY2*P2SQ(I)*D2P(I))/PSI
      G2M(I)=(-WEP*GY2*A2M(I)-PHI*P2SQ(I)*D2P(I))/PSI
      A1(I)=RDC*A2P(I)/(QAM(I)*PXN1(I)*PXN2(I))
      D1(I)=D2M(I)/(QDP(I)*PXN1(I)*PXN2(I))
      EXADI(I)=A1(I)*HC1(I)
      HXADI(I)=D1(I)*HSP1(I)
      B1(I)=(GY2*P1SQ(I)*A1(I)-WU*PHI*D1(I))/PSI
      C1(I)=(-PHI*P1SQ(I)*A1(I)-WU*GY2*D1(I))/PSI
      F1(I)=(WEFS*PHI*A1(I)-GY2*D1(I))/PSI
      G1(I)=(-WEFS*GY2*A1(I)-PHI*D1(I))/PSI
      EYADI(I)=B1(I)*HSP1(I)
      EZADI(I)=C1(I)*HSP1(I)
      HYADI(I)=F1(I)*HC1(I)
685   HZADI(I)=G1(I)*HC1(I)
      DO 690 I=1,NTERMS,1
      F3R(I)=0.0
      G3R(I)=0.0
      DO 690 J=1,NTERMS,1
      F3R(I)=F3R(I)+(SMHY(I,J)*F2P(J))
690   G3R(I)=G3R(I)+(SMHZ(I,J)*G2P(J))
      DO 699 I=1,NTERMS,1
      ZONE=0.0
      IF(IFFC.EQ.0.AND.NMODE.EQ.0.AND.I.EQ.1)ZONE=1.0
```

```
45200          PSI=GNX3SQ(I)+ZONE
45300          PHI=BETA+ZONE
45400          WD=P3SQ(I)
45500          WA=1.0
45600          IF(MED.LT.0)GO TO 695
45700          WD=1.0
45800          WA=P3SQ(I)
45900   695    PMK3=MED*GY3(I)
46000          F3(I)=F3R(I)/HH3(I)
46100          G3(I)=G3R(I)/HH3(I)
46200          A3(I)=(PHI*F3(I)-PMK3*G3(I))/WER
46300          D3(I)=(-PMK3*F3(I)-PHI*G3(I))/WD
46400          C3(I)=(-PHI*WA*A3(I)-WU*PMK3*D3(I))/PSI
46500          B3(I)=(PMK3*WA*A3(I)-WU*PHI*D3(I))/PSI
46600          A3R(I)=A3(I)*HH3(I)
46700          B3R(I)=B3(I)*HE3(I)
46800          C3R(I)=C3(I)*HE3(I)
46900   699    D3R(I)=D3(I)*HE3(I)
47000          NCAMP=0
47100   C **** PRINT OUT MODAL COMPONENT COEFFICIENTS IF REQUESTED
47200          IF(IFMCAP.NE.1)GO TO 738
47300          TYPE 703
47400   703    FORMAT(/'  N'4X'EXADI(N)'4X'EYADI(N)'3X'EZADI(N)'
47500        1 3X'HXADI(N)'3X'HYADI(N)'3X'HZADI(N)')
47600          DO 705 I=1,NTERMS,1
47700   705    TYPE 729,I,EXADI(I),EYADI(I),EZADI(I),HXADI(I),
47800        1 HYADI(I),HZADI(I)
47900          TYPE 706
48000   706    FORMAT(/'  N'6X'A3R(N)'6X'B3R(N)'5X'C3R(N)'
48100        1 5X'D3R(N)'5X'F3R(N)'5X'G3R(N)')
48200          DO 710 I=1,NTERMS,1
48300   710    TYPE 729,I,A3R(I),B3R(I),C3R(I),D3R(I),F3R(I),G3R(I)
48400          TYPE 711
48500   711    FORMAT(/'  N'7X'A1(N)'7X'B1(N)'6X'C1(N)'6X'D1(N)'
48600        1 6X'F1(N)'6X'G1(N)')
48700          DO 715 I=1,NTERMS,1
48800   715    TYPE 729,I,A1(I),B1(I),C1(I),D1(I),F1(I),G1(I)
48900          TYPE 716
49000   716    FORMAT(/'  N'6X'A2M(N)'6X'B2M(N)'5X'C2M(N)'
49100        1 5X'D2M(N)'5X'F2M(N)'5X'G2M(N)')
49200          DO 720 I=1,NTERMS,1
49300   720    TYPE 729,I,A2M(I),B2M(I),C2M(I),D2M(I),F2M(I),G2M(I)
49400          TYPE 721
49500   721    FORMAT(/'  N'6X'A2P(N)'6X'B2P(N)'5X'C2P(N)'
49600        1 5X'D2P(N)'5X'F2P(N)'5X'G2P(N)')
49700          DO 725 I=1,NTERMS,1
49800   725    TYPE 729,I,A2P(I),B2P(I),C2P(I),D2P(I),F2P(I),G2P(I)
49900          TYPE 726
50000   726    FORMAT(/'  N'7X'A3(N)'7X'B3(N)'6X'C3(N)'6X'D3(N)'
50100        3 6X'F3(N)'6X'G3(N)')
50200          DO 728 I=1,NTERMS,1
50300   728    TYPE 729,I,A3(I),B3(I),C3(I),D3(I),F3(I),G3(I)
50400   729    FORMAT(I3,2E12.4,4E11.3)
50500          TYPE 731
50600   731    FORMAT(/'  N'5X'P1SQ(N)'5X'P2SQ(N)'5X'P3SQ(N)')
50700          DO 735 I=1,NTERMS,1
50800   735    TYPE 736,I,P1SQ(I),P2SQ(I),P3SQ(I)
50900   736    FORMAT(I3,3E12.4)
51000   738    CONTINUE
51100          IF(IFPAA.NE.1)GO TO 790
51200          SURFRS=SQRT(FREQ/WGCNCU)*8.25E-03
51300          WL1=0.0
51400          WL2=0.0
51500          WL3=0.0
51600          WL4=0.0
51700          WL5=0.0
51800          WLDS2=0.0
51900          WLDS3=0.0
52000          PWRN1=0.0
```

```
52100          PWRN2=0.0
52200          PWRN3=0.0
52300          DO 754 N=1,NTERMS,1
52400          F12N1=1.0
52500          IF(N.EQ.1)F12N1=2.0
52600          F01N1=2.0-F12N1
52700          WL1=WL1+BDIM*(F01N1*F1(N)**2+F12N1*G1(N)**2)
52800          DO 754 M=1,NTERMS,1
52900          IF(M.NE.N)GO TO 750
53000   740    PSS1=0.5*(HSP1(N)*HC1(N)-AX1)/P1SQ(N)
53100          PCC1=0.5*(HSP1(N)*HC1(N)+AX1)
53200          PCS2=(1.0-(HC2(N))**2)/(2.0*P2SQ(N))
53300          PSC2=PCS2
53400          ARG=6.283185*HR*(N-1)
53500          IF(N.GT.1)GO TO 743
53600          SS2=0.0
53700          CC2=0.5*(BDIM-DDIM)
53800          GO TO 745
53900   743    SS2=0.25*(BDIM-DDIM+DDIM*SIN(ARG)/ARG)
54000          CC2=0.25*(BDIM-DDIM-DDIM*SIN(ARG)/ARG)
54100   745    PSS3=0.5*(-HH3(N)*HE3(N)-AX3)/P3SQ(N)
54200          PCC3=0.5*(-HH3(N)*HE3(N)+AX3)
54300          RCSQA=HC1(N)*HSP2(N)/(QAM(N)*PXN1(N)*PXN2(N))
54400          RSSQA=RCSQA*HSP1(N)/HC1(N)
54500          RCSQD=HC1(N)*HSP2(N)/(QDP(N)*PXN1(N)*PXN2(N))
54600          RSSQD=RCSQD*HSP1(N)/HC1(N)
54700          SEXN=0.5*F01N1*(AX2*(A2P(N)**2-(A2M(N)**2)/P2SQ(N))+
54800        1 RCSQA*A2P(N)**2+RDC*P1SQ(N)*RSSQA*A2P(N)*
54900        2 A2M(N)/P2SQ(N))
55000          SEYN=0.5*F12N1*(AX2*(B2P(N)**2-(B2M(N)**2)/
55100        1 P2SQ(N))+(GY1(N)*A2P(N)*(RDC*P1SQ(N)*RSSQA*B2P(N)
55200        2 +RCSQA*B2M(N))-WU*BETA*D2M(N)*(RSSQD*B2P(N)
55300        3 +RCSQD*B2M(N)/P2SQ(N)))/GNX1SQ(N))
55400          SEZN=0.5*F01N1*(AX2*(C2P(N)**2-(C2M(N)**2)/
55500        1 P2SQ(N))-(BETA*A2P(N)*(RDC*P1SQ(N)*RSSQA*C2P(N)
55600        2 +RCSQA*C2M(N))+WU*GY1(N)*D2M(N)*(RSSQD*C2P(N)
55700        3 +RCSQD*C2M(N)/P2SQ(N)))/GNX1SQ(N))
55800          WLDS2N=SEXN+SEYN+SEZN
55900          WLDS3N=F01N1*(PSS3*A3(N)**2+PCC3*C3(N)**2)
56000        1 +F12N1*PCC3*B3(N)**2
56100          WLDS2=WLDS2+WLDS2N
56200          WLDS3=WLDS3+WLDS3N
56300          PWR1TN=0.5*BDIM*(F01N1*A1(N)*F1(N)*PCC1
56400        1 -F12N1*B1(N)*D1(N)*PSS1)
56500          PWRN1=PWRN1+PWR1TN
56600          PWR2AF=0.5*F01N1*(AX2*(A2P(N)*F2P(N)-A2M(N)
56700        1 *F2M(N)/P2SQ(N))+A2P(N)*(RCSQA*F2P(N)+RDC*P1SQ(N)
56800        2 *RSSQA*F2M(N)/P2SQ(N)))
56900          PWR2BD=0.5*F12N1*(AX2*(B2P(N)*D2P(N)-B2M(N)
57000        1 *D2M(N)/P2SQ(N))+D2M(N)*(RSSQD*B2P(N)+RCSQD
57100        2 *B2M(N)/P2SQ(N)))
57200          PWR2TN=0.5*BDIM*(PWR2AF-PWR2BD)
57300          PWRN2=PWRN2+PWR2TN
57400   748    PWR3TN=0.5*DDIM*(F01N1*A3(N)*F3(N)*PSS3
57500        1 -F12N1*B3(N)*D3(N)*PCC3)
57600          PWRN3=PWRN3+PWR3TN
57700          HZZ0=0.5*AX2*(G2P(N)**2-(G2M(N)**2)/P2SQ(N))
57800          HZZ1=-0.5*G2P(N)*(GY1(N)*WEP*RCSQA*A2P(N)
57900        1 +BETA*RCSQD*D2M(N))/GNX1SQ(N)
58000          HZZ2=-0.5*G2M(N)*(GY1(N)*WEP*RDC*P1SQ(N)*RSSQA
58100        1 *A2P(N)/P2SQ(N)+BETA*RSSQD*D2M(N))/GNX1SQ(N)
58200          HZZNM=HZZ0+HZZ1+HZZ2
58300          HXX0=0.5*AX2*(D2P(N)**2-(D2M(N)**2)/P2SQ(N))
58400          HXX1=0.5*D2M(N)*(RSSQD*D2P(N)+RCSQD*D2M(N)/P2SQ(N))
58500          HXXNM=HXX0+HXX1
58600          GO TO 752
58700   750    PSS1=(HC1(N)*HSP1(M)-HSP1(N)*HC1(M))
58800        1 /(P1SQ(N)-P1SQ(M))
```

```
      PCC1=(P1SQ(N)*HSP1(N)*HC1(M)-P1SQ(M)
     1 *HC1(N)*HSP1(M))/(P1SQ(N)-P1SQ(M))
      QNN=1.0/(PXN1(N)*PXN2(N))
      RCQAN=HC1(N)*QNN/QAM(N)
      RSQAN=HSP1(N)*QNN/QAM(N)
      RCQDN=HC1(N)*QNN/QDP(N)
      RSQDN=HSP1(N)*QNN/QDP(N)
      QNM=1.0/(PXN1(M)*PXN2(M))
      RCQAM=HC1(M)*QNM/QAM(M)
      RSQAM=HSP1(M)*QNM/QAM(M)
      RCQDM=HC1(M)*QNM/QDP(M)
      RSQDM=HSP1(M)*QNM/QDP(M)
      TDENOM=1.0/(GNX1SQ(N)*GNX1SQ(M)*(P2SQ(N)
     1 -P2SQ(M))
      HZZ0=(G2M(N)*G2P(M)-G2P(N)*G2M(M))/(P2SQ(N)
     1 -P2SQ(M))
      HZZ1=A2P(N)*A2P(M)*WEP*WEP*GY1(N)*GY1(M)*RDC*(P1SQ(M)
     1 *RCQAN*RSQAM-P1SQ(N)*RSQAN*RCQAM)*TDENOM
      HZZ2=D2M(N)*D2M(M)*BETASQ*(P2SQ(M)*RCQDN*RSQDM
     1 -P2SQ(N)*RSQDN*RCQDM)*TDENOM
      HZZ3=A2P(N)*D2M(N)*BETA*WEP*GY1(N)*(P2SQ(M)
     1 *RCQAN*RSQDM-RDC*P1SQ(N)*RSQAN*RCQDM)*TDENOM
      HZZ4=A2P(M)*D2M(N)*BETA*WEP*GY1(M)*(RDC*P1SQ(M)
     1 *RCQDN*RSQAM-P2SQ(N)*RSQDN*RCQAM)*TDENOM
      HZZNM=HZZ0+HZZ1+HZZ2+HZZ3+HZZ4
      HXX0=(D2M(N)*D2P(M)-D2P(N)*D2M(M))/(P2SQ(N)-P2SQ(M))
      HXX1=D2M(N)*D2M(M)*(RSQDN*RCQDM-RCQDN*RSQDM)/(P2SQ(N)
     1 -P2SQ(M))
      HXXNM=HXX0+HXX1
      ARGP=3.141593*HF*(N+M-2)
      ARGM=3.141593*HF*(N-M)
      SS2=-0.25*DDIM*(SIN(ARGM)/ARGM-SIN(ARGP)/ARGP)
      CC2=-0.25*DDIM*(SIN(ARGM)/ARGM+SIN(ARGP)/ARGP)
      PCC3=-(P3SQ(N)*HH3(N)*HE3(M)-P3SQ(M)
     1 *HE3(N)*HH3(M))/(P3SQ(N)-P3SQ(M))
      PSS3=-(HE3(N)*HH3(M)-HH3(N)*HE3(M))
     1 /(P3SQ(N)-P3SQ(M))
752   ONEPM=(-1.0)**(N+M)
      WL2=WL2+4.0*ONEPM*(D1(N)*D1(M)*PSS1
     1 +G1(N)*G1(M)*PCC1)
      WL3=WL3+4.0*ONEPM*(HXXNM+HZZNM)
      WL4=WL4+4.0*(F2P(N)*F2P(M)*SS2+G2P(N)*G2P(M)*CC2)
      WL5=WL5+4.0*ONEPM*(D3(N)*D3(M)*PCC3+G3(N)*G3(M)*PSS3)
754   CONTINUE
      PWRN=PWRN1+PWRN2+PWRN3
      TYPE 756,PWRN
756   FORMAT(/' NORMALLIZED POWER = 'E12.4/)
      ECLN=0.0
      DO 760 I=1,NTERMS,1
760   ECLN=ECLN+ABS(B3(I))
      EM2ADI=0.0
      DO 773 I=1,33,1
      EXMADI=0.0
      EYMADI=0.0
      DO 764 J=1,NTERMS,1
      ARG=(I-1)*GY1(J)*DDIM/64.0
      EXMADI=EXMADI+EXADI(J)*SIN(ARG)
764   EYMADI=EYMADI+EYADI(J)*COS(ARG)
      EM2I=EXMADI**2+EYMADI**2
C **** SKIP PRINTOUT FOR MOST APPLICATIONS
      GO TO 770
      I32THS=I-1
      TYPE 766,EM2I,I32THS
766   FORMAT(4X'(ETRANS)**2 AT ADI = 'E12.4' FOR Y = 'I2' 32THS
     1 OF D/2')
770   CONTINUE
      IF(EM2I.GT.EM2ADI)EM2ADI=EM2I
773   CONTINUE
      PRDADI=5.8064E+06*PWRN/EM2ADI
```

```
65800          PBDCL=0.001*PWRN*(76200*BDSD/ECLN)**2
65900          TYPE 776,PBDADI,PBDCL
66000   776    FORMAT(/' POWER CAPACITY (AIR BREAKDOWN) ='F10.3'
66100        1 KILOWATTS'/' POWER CAPACITY (DIELECTRIC BREAKDOWN) ='
66200        2 F10.3' KILOWATTS')
66300          WLC=(WL1+WL2+WL3+WL4+WL5)*SURFRS*0.5
66400          ALMC=WLC/(2.0*PWRN)
66500          ALCDBL=8.68589*ALMC*WGWL
66600          ALCDBF=ALCDBL*12.0/WGWL
66700          TYPE 779,WGCNCU
66800   779    FORMAT(/'  CONDUCTIVITY (NORMALLIZED TO COPPER) OF
66900        1 WAVEGUIDE WALLS = 'F4.2)
67000          TYPE 781,ALMC,ALCDBF,ALCDBL
67100   781    FORMAT('  ATTENUATION FROM CONDUCTOR LOSSES -- ALPHA ='
67200        1 E11.4/6X'='F7.5' DB/FOOT OR 'F7.5' DB/WAVELENGTH')
67300          FLDF=WER*DLT/(4.0*PWRN)
67400          ALD2=WLDS2*BDIM*FLDF
67500          ALD3=WLDS3*DDIM*FLDF
67600          ALDL=ALD2+ALD3
67700          ALDDBF=8.68589*ALDL*12.0
67800          ALDDBL=WGWL*ALDDBF/12.0
67900          TYPE 785,DLT
68000   785    FORMAT(/'  DIELECTRIC LOSS TANGENT = 'E9.3)
68100          TYPE 786,ALDL,ALDDBF,ALDDBL
68200   786    FORMAT(' ATTENUATION FROM DIELECTRIC LOSSES -- ALPHA =
68300        1 'E11.5/6X'='F7.5' DB/FOOT OR 'F7.5' DB/WAVELENGTH')
68400   790    CONTINUE
68500          IF(IFFC.EQ.0)GO TO 840
68600   795    TYPE 796
68700   796    FORMAT(/' WISH NEW FREQUENCY? '$)
68800          ACCEPT 210,IFFREQ
68900          IF(IFFREQ.EQ.1)GO TO 875
69000          GO TO 960
69100   800    DD1=1.0
69200          CALL LINV3F(TMATX,DUMMY,4,MXSIZE,32,DD1,DD2,
69300        1 WKAREA,IER)
69400          DET=DD1*2.0**DD2
69500          XX=FREQ
69600          IF(IFFC.EQ.1)XX=BDG
69700          IF(MRSF.NE.1)GO TO 820
69800          IF(NCOUNT.NE.1)GO TO 810
69900          FN1=DET
70000          XXNEW=XUL
70100          GO TO 818
70200   810    DRX=0.0001
70300          IF(IFFC.EQ.1)DRX=0.01
70400          IF(ABS(XX-XXOLD).GT.DRX.OR.ABS(DET/FN1).GT.0.01)GO
70500        1 TO 813
70600          GO TO 831
70700   813    XXNEW=XX-FOLD*(XXOLD-XX)/(FOLD-DET)
70800          IF(DET*FOLD.LT.0.0)GO TO 815
70900          IF(XX.GT.XXOLD)XLL=XX
71000          IF(XX.LT.XXOLD)XUL=XX
71100          GO TO 817
71200   815    IF(XX.GT.XXOLD)XUL=XX
71300          IF(XX.LT.XXOLD)XLL=XX
71400   817    IF(XXNEW.GT.XUL.OR.XXNEW.LT.XLL)XXNEW=0.5*(XUL+XLL)
71500   818    FOLD=DET
71600          XXOLD=XX
71700          GO TO 825
71800   820    TYPE 821,FREQ,BDG,DET,IER,P3SO(1),P2SO(1),HH3(1)
71900   821    FORMAT(2F9.3,E13.3,I4,3E12.3)
72000          IF(XX.GE.XX2)GO TO 829
72100          XXNEW=XX+XDEL
72200   825    CONTINUE
72300          IF(IFFC.EQ.1)GO TO 828
72400          FREQ=XXNEW
72500          GO TO 290
72600   828    BDG=XXNEW
```

```
72700          GO TO 295
72800   829    TYPE 830
72900   830    FORMAT(/' WISH NEW TRYS AT ROOT? '$)
73000          ACCEPT 210,INEWXX
73100          IF(INEWXX.EQ.0)GO TO 980
73200          IF(IFFC.EQ.0)GO TO 245
73300          GO TO 878
73400   831    IFROOT=1
73500   C **** ROOT NOW KNOWN
73600   833    IF(IFFC.EQ.1)GO TO 890
73700          FCGHZ=FREQ
73800   835    TYPE 836,FCGHZ
73900   836    FORMAT(/' CUTOFF FREQ IN GHZ ='F8.4)
74000          IFMCAP=0
74100          IF(MMODE.NE.1.OR.NMODE.NE.0.OR.JTTYPE.NE.1)GO TO 840
74200   C MODAL COMPONENT AMPLITUDES ARE CALCULATED ONLY FOR
74300   C OLSE(1,0) MODES WITH TDIM GREATER THAN SDIM.
74400          TYPE 838
74500   838    FORMAT(/' WISH MODAL COMPONENT AMPLITUDES? '$)
74600          ACCEPT 210,IFMCAP
74700          IF(IFMCAP.NE.1)GO TO 840
74800          IFPAA=0
74900          MCAMP=1
75000          GO TO 560
75100   840    TYPE 841
75200   841    FORMAT(' DO YOU WISH CALCULATIONS FOR FREQUENCIES
75300        1 ABOVE CUTOFF? NO=0, YES=1    ?'$)
75400          ACCEPT 210,IFFREQ
75500          IF(IFFREQ.EQ.1)GO TO 843
75600          IF(IFFREQ.EQ.0)GO TO 960
75700          GO TO 840
75800   843    IFFC=1
75900          IFPAA=0
76000          IF(MMODE.NE.1.OR.NMODE.NE.0.OR.JTTYPE.NE.1)GO TO 875
76100          TYPE 846
76200   846    FORMAT(' WISH POWER BREAKDOWN AND ATTENUATION? '$)
76300          ACCEPT 210,IFPAA
76400          IF(IFPAA.NE.1)GO TO 870
76500   850    TYPE 851
76600   851    FORMAT(' BREAKDOWN STRENGTH (RELATIVE TO THAT OF
76700        1 DRY AIR) OF DIELECTRIC: '$)
76800          READ(5,*)BDSD
76900          IF(BDSD.GE.1.0)GO TO 858
77000          TYPE 856
77100   856    FORMAT(' RELATIVE BREAKDOWN STRENGTH OF DIELECTRIC
77200        1 SHOULD BE UNITY OR GREATER')
77300          GO TO 850
77400   858    TYPE 861
77500   861    FORMAT(' CONDUCTIVITY (RELATIVE TO COPPER) OF WAVEGUIDE
77600        1 WALLS: '$)
77700          READ(5,*)WGCNCU
77800   865    TYPE 866
77900   866    FORMAT(' LOSS TANGENT OF DIELECTRIC: '$)
78000          READ(5,*)DLT
78100   870    TYPE 871
78200   871    FORMAT(' WISH MODAL COMPONENT AMPLITUDES (YES=1) ?'$)
78300          ACCEPT 210,IFMCAP
78400   875    TYPE 876
78500   876    FORMAT(' DESIRED FREQUENCY IN GHZ: '$)
78600          READ(5,*)FREQ
78700          IF(FREQ.GT.FCGHZ)GO TO 878
78800          TYPE 877
78900   877    FORMAT(' FREQUENCY MUST BE GREATER THAN CUTOFF FREQUENCY')
79000          GO TO 875
79100   878    TYPE 879
79200   879    FORMAT(/' WISH BETA SEARCH(0) OR FIX(1)? '$)
79300          ACCEPT 210,MPSF
79400          IF(MPSF.EQ.0)GO TO 880
```

```
79500            IF(MRSF.EQ.1)GO TO 885
79600            GO TO 878
79700   880      TYPE 881
79800   881      FORMAT(' BETA (DEG/IN) - - START,STOP,INCREMENT: '$)
79900            READ(5,*)XX1,XX2,XDEL
80000            BDG=XX1
80100            GO TO 265
80200   885      TYPE 886
80300   886      FORMAT(' SET LOWER,UPPER LIMITS ON BETA (DEG/IN): '$)
80400            READ(5,*)XLL,XUL
80500            BDG=XLL
80600            XDEL=0.5*(XUL-XLL)
80700            GO TO 265
80800   890      BDGR=BDG
80900            WGWL=360.0/BDGR
81000            TYPE 894,FREQ,BDGR
81100   894      FORMAT(6X'FREQ'11X'BETA'/F10.3,F15.3)
81200            MCAMP=0
81300            IF(IFPAA.NE.1.AND.IFMCAP.NE.1)GO TO 795
81400            MCAMP=1
81500            GO TO 560
81600   960      TYPE 962
81700   962      FORMAT(////' WAVEGUIDE PARAMETERS -- DIMENSIONS IN
81800         1 INCHES'/9X'A'9X'B'9X'D'9X'S'9X'T'7X'RDC')
81900            TYPE 963,ADIM,BDIM,DDIM,SDIM,TDIM,RDC
82000   963      FORMAT(7F10.4)
82100            TYPE 965,EMMODE,MMODE,NMODE,FCGHZ,NHOM
82200   965      FORMAT(/' WAVEGUIDE MODE IS OLS'A1'('I1','I1')'5X
82300         1 'CUTOFF FREQUENCY IN GHZ ='F9.4/' NUMBER OF HIGHER ORDER
82400         2 MODES USED IN ANALYSIS = 'I2/)
82500            IF(IFFREQ.EQ.0)GO TO 980
82600   980      TYPE 981
82700   981      FORMAT(////' DO YOU WISH A RERUN? '$)
82800            READ(5,*)NRERUN
82900            GO TO(999,984,124,128,132,136,140,175,200,190,110
83000         1 ,980)NRERUN+1
83100   984      TYPE 985
83200   985      FORMAT(' TO CHANGE: A=2, B=3, D=4, S=5, T=6, EPSR=7,
83300         1 NUMBER OF MODES IN ANALYSIS=8,'/' DESIRED MODE=9,START
83400         1 FROM SCRATCH=10')
83500            GO TO 980
83600   999      END
83700            FUNCTION SINC(KSINC,MFS12,KINT,KHR,HRATIO)
83800            SCXP=1.570796*(KINT+KHR*HRATIO)
83900            SCXM=1.570796*(KINT-KHR*HRATIO)
84000            IF(KINT.NE.0.AND.KHR.NE.0)GO TO 1120
84100            IF(KINT.EQ.0.AND.KHR.NE.0)GO TO 1110
84200            IF(KINT.NE.0.AND.KHR.EQ.0)GO TO 1100
84300            SINC=1.0
84400            IF(MFS12.EQ.0)SINC=0.0
84500            GO TO 1130
84600   1100     SINC=0.0
84700            GO TO 1130
84800   1110     SINC=MFS12*SIN(SCXP)/SCXP
84900            GO TO 1130
85000   1120     IF(ABS(SCXM).GT.1.0E-05)GO TO 1125
85100            SINC=KSINC*SIN(SCXP)/SCXP+1.0
85200            GO TO 1130
85300   1125     SINC=KSINC*SIN(SCXP)/SCXP+SIN(SCXM)/SCXM
85400   1130     CONTINUE
85500            RETURN
85600            END
```

PROGRAM CROOT3

```
00100   C PROGRAM CROOT3.FOR
00200            DIMENSION XL(3),TDB(3),TANGD(3),CA(3),CBD(3)
00300            COMPLEX CT1,CT2,CT3,CG12,CG31,CG23,PG
```

```
00400          COMPLEX CF,PGA,CGSQ,TC1,TC2
00500          TYPE 20
00600    20    FORMAT(' PROGRAM CROOT3 CALCULATES THE COMPLEX
00700        1 PROPAGATION CONSTANT OF A GIVEN'/' TRANSMISSION LINE
00800        2 BY USING THE MEASURED TRANSMISSION COEFFICIENTS
00900        3 '/' OF THREE DIFFERENT LENGTH SAMPLES TO
01000        4 CORRECT FOR MISMATCH EFFECTS'//)
01100          TYPE 21
01200    21    FORMAT(' WISH PRINTOUT AS ROOT IS SOUGHT?'$)
01300          ACCEPT 215,IFRSPO
01400    24    TYPE 25
01500    25    FORMAT(' LENGTHS ARE IN INCHES')
01600          DO 28 I=1,3,1
01700          TYPE 27,I
01800    27    FORMAT(' LENGTH OF SAMPLE #'I1': '$)
01900          READ(5,*)XL(I)
02000    28    CONTINUE
02100          TYPE 30
02200    30    FORMAT('/' MEASURED TRANSMISSION DATA IS TO BE ENTERED
02300        1 AS LOSS IN DB, PHASE IN DEGREES')
02400    31    TYPE 32
02500    32    FORMAT('/' FREQUENCY IN GHZ: '$)
02600          READ(5,*)FREQ
02700          DO 35 I=1,3,1
02800          TYPE 33,XL(I)
02900    33    FORMAT(' LOSS, PHASE OF'F6.3' INCH SAMPLE: '$)
03000          READ(5,*)TDB(I),TANGD(I)
03100    35    CONTINUE
03200          TYPE 40
03300    40    FORMAT('/' ENTER FIRST TRY VALUES FOR ALPHA, BETA(DEG/IN): '$)
03400          READ(5,*)A1,BDI1
03500          T1MAG=10.0**(-TDB(1)/20.0)
03600          T2MAG=10.0**(-TDB(2)/20.0)
03700          T3MAG=10.0**(-TDB(3)/20.0)
03800          T1ANGR=TANGD(1)/57.2957795
03900          T2ANGR=TANGD(2)/57.2957795
04000          T3ANGR=TANGD(3)/57.2957795
04100          TR21=T2MAG*T1MAG*COS(T2ANGR+T1ANGR)
04200          TI21=T2MAG*T1MAG*SIN(T2ANGR+T1ANGR)
04300          TR13=T1MAG*T3MAG*COS(T1ANGR+T3ANGR)
04400          TI13=T1MAG*T3MAG*SIN(T1ANGR+T3ANGR)
04500          TR32=T3MAG*T2MAG*COS(T3ANGR+T2ANGR)
04600          TI32=T3MAG*T2MAG*SIN(T3ANGR+T2ANGR)
04700          DL13=XL(1)-XL(3)
04800          DL32=XL(3)-XL(2)
04900          DL21=XL(2)-XL(1)
05000          ITRY=1
05100          ALPHA=A1
05200          BETA=BDI1/57.2957795
05300    50    HCA13=COSH(ALPHA*DL13)
05400          HSA13=SINH(ALPHA*DL13)
05500          HCA21=COSH(ALPHA*DL21)
05600          HCA21=SINH(ALPHA*DL21)
05700          HCA32=COSH(ALPHA*DL32)
05800          HSA32=SINH(ALPHA*DL32)
05900          CB13=COS(BETA*DL13)
06000          SB13=SIN(BETA*DL13)
06100          CB21=COS(BETA*DL21)
06200          SB21=SIN(BETA*DL21)
06300          CB32=COS(BETA*DL32)
06400          SB32=SIN(BETA*DL32)
06500          HSS13=HSA13*SB13
06600          HSC13=HSA13*CB13
06700          HCS13=HCA13*SB13
06800          HCC13=HCA13*CB13
06900          HSS21=HSA21*SB21
07000          HSC21=HSA21*CB21
07100          HCS21=HCA21*SB21
```

```
07200          HCC21=HCA21*CB21
07300          HSS32=HSA32*SB32
07400          HSC32=HSA32*CB32
07500          HCS32=HCA32*SB32
07600          HCC32=HCA32*CB32
07700          FR=TR32*HSC32-TI32*HCS32+TR21*HSC21-TI21*HCS21
07800        1 +TR13*HSC13-TI13*HCS13
07900          FI=TR32*HCS32+TI32*HSC32+TR21*HCS21+TI21*HSC21
08000        1 +TR13*HCS13+TI13*HSC13
08100          FMAG=SQRT(FR*FR+FI*FI)
08200          IF(IFRSPD.NE.1)GO TO 60
08300          TYPE 58,ALPHA,BETA,FR,FI,FMAG
08400   58     FORMAT(2F10.5,3E10.3)
08500   60     CONTINUE
08600          IF(FMAG.LT.1.0E-07)GO TO 80
08700          IF(ITRY.LT.11)GO TO 70
08800          TYPE 65
08900   65     FORMAT(' MORE THAN 10 TRYS AT ROOT')
09000          GO TO 80
09100   70     PFRA=DL32*(TR32*HCC32-TI32*HSS32)+DL21*(TR21*HCC21
09200        1 -TI21*HSS21)+DL13*(TR13*HCC13-TI13*HSS13)
09300          PFRB=-DL32*(TR32*HSS32+TI32*HCC32)-DL21*(TR21*HSS21
09400        1+TI21*HCC21)-DL13*(TR13*HSS13+TI13*HCC13)
09500          DET=PFRA*PFRA+PFRB*PFRB
09600          DELA=-(PFRA*FR-PFRB*FI)/DET
09700          DELB=-(PFRB*FR+PFRA*FI)/DET
09800          ALPHA=ALPHA+DELA
09900          BETA=BETA+DELB
10000          ITRY=ITRY+1
10100          GO TO 50
10200   80     EDI=57.2957795*BETA
10300          TYPE 90
10400   90     FORMAT(/// MEAS #'3X'LENGTH(IN)'3X'TMAG(DB LOSS)
10500        1 TANG(DEG)')
10600          DO 95 I=1,3,1
10700          TYPE 94,I,XL(I),TDB(I),TANGD(I)
10800   94     FORMAT(I7,F13.4,F16.3,F12.2)
10900   95     CONTINUE
11000          TYPE 100,FREQ,ALPHA,EDI
11100  100     FORMAT(/' FREQUENCY(GHZ) ='F7.3,5X'ALPHA ='F6.4,4X'
11200        1 BETA(DEG/INCH) ='F8.2)
11300  200     TYPE 210
11400  210     FORMAT(/// WISH NEW FREQUENCY DATA? '$)
11500          ACCEPT 215,NRERUN
11600  215     FORMAT(I1)
11700          GO TO(225,31,225)NRERUN+1
11800  225     END
```


GPO 922-236

END
FILMED

6-86

DTIC